ISSN 1007-9327
CN 14-1219/R

World Journal of Gastroenterology®

Indexed and Abstracted in:
Current Contents®/Clinical Medicine, Science Citation Index Expanded (also known as SciSearch®), Journal Citation Reports®, Index Medicus, MEDLINE, PubMed, PubMed Central, Digital Object Identifer, and EMBASE/Excerpta Medica. ISI, Thomson Reuters, 2008 Impact Factor: 2.081 (32/55 Gastroenterology and Hepatology).

Volume 16 Number 13
April 7, 2010
World J Gastroenterol
2010 April 7; 16(13): 1555-1682

Online Submissions
www.wjgnet.com/1007-9327offce
www.wjgnet.com
Printed on Acid-free Paper
世界胃肠病学杂志

World Journal of Gastroenterology

A peer-reviewed, online, open-access journal of gastroenterology and hepatology

Editorial Board

2010-2013

The *World Journal of Gastroenterology* Editorial Board consists of 1096 members, representing a team of worldwide experts in gastroenterology and hepatology. They are from 60 countries, including Albania (1), Argentina (7), Australia (28), Austria (13), Belgium (11), Brazil (8), Brunei Darussalam (1), Bulgaria (2), Canada (18), Chile (3), China (66), Colombia (1), Croatia (2), Cuba (1), Czech (4), Denmark (8), Ecuador (1), Egypt (2), Estonia (2), Finland (7), France (22), Germany (72), Greece (14), Hungary (10), India (25), Iran (6), Ireland (6), Israel (12), Italy (94), Japan (107), Jordan (1), Kuwait (1), Lebanon (3), Lithuania (2), Malaysia (1), Mexico (9), Moldova (1), Netherlands (27), New Zealand (2), Norway (11), Pakistan (2), Poland (10), Portugal (4), Romania (3), Russia (1), Saudi Arabia (3), Serbia (3), Singapore (9), South Africa (2), South Korea (32), Spain (36), Sweden (17), Switzerland (11), Thailand (1), Trinidad and Tobago (1), Turkey (24), United Arab Emirates (2), United Kingdom (80), United States (242), and Uruguay (1).

William Kemp, *Melbourne*
Finlay A Macrae, *Victoria*
Daniel Markovich, *Brisbane*
Vance Matthews, *Melbourne*
Phillip S Oates, *Perth*
Shan Rajendra, *Tasmania*
Rajvinder Singh, *Elizabeth Vale*
Ross C Smith, *Sydney*
Kevin J Spring, *Brisbane*
Nathan Subramaniam, *Brisbane*
Phil Sutton, *Melbourne*
Cuong D Tran, *North Adelaide*
Debbie Trinder, *Fremantle*
David Ian Watson, *Bedford Park*

Austria

Herwig H Cerwenka, *Graz*
Ashraf Dahaba, *Graz*
Peter Ferenci, *Vienna*
Valentin Fuhrmann, *Vienna*
Alfred Gangl, *Vienna*
Alexander M Hirschl, *Wien*
Kurt Lenz, *Linz*
Dietmar Öfner, *Salzburg*
Markus Peck-Radosavljevic, *Vienna*
Markus Raderer, *Vienna*
Georg Roth, *Vienna*
Michael Trauner, *Graz*
Thomas Wild, *Kapellerfeld*

Belgium

Rudi Beyaert, *Gent*
Benedicte Y De Winter, *Antwerp*
Inge I Depoortere, *Leuven*
Olivier Detry, *Liège*
Marc Peeters, *De Pintelaan*
Freddy Penninckx, *Leuven*
Jean-Yves L Reginster, *Liège*
Mark De Ridder, *Brussels*
Etienne M Sokal, *Brussels*
Kristin Verbeke, *Leuven*
Eddie Wisse, *Keerbergen*

Brazil

José LF Caboclo, *São José do Rio Preto*
Roberto J Carvalho-Filho, *São Paulo*
Jaime Natan Eisig, *São Paulo*
Andre Castro Lyra, *Salvador*
Marcelo Lima Ribeiro, *Braganca Paulista*
Heitor Rosa, *Goiania*
Damiao C Moraes Santos, *Rio de Janeiro*
Eduardo Garcia Vilela, *Belo Horizonte*

Brunei Darussalam

Vui Heng Chong, *Bandar Seri Begawan*

Bulgaria

Zahariy Krastev, *Sofia*
Mihaela Petrova, *Sofia*

Canada

Alain Bitton, *Montreal*
Michael F Byrne, *Vancouver*
Kris Chadee, *Calgary*
Ram Prakash Galwa, *Ottawa*
Philip H Gordon, *Montreal*
Waliul Khan, *Ontario*
John K Marshall, *Ontario*
Andrew L Mason, *Alberta*
Kostas Pantopoulos, *Quebec*
Nathalie Perreault, *Sherbrooke*
Baljinder Singh Salh, *Vancouver*
Eldon Shaffer, *Calgary*
Martin Storr, *Calgary*
Pingchang Yang, *Hamilton*
Eric M Yoshida, *Vancouver*
Claudia Zwingmann, *Montreal*

Chile

Marcelo A Beltran, *La Serena*
Xabier De Aretxabala, *Santiago*
Silvana Zanlungo, *Santiago*

China

Hui-Jie Bian, *Xi'an*
San-Jun Cai, *Shanghai*
Guang-Wen Cao, *Shanghai*
Xiao-Ping Chen, *Wuhan*
Chi-Hin Cho, *Hong Kong*
Zong-Jie Cui, *Beijing*
Jing-Yuan Fang, *Shanghai*
De-Liang Fu, *Shanghai*
Chun-Yi Hao, *Beijing*
Ming-Liang He, *Hong Kong*
Simon Law, *Hong Kong*
Yuk-Tong Lee, *Hong Kong*
En-Min Li, *Shantou*
Fei Li, *Beijing*
Yu-Yuan Li, *Guangzhou*
Zhao-Shen Li, *Shanghai*
Xing-Hua Lu, *Beijing*
Yi-Min Mao, *Shanghai*
Qin Su, *Beijing*
Paul Kwong-Hang Tam, *Hong Kong*
Yuk Him Tam, *Hong Kong*
Ren-Xiang Tan, *Nanjing*
Eric WC Tse, *Hong Kong*
Fu-Sheng Wang, *Beijing*
Xiang-Dong Wang, *Shanghai*
Nathalie Wong, *Hong Kong*
Justin CY Wu, *Hong Kong*
Wen-Rong Xu, *Zhenjiang*
An-Gang Yang, *Xi'an*
Wei-Cheng You, *Beijing*
Chun-Qing Zhang, *Jinan*
Jian-Zhong Zhang, *Beijing*
Xiao-Peng Zhang, *Beijing*
Xuan Zhang, *Beijing*

Colombia

Germán Campuzano-Maya, *Medellín*

Croatia

Tamara Cacev, *Zagreb*
Marko Duvnjak, *Zagreb*

Cuba

Damian C Rodriguez, *Havana*

Czech

Jan Bures, *Hradec Kralove*
Milan Jirsa, *Praha*
Marcela Kopacova, *Hradec Kralove*
Pavel Trunečka, *Prague*

Denmark

Leif Percival Andersen, *Copenhagen*
Asbjørn M Drewes, *Aalborg*
Morten Frisch, *Copenhagen*
Jan Mollenhauer, *Odense*
Morten Hylander Møller, *Holte*
Søren Rafaelsen, *Vejle*
Jorgen Rask-Madsen, *Skodsborg*
Peer Wille-Jørgensen, *Copenhagen*

Ecuador

Fernando E Sempértegui, *Quito*

Egypt

Zeinab Nabil Ahmed, *Cairo*
Hussein M Atta, *El-Minia*

Estonia

Riina Salupere, *Tartu*
Tamara Vorobjova, *Tartu*

Finland

Saila Kauhanen, *Turku*
Kaija-Leena Kolho, *Helsinki*
Jukka-Pekka Mecklin, *Jyvaskyla*
Minna Nyström, *Helsinki*
Pauli Antero Puolakkainen, *Turku*
Juhani Sand, *Tampere*
Lea Veijola, *Helsinki*

France

Claire Bonithon-Kopp, *Dijon*
Lionel Bueno, *Toulouse*
Sabine Colnot, *Paris*
Catherine Daniel, *Lille Cedex*
Thabut Dominique, *Paris*
Francoise L Fabiani, *Angers*
Jean-Luc Faucheron, *Grenoble*
Jean Paul Galmiche, *Nantes cedex*

Boris Guiu, *Dijon*
Paul Hofman, *Nice*
Laurent Huwart, *Paris*
Abdel-Majid Khatib, *Paris*
Philippe Lehours, *Bordeaux*
Flavio Maina, *Marseille*
Patrick Marcellin, *Paris*
Rene Gerolami Santandera, *Marseille*
Annie Schmid-Alliana, *Nice cedex*
Alain L Servin, *Châtenay-Malabry*
Stephane Supiot, *Nantes*
Baumert F Thomas, *Strasbourg*
Jean-Jacques Tuech, *Rouen*
Frank Zerbib, *Bordeaux Cedex*

Germany

Erwin Biecker, *Siegburg*
Hubert Blum, *Freiburg*
Thomas Bock, *Tuebingen*
Dean Bogoevski, *Hamburg*
Elfriede Bollschweiler, *Köln*
Jürgen Borlak, *Hannover*
Christa Buechler, *Regensburg*
Jürgen Büning, *Lübeck*
Elke Cario, *Essen*
Bruno Christ, *Halle/Saale*
Christoph F Dietrich, *Bad Mergentheim*
Ulrich R Fölsch, *Kiel*
Nikolaus Gassler, *Aachen*
Markus Gerhard, *Munich*
Dieter Glebe, *Giessen*
Ralph Graeser, *Freiburg*
Axel M Gressner, *Aachen*
Nils Habbe, *Marburg*
Thilo Hackert, *Heidelberg*
Wolfgang Hagmann, *Heidelberg*
Dirk Haller, *Freising*
Philip D Hard, *Giessen*
Claus Hellerbrand, *Regensburg*
Klaus R Herrlinger, *Stuttgart*
Eberhard Hildt, *Berlin*
Andrea Hille, *Goettingen*
Joerg C Hoffmann, *Berlin*
Andrej Khandoga, *Munich*
Jorg Kleeff, *Munich*
Ingmar Königsrainer, *Tübingen*
Peter Konturek, *Erlangen*
Stefan Kubicka, *Hannover*
Joachim Labenz, *Siegen*
Michael Linnebacher, *Rostock*
Jutta Elisabeth Lüttges, *Riegelsberg*
Peter Malfertheiner, *Magdeburg*
Oliver Mann, *Hamburg*
Peter N Meier, *Hannover*
Sabine Mihm, *Göttingen*
Klaus Mönkemüller, *Bottrop*
Jonas Mudter, *Erlangen*
Sebastian Mueller, *Heidelberg*
Robert Obermaier, *Freiburg*
Matthias Ocker, *Erlangen*
Stephan Johannes Ott, *Kiel*
Christoph Reichel, *Bad Brückenau*
Markus Reiser, *Bochum*
Steffen Rickes, *Magdeburg*
Elke Roeb, *Giessen*
Christian Rust, *Munich*
Hans Scherubl, *Berlin*
Martin K Schilling, *Homburg*
Rene Schmidt, *Freiburg*
Andreas G Schreyer, *Regensburg*
Karsten Schulmann, *Bochum*
Henning Schulze-Bergkamen, *Mainz*
Manfred V Singer, *Mannheim*
Jens Standop, *Bonn*
Jurgen M Stein, *Frankfurt*
Ulrike S Stein, *Berlin*
Wolfgang R Stremmel, *Heidelberg*
Harald F Teutsch, *Ulm*
Hans L Tillmann, *Leipzig*
Christian Trautwein, *Aachen*
Joerg Trojan, *Frankfurt*
Arndt Vogel, *Hannover*
Siegfried Wagner, *Deggendorf*
Frank Ulrich Weiss, *Greifswald*
Fritz von Weizsäcker, *Berlin*
Thomas Wex, *Magdeburg*
Stefan Wirth, *Wuppertal*
Marty Zdichavsky, *Tübingen*

Greece

Helen Christopoulou-Aletra, *Thessaloniki*
T Choli-Papadopoulou, *Thessaloniki*
Tsianos Epameinondas, *Ioannina*
Ioannis Kanellos, *Thessaloniki*
Elias A Kouroumalis, *Heraklion*
Ioannis E Koutroubakis, *Heraklion*
Michael Koutsilieris, *Athens*
Andreas Larentzakis, *Athens*
Emanuel K Manesis, *Athens*
Spilios Manolakopoulos, *Athens*
Konstantinos Mimidis, *Alexandroupolis*
George Papatheodoridis, *Athens*
Spiros Sgouros, *Athens*
Evangelos Tsiambas, *Ag Paraskevi Attiki*

Hungary

György M Buzás, *Budapest*
László Czakó, *Szeged*
Gyula Farkas, *Szeged*
Peter Hegyi, *Szeged*
Peter L Lakatos, *Budapest*
Yvette Mándi, *Szeged*
Zoltan Rakonczay, *Szeged*
Ferenc Sipos, *Budapest*
Zsuzsa Szondy, *Debrecen*
Gabor Veres, *Budapest*

India

Philip Abraham, *Mumbai*
Vineet Ahuja, *New Delhi*
Devinder Kumar Dhawan, *Chandigarh*
Radha K Dhiman, *Chandigarh*
Pankaj Garg, *Panchkula*
Pramod Kumar Garg, *New Delhi*
Debidas Ghosh, *Midnpore*
Uday C Ghoshal, *Lucknow*
Bhupendra Kumar Jain, *Delhi*
Ashok Kumar, *Lucknow*
Bikash Medhi, *Chandigarh*
Sri P Misra, *Allahabad*
Gopal Nath, *Varanasi*
Samiran Nundy, *New Delhi*
Jagannath Palepu, *Mumbai*
Vandana Panda, *Mumbai*
Benjamin Perakath, *Tamil Nadu*
Ramesh Roop Rai, *Jaipur*
Nageshwar D Reddy, *Hyderabad*
Barjesh Chander Sharma, *New Delhi*
Virendra Singh, *Chandigarh*
Rupjyoti Talukdar, *Guwahati*
Rakesh Kumar Tandon, *New Delhi*
Jai Dev Wig, *Chandigarh*

Iran

Mohammad Abdollahi, *Tehran*
Peyman Adibi, *Isfahan*
Seyed-Moayed Alavian, *Tehran*
Seyed Mohsen Dehghani, *Shiraz*
Reza Malekzadeh, *Tehran*
Alireza Mani, *Tehran*

Ireland

Billy Bourke, *Dublin*
Ted Dinan, *Cork*
Catherine Greene, *Dublin*
Ross McManus, *Dublin*
Marion Rowland, *Dublin*

Israel

Simon Bar-Meir, *Hashomer*
Alexander Becker, *Afula*
Abraham R Eliakim, *Haifa*
Sigal Fishman, *Tel Aviv*
Boris Kirshtein, *Beer Sheva*
Eli Magen, *Ashdod*
Menachem Moshkowitz, *Tel-Aviv*
Assy Nimer, *Safed*
Shmuel Odes, *Beer Sheva*
Mark Pines, *Bet Dagan*
Ron Shaoul, *Haifa*
Ami D Sperber, *Beer-Sheva*

Italy

Donato F Altomare, *Bari*
Piero Amodio, *Padova*
Paolo Angeli, *Padova*
Bruno Annibale, *Rome*
Paolo Aurello, *Rome*
Salvatore Auricchio, *Naples*
Antonio Basoli, *Rome*
Claudio Bassi, *Verona*
Gabrio Bassotti, *Perugia*
Mauro Bernardi, *Bologna*
Alberto Biondi, *Rome*
Luigi Bonavina, *Milano*
Guglielmo Borgia, *Naples*
Roberto Berni Canani, *Naples*
Fausto Catena, *Bologna*
Giuseppe Chiarioni, *Valeggio*
Michele Cicala, *Rome*
Dario Conte, *Milano*
Francesco Costa, *Pisa*
Giuseppe Currò, *Messina*
Mario M D'Elios, *Florence*
Mirko D'Onofrio, *Verona*
Silvio Danese, *Milano*
Roberto de Franchis, *Milano*
Paola De Nardi, *Milan*
Giovanni D De Palma, *Naples*

Giuliana Decorti, *Trieste*
Gianlorenzo Dionigi, *Varese*
Massimo Falconi, *Verona*
Silvia Fargion, *Milan*
Giammarco Fava, *Ancona*
Francesco Feo, *Sassari*
Alessandra Ferlini, *Ferrara*
Alessandro Ferrero, *Torino*
Luca Frulloni, *Verona*
Giovanni B Gaeta, *Napoli*
Antonio Gasbarrini, *Rome*
Edoardo G Giannini, *Genoa*
Alessandro Granito, *Bologna*
Fabio Grizzi, *Milan*
Salvatore Gruttadauria, *Palermo*
Pietro Invernizzi, *Milan*
Achille Iolascon, *Naples*
Angelo A Izzo, *Naples*
Ezio Laconi, *Cagliari*
Giovanni Latella, *L'Aquila*
Massimo Levrero, *Rome*
Francesco Luzza, *Catanzaro*
Lucia Malaguarnera, *Catania*
Francesco Manguso, *Napoli*
Pier Mannuccio Mannucci, *Milano*
Giancarlo Mansueto, *Verona*
Giulio Marchesini, *Bologna*
Mara Massimi, *Coppito*
Giovanni Milito, *Rome*
Giuseppe Montalto, *Palermo*
Giovanni Monteleone, *Rome*
Luca Morelli, *Trento*
Giovanni Musso, *Torino*
Mario Nano, *Torino*
Gerardo Nardone, *Napoli*
Riccardo Nascimbeni, *Brescia*
Valerio Nobili, *Rome*
Fabio Pace, *Milano*
Nadia Peparini, *Rome*
Mario Pescatori, *Rome*
Raffaele Pezzilli, *Bologna*
Alberto Piperno, *Monza*
Anna C Piscaglia, *Rome*
Piero Portincasa, *Bari*
Michele Reni, *Milan*
Vittorio Ricci, *Pavia*
Oliviero Riggio, *Rome*
Mario Rizzetto, *Torino*
Ballarin Roberto, *Modena*
Franco Roviello, *Siena*
Cesare Ruffolo, *Treviso*
Massimo Rugge, *Padova*
Marco Scarpa, *Padova*
C armelo Scarpignato, *Parma*
Giuseppe Sica, *Rome*
Marco Silano, *Rome*
Pierpaolo Sileri, *Rome*
Vincenzo Stanghellini, *Bologna*
Fiorucci Stefano, *Perugia*
Giovanni Tarantino, *Naples*
Alberto Tommasini, *Trieste*
Guido Torzilli, *Rozzano Milano*
Cesare Tosetti, *Porretta Terme*
Antonello Trecca, *Rome*
Vincenzo Villanacci, *Brescia*
Lucia Ricci Vitiani, *Rome*
Marco Vivarelli, *Bologna*

Japan

Kyoichi Adachi, *Izumo*
Yasushi Adachi, *Sapporo*
Takafumi Ando, *Nagoya*
Akira Andoh, *Otsu*
Masahiro Arai, *Tokyo*
Hitoshi Asakura, *Tokyo*
Kazuo Chijiiwa, *Miyazaki*
Yuichiro Eguchi, *Saga*
Itaru Endo, *Yokohama*
Munechika Enjoji, *Fukuoka*
Yasuhiro Fujino, *Akashi*
Mitsuhiro Fujishiro, *Tokyo*
Kouhei Fukushima, *Sendai*
Masanori Hatakeyama, *Tokyo*
Keiji Hirata, *Kitakyushu*
Toru Hiyama, *Higashihiroshima*
Masahiro Iizuka, *Akita*
Susumu Ikehara, *Osaka*
Kenichi Ikejima, *Bunkyo-ku*
Yutaka Inagaki, *Kanagawa*
Hiromi Ishibashi, *Nagasaki*
Shunji Ishihara, *Izumo*
Toru Ishikawa, *Niigata*
Toshiyuki Ishiwata, *Tokyo*
Yoshiaki Iwasaki, *Okayama*
Satoru Kakizaki, *Gunma*
Terumi Kamisawa, *Tokyo*
Mototsugu Kato, *Sapporo*
Naoya Kato, *Tokyo*
Takumi Kawaguchi, *Kurume*
Yohei Kida, *Kainan*
Shogo Kikuchi, *Aichi*
Tsuneo Kitamura, *Chiba*
Takashi Kobayashi, *Tokyo*
Yasuhiro Koga, *Isehara*
Takashi Kojima, *Sapporo*
Norihiro Kokudo, *Tokyo*
Masatoshi Kudo, *Osaka*
Shin Maeda, *Tokyo*
Satoshi Mamori, *Hyogo*
Atsushi Masamune, *Sendai*
Yasushi Matsuzaki, *Tsukuba*
Kenji Miki, *Tokyo*
Hiroto Miwa, *Hyogo*
Kotaro Miyake, *Tokushima*
Manabu Morimoto, *Yokohama*
Yoshiharu Motoo, *Kanazawa*
Yoshiaki Murakami, *Hiroshima*
Kunihiko Murase, *Tusima*
Akihito Nagahara, *Tokyo*
Yuji Naito, *Kyoto*
Atsushi Nakajima, *Yokohama*
Hisato Nakajima, *Tokyo*
Hiroki Nakamura, *Yamaguchi*
Shotaro Nakamura, *Fukuoka*
Akimasa Nakao, *Nagogya*
Shuhei Nishiguchi, *Hyogo*
Mikio Nishioka, *Niihama*
Keiji Ogura, *Tokyo*
Susumu Ohmada, *Maebashi*
Hirohide Ohnishi, *Akita*
Kenji Okajima, *Nagoya*
Kazuichi Okazaki, *Osaka*
Morikazu Onji, *Ehime*
Satoshi Osawa, *Hamamatsu*
Hidetsugu Saito, *Tokyo*
Yutaka Saito, *Tokyo*
Naoaki Sakata, *Sendai*
Yasushi Sano, *Chiba*
Tokihiko Sawada, *Tochigi*
Tomohiko Shimatan, *Hiroshima*
Yukihiro Shimizu, *Kyoto*
Shinji Shimoda, *Fukuoka*
Yoshio Shirai, *Niigata*
Masayuki Sho, *Nara*
Shoichiro Sumi, *Kyoto*
Hidekazu Suzuki, *Tokyo*
Masahiro Tajika, *Nagoya*
Yoshihisa Takahashi, *Tokyo*
Toshinari Takamura, *Kanazawa*
Hiroaki Takeuchi, *Kochi*
Yoshitaka Takuma, *Okayama*
Akihiro Tamori, *Osaka*
Atsushi Tanaka, *Tokyo*
Shinji Tanaka, *Hiroshima*
Satoshi Tanno, *Hokkaido*
Shinji Togo, *Yokohama*
Hitoshi Tsuda, *Tokyo*
Hiroyuki Uehara, *Osaka*
Masahito Uemura, *Kashihara*
Yoshiyuki Ueno, *Sendai*
Mitsuyoshi Urashima, *Tokyo*
Satoshi Yamagiwa, *Niigata*
Taketo Yamaguchi, *Chiba*
Mitsunori Yamakawa, *Yamagata*
Takayuki Yamamoto, *Yokkaichi*
Yutaka Yata, *Maebashi*
Hiroshi Yoshida, *Tokyo*
Norimasa Yoshida, *Kyoto*
Yuichi Yoshida, *Osaka*
Kentaro Yoshika, *Toyoake*
Katsutoshi Yoshizato, *Higashihiroshima*
Tomoharu Yoshizumi, *Fukuoka*

Jordan

Ismail Matalka, *Irbid*

Kuwait

Islam Khan, *Safat*

Lebanon

Bassam N Abboud, *Beirut*
Ala I Sharara, *Beirut*
Rita Slim, *Beirut*

Lithuania

Giedrius Barauskas, *Kaunas*
Limas Kupcinskas, *Kaunas*

Malaysia

Andrew Seng Boon Chua, *Ipoh*

Mexico

Richard A Awad, *Mexico*
Aldo Torre Delgadillo, *Mexico*
Diego Garcia-Compean, *Monterrey*
Paulino M Hernández Magro, *Celaya*
Miguel Angel Mercado, *Distrito Federal*
Arturo Panduro, *Jalisco*
Omar Vergara-Fernandez, *Tlalpan*
Saúl Villa-Trevio, *Mexico*

Moldova

Igor Mishin, *Kishinev*

Netherlands

Ulrich Beuers, *Amsterdam*
Lee Bouwman, *Leiden*
Albert J Bredenoord, *Nieuwegein*
Lodewijk AA Brosens, *Utrecht*
J Bart A Crusius, *Amsterdam*
Wouter de Herder, *Rotterdam*
Pieter JF de Jonge, *Rotterdam*
Robert J de Knegt, *Rotterdam*
Wendy W Johanna de Leng, *Utrecht*
Annemarie de Vries, *Rotterdam*
James CH Hardwick, *Leiden*
Frank Hoentjen, *Haarlem*
Misha Luyer, *Sittard*
Gerrit A Meijer, *Amsterdam*
Servaas Morré, *Amsterdam*
Chris JJ Mulder, *Amsterdam*
John Plukker, *Groningen*
Albert Frederik Pull ter Gunne, *Tilburg*
Paul E Sijens, *Groningen*
BW Marcel Spanier, *Arnhem*
Maarten Tushuizen, *Amsterdam*
Jantine van Baal, *Heidelberglaan*
Astrid van der Velde, *The Hague*
Karel van Erpecum, *Utrecht*
Loes van Keimpema, *Nijmegen*
Robert Christiaan Verdonk, *Groningen*
Erwin G Zoetendal, *Wageningen*

New Zealand

Andrew S Day, *Christchurch*

Norway

Olav Dalgard, *Oslo*
Trond Peder Flaten, *Trondheim*
Reidar Fossmark, *Trondheim*
Rasmus Goll, *Tromso*
Ole Høie, *Arendal*
Asle W Medhus, *Oslo*
Espen Melum, *Oslo*
Trine Olsen, *Tromso*
Eyvind J Paulssen, *Tromso*
Jon Arne Søreide, *Stavanger*
Kjetil Soreide, *Stavanger*

Pakistan

Shahab Abid, *Karachi*
Syed MW Jafri, *Karachi*

Poland

Marek Bebenek, *Wroclaw*
Tomasz Brzozowski, *Cracow*
Halina Cichoż-Lach, *Lublin*
Andrzej Dabrowski, *Bialystok*
Hanna Gregorek, *Warsaw*
Marek Hartleb, *Katowice*
Beata Jolanta Jablońska, *Katowice*
Stanislaw J Konturek, *Krakow*
Jan Kulig, *Krakow*
Julian Swierczynski, *Gdansk*

Portugal

Raquel Almeida, *Porto*
Ana Isabel Lopes, *Lisboa Codex*
Ricardo Marcos, *Porto*
Guida Portela-Gomes, *Estoril*

Romania

Dan L Dumitrascu, *Cluj*
Adrian Saftoiu, *Craiova*
Andrada Seicean, *Cluj-Napoca*

Russia

Vasiliy I Reshetnyak, *Moscow*

Saudi Arabia

Ibrahim A Al Mofleh, *Riyadh*
Abdul-Wahed Meshikhes, *Qatif*
Faisal Sanai, *Riyadh*

Serbia

Tamara M Alempijevic, *Belgrade*
Dusan M Jovanovic, *Sremska Kamenica*
Zoran Krivokapic, *Belgrade*

Singapore

Madhav Bhatia, *Singapore*
Kong Weng Eu, *Singapore*
Brian Kim Poh Goh, *Singapore*
Khek-Yu Ho, *Singapore*
Kok Sun Ho, *Singapore*
Fock Kwong Ming, *Singapore*
London Lucien Ooi, *Singapore*
Nagarajan Perumal, *Singapore*
Francis Seow-Choen, *Singapore*

South Africa

Rosemary Joyce Burnett, *Pretoria*
Michael Kew, *Cape Town*

South Korea

Sang Hoon Ahn, *Seoul*
Sung-Gil Chi, *Seoul*
Myung-Gyu Choi, *Seoul*
Hoon Jai Chun, *Seoul*
Yeun-Jun Chung, *Seoul*
Young-Hwa Chung, *Seoul*
Kim Donghee, *Seoul*
Ki-Baik Hahm, *Incheon*
Sun Pyo Hong, *Geonggi-do*
Seong Gyu Hwang, *Seongnam*
Hong Joo Kim, *Seoul*
Jae J Kim, *Seoul*
Jin-Hong Kim, *Suwon*
Nayoung Kim, *Seongnam-si*
Sang Geon Kim, *Seoul*
Seon Hahn Kim, *Seoul*
Sung Kim, *Seoul*
Won Ho Kim, *Seoul*
Jeong Min Lee, *Seoul*
Kyu Taek Lee, *Seoul*
Sang Kil Lee, *Seoul*
Sang Yeoup Lee, *Gyeongsangnam-do*
Yong Chan Lee, *Seoul*
Eun-Yi Moon, *Seoul*
Hyoung-Chul Oh, *Seoul*
Seung Woon Paik, *Seoul*
Joong-Won Park, *Goyang*
Ji Kon Ryu, *Seoul*
Si Young Song, *Seoul*
Marie Yeo, *Suwon*
Byung Chul Yoo, *Seoul*
Dae-Yeul Yu, *Daejeon*

Spain

Maria-Angeles Aller, *Madrid*
Raul J Andrade, *Málaga*
Luis Aparisi, *Valencia*
Gloria González Aseguinolaza, *Navarra*
Matias A Avila, *Pamplona*
Fernando Azpiroz, *Barcelona*
Ramon Bataller, *Barcelona*
Belén Beltrán, *Valencia*
Adolfo Benages, *Valencia*
Josep M Bordas, *Barcelona*
Lisardo Boscá, *Madrid*
Luis Bujanda, *San Sebastián*
Juli Busquets, *Barcelona*
Matilde Bustos, *Pamplona*
José Julián calvo Andrés, *Salamanca*
Andres Cardenas, *Barcelona*
Antoni Castells, *Barcelona*
Fernando J Corrales, *Pamplona*
J E Domínguez-Muñoz, *Santiago de Compostela*
Juan Carlos Laguna Egea, *Barcelona*
Isabel Fabregat, *Barcelona*
Antoni Farré, *Barcelona*
Vicente Felipo, *Valencia*
Laureano Fernández-Cruz, *Barcelona*
Luis Grande, *Barcelona*
Angel Lanas, *Zaragoza*
Juan-Ramón Larrubia, *Guadalajara*
María IT López, *Jaén*
Juan Macías, *Seville*
Javier Martin, *Granada*
José Manuel Martin-Villa, *Madrid*
Julio Mayol, *Madrid*
Mireia Miquel, *Sabadell*
Jesús M Prieto, *Pamplona*
Pedro L Majano Rodriguez, *Madrid*
Eva Vaquero, *Barcelona*

Sweden

Lars Erik Agréus, *Stockholm*
Roland Andersson, *Lund*
Mauro D'Amato, *Huddinge*
Evangelos Kalaitzakis, *Gothenburg*
Greger Lindberg, *Stockholm*
Annika Lindblom, *Stockholm*

Sara Lindén, *Göteborg*
Hanns-Ulrich Marschall, *Stockholm*
Pär Erik Myrelid, *Linköping*
Åke Nilsson, *Lund*
Helena Nordenstedt, *Stockholm*
Kjell Öberg, *Uppsala*
Lars A Pahlman, *Uppsala*
Stefan G Pierzynowski, *Lund*
Sara Regnér, *Malmö*
Bobby Tingstedt, *Lund*
Zongli Zheng, *Stockholm*

Switzerland

Pascal Bucher, *Geneva*
Michelangelo Foti, *Geneva*
Jean L Frossard, *Geneva*
Andreas Geier, *Zürich*
Pascal Gervaz, *Geneva*
Gerd A Kullak-Ublick, *Zürich*
Fabrizio Montecucco, *Geneva*
Paul M Schneider, *Zürich*
Felix Stickel, *Berne*
Bruno Stieger, *Zürich*
Inti Zlobec, *Basel*

Trinidad and Tobago

Shivananda Nayak, *Mount Hope*

Turkey

Sinan Akay, *Tekirdag*
Metin Basaranoglu, *Istanbul*
Yusuf Bayraktar, *Ankara*
A Mithat Bozdayi, *Ankara*
Hayrullah Derici, *Balıkesir*
Eren Ersoy, *Ankara*
Mukaddes Esrefoglu, *Malatya*
Can Goen, *Kutahya*
Selin Kapan, *Istanbul*
Aydin Karabacakoglu, *Konya*
Cuneyt Kayaalp, *Malatya*
Kemal Kismet, *Ankara*
Seyfettin Köklü, *Ankara*
Mehmet Refik Mas, *Etlik-Ankara*
Osman C Ozdogan, *Istanbul*
Bülent Salman, *Ankara*
Salih Sanlioglu, *Antalya*
Orhan Sezgin, *Mersin*
Ilker Tasci, *Ankara*
Ahmet Tekin, *Mersin*
Mesut Tez, *Ankara*
Ekmel Tezel, *Ankara*
Özlem Yilmaz, *Izmir*

United Arab Emirates

Fikri M Abu-Zidan, *Al-Ain*
Sherif M Karam, *Al-Ain*

United Kingdom

Simon Afford, *Birmingham*
Navneet K Ahluwalia, *Stockport*
Mohamed H Ahmed, *Southampton*
Basil Ammori, *Salford*
Lesley A Anderson, *Belfast*
Chin Wee Ang, *Liverpool*
Yeng S Ang, *Wigan*
Anthony TR Axon, *Leeds*
Kathleen B Bamford, *London*
Jim D Bell, *London*
John Beynon, *Swansea*
Chris Briggs, *Sheffield*
Geoffrey Burnstock, *London*
Alastair D Burt, *Newcastle*
Jeff Butterworth, *Shrewsbury*
Jeremy FL Cobbold, *London*
Jean E Crabtree, *Leeds*
Tatjana Crnogorac-Jurcevic, *London*
William Dickey, *Londonderry*
Sunil Dolwani, *Cardiff*
Emad M El-Omar, *Aberdeen*
A M El-Tawil, *Birmingham*
Charles B Ferguson, *Belfast*
Andrew Fowell, *Southampton*
Piers Gatenby, *London*
Daniel R Gaya, *Edinburgh*
Anil George, *London*
Rob Glynne-Jones, *Northwood*
Jason CB Goh, *Birmingham*
Gianpiero Gravante, *Leicester*
Brian Green, *Belfast*
William Greenhalf, *Liverpool*
Indra N Guha, *Nottingham*
Stefan G Hübscher, *Birmingham*
Robin Hughes, *London*
Pali Hungin, *Stockton*
Nawfal Hussein, *Nottingham*
Clement W Imrie, *Glasgow*
Janusz AZ Jankowski, *Oxford*
Sharad Karandikar, *Birmingham*
Peter Karayiannis, *London*
Shahid A Khan, *London*
Patricia F Lalor, *Birmingham*
John S Leeds, *Sheffield*
Ian Lindsey, *Oxford*
Hong-Xiang Liu, *Cambridge*
Dileep N Lobo, *Nottingham*
Graham MacKay, *Glasgow*
Anne McCune, *Bristol*
Donald Campbell McMillan, *Glasgow*
Giorgina Mieli-Vergani, *London*
Jamie Murphy, *London*
Guy Fairbairn Nash, *Poole*
James Neuberger, *Birmingham*
Patrick O'Dwyer, *Glasgow*
Christos Paraskeva, *Bristol*
Richard Parker, *North Staffordshire*
Thamara Perera, *Birmingham*
Kondragunta Rajendra Prasad, *Leeds*
D Mark Pritchard, *Liverpool*
Alberto Quaglia, *London*
Akhilesh B Reddy, *Cambridge*
Kevin Robertson, *Glasgow*
John B Schofield, *Kent*
Marco Senzolo, *Padova*
Venkatesh Shanmugam, *Derby*
Paul Sharp, *London*
Chew Thean Soon, *Manchester*
Aravind Suppiah, *East Yorkshire*
Noriko Suzuki, *Middlesex*
Simon D Taylor-Robinson, *London*
Frank I Tovey, *London*
A McCulloch Veitch, *Wolverhampton*
Vamsi R Velchuru, *Lowestoft*
Sumita Verma, *Brighton*
Catherine Walter, *Cheltenham*
Julian RF Walters, *London*
Roger Williams, *London*

United States

Kareem M Abu-Elmagd, *Pittsburgh*
Sami R Achem, *Florida*
Golo Ahlenstiel, *Bethesda*
Bhupinder S Anand, *Houston*
M Ananthanarayanan, *New York*
Balamurugan N Appakalal, *Minneapolis*
Dimitrios V Avgerinos, *New York*
Shashi Bala, *Worcester*
Anthony J Bauer, *Pittsburgh*
Kevin E Behrns, *Gainesville*
Roberto Bergamaschi, *New York*
Henry J Binder, *New Haven*
Edmund J Bini, *New York*
Wojciech Blonski, *Philadelphia*
Mark Bloomston, *Columbus*
Edward L Bradley III, *Sarasota*
Carla W Brady, *Durham*
David A Brenner, *San Diego*
Adeel A Butt, *Pittsburgh*
Shi-Ying Cai, *New Haven*
Justin MM Cates, *Nashville*
Eugene P Ceppa, *Durham*
Jianyuan Chai, *Long Beach*
Ronald S Chamberlain, *Livingston*
Xian-Ming Chen, *Omaha*
Ramsey Chi-man Cheung, *Palo Alto*
Denesh Chitkara, *East Brunswick*
Clifford S Cho, *Madison*
Parimal Chowdhury, *Arkansas*
John David Christein, *Birmingham*
Thomas Clancy, *Boston*
Ana J Coito, *Los Angeles*
Ricardo Alberto Cruciani, *New York*
Joseph J Cullen, *Iowa City*
Mark J Czaja, *New York*
Mariana D Dabeva, *Bronx*
Jessica A Davila, *Houston*
Conor P Delaney, *Cleveland*
Laurie DeLeve, *Los Angeles*
Anthony J Demetris, *Pittsburgh*
Sharon DeMorrow, *Temple*
Bijan Eghtesad, *Cleveland*
Yoram Elitsur, *Huntington*
Mohamad A Eloubeidi, *Alabama*
Wael El-Rifai, *Nashville*
Giamila Fantuzzi, *Chicago*
Ashkan Farhadi, *Irvine*
Ronnie Fass, *Tucson*
Martín E Fernández-Zapico, *Rochester*
Alessandro Fichera, *Chicago*
Josef E Fischer, *Boston*
Piero Marco Fisichella, *Maywood*
Fritz Francois, *New York*
Glenn T Furuta, *Aurora*
T Clark Gamblin, *Pittsburgh*
Henning Gerke, *Iowa City*
Jean-Francois Geschwind, *Baltimore*
R Mark Ghobrial, *Texas*
John F Gibbs, *Buffalo*
Shannon S Glaser, *Temple*
Ajay Goel, *Dallas*
Jon C Gould, *Madison*
Eileen F Grady, *San Francisco*
James H Grendell, *New York*

World Journal of Gastroenterology

Contents

Weekly Volume 16 Number 13 April 7, 2010

World Journal of Gastroenterology
Volume 16 Number 13 April 7, 2010

Contents

AIM AND SCOPE

World Journal of Gastroenterology (*World J Gastroenterol*, *WJG*, print ISSN 1007-9327, DOI: 10.3748) is a weekly, open-access, peer-reviewed journal supported by an editorial board of 1096 experts in gastroenterology and hepatology from 60 countries.

The major task of *WJG* is to report rapidly the most recent results in basic and clinical research on esophageal, gastrointestinal, liver, pancreas and biliary tract diseases, *Helicobacter pylori*, endoscopy and gastrointestinal surgery, including: gastroesophageal reflux disease, gastrointestinal bleeding, infection and tumors; gastric and duodenal disorders; intestinal inflammation, microflora and immunity; celiac disease, dyspepsia and nutrition; viral hepatitis, portal hypertension, liver fibrosis, liver cirrhosis, liver transplantation, and metabolic liver disease; molecular and cell biology; geriatric and pediatric gastroenterology; diagnosis and screening, imaging and advanced technology.

NAME OF JOURNAL
World Journal of Gastroenterology

LAUNCH DATE
October 1, 1995

RESPONSIBLE INSTITUTION
Department of Science and Technology of Shanxi Province

SPONSOR
Taiyuan Research and Treatment Center for Digestive Diseases, 77 Shuangta Xijie, Taiyuan 030001, Shanxi Province, China

EDITING
Editorial Board of *World Journal of Gastroenterology*,
Room 903, Building D, Ocean International Center,
No. 62 Dongsihuan Zhonglu, Chaoyang District,
Beijing 100025, China
Telephone: +86-10-5908-0039
Fax: +86-10-8538-1893
E-mail: wjg@wjgnet.com
http://www.wjgnet.com

PUBLISHING
Beijing Baishideng BioMed Scientific Co., Ltd.,
Room 903, Building D, Ocean International Center,
No. 62 Dongsihuan Zhonglu, Chaoyang District,
Beijing 100025, China
Telephone: +86-10-8538-1892
Fax: +86-10-8538-1893
E-mail: baishideng@wjgnet.com
http://www.wjgnet.com

SUBSCRIPTION
Beijing Baishideng BioMed Scientific Co., Ltd.,
Room 903, Building D, Ocean International Center,
No. 62 Dongsihuan Zhonglu, Chaoyang District,
Beijing 100025, China
Telephone: +86-10-8538-1892
Fax: +86-10-8538-1893
E-mail: baishideng@wjgnet.com
http://www.wjgnet.com

PRINT SUBSCRIPTION
RMB 245 Yuan for each issue, RMB 11760 Yuan for one year.

ONLINE SUBSCRIPTION
One-Year Price 864.00 USD

PUBLICATION DATE
April 7, 2010

CSSN
ISSN 1007-9327 (print)
CN 14-1219/R

EDITORIAL OFFICE
Jian-Xia Cheng, Director
World Journal of Gastroenterology
Room 903, Building D, Ocean International Center,
No. 62 Dongsihuan Zhonglu, Chaoyang District,
Beijing 100025, China
Telephone: +86-10-5908-0039
Fax: +86-10-8538-1893
E-mail: wjg@wjgnet.com
http://www.wjgnet.com

INSTRUCTIONS TO AUTHORS
Full instructions are available online at http://www.wjgnet.com/1007-9327/g_info_20100315215714.htm. If you do not have web access please contact the editorial office.

ONLINE SUBMISSION
http://www.wjgnet.com/1007-9327office

World Journal of Gastroenterology

Online Submissions: http://www.wjgnet.com/1007-9327office
wjg@wjgnet.com
doi:10.3748/wjg.v16.i13.1555

World J Gastroenterol 2010 April 7; 16(13): 1555-1557
ISSN 1007-9327 (print)

EDITORIAL

Ezetimbe as potential treatment for cholesterol gallstones: The need for clinical trials

Mohamed H Ahmed

Mohamed H Ahmed, Chemical Pathology Department, Southampton University Hospital NHS Trust, Southampton SO16 6YD, United Kingdom
Author contributions: Ahmed MH wrote the paper.
Correspondence to: Mohamed H Ahmed, MD, PhD, Chemical Pathology Department, Mail point 6-Level D, South Academic Block, Southampton University Hospitals NHS Trust, Southampton SO16 6YD, United Kingdom. elziber@yahoo.com
Telephone: +44-23-80793465 Fax: +44-23-80796339
Received: November 27, 2009 Revised: December 24, 2009
Accepted: December 31, 2009
Published online: April 7, 2010

Abstract

Obesity is associated with insulin resistance, non-alcoholic fatty liver disease (NAFLD) and gallstones. High fat diets (unsaturated fats) rich in cholesterol have been demonstrated to produce not only gallstones but also NAFLD and insulin resistance. Interestingly, a high incidence of gallstones is being reported in association with insulin resistance and NAFLD. Laparoscopic cholecystectomy is the best definitive therapy for symptomatic gallbladder disease. Ezetimibe is a drug that inhibits the absorption of both dietary and biliary cholesterol in the small intestine. Importantly, ezetimibe showed potential benefit not only in treating and preventing gallstones but also in insulin resistance and NAFLD. Further studies are required before the use of ezetimibe for the treatment of gallstones can be advocated.

Key words: Ezetimibe; Gallstones; Insulin resistance; Non-alcoholic fatty liver disease

Peer reviewers: Dr. Kaye M Reid Lombardo, MD, Assistant Professor, Department of General Surgery, Mayo Clinic, 200 First St. SW, Rochester, MN 55905, United States; Kyu Taek Lee, MD, PhD, Professor, Department of Medicine Samsung Medical Center, Sungkyunkwan, University School of Medicine, #50, Irwon-dong, Gangnam-gu, Seoul 135-710, South Korea

Ahmed MH. Ezetimbe as potential treatment for cholesterol gallstones: The need for clinical trials. *World J Gastroenterol* 2010; 16(13): 1555-1557 Available from: URL: http://www.wjgnet.com/1007-9327/full/v16/i13/1555.htm DOI: http://dx.doi.org/10.3748/wjg.v16.i13.1555

INTRODUCTION

Gallstones are a common problem and is likely to have existed since the appearance of mankind on Earth. Interestingly, gallstones have been identified in autopsy studies of Egyptian mummies[1]. Gallstones and associated complications cost approximately 6.5 billion dollars annually in the USA. The incidence of gallstones is more frequent in females than males and increase with age. The role of ethnicity and genetics is known in gallstone formation. Importantly, the distribution of gallstones in different populations appears to be related to high dietary intake of cholesterol and fats (Western diets). Furthermore, gallstones are primarily cholesterol or black pigment stones (bilirubin polymers) or brown pigment stones (calcium bilirubinate). The only established dietary risk is a high caloric intake. Other modifiable risk factors for gallstones are obesity, the metabolic syndrome, rapid weight loss, certain diseases (cirrhosis, Crohn's disease) and gallbladder stasis (from spinal cord injury or drugs such as somatostatin). Therefore, it is anticipated that diets containing fibre, vegetable protein, nuts, calcium, vitamin C, coffee, plus physical activity are all regarded as protective factors. In developed countries, cholesterol gallstones predominate; 15% are black pigment stones. It is thought that gallstones affect around 15% of white adults in developed countries. East Asians develop brown pigment stones in bile ducts, associated with biliary infection or parasites, or in intrahepatic ducts (hepatolithiasis). In view of the high prevalence of obesity and metabolic

syndrome, the burden of disease is epidemic in American Indians at around 60%-70%. The frequency of gallstones is reduced in Black Americans, Hispanics of mixed Indian origin, East Asians and sub-Saharan Africans[2,3]. Most asymptomatic gallstone carriers require no therapy. Laparoscopic cholecystectomy is the best definitive therapy for symptomatic gallstone disease. Primary prevention is unproven but focuses on early identification and risk alteration to decrease the possibility of developing gallstones. Ursodeoxycholic acid has a limited role in stone dissolution but can prevent stone development in severe obesity during rapid weight reduction with diet therapy or after bariatric surgery[4].

EZETIMIBE AND CHOLESTEROL GALLSTONES

Recently, it was shown both in animal models and humans that ezetimibe may prevent and treat cholesterol gallstones[5]. Ezetimibe inhibits intestinal uptake of cholesterol with a half life of approximately of 22 h. The major metabolic pathway for ezetimibe consists of glucuronidation of the 4-hydroxyphenyl group by uridine 5'-diphosphate-glucuronosyltransferase isoenzymes to form ezetimibe-glucuronide in the intestine and liver. Approximately 78% of the dose is excreted in the faeces predominantly as ezetimibe, with the balance found in the urine mainly as ezetimibe-glucuronide[6]. Niemann-Pick C1 like1 (NPC1L1), highly expressed in the jejunum of different species and only in human liver, is the main transporter of intestinal cholesterol. Mice deficient in NPC1L1 showed a significant > 70% reduction in cholesterol absorption, and a further reduction in cholesterol level with ezetimibe administration was not achievable. It was concluded that eztimibe reduces intestinal absorption by inhibiting the action of NPC1L1. Ezetimibe significantly reduces low-density lipoprotein (LDL) cholesterol and is used as monotherapy or in combination with statins to treat hyperlipidaemia[7].

Wang *et al*[5] showed that ezetimibe treatment for 8 to 12 wk in male gallstone-susceptible C57L mice and in 7 patients (treated with 20 mg ezetimibe for 30 d) resulted in a decrease in intestinal cholesterol absorption and biliary cholesterol secretion. Ezetimibe also protected gallbladder motility function by desaturating bile. Furthermore, ezetimibe treatment promoted the dissolution of gallstones by forming an abundance of unsaturated micelles and reduced biliary cholesterol saturation. However, Tamel *et al*[8] found that mice transgenic for *NPC1L1* gene, displayed an increase in biliary cholesterol concentration, suggesting that ezetimibe treatment may reduce biliary cholesterol secretion and increase the cholesterol saturation index. This is not in agreement with previous studies which showed the potential benefit of ezetimibe in treating gallstones, and may lead to speculation that it is actually intestinal cholesterol absorption which is largely responsible for the formation of cholesterol gallstones.

Furthermore, administration of ezetimibe in Golden Syrian hamsters fed a diet high in cholesterol and sunflower oil resulted in a significant reduction in absolute and relative cholesterol levels in bile[9]. Ezetimibe treatment in C5BL female mice, prevented biliary crystals and normalized gallbladder wall fat and function[10]. Importantly, gallstone-susceptible C57BL/6 inbred mice were fed control and lithogenic diets with or without simultaneous ezetimibe administration. Lithogenic diets increased biliary cholesterol content and secretion, and induced sludge or gallstone formation in 100% of the animals. Ezetimibe administration reduced intestinal cholesterol absorption by 90% in control animals and by 35% in mice receiving the lithogenic diets. Ezetimibe prevented the appearance of cholesterol crystals and gallstones. In addition, mice fed the lithogenic diets plus ezetimibe exhibited a 60% reduction in the biliary cholesterol saturation index. Of note, ezetimibe treatment caused a significant increase in bile flow (+50%, $P < 0.01$) as well as bile salt, phospholipid and glutathione secretion rates (+60%, +44% and +100%, respectively, $P < 0.01$), which was associated with a moderately increased expression of hepatic bile salt transporters[11]. From the above discussion it is possible to suggest that ezetimibe acts by decreasing intestinal cholesterol absorption and biliary cholesterol secretion, preserving gallbladder motility function by de-saturating bile in mice, promoting the dissolution of gallstones by forming an abundance of unsaturated micelles and significantly reducing biliary cholesterol saturation and retarding cholesterol crystallization in the bile of patients with gallstones.

Another important precipitating factor for gallstones and a therapeutic target for ezetimibe is insulin resistance. Interestingly, Chang *et al*[12] showed in 19 503 Korean men, that the prevalence of obesity, abdominal obesity, and metabolic syndromes in the subjects with gallstones were higher than in those without gallstones. The prevalence of elevated homeostatic model assessment (HOMA) (> 75 percentile) in subjects with gallstones was significantly higher than in those without gallstones, and this association remained even after the obesity stratification was applied. In multiple logistic regression analyses, only age and HOMA proved to be independent predictors of gallstones. Insulin resistance was positively associated with gallstones in non-diabetic Korean men, and this occurred regardless of obesity. Importantly, gallstones appear to be a marker for insulin resistance, even in non-diabetic, non-obese men. Furthermore, hepatic insulin resistance directly promotes the formation of cholesterol gallstones in mice[13]. Nakeeb *et al*[14] showed that in lean, non-diabetic volunteers without gallstones, gallbladder dysmotility is associated with an elevated fasting glucose as well as a high index of insulin resistance, and their conclusion was that insulin resistance alone may be responsible for gallbladder dysmotility which may result in acalculous cholecystitis or gallstone formation. Insulin resistance is also associated with non-alcoholic fatty liver disease (NAFLD)[15]. Loria *et al*[16] showed a higher prevalence of gallstones in association with NAFLD compared with a normal population. In liver biopsy screening for NAFLD, it was documented that 55% of subjects have gallstones[17]. Recent studies showed the potential benefit of ezetimibe as treat-

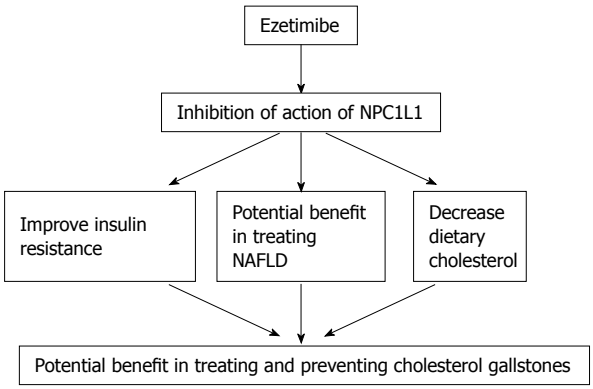

Figure 1 Mechanism of action of ezetimibe and ezetimibe may not only be of potential benefit in the treatment of cholesterol gallstones but also insulin resistance and NAFLD.

ment for NAFLD and associated hyperlipidaemia and insulin resistance. Interestingly, Zheng *et al*[18] showed that ezetimibe treatment for 4 wk reduced alanine transaminase (ALT), hepatic triglyceride, hepatomegaly, cholesterol ester and free cholesterol in diet-induced obese mice fed a high fat/cholesterol diet for 7 mo with proof of NAFLD. Importantly, administration of ezetimibe in obese Zucker rats (a model of NAFLD and metabolic syndrome) resulted in a significant improvement in both cholesterol and triglyceride levels, hepatic steatosis and improved insulin resistance[19]. This is in accordance with a recent study by Nomura *et al*[20] who showed that ezetimibe improved hepatic insulin sensitivity.

CONCLUSION

In summary, Ezetimibe is a unique medication with potential for treating not only gallbladder stones but also insulin resistance and NAFLD (Figure 1). Taking all these factors into consideration, it is possible to suggest that a clinical trial designed to investigate the potential of ezetimibe for reducing biliary cholesterol saturation and insulin resistance in populations with a predisposition to cholelithiasis is now warranted.

REFERENCES

1 **Shaffer EA**. Epidemiology and risk factors for gallstone disease: has the paradigm changed in the 21st century? *Curr Gastroenterol Rep* 2005; **7**: 132-140
2 **Shaffer EA**. Gallstone disease: Epidemiology of gallbladder stone disease. *Best Pract Res Clin Gastroenterol* 2006; **20**: 981-996
3 **Tazuma S**. Gallstone disease: Epidemiology, pathogenesis, and classification of biliary stones (common bile duct and intrahepatic). *Best Pract Res Clin Gastroenterol* 2006; **20**: 1075-1083
4 **Williams CI**, Shaffer EA. Gallstone disease: current therapeutic practice. *Curr Treat Options Gastroenterol* 2008; **11**: 71-77
5 **Wang HH**, Portincasa P, Mendez-Sanchez N, Uribe M, Wang DQ. Effect of ezetimibe on the prevention and dissolution of cholesterol gallstones. *Gastroenterology* 2008; **134**: 2101-2110
6 **Kosoglou T**, Statkevich P, Johnson-Levonas AO, Paolini JF, Bergman AJ, Alton KB. Ezetimibe: a review of its metabolism, pharmacokinetics and drug interactions. *Clin Pharmacokinet* 2005; **44**: 467-494
7 **Davis HR Jr**, Altmann SW. Niemann-Pick C1 Like 1 (NPC1L1) an intestinal sterol transporter. *Biochim Biophys Acta* 2009; **1791**: 679-683
8 **Temel RE**, Tang W, Ma Y, Rudel LL, Willingham MC, Ioannou YA, Davies JP, Nilsson LM, Yu L. Hepatic Niemann-Pick C1-like 1 regulates biliary cholesterol concentration and is a target of ezetimibe. *J Clin Invest* 2007; **117**: 1968-1978
9 **Valasek MA**, Repa JJ, Quan G, Dietschy JM, Turley SD. Inhibiting intestinal NPC1L1 activity prevents diet-induced increase in biliary cholesterol in Golden Syrian hamsters. *Am J Physiol Gastrointest Liver Physiol* 2008; **295**: G813-G822
10 **Mathur A**, Walker JJ, Al-Azzawi HH, Lu D, Swartz-Basile DA, Nakeeb A, Pitt HA. Ezetimibe ameliorates cholecystosteatosis. *Surgery* 2007; **142**: 228-233
11 **Zúñiga S**, Molina H, Azocar L, Amigo L, Nervi F, Pimentel F, Jarufe N, Arrese M, Lammert F, Miquel JF. Ezetimibe prevents cholesterol gallstone formation in mice. *Liver Int* 2008; **28**: 935-947
12 **Chang Y**, Sung E, Ryu S, Park YW, Jang YM, Park M. Insulin resistance is associated with gallstones even in non-obese, non-diabetic Korean men. *J Korean Med Sci* 2008; **23**: 644-650
13 **Biddinger SB**, Haas JT, Yu BB, Bezy O, Jing E, Zhang W, Unterman TG, Carey MC, Kahn CR. Hepatic insulin resistance directly promotes formation of cholesterol gallstones. *Nat Med* 2008; **14**: 778-782
14 **Nakeeb A**, Comuzzie AG, Al-Azzawi H, Sonnenberg GE, Kissebah AH, Pitt HA. Insulin resistance causes human gallbladder dysmotility. *J Gastrointest Surg* 2006; **10**: 940-948; discussion 948-949
15 **Ahmed MH**, Byrne CD. Modulation of sterol regulatory element binding proteins (SREBPs) as potential treatments for non-alcoholic fatty liver disease (NAFLD). *Drug Discov Today* 2007; **12**: 740-747
16 **Loria P**, Lonardo A, Lombardini S, Carulli L, Verrone A, Ganazzi D, Rudilosso A, D'Amico R, Bertolotti M, Carulli N. Gallstone disease in non-alcoholic fatty liver: prevalence and associated factors. *J Gastroenterol Hepatol* 2005; **20**: 1176-1184
17 **Ramos-De la Medina A**, Remes-Troche JM, Roesch-Dietlen FB, Pérez-Morales AG, Martinez S, Cid-Juarez S. Routine liver biopsy to screen for nonalcoholic fatty liver disease (NAFLD) during cholecystectomy for gallstone disease: is it justified? *J Gastrointest Surg* 2008; **12**: 2097-2102; discussion 2102
18 **Zheng S**, Hoos L, Cook J, Tetzloff G, Davis H Jr, van Heek M, Hwa JJ. Ezetimibe improves high fat and cholesterol diet-induced non-alcoholic fatty liver disease in mice. *Eur J Pharmacol* 2008; **584**: 118-124
19 **Deushi M**, Nomura M, Kawakami A, Haraguchi M, Ito M, Okazaki M, Ishii H, Yoshida M. Ezetimibe improves liver steatosis and insulin resistance in obese rat model of metabolic syndrome. *FEBS Lett* 2007; **581**: 5664-5670
20 **Nomura M**, Ishii H, Kawakami A, Yoshida M. Inhibition of Hepatic Neiman-Pick C1-Like 1 Improves Hepatic Insulin Resistance. *Am J Physiol Endocrinol Metab* 2009; Epub ahead of print

S- Editor Wang YR **L- Editor** Webster JR **E- Editor** Ma WH

World Journal of Gastroenterology

Online Submissions: http://www.wjgnet.com/1007-9327office
wjg@wjgnet.com
doi:10.3748/wjg.v16.i13.1558

World J Gastroenterol 2010 April 7; 16(13): 1558-1559
ISSN 1007-9327 (print)

EDITORIAL

Liver magnetic resonance imaging: State of the art

Paul E Sijens

Paul E Sijens, Department of Radiology, University Medical Center Groningen and University of Groningen, Hanzeplein 1, 9713 GZ Groningen, The Netherlands
Author contributions: Sijens PE, series editor of the Topic Highlight "MRI of the liver, state of the art" wrote this introduction.
Correspondence to: Dr. Paul E Sijens, PhD, Associate Professor, Department of Radiology, University Medical Center Groningen and University of Groningen, Hanzeplein 1, 9713 GZ Groningen, The Netherlands. p.e.sijens@rad.umcg.nl
Telephone: +31-50-3613534 Fax: +31-50-3611798
Received: March 19, 2010 Revised: March 22, 2010
Accepted: March 29, 2010
Published online: April 7, 2010

Abstract

Magnetic resonance imaging (MRI) has now been used for about three decades to characterize the human liver in a non-invasive way, that is without the need of using ionizing radiation or removing tissue samples. During the past few years, technical progress has been considerable and novel applications of MRI have been implemented in the clinic. The beginning of a new decade offers an excellent opportunity for having five experts to present their view on the current status of MRI (and magnetic resonance spectroscopy) in the study of perfusion, fat and iron contents, diffusion and the metabolism of diffuse liver diseases. This topic highlight series thus provides an update of current knowledge in the field of liver MRI.

Key words: Liver; Magnetic resonance imaging

Sijens PE. Liver magnetic resonance imaging: State of the art. *World J Gastroenterol* 2010; 16(13): 1558-1559 Available from: URL: http://www.wjgnet.com/1007-9327/full/v16/i13/1558.htm DOI: http://dx.doi.org/10.3748/wjg.v16.i13.1558

In this Topic Highlight "Liver MRI, state of the art", we focus on five magnetic resonance imaging (MRI) methods offering opportunities for parametric exploration of the liver[1]. The first contribution focuses on the microcirculatory status in liver parenchyma and liver lesions as studied by perfusion MRI, i.e. MRI with the use of (contrast) agents to improve the contrast between the features on images[2]. Great progress has been made in turning perfusion weighted imaging into a quantitative method for detecting tumor, evaluating tumor viability after therapy and, for instance, the diagnosis of liver cirrhosis and its severity. Another important development is that nowadays, the sampling of liver tissue for the assessment of hepatic steatosis, related to alcoholic and non-alcoholic liver disease, metabolic syndrome, obesity and insuline resistance, can be replaced by the use of MRI or magnetic resonance spectroscopy (MRS) for determining liver fat content[3]. The next review is a thorough assessment of the present status in another novel application of MRI presenting an alternative to biopsy: liver iron content determination[4]. Accurate evaluation of iron overload is necessary to establish the diagnosis of hemochromatosis and guide chelation treatment in transfusion-dependent anemia. Diffusion weighted imaging (DWI), best used in combination with conventional unenhanced MRI and perfusion weighted MRI, is a promising tool used in predicting tumor responsiveness and following up oncological treatment since DWI might be capable of detecting recurrent disease earlier than conventional imaging[5]. The final contribution features the use of MRS to study metabolism in diffuse liver diseases, diabetes and cancer[6]. Although this method still is in the preclinical stage, it is anticipated that future developments such as clinical magnets with a higher field strength (3 T, 7 T) and improved delineation of multi-component signals, will lead to intensified research in metabolic syndrome, cardiovascular disease, hepato-biliary diseases, *etc.* We believe that this issue will be of interest not only to gastroenterologists, but also to those involved in metabolic studies, cell physiology and pathology.

REFERENCES

1 **Sijens PE**. Parametric exploration of the liver by magnetic

resonance methods. *Eur Radiol* 2009; **19**: 2594-2607
2 **Thng CH**, Koh TS, Collins DJ, Koh DM. Perfusion magnetic resonance imaging of the liver. *World J Gastroenterol* 2010; **16**: 1598-1609
3 **Springer F**, Machann J, Claussen CD, Schick F, Schwenzer NF. Liver fat content determined by magnetic resonance imaging and spectroscopy. *World J Gastroenterol* 2010; **16**: 1560-1566
4 **Tziomalos K**, Perifanis V. Liver iron content determination by magnetic resonance imaging. *World J Gastroenterol* 2010; **16**: 1587-1597
5 **Kele PG**, van der Jagt EJ. Diffusion weighted imaging in the liver. *World J Gastroenterol* 2010; **16**: 1567-1576
6 **Dagnelie PC**, Leij-Halfwerk S. Magnetic resonance spectroscopy to study hepatic metabolism in diffuse liver diseases, diabetes and cancer. *World J Gastroenterol* 2010; **16**: 1577-1586

S- Editor Tian L **L- Editor** Wang XL **E- Editor** Ma WH

World Journal of Gastroenterology

Online Submissions: http://www.wjgnet.com/1007-9327office
wjg@wjgnet.com
doi:10.3748/wjg.v16.i13.1560

World J Gastroenterol 2010 April 7; 16(13): 1560-1566
ISSN 1007-9327 (print)

TOPIC HIGHLIGHT

Paul E Sijens, PhD, Associate Professor, *Series Editor*

Liver fat content determined by magnetic resonance imaging and spectroscopy

Fabian Springer, Jürgen Machann, Claus D Claussen, Fritz Schick, Nina F Schwenzer

Fabian Springer, Jürgen Machann, Fritz Schick, Nina F Schwenzer, Section on Experimental Radiology, Department of Diagnostic and Interventional Radiology, University Hospital Tübingen, 72076 Tübingen, Germany
Claus D Claussen, Department of Diagnostic and Interventional Radiology, University Hospital Tübingen, 72076 Tübingen, Germany
Author contributions: Springer F, Schwenzer NF and Machann J contributed equally to this work; Springer F, Machann J, Schwenzer NF and Schick F performed the literature research and wrote the manuscript; Springer F, Machann J, Schwenzer NF, Claussen CD and Schick F thoroughly edited the manuscript during the review process.
Correspondence to: Dr. Fabian Springer, MD, Section on Experimental Radiology, Department of Diagnostic and Interventional Radiology, University Hospital Tübingen, Hoppe-Seyler-Str. 3, 72076 Tübingen,
Germany. fabian.springer@med.uni-tuebingen.de
Telephone: +49-7071-2987751 Fax: +49-7071-295392
Received: February 3, 2010 Revised: February 25, 2010
Accepted: March 4, 2010
Published online: April 7, 2010

Abstract

Hepatic steatosis as the most prevalent liver disorder can either be related to alcoholic liver disease (ALD) or non-alcoholic fatty liver disease (NAFLD). In both conditions, hepatocytes excessively accumulate fat-containing vacuoles within their cytoplasm, which is the key histological feature. In contrast to ALD, NAFLD is commonly associated with metabolic syndrome, obesity and insulin resistance. To determine increased liver fat content, liver biopsy is currently considered the gold standard. Besides the invasive technique, various other non-invasive techniques have been developed, such as ultrasound, computed tomography (CT), magnetic resonance spectroscopy (MRS) and magnetic resonance imaging (MRI) based methods. Among these techniques, ultrasound and CT provide only qualitative information about hepatic steatosis, whereas MRS- or MRI-based methods are able to determine even small amounts of fat accurately. These non-invasive magnetic resonance techniques have already proven their great potential, especially in longitudinal and cross-sectional studies regarding various metabolic conditions and medical treatment regimens. In this review, the most common, non-invasive MRS/MRI techniques for assessment of intrahepatic lipid content are described with their inherent advantages and limitations.

Key words: Hepatic steatosis; Magnetic resonance imaging; Proton magnetic resonance spectroscopy; Lipids

Peer reviewer: Paul E Sijens, PhD, Associate Professor, Radiology, UMCG, Hanzeplein 1, 9713GZ Groningen, The Netherlands

Springer F, Machann J, Claussen CD, Schick F, Schwenzer NF. Liver fat content determined by magnetic resonance imaging and spectroscopy. *World J Gastroenterol* 2010; 16(13): 1560-1566 Available from: URL: http://www.wjgnet.com/1007-9327/full/v16/i13/1560.htm DOI: http://dx.doi.org/10.3748/wjg.v16.i13.1560

INTRODUCTION

Hepatic steatosis is a common finding during liver examination and is found in a broad spectrum of diseases. It is related to an increased deposition of triglycerides within the cytoplasm of hepatocytes. Besides alcoholic liver disease (ALD), intrahepatic accumulation of lipids can also be associated with obesity, insulin resistance and metabolic syndrome, and is then termed non-alcoholic fatty liver disease (NAFLD). NAFLD is constantly gaining prevalence throughout the western world and is related to obesity as an increasing problem in recent decades[1,2]. Nevertheless, NAFLD can also be found in non-obese subjects with a body mass index within the normal range. Those patients

often suffer from insulin resistance. Thus, intrahepatic fat fraction denotes an interesting metabolic parameter for longitudinal or cross-sectional studies regarding various metabolic conditions. Moreover, it is considered an independent risk factor for insulin resistance and atherosclerosis[3-7]. The current gold standard for quantification of intrahepatic lipid content is based on invasive liver biopsies and subsequent histological analysis. However, due to its invasive character, it is not useful for longitudinal studies or metabolic studies on otherwise healthy subjects.

Magnetic resonance spectroscopy (MRS) and magnetic resonance imaging (MRI) provide non-invasive means to accurately quantify intrahepatic lipid content[8-10]. In contrast to other modalities such as ultrasound and computed tomography (CT), MRI/MRS are capable of detecting even small amounts of intrahepatic lipid accumulation[10]. Therefore, MRI/MRS are especially useful to measure changes in hepatic steatosis during various treatment regimens. During recent years, clinical and research investigations have been performed on this subject.

This review gives an overview of various magnetic-resonance-based methods that are capable of quantifying intrahepatic lipid content non-invasively. Different strategies of ^{1}H-MRS, as well as phase-sensitive and frequency-selective MRI methods are described.

^{1}H-MRS

In 1993, Longo *et al*[11,12] first published their results of ^{1}H-MRS of liver parenchyma and correlated the data with CT studies and biopsies. In these studies, they found an excellent agreement between the different investigated methods. Since then, several studies have been performed that have further verified these results by means of whole-body MR scanning[13-15].

However, various strategies have been developed to obtain volume-selective ^{1}H-MR spectra from liver parenchyma *in vivo*. Spectra are usually recorded from volumes ranging from 1 to 27 cm^3, which are small enough to be positioned well in the liver parenchyma. To record reliable spectra from pure liver parenchyma, voxels have to be carefully placed in order to avoid artificial signal contributions from surrounding adipose tissue or intrahepatic blood vessels.

Two main strategies are used for single-voxel spectroscopy (SVS): point resolved spectroscopy (PRESS) or stimulated-echo acquisition mode (STEAM)[16,17]. The PRESS acquisition scheme (multi-echo single-shot technique) uses a 90°-180°-180° pulse sequence with long echo time (TE) and allows for better visualization of metabolites with long T1 relaxation times. In contrast, the STEAM sequence applies a 90°-90°-90° pulse sequence and is less sensitive to J-coupling effects. The STEAM sequence provides shorter TE and lower signal yield compared to PRESS, which is usually not a limitation for fat quantification in the liver. However, both techniques can be applied for intrahepatic fat quantification in clinical examinations.

Since both techniques only provide spectra of a small sub-region of the liver parenchyma, so-called spectroscopic imaging techniques with 2D or even 3D matrices of spectra have been developed to obtain detailed information on lipid distribution[18,19]. Compared to SVS, these techniques are rarely used clinically for routine investigation of liver parenchyma, due to their rather long acquisition and post-processing times[20,21]. In most cases of NAFLD, hepatic lipid distribution has been shown to be relatively homogeneous, which allows one to quantify intrahepatic fat fraction by only one single representative voxel[22-24]. However, it should be noted that significant differences in sub-regions of both liver lobes have also been reported[13].

The above-mentioned ^{1}H-MRS techniques have been applied in studies investigating NAFLD in the general adult population[25]. Moreover, an increasing number of longitudinal clinical studies have been performed evaluating intrahepatic fat fraction in the obese population or patients at risk for developing type 2 diabetes[26-31]. Intrahepatic fat fraction has also been evaluated in morbidly obese patients undergoing bariatric surgery[32-35]. Moreover, additional cross-sectional studies have revealed different intrahepatic fat fractions depending on genetic background or hormonal status of the examined subjects[36-42].

All of these MRS fat quantification techniques have been shown to be safe and non-invasive alternatives to the current invasive gold standard (liver biopsy). They have been tested regarding their accuracy and have shown high intra-individual reproducibility in repeated measurements[13,23,25]. However, one has to consider that MR spectroscopic fat quantification relies on determination of overall volume fraction of lipids in the liver parenchyma. In contrast, in histological examinations, the percentage of hepatocytes that show distinct fat droplets is used for quantification. Thus, the reported percentage values that characterize steatosis from MR examinations might differ from those in histological analysis. On the other hand, data from MRI and histology correlate with each other and both techniques allow, nevertheless, for reliable quantification of intrahepatic lipid content.

It should be also mentioned that spectroscopic examinations are especially recommended for assessment of small lipid fractions in the liver, because sensitivity to low signal intensities from fat is higher than for imaging-based strategies. Furthermore, water and fat signals can be well distinguished.

FAT-SENSITIVE IMAGING METHODS

^{1}H-MRS capabilities are still not available on all standard clinical scanners and require dedicated prerequisites including spectroscopic sequences and post-processing software. Therefore, ^{1}H-MRS still remains a research tool for clinical studies and is usually not used in daily routine liver examinations. There are, nevertheless, MRI sequences that allow for reliable and accurate quantification of intrahepatic lipid content.

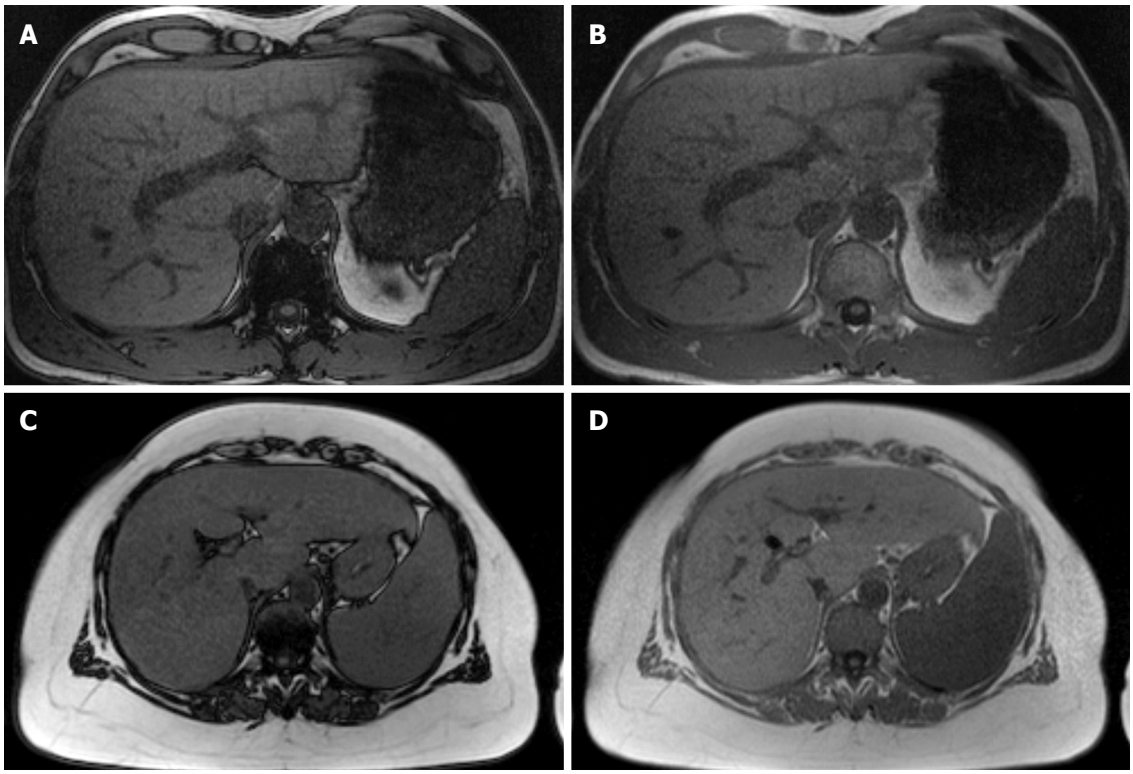

Figure 1 T1-weighted gradient echo images recorded with OP (parts A and C) and IP (B and D) conditions. A and B show a lean subject with almost equal signal intensity of the liver under OP (A) and IP (B) conditions, since no intrahepatic lipid storage is present. In contrast, C and D show an obese subject with lower signal intensity under OP conditions compared to IP conditions, which indicated relevant intrahepatic lipid storage.

Techniques based on differences in signal phase of water and fat

So-called in-phase/opposed-phase (IP/OP) techniques are available on most MR units and can be performed easily in routine examinations. Using this technique, T1-weighted images can be acquired extremely fast, with the use of multi-segment phased array coils and parallel imaging techniques. Moreover, T1-weighted gradient echo sequences can cover most of the liver parenchyma within a single breath-hold[43-46]. The IP/OP technique is based upon the fact that, during TE, transverse magnetization vectors of fat and water develop a phase difference that results in decreased overall length of the magnetization vector under OP conditions. At a main magnetic field strength of 1.5 T, the frequency shift between fat and water is approximately 220 Hz, which results in OP conditions at a TE of about 2.4 ms and in-phase conditions at a TE of about 4.8 ms[47-49]. The hepatic fat fraction can then be quantified by calculating the loss of signal intensity in OP images compared to IP images[50-52], as shown in Figure 1. From congruent sets of IP and OP images, acquired within the same breath-hold, the fat fraction can be calculated pixel-wise and misregistration errors can be avoided. Thus, maps of intrahepatic fat fraction can be obtained to estimate liver fat content and show differences in regional fat distribution.

However, not only the phase difference between water and fat protons contribute to the observed signal loss in OP images, but also additional transverse and longitudinal relaxation effects may play a major role. Recent studies have shown that especially transverse relaxation time can vary largely between different individuals, as well as intra-individually in the time-course of longitudinal studies[46,53,54]. These changes in transverse relaxation time are mainly due to increased iron deposition in the liver parenchyma; either artificially acquired or, for example, hemochromatosis-associated[55]. It has been shown that transverse relaxivity correlates well with serum ferritin levels[53,56]. Thus, transverse relaxation time of liver parenchyma has to be measured additionally using a multi-echo gradient echo sequence. The data necessary for estimation of T2* can than be obtained within a single additional breath-hold. Integration of individual T2* values in the calculation of the fat fraction requires a somewhat more sophisticated approach[57].

In contrast, longitudinal relaxation times are relatively stable throughout the population and individual calculation requires additional time-consuming sequences. Therefore, it seems legitimate for the general population to account for longitudinal relaxivity using constant values for longitudinal relaxation time of liver parenchyma.

Compared to the above-described gradient-echo-based IP/OP technique, Dixon *et al*[47] described in 1984 the use of a spin-echo technique with a small timing-offset of the 180° refocusing pulse, which is used to create a so-called OP image. The IP image is then acquired using a conventional spin-echo sequence. From these two images, fat- and water-selective images can be subsequently obtained. However, sensitivity to magnetic field inhomogeneity cannot be neglected and has prevented the wides-

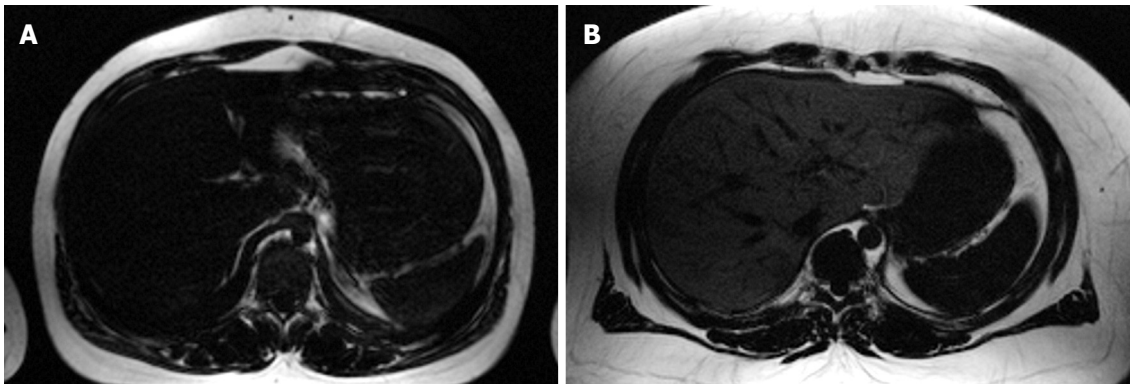

Figure 2 A and B show fat-selective spectral-spatial imaging of the body trunk. A lean subject with almost no intrahepatic lipid storage (A) and an obese subject with markedly increased lipid storage in the liver parenchyma is shown (B).

pread routine clinical usage of the Dixon technique. Since its introduction more than 20 years ago, several modifications have been reported that have aimed at overcoming its inherent limitations[45,48,58,59]. Three-point Dixon methods have been developed that additionally acquire a third image with a phase shift of -180° or 360°. Then, using three different images and sophisticated phase-correction algorithms, true fat- and water-selective images are derived from the recorded data. This technique allows one to distinguish which constituent (water or fat) is predominant in each voxel[60-66]. Acquiring all three images in a single breath-hold is often not possible, whereas recording in multiple breath-holds poses the problem of misregistration artefacts due to variable positions of the liver parenchyma.

Another approach was first described by Reeder *et al*[67-69] and is termed the IDEAL technique (iterative decomposition of water and fat with echo asymmetry and least squares estimation). Using optimized echo shifts and gradient echo imaging, it provides robust quantification of the intrahepatic fat fraction. This technique allows for fat quantification even in the presence of moderate inhomogeneities of the static magnetic field, which are often encountered in examinations of extremely obese patients on wide-bore MRI scanners. However, it is not free of limitations. Liu *et al*[70] have reported techniques for reduction of noise bias and longitudinal relaxation effects that affect quantification of the hepatic fat fraction in the IDEAL technique. These drawbacks can be partially overcome by small- or dual-flip angle approaches, magnitude discrimination and phase-constrained methods. Besides its capabilities in measuring parenchymal fat content, the IDEAL method has also been used for fat suppression in clinical studies of various body regions[71-75].

Techniques based on frequency selective excitation

Previous studies have described a so-called spectral-spatial excitation technique to quantify fat content accurately in parenchymal organs and muscles[57,76]. A combination of chemical shift selectivity and slice-selective excitation in gradient echo or spin echo imaging sequences provides a high sensitivity to detect even small amounts of fat[23,49,77,78]. Furthermore, spatial information about parenchymal lipid distribution is also obtained. Slice-selectivity is implemented using six equidistant radio frequency pulses (time increment between pulses, 2.38 ms at 1.5 T) with nearly binomial amplitude ratios. These radio frequency pulses excite the methylene and methyl signal of fatty acids (0.8-2.0 ppm) selectively, as shown in Figure 2. Thus, signal contributions from water protons are below the noise level. To achieve this optimal spectral-spatial excitation, relatively homogeneous static magnetic fields are required, which makes adequate shimming procedures necessary. However, especially in wide-bore MR scanners that are designed to examine extremely obese patients, the inhomogeneity of the static magnetic field is often problematic. Even time-consuming shimming procedures might fail. For quantitative assessment of intrahepatic fat, adjacent subcutaneous or visceral fat is used as an internal reference because it contains almost 100% fat. The spectral-spatial excitation method is capable of detecting even small amounts of lipids (starting at 1%-2% volume fraction of fat in the liver), with additional spatial information about its distribution[23]. However, some advantages and disadvantages of this technique should be noted. As a result of highly selective visualization of fat, the technique offers relatively low soft tissue contrast compared to conventional gradient echo sequences (Figure 3). Moreover, only a small number of representative slices can be acquired during a single breath-hold. Since only a reference region-of-interest in subcutaneous adipose tissue adjacent to liver parenchyma is needed for quantification of fat fraction, the calculation of intrahepatic lipid content can easily be done. Furthermore, there is no need for additional time-consuming sequences that are necessary to correct for transverse and longitudinal relaxation effects.

CONCLUSION

Several non-invasive methods have been developed for quantification of intrahepatic fat content using whole-body MRI scanners. Being aware of the inherent advantages and disadvantages of each technique, one has to choose carefully the appropriate method for specific examination

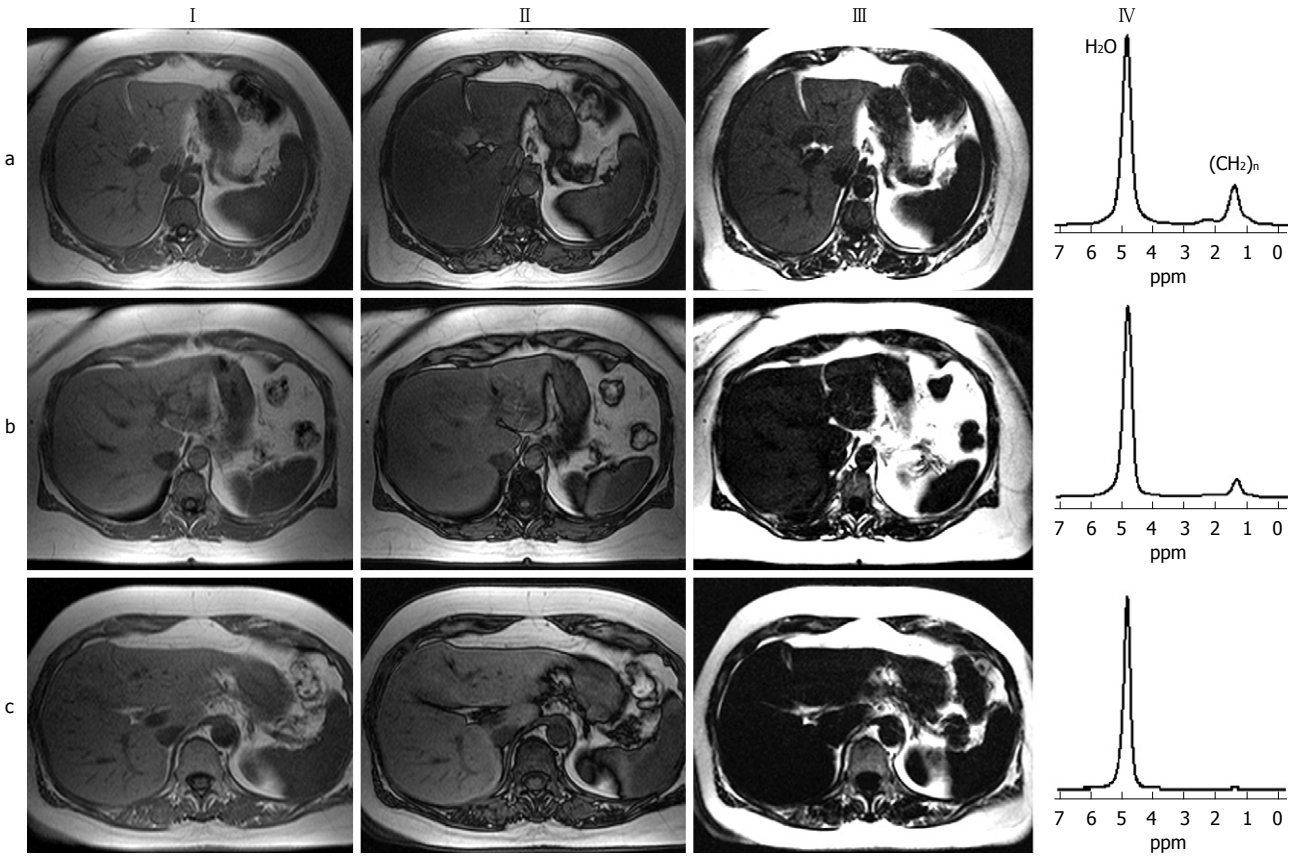

Figure 3 Three subjects with different intrahepatic lipid contents are compared. The subject in row (a) shows intrahepatic lipid content of about 20%; the subject in row (b) shows intrahepatic lipid content of about 10%; and the subject in row (c) shows intrahepatic lipid content in the normal range (about 1%). The figure shows IP (column Ⅰ) and OP (column Ⅱ) images of a T1-weighted gradient echo sequence. Column Ⅲ shows the results of a fat-selective spectral-spatial imaging sequence, and column Ⅳ shows the results from single-volume ^{1}H-MRS using a STEAM sequence.

circumstances, as well as for hard- and software capabilities. Correctly applied, each technique (MRS/MRI) provides accurate data on intrahepatic fat fraction, correlating well with findings in liver biopsies, which is often considered as the current gold standard. The methods described above provide non-invasive quantification of the intrahepatic fat fraction, and give a reliable basis for longitudinal clinical and research studies. Thus, the influence of various medical treatments and diseases on intrahepatic lipid storage can be easily investigated in a non-invasive way.

REFERENCES

1 **Angulo P**. Obesity and nonalcoholic fatty liver disease. *Nutr Rev* 2007; **65**: S57-S63
2 **Schwimmer JB**, Deutsch R, Kahen T, Lavine JE, Stanley C, Behling C. Prevalence of fatty liver in children and adolescents. *Pediatrics* 2006; **118**: 1388-1393
3 **Stefan N**, Kantartzis K, Häring HU. Causes and metabolic consequences of Fatty liver. *Endocr Rev* 2008; **29**: 939-960
4 **Targher G**. Non-alcoholic fatty liver disease, the metabolic syndrome and the risk of cardiovascular disease: the plot thickens. *Diabet Med* 2007; **24**: 1-6
5 **Stefan N**, Kantartzis K, Machann J, Schick F, Thamer C, Rittig K, Balletshofer B, Machicao F, Fritsche A, Häring HU. Identification and characterization of metabolically benign obesity in humans. *Arch Intern Med* 2008; **168**: 1609-1616
6 **Kotronen A**, Westerbacka J, Bergholm R, Pietiläinen KH, Yki-Järvinen H. Liver fat in the metabolic syndrome. *J Clin Endocrinol Metab* 2007; **92**: 3490-3497
7 **Roden M**. Mechanisms of Disease: hepatic steatosis in type 2 diabetes--pathogenesis and clinical relevance. *Nat Clin Pract Endocrinol Metab* 2006; **2**: 335-348
8 **Sijens PE**. Parametric exploration of the liver by magnetic resonance methods. *Eur Radiol* 2009; **19**: 2594-2607
9 **Mehta SR**, Thomas EL, Bell JD, Johnston DG, Taylor-Robinson SD. Non-invasive means of measuring hepatic fat content. *World J Gastroenterol* 2008; **14**: 3476-3483
10 **Schwenzer NF**, Springer F, Schraml C, Stefan N, Machann J, Schick F. Non-invasive assessment and quantification of liver steatosis by ultrasound, computed tomography and magnetic resonance. *J Hepatol* 2009; **51**: 433-445
11 **Longo R**, Ricci C, Masutti F, Vidimari R, Crocé LS, Bercich L, Tiribelli C, Dalla Palma L. Fatty infiltration of the liver. Quantification by 1H localized magnetic resonance spectroscopy and comparison with computed tomography. *Invest Radiol* 1993; **28**: 297-302
12 **Longo R**, Pollesello P, Ricci C, Masutti F, Kvam BJ, Bercich L, Crocè LS, Grigolato P, Paoletti S, de Bernard B. Proton MR spectroscopy in quantitative in vivo determination of fat content in human liver steatosis. *J Magn Reson Imaging* 1995; **5**: 281-285
13 **Cowin GJ**, Jonsson JR, Bauer JD, Ash S, Ali A, Osland EJ, Purdie DM, Clouston AD, Powell EE, Galloway GJ. Magnetic resonance imaging and spectroscopy for monitoring liver steatosis. *J Magn Reson Imaging* 2008; **28**: 937-945
14 **Szczepaniak LS**, Babcock EE, Schick F, Dobbins RL, Garg A, Burns DK, McGarry JD, Stein DT. Measurement of intracellular triglyceride stores by H spectroscopy: validation in vivo. *Am J Physiol* 1999; **276**: E977-E989

15 **Thomsen C**, Becker U, Winkler K, Christoffersen P, Jensen M, Henriksen O. Quantification of liver fat using magnetic resonance spectroscopy. *Magn Reson Imaging* 1994; **12**: 487-495
16 **Bottomley PA**. Spatial localization in NMR spectroscopy in vivo. *Ann N Y Acad Sci* 1987; **508**: 333-348
17 **Frahm J**, Bruhn H, Gyngell ML, Merboldt KD, Hänicke W, Sauter R. Localized high-resolution proton NMR spectroscopy using stimulated echoes: initial applications to human brain in vivo. *Magn Reson Med* 1989; **9**: 79-93
18 **Pykett IL**, Rosen BR. Nuclear magnetic resonance: in vivo proton chemical shift imaging. Work in progress. *Radiology* 1983; **149**: 197-201
19 **Skoch A**, Jiru F, Bunke J. Spectroscopic imaging: basic principles. *Eur J Radiol* 2008; **67**: 230-239
20 **Sijens PE**, Smit GP, Borgdorff MA, Kappert P, Oudkerk M. Multiple voxel 1H MR spectroscopy of phosphorylase-b kinase deficient patients (GSD IXa) showing an accumulation of fat in the liver that resolves with aging. *J Hepatol* 2006; **45**: 851-855
21 **Irwan R**, Edens MA, Sijens PE. Assessment of the variations in fat content in normal liver using a fast MR imaging method in comparison with results obtained by spectroscopic imaging. *Eur Radiol* 2008; **18**: 806-813
22 **Machann J**, Stefan N, Schick F. (1)H MR spectroscopy of skeletal muscle, liver and bone marrow. *Eur J Radiol* 2008; **67**: 275-284
23 **Machann J**, Thamer C, Schnoedt B, Stefan N, Haring HU, Claussen CD, Fritsche A, Schick F. Hepatic lipid accumulation in healthy subjects: a comparative study using spectral fat-selective MRI and volume-localized 1H-MR spectroscopy. *Magn Reson Med* 2006; **55**: 913-917
24 **Thomas EL**, Hamilton G, Patel N, O'Dwyer R, Doré CJ, Goldin RD, Bell JD, Taylor-Robinson SD. Hepatic triglyceride content and its relation to body adiposity: a magnetic resonance imaging and proton magnetic resonance spectroscopy study. *Gut* 2005; **54**: 122-127
25 **Szczepaniak LS**, Nurenberg P, Leonard D, Browning JD, Reingold JS, Grundy S, Hobbs HH, Dobbins RL. Magnetic resonance spectroscopy to measure hepatic triglyceride content: prevalence of hepatic steatosis in the general population. *Am J Physiol Endocrinol Metab* 2005; **288**: E462-E468
26 **Belfort R**, Harrison SA, Brown K, Darland C, Finch J, Hardies J, Balas B, Gastaldelli A, Tio F, Pulcini J, Berria R, Ma JZ, Dwivedi S, Havranek R, Fincke C, DeFronzo R, Bannayan GA, Schenker S, Cusi K. A placebo-controlled trial of pioglitazone in subjects with nonalcoholic steatohepatitis. *N Engl J Med* 2006; **355**: 2297-2307
27 **Thamer C**, Machann J, Stefan N, Schäfer SA, Machicao F, Staiger H, Laakso M, Böttcher M, Claussen C, Schick F, Fritsche A, Haring HU. Variations in PPARD determine the change in body composition during lifestyle intervention: a whole-body magnetic resonance study. *J Clin Endocrinol Metab* 2008; **93**: 1497-1500
28 **Thomas EL**, Brynes AE, Hamilton G, Patel N, Spong A, Goldin RD, Frost G, Bell JD, Taylor-Robinson SD. Effect of nutritional counselling on hepatic, muscle and adipose tissue fat content and distribution in non-alcoholic fatty liver disease. *World J Gastroenterol* 2006; **12**: 5813-5819
29 **Thomas EL**, Potter E, Tosi I, Fitzpatrick J, Hamilton G, Amber V, Hughes R, North C, Holvoet P, Seed M, Betteridge DJ, Bell JD, Naoumova RP. Pioglitazone added to conventional lipid-lowering treatment in familial combined hyperlipidaemia improves parameters of metabolic control: relation to liver, muscle and regional body fat content. *Atherosclerosis* 2007; **195**: e181-e190
30 **Westerbacka J**, Lammi K, Häkkinen AM, Rissanen A, Salminen I, Aro A, Yki-Järvinen H. Dietary fat content modifies liver fat in overweight nondiabetic subjects. *J Clin Endocrinol Metab* 2005; **90**: 2804-2809
31 **Borra R**, Lautamäki R, Parkkola R, Komu M, Sijens PE, Hällsten K, Bergman J, Iozzo P, Nuutila P. Inverse association between liver fat content and hepatic glucose uptake in patients with type 2 diabetes mellitus. *Metabolism* 2008; **57**: 1445-1451
32 **Heath ML**, Kow L, Slavotinek JP, Valentine R, Toouli J, Thompson CH. Abdominal adiposity and liver fat content 3 and 12 months after gastric banding surgery. *Metabolism* 2009; **58**: 753-758
33 **Verna EC**, Berk PD. Role of fatty acids in the pathogenesis of obesity and fatty liver: impact of bariatric surgery. *Semin Liver Dis* 2008; **28**: 407-426
34 **Wolf AM**, Beisiegel U. The effect of loss of excess weight on the metabolic risk factors after bariatric surgery in morbidly and super-obese patients. *Obes Surg* 2007; **17**: 910-919
35 **Phillips ML**, Boase S, Wahlroos S, Dugar M, Kow L, Stahl J, Slavotinek JP, Valentine R, Toouli J, Thompson CH. Associates of change in liver fat content in the morbidly obese after laparoscopic gastric banding surgery. *Diabetes Obes Metab* 2008; **10**: 661-667
36 **Kantartzis K**, Peter A, Machicao F, Machann J, Wagner S, Königsrainer I, Königsrainer A, Schick F, Fritsche A, Häring HU, Stefan N. Dissociation between fatty liver and insulin resistance in humans carrying a variant of the patatin-like phospholipase 3 gene. *Diabetes* 2009; **58**: 2616-2623
37 **Kantartzis K**, Machicao F, Machann J, Schick F, Fritsche A, Häring HU, Stefan N. The DGAT2 gene is a candidate for the dissociation between fatty liver and insulin resistance in humans. *Clin Sci* (Lond) 2009; **116**: 531-537
38 **Kantartzis K**, Rittig K, Cegan A, Machann J, Schick F, Balletshofer B, Fritsche A, Schleicher E, Häring HU, Stefan N. Fatty liver is independently associated with alterations in circulating HDL2 and HDL3 subfractions. *Diabetes Care* 2008; **31**: 366-368
39 **Stefan N**, Hennige AM, Staiger H, Machann J, Schick F, Schleicher E, Fritsche A, Häring HU. High circulating retinol-binding protein 4 is associated with elevated liver fat but not with total, subcutaneous, visceral, or intramyocellular fat in humans. *Diabetes Care* 2007; **30**: 1173-1178
40 **Stefan N**, Peter A, Cegan A, Staiger H, Machann J, Schick F, Claussen CD, Fritsche A, Häring HU, Schleicher E. Low hepatic stearoyl-CoA desaturase 1 activity is associated with fatty liver and insulin resistance in obese humans. *Diabetologia* 2008; **51**: 648-656
41 **Silbernagel G**, Stefan N, Hoffmann MM, Machicao-Arano F, Machann J, Schick F, Winkelmann BR, Boehm BO, Häring HU, Fritsche A, März W. The L162V polymorphism of the peroxisome proliferator activated receptor alpha gene (PPARA) is not associated with type 2 diabetes, BMI or body fat composition. *Exp Clin Endocrinol Diabetes* 2009; **117**: 113-118
42 **Haupt A**, Thamer C, Heni M, Tschritter O, Machann J, Schick F, Machicao F, Häring HU, Staiger H, Fritsche A. Impact of variation near MC4R on whole-body fat distribution, liver fat, and weight loss. *Obesity* (Silver Spring) 2009; **17**: 1942-1945
43 **Park HW**, Kim YH, Cho ZH. Fast gradient-echo chemical-shift imaging. *Magn Reson Med* 1988; **7**: 340-345
44 **Chen Q**, Stock KW, Prasad PV, Hatabu H. Fast magnetic resonance imaging techniques. *Eur J Radiol* 1999; **29**: 90-100
45 **Hussain HK**, Chenevert TL, Londy FJ, Gulani V, Swanson SD, McKenna BJ, Appelman HD, Adusumilli S, Greenson JK, Conjeevaram HS. Hepatic fat fraction: MR imaging for quantitative measurement and display--early experience. *Radiology* 2005; **237**: 1048-1055
46 **Alústiza JM**, Castiella A. Liver fat and iron at in-phase and opposed-phase MR imaging. *Radiology* 2008; **246**: 641
47 **Dixon WT**. Simple proton spectroscopic imaging. *Radiology* 1984; **153**: 189-194
48 **Fishbein MH**, Gardner KG, Potter CJ, Schmalbrock P, Smith MA. Introduction of fast MR imaging in the assessment of hepatic steatosis. *Magn Reson Imaging* 1997; **15**: 287-293

49 **Machann J**, Bachmann OP, Brechtel K, Dahl DB, Wietek B, Klumpp B, Häring HU, Claussen CD, Jacob S, Schick F. Lipid content in the musculature of the lower leg assessed by fat selective MRI: intra- and interindividual differences and correlation with anthropometric and metabolic data. *J Magn Reson Imaging* 2003; **17**: 350-357

50 **Fishbein MH**, Stevens WR. Rapid MRI using a modified Dixon technique: a non-invasive and effective method for detection and monitoring of fatty metamorphosis of the liver. *Pediatr Radiol* 2001; **31**: 806-809

51 **Namimoto T**, Yamashita Y, Mitsuzaki K, Nakayama Y, Makita O, Kadota M, Takahashi M. Adrenal masses: quantification of fat content with double-echo chemical shift in-phase and opposed-phase FLASH MR images for differentiation of adrenal adenomas. *Radiology* 2001; **218**: 642-646

52 **Ma X**, Holalkere NS, Kambadakone R A, Mino-Kenudson M, Hahn PF, Sahani DV. Imaging-based quantification of hepatic fat: methods and clinical applications. *Radiographics* 2009; **29**: 1253-1277

53 **Schwenzer NF**, Machann J, Haap MM, Martirosian P, Schraml C, Liebig G, Stefan N, Häring HU, Claussen CD, Fritsche A, Schick F. T2* relaxometry in liver, pancreas, and spleen in a healthy cohort of one hundred twenty-nine subjects-correlation with age, gender, and serum ferritin. *Invest Radiol* 2008; **43**: 854-860

54 **Westphalen AC**, Qayyum A, Yeh BM, Merriman RB, Lee JA, Lamba A, Lu Y, Coakley FV. Liver fat: effect of hepatic iron deposition on evaluation with opposed-phase MR imaging. *Radiology* 2007; **242**: 450-455

55 **Olthof AW**, Sijens PE, Kreeftenberg HG, Kappert P, van der Jagt EJ, Oudkerk M. Non-invasive liver iron concentration measurement by MRI: comparison of two validated protocols. *Eur J Radiol* 2009; **71**: 116-121

56 **Olthof AW**, Sijens PE, Kreeftenberg HG, Kappert P, Irwan R, van der Jagt EJ, Oudkerk M. Correlation between serum ferritin levels and liver iron concentration determined by MR imaging: impact of hematologic disease and inflammation. *Magn Reson Imaging* 2007; **25**: 228-231

57 **Schwenzer NF**, Machann J, Martirosian P, Stefan N, Schraml C, Fritsche A, Claussen CD, Schick F. Quantification of pancreatic lipomatosis and liver steatosis by MRI: comparison of in/opposed-phase and spectral-spatial excitation techniques. *Invest Radiol* 2008; **43**: 330-337

58 **Levenson H**, Greensite F, Hoefs J, Friloux L, Applegate G, Silva E, Kanel G, Buxton R. Fatty infiltration of the liver: quantification with phase-contrast MR imaging at 1.5 T vs biopsy. *AJR Am J Roentgenol* 1991; **156**: 307-312

59 **Zhang X**, Tengowski M, Fasulo L, Botts S, Suddarth SA, Johnson GA. Measurement of fat/water ratios in rat liver using 3D three-point dixon MRI. *Magn Reson Med* 2004; **51**: 697-702

60 **Glover GH**, Schneider E. Three-point Dixon technique for true water/fat decomposition with B0 inhomogeneity correction. *Magn Reson Med* 1991; **18**: 371-383

61 **Glover GH**. Multipoint Dixon technique for water and fat proton and susceptibility imaging. *J Magn Reson Imaging* 1991; **1**: 521-530

62 **Borrello JA**, Chenevert TL, Meyer CR, Aisen AM, Glazer GM. Chemical shift-based true water and fat images: regional phase correction of modified spin-echo MR images. *Radiology* 1987; **164**: 531-537

63 **Lodes CC**, Felmlee JP, Ehman RL, Sehgal CM, Greenleaf JF, Glover GH, Gray JE. Proton MR chemical shift imaging using double and triple phase contrast acquisition methods. *J Comput Assist Tomogr* 1989; **13**: 855-861

64 **Szumowski J**, Coshow WR, Li F, Quinn SF. Phase unwrapping in the three-point Dixon method for fat suppression MR imaging. *Radiology* 1994; **192**: 555-561

65 **Szumowski J**, Coshow W, Li F, Coombs B, Quinn SF. Double-echo three-point-Dixon method for fat suppression MRI. *Magn Reson Med* 1995; **34**: 120-124

66 **Coombs BD**, Szumowski J, Coshow W. Two-point Dixon technique for water-fat signal decomposition with B0 inhomogeneity correction. *Magn Reson Med* 1997; **38**: 884-889

67 **Reeder SB**, Pineda AR, Wen Z, Shimakawa A, Yu H, Brittain JH, Gold GE, Beaulieu CH, Pelc NJ. Iterative decomposition of water and fat with echo asymmetry and least-squares estimation (IDEAL): application with fast spin-echo imaging. *Magn Reson Med* 2005; **54**: 636-644

68 **Reeder SB**, McKenzie CA, Pineda AR, Yu H, Shimakawa A, Brau AC, Hargreaves BA, Gold GE, Brittain JH. Water-fat separation with IDEAL gradient-echo imaging. *J Magn Reson Imaging* 2007; **25**: 644-652

69 **Reeder SB**, Hargreaves BA, Yu H, Brittain JH. Homodyne reconstruction and IDEAL water-fat decomposition. *Magn Reson Med* 2005; **54**: 586-593

70 **Liu CY**, McKenzie CA, Yu H, Brittain JH, Reeder SB. Fat quantification with IDEAL gradient echo imaging: correction of bias from T(1) and noise. *Magn Reson Med* 2007; **58**: 354-364

71 **Chen CA**, Lu W, John CT, Hargreaves BA, Reeder SB, Delp SL, Siston RA, Gold GE. Multiecho IDEAL gradient-echo water-fat separation for rapid assessment of cartilage volume at 1.5 T: initial experience. *Radiology* 2009; **252**: 561-567

72 **Grayev A**, Shimakawa A, Cousins J, Turski P, Brittain J, Reeder S. Improved time-of-flight magnetic resonance angiography with IDEAL water-fat separation. *J Magn Reson Imaging* 2009; **29**: 1367-1374

73 **Kijowski R**, Tuite M, Passov L, Shimakawa A, Yu H, Reeder SB. Cartilage imaging at 3.0T with gradient refocused acquisition in the steady-state (GRASS) and IDEAL fat-water separation. *J Magn Reson Imaging* 2008; **28**: 167-174

74 **Costa DN**, Pedrosa I, McKenzie C, Reeder SB, Rofsky NM. Body MRI using IDEAL. *AJR Am J Roentgenol* 2008; **190**: 1076-1084

75 **Reeder SB**, Markl M, Yu H, Hellinger JC, Herfkens RJ, Pelc NJ. Cardiac CINE imaging with IDEAL water-fat separation and steady-state free precession. *J Magn Reson Imaging* 2005; **22**: 44-52

76 **Schick F**, Machann J, Brechtel K, Strempfer A, Klumpp B, Stein DT, Jacob S. MRI of muscular fat. *Magn Reson Med* 2002; **47**: 720-727

77 **Schick F**. Simultaneous highly selective MR water and fat imaging using a simple new type of spectral-spatial excitation. *Magn Reson Med* 1998; **40**: 194-202

78 **Schick F**, Forster J, Machann J, Huppert P, Claussen CD. Highly selective water and fat imaging applying multislice sequences without sensitivity to B1 field inhomogeneities. *Magn Reson Med* 1997; **38**: 269-274

S- Editor Tian L **L- Editor** Kerr C **E- Editor** Ma WH

World Journal of Gastroenterology

Online Submissions: http://www.wjgnet.com/1007-9327office
wjg@wjgnet.com
doi:10.3748/wjg.v16.i13.1567

World J Gastroenterol 2010 April 7; 16(13): 1567-1576
ISSN 1007-9327 (print)

TOPIC HIGHLIGHT

Paul E Sijens, PhD, Associate Professor, *Series Editor*

Diffusion weighted imaging in the liver

Petra G Kele, Eric J van der Jagt

Petra G Kele, Eric J van der Jagt, Department of Radiology, University Medical Center Groningen, University of Groningen, 9700 RB Groningen, The Netherlands
Author contributions: Kele PG wrote the manuscript; van der Jagt EJ, expert in abdominal radiology, commented the manuscript.
Correspondence to: Petra G Kele, MD, Research Officer, Department of Radiology, University Medical Center Groningen, University of Groningen, 9700 RB Groningen, The Netherlands. p.g.kele@rad.umcg.nl
Telephone: +31-50-3611098 Fax: +31-50-3617008
Received: February 3, 2010 Revised: February 25, 2010
Accepted: March 4, 2010
Published online: April 7, 2010

Abstract

Diffusion weighted magnetic resonance imaging (DWI) is an imaging technique which provides tissue contrast by the measurement of diffusion properties of water molecules within tissues. Diffusion is expressed in an apparent diffusion coefficient (ADC), which reflects the diffusion properties unique to each type of tissue. DWI has been originally used in neuroradiology. More recently, DWI has increasingly been used in addition to conventional unenhanced and enhanced magnetic resonance imaging (MRI) in other parts of the body. The reason for this delay was a number of technical problems inherent to the technique, making DWI very sensitive to artifacts, which had to be overcome. With assessment of ADC values, DWI proved to be helpful in characterization of focal liver lesions. However, DWI should always be used in conjunction to conventional MRI since there is considerable overlap between ADC values of benign and malignant lesions. DWI is useful in the detection of hepatocellular carcinoma in the cirrhotic liver and detection of liver metastases in oncological patients. In addition, DWI is a promising tool in the prediction of tumor responsiveness to chemotherapy and the follow-up of oncological patients after treatment, as DWI may be capable of detecting recurrent disease earlier than conventional imaging. This review focuses on the most common applications of DWI in the liver.

Key words: Diffusion; Magnetic resonance imaging; Diffusion weighted imaging; Benign neoplasms; Liver neoplasms

Peer reviewer: Paul E Sijens, PhD, Associate Professor, Radiology, UMCG, Hanzeplein 1, 9713GZ Groningen, The Netherlands

Kele PG, van der Jagt EJ. Diffusion weighted imaging in the liver. *World J Gastroenterol* 2010; 16(13): 1567-1576 Available from: URL: http://www.wjgnet.com/1007-9327/full/v16/i13/1567.htm DOI: http://dx.doi.org/10.3748/wjg.v16.i13.1567

INTRODUCTION

Magnetic resonance imaging (MRI) is an imaging technique which is used to visualize the internal structure and function of the body. MRI provides excellent tissue contrast, which is much greater than that of any other imaging modality[1,2]. Tissue contrast is realized by a wide range of pulse sequences. For example, tissue contrast on T1- and T2-weighted images is based on the rate at which signals from protons in water molecules in a static magnetic field decay following excitation by a sequence of radiofrequency (RF) pulses. Diffusion weighted imaging (DWI) is another mechanism for developing image contrast and relies on changes in the diffusion properties of water molecules in tissues. DWI is a widely accepted technique in neuroradiology for detecting early ischemia in cerebrovascular accidents and characterization of brain tumors and intracranial infections[1-3]. The use of DWI in other parts of the body is relatively new, but very promising for the detection and differentiation of benign and malignant lesions, imaging for dissemination (i.e. staging) in oncological patients before treatment and

for follow-up after treatment of liver tumors. Besides this, DWI is thought to be capable of predicting the response to therapy of malignant tumors (especially chemotherapy)[4].

BASIC PRINCIPLES OF DWI

Diffusion

Diffusion is a physical property, which describes the microscopic random movement of (water) molecules driven by their internal thermal energy. This movement is known as Brownian motion. In biological tissues, water diffusion is movement of water molecules in intracellular, extracellular and intravascular spaces. Diffusion is affected by the biophysical properties of tissue cell organization (cell membranes, fibers and macromolecules), density, microstructure and microcirculation. Intracellular water diffusion is more hindered than that in the extracellular spaces which are lacking natural barriers. Pathological processes which change the volume ratio or physical nature of intra- and extracellular spaces affect the diffusion of water molecules. Restricted or impeded diffusion is seen in tissues with high cellularity, e.g. tumors, abscesses, fibrosis and cytotoxic edema. Relative free or unimpeded diffusion is encountered in tissues with low cellularity or tissues with disrupted cell membranes, for example in cysts and necrotic tissues[3-5] (Figure 1A and B).

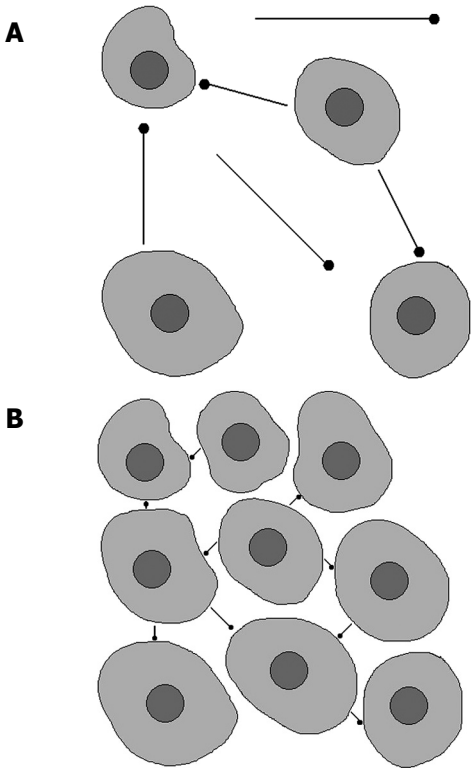

Figure 1 Brownian movements in hypocellular (A) and hypercellular (B) environment. A: Tissue with low cellularity permits movement of the water molecules; B: Tissue with high cellularity restricts the movement of water molecules.

DWI

DWI relies on measuring diffusion of water molecules in the tissue by MRI. It uses a pulse sequence (T2-weighted spin echo sequence) and 2 strong motion probing gradients on either side of the 180° refocusing pulse, known as the Stejskal-Tanner sequence. The first gradient, prior to the 180° RF pulse is the dephasing (diffusion sensitizing) gradient. The second gradient, after the RF pulse, is the rephasing gradient. In tissues with restricted diffusion, the effect of the dephasing gradient is cancelled out by the rephasing gradient. This causes little impact on the overall T2 decay, reflected as a maintained T2 signal in the tissue. When diffusion is not impeded, water molecules can move a considerable distance between the dephasing and rephasing gradients. The mobile water molecules will not be fully rephased and a reduction in overall T2 signal intensity follows.

DWI is sensitive to very small scale motion of water molecules at a microscopic level. The sensitivity of a DWI sequence is characterized by its b-value, expressed in s/mm^2. The b-value summarizes the influence of the gradients in DWI. The higher the b-value, the more sensitive the sequence is to diffusion effects. DWI is performed with at least two b-values. Diffusion is quantitatively reflected in a diffusion coefficient. The diffusion coefficient is related to the molecular mobility of water molecules and reflects tissue properties such as the size of the extracellular space, viscosity and cellularity. Diffusion coefficients in DWI are reflected in the *apparent diffusion coefficient* (ADC, expressed in mm^2/s), apparent because it is a mean value of diffusion contributed by movement of intracellular, extracellular and vascular water molecules within an image voxel (volumetric pixel) at different b-values. Analysis of ADC is an automated process, available as an application on most scanners or workstations. Calculation of ADC is made for each voxel of an image and can be displayed as a parametric (ADC) map. ADC measurements are then recorded for a given region by drawing regions of interest (ROIs) on the ADC map. Low ADC values mean restricted diffusion, thus in tissues which are highly cellular. High ADC values are seen in areas with relative free diffusion, thus in tissues with low cellularity[1,3-5].

Problems encountered in DWI

DWI can be performed with different techniques, including spin-echo (SE), fast spin echo (FSE), gradient echo (GE) and echo-planar imaging (EPI). EPI is the gold standard DWI technique. When DWI is performed in the body, scanning can be carried out with free breathing, breath hold or respiratory triggered. There are some important limitations of DWI[2,6].

Firstly, the signal-to-noise ratio (SNR, describes the relative contributions of the true signal and background noise to a detected signal) and spatial resolution are low due to hardware limitations and high bandwidth (a measure of frequency range, the range between the highest and lowest frequency allowed in the signal), inherent to the technique and EPI sequence. SNR will be decreased in incomplete spin echo formation, as is the case with

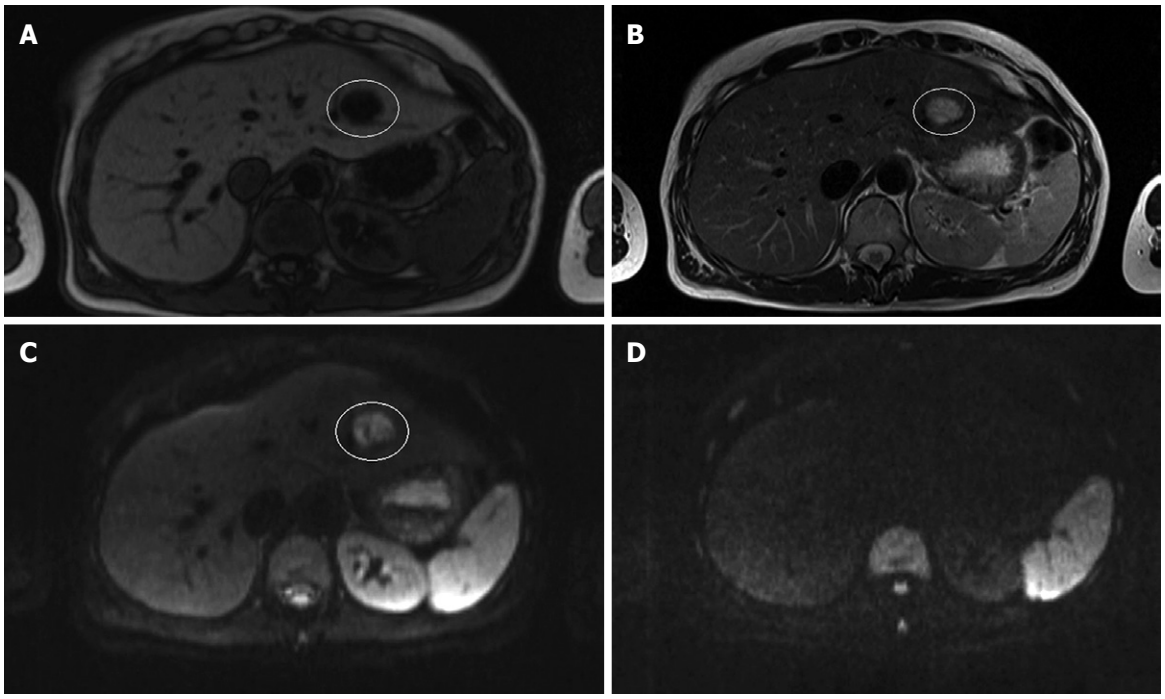

Figure 2 Magnetic resonance imaging (MRI) and diffusion weighted imaging (DWI) of a cyst. A: T1-weighted MRI; B: T2-weighted MRI; C: Diffusion weighted image (b-value 50 s/mm^2); D: Diffusion weighted image (b-value 1000 s/mm^2) in a 33-year old woman with multiple liver lesions. The cyst is hypo-intense on the T1-weighted image, hyper-intense on the T2-weighted image and the diffusion weighted image at a b-value 50 s/mm^2. Note that the cyst totally disappears on the diffusion weighted image at a b-value 1000 s/mm^2.

the most common DWI technique, the EPI sequence. SNR can be increased, but then spatial resolution is sacrificed[2,3,6-8].

Secondly, DWI is susceptible to a number of artifacts. Ghosting images and blurring may arise from motion, caused by respiratory, cardiac and voluntary movements. Tissue contrast is maintained during free-breathing scanning, but breath hold and respiratory triggered techniques reduce image blurring. Breath hold scans have very short acquisition times of 20-30 s (i.e. the time the patient holds his or her breath) and are theoretically less likely to be degraded by motion-related artifacts. A disadvantage of breath-hold scanning is that the patient needs to hold his or her breath for a considerable time, which may be difficult when the physical condition does not allow him or her to do so. Respiratory triggering will make the acquisition time of the images longer (5 min), especially when the patient is breathing irregularly or slowly, but this is a minimal time penalty. Respiratory triggering provides substantially improved signal, spatial resolution and the ADC values are comparable to breath-hold DWI. In respiratory triggering, multiple b-values can be used to reduce errors in ADC calculation[2,3,6,7,9-11].

Motion artifacts caused by the heart beating alter ADC in the left lobe of the liver, making measurements unreliable. Cardiac motion can be overcome by using electrocardiographic-triggering, but cardiac gating is not always reliable and increases acquisition times significantly[2,3,6,7,12].

Susceptibility artifacts are due to magnetic field inhomogeneity (to be overcome by shimming techniques) or metal artifacts and are seen as bright spots, spatial distortion or signal drop out. Susceptibility artifacts occur especially in fast imaging techniques like EPI[2,6,7].

Artifacts caused by air-tissue interfaces or fat-water interfaces (chemical shift) appear as black or bright bands at the edge of an anatomical structure. Other artifacts are eddy currents, resulting from the rapid on and off switching of the gradients, leading to geometrical distortion and image shearing artifacts[2,6,7].

Pathological diffusion

When evaluating diffusion on DWI images, the radiologist focuses on the measurement of extracellular diffusion. As mentioned earlier, the higher the cellularity in a tissue, the less far is extracellular water able to diffuse during the MR observation period without being blocked by cell membranes. Highly cellular tissues provide a short path of diffusion, resulting in low ADC values, as is seen in solid liver lesions and abscesses. Low cellularity means that there are fewer structural barriers, making the diffusion path longer. This results in high ADC values as is seen in cysts and necrotic lesions. In summary, ADC maps, derived from DWI provide a non-invasive measure of cellularity. This makes DWI a potential tool in diagnosis, treatment planning and monitoring, especially in oncology[3-5]. Examples of different types of lesions and their diffusion weighted images are seen in Figures 2-5.

DWI IN THE LIVER

There are an increasing number of studies dealing with quantitative measurements of ADC in liver lesions, but

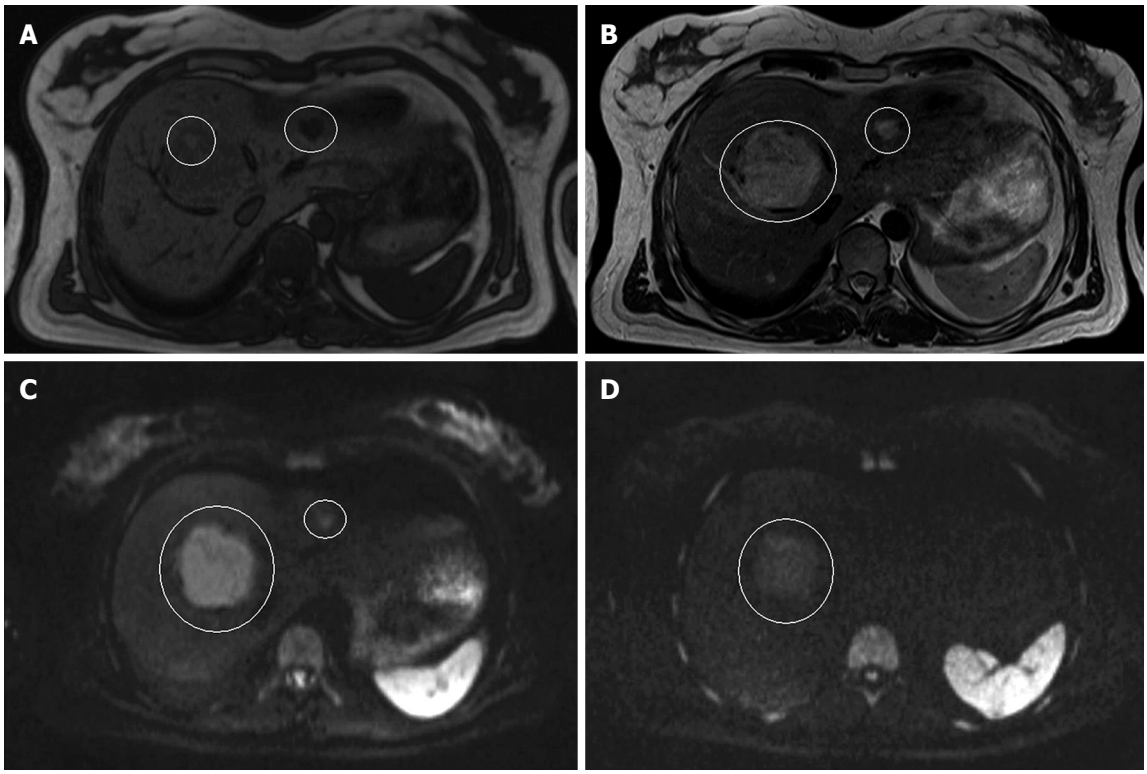

Figure 3 MRI and DWI of an adenoma and a hemangioma. A: T1-weighted MRI; B: T2-weighted MRI; C: Diffusion weighted image (b-value 50 s/mm^2); D: Diffusion weighted image (b-value 1000 s/mm^2) in a 41-year-old women with multiple liver lesions. The large lesion in segment 8 is an adenoma and the small one in segment 2-3 is a hemangioma. On the T1-weighted image, the adenoma is slightly hypo-intense to the normal liver parenchyma, and hyper-intense on the T2-weighted image. On the diffusion weighted images, it remains hyper-intense at both b-values. The hemangioma is also hypo-intense on the T1-weighted image and hyper-intense on the T2-weighted image. However, in contrast to the adenoma, it totally disappears at a b-value of 1000 mm/s^2.

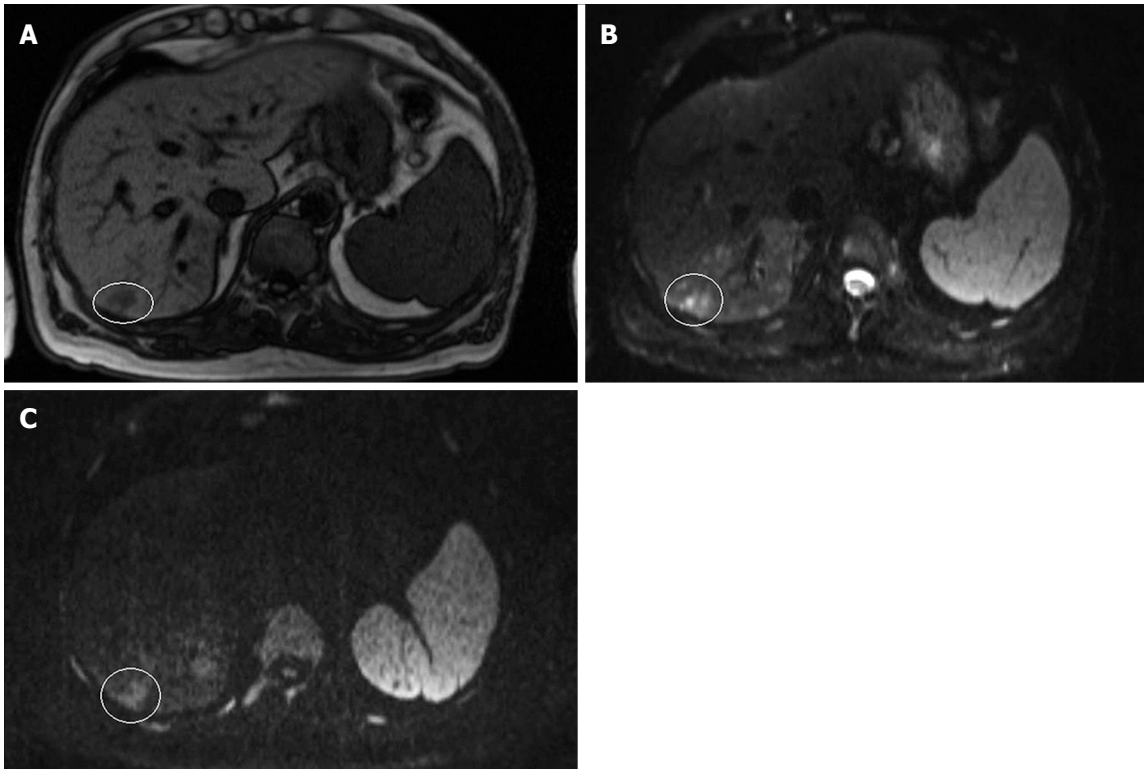

Figure 4 MRI and DWI of hepatocellular carcinoma. A: T1-weighted; B: DWI (b-value 50 s/mm^2); C: Diffusion weighted image (b-value 1000 s/mm^2) in a 67-year-old male with hemophilia, hepatitis C-based liver cirrhosis and HCC in segment 7. The HCC is hypo-intense on the T1-weighted image and hyper-intense on the diffusion weighted images at both b-values. Note that the lesion remains hyper-intense on the image with a b-value 1000 s/mm^2.

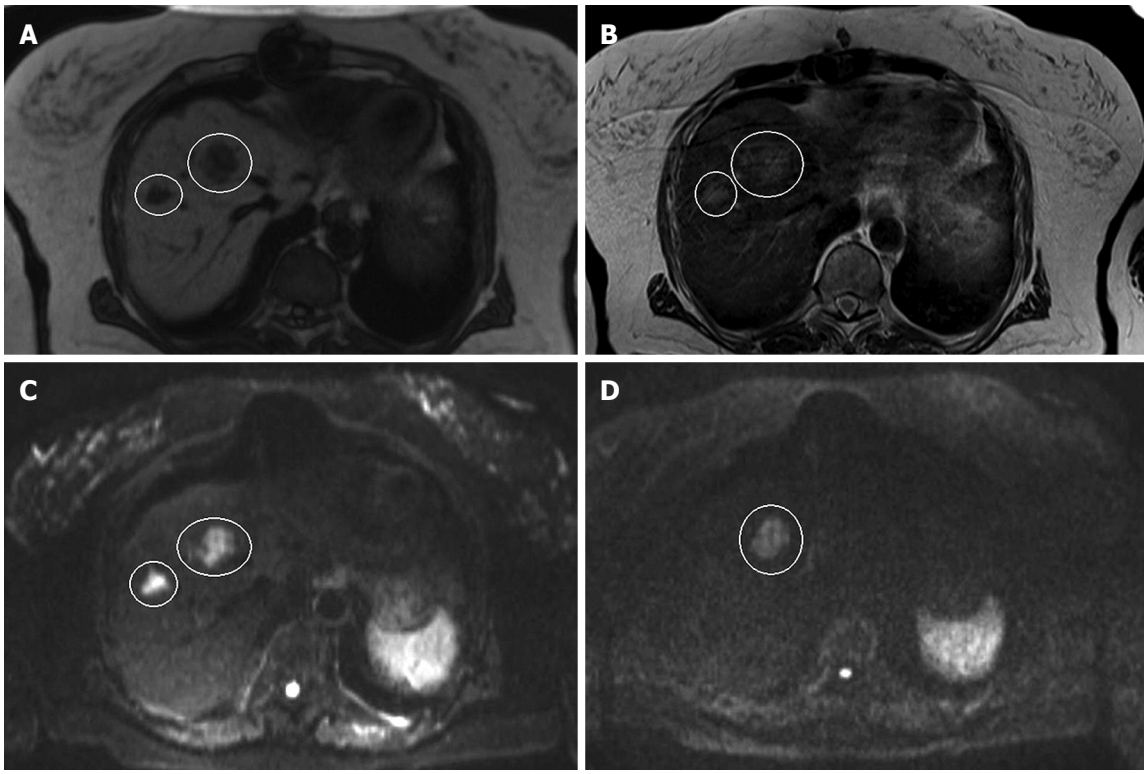

Figure 5 MRI and DWI of hepatic metastases. A: T1-weighted; B: T2-weighted; C: Diffusion weighted image (b-value 50 s/mm^2); D: Diffusion weighted image (b-value 1000 s/mm^2) in a 74-year-old woman with a history of rectal cancer, recently diagnosed with lung and liver metastases in segment 4 and 8, respectively. The lesions are hypo-intense to the liver parenchyma on the T1-weighted image and hyper-intense on the T2-weighted image. On the diffusion weighted image at a b-value 50 s/mm^2, both lesions appear hyper-intense, but at a b-value 1000 s/mm^2, only the lesion in segment 4 remains hyper-intense. The lesion in segment 8 has completely disappeared.

there are as many discrepancies in the reported ADC values (Table 1). This is often associated with the choice of b-values and other technical parameters. Low b-values lead to overestimation of the ADC due to the contribution of perfusion to the diffusion measurement. Large b-values underestimate ADC due to increasing contributions from low ADC components and SNR.

DWI as a tool for characterization of liver lesions

Several studies have suggested that the measurement of ADC values is useful in the characterization of focal liver lesions[13-26]. Reduced ADC values have been reported for most malignant tumors. This finding is thought to be the result of cellular membranes impeding the mobility of water molecules. However, solid benign lesions, which are also highly cellular, exhibit decreased ADC values as well. Abscesses do so too because their viscose content with bacteria, inflammatory cells, mucoid proteins and cell debris result in restricted diffusion, thus low ADC values. On the other hand, necrotic and cystic malignancies show high ADC values resulting from larger diffusion distances as a consequence of lost membrane integrity. Benign lesions as simple cysts and hemangiomas show high ADC values because of their liquid content and large extracellular spaces. However, ADC values cannot discriminate between solid benign and malignant lesions, since there is considerable overlap. According to Feuerlein *et al*[15], the pretest probability of malignancy is very important in the determination to which degree a large ADC value is predictive for a malignancy, i.e. the history, demography and clinical picture of the individual patient. Even ADC values of lesions of the same kind show overlap and there is no cut-off value for ADC values in normal parenchyma, benign and malignant lesions. In the literature, ADC values vary between 0.94-2.85 × 10^{-3} mm^2/s for metastases and 0.69-2.28 × 10^{-3} mm^2/s for normal liver parenchyma. This is mainly because every study group uses their own scanning parameters. Differences in b-values are the main cause of non-equivocal results. Breath-hold, respiratory triggered and navigator echo techniques can also give different ADC values. There is need for an uniformly applicable scanning protocol to eliminate discrepancies in ADC values caused by different scanning parameters[13].

DWI alone is not suitable for the characterization of liver lesions, because solid benign lesions also can show restricted diffusion, and cystic or necrotic malignant lesions have unimpeded diffusion. DWI can help direct the attention of the radiologist to findings that may otherwise be overlooked. Unenhanced and dynamic MRI contrast series alone are very capable in the discrimination of different types of liver lesions, but a combination of DWI and MRI increases the accuracy of the characterization of benign and malignant lesions[15-17].

Detection of hepatocellular carcinoma

Multiphase multidetector contrast enhanced computed tomography (CT) has reached a high standard for the

Table 1 Reported ADC values in different types of lesions in the liver

Study	Type of lesion	*n*	ADC value mm^2/s, BH (SD)	ADC value mm^2/s, RT (SD)
Taouli *et al*[10]				
b-values	Benign	18	2.21 (0.60)	2.39 (0.44)
0, 50, 500 s/mm^2	Malignant	11	1.04 (0.27)	1.16 (0.33)
Goshima *et al*[13]				
b-values	Hemangioma	12	1.23-2.23 (0.2-1.2)[2]	
100, 200, 400, 800 s/mm^2	Cyst	15	3.70-4.72 (0.9-1.2)[2]	
	Metastases	7	0.99-1.70 (0.5-1.1)[2]	
	HCC	21	1.08-1.79 (0.3-10.9)[2]	
Kandpal *et al*[14]				
b-value	Hemangioma	11	2.22 (0.45)	2.36 (0.48)
0, 500 s/mm^2	Cyst	11	2.66 (0.44)	2.90 (0.51)
	FNH	3	2.03 (0.24)	2.15 (0.18)
	Abscess	6	1.21 (0.36)	1.13 (0.43)
	Metastases	38	1.06 (0.36)	1.13 (0.41)
	HCC	12	1.22 (0.34)	1.27 (0.42)
Gourtsoyianni *et al*[18][1]				
b-values	Hemangioma	7		1.90
0, 50, 500, 1000 s/mm^2	Cyst	15		2.55
	Metastases	13		0.99 (0.22)
	HCC	2		1.38
Oner *et al*[19]				
b-values	Hemangioma	5	1.72 (0.30)	
0, 500 s/mm^2	Cyst	3	2.34 (0.36)	
	Metastases	6	1.03 (0.24)	
Demir *et al*[23][1]				
0, 1000 s/mm^2	Benign	24	1.09-3.36 (0.32/0.28)[3]	
	Malignant	17	0.54-1.24 (0.07/0.14)[3]	
Bruegel *et al*[24][1]				
b-values	Hemangioma	56		1.92 (0.34)
50, 300, 600 s/mm^2	Cyst	51		3.02 (0.31)
	FNH	4		1.40 (0.15)
	Metastases	82		1.22 (0.31)
	HCC	11		1.05 (0.09)
Holzapfel *et al*[25][1]				
b-values	Hemangioma	18		1.69 (0.34)
50, 300, 600 s/mm^2	Cyst	71		2.61 (0.57)
	FNH/adenoma	6/9		1.43 (0.22)
	Metastases	76		1.08 (0.32)
	HCC	17		1.12 (0.28)

[1]These studies found significantly higher ADC values in benign liver lesions than in malignant liver lesions; [2]This study evaluated the ADC values at different b-values. The lowest and highest ADC values are reported here. The lowest ADC value corresponds with the highest b-value, the highest ADC value with the lowest b-value; [3]This study evaluated the ADC values of different types of benign and malignant lesions. The lowest and highest ADC values are reported here. ADC: Apparent diffusion coefficient; BH: Breath-hold; RT: Respiratory triggered; SD: Standard deviation; FNH: Focal nodular hyperplasia; HCC: Hepatocellular carcinoma.

evaluation of the cirrhotic liver and for the detection of hepatocellular carcinoma (HCC). On CT images, diagnosis of HCC is made based on neovascularization with increased arterial enhancement and rapid portal venous wash-out. In the last few years, (liver-specific) contrast enhanced multiphase dynamic MRI has increasingly been used for the detection of HCC. MRI proved to be superior to CT in the detection of HCC and for the characterization of nodules in patients with liver cirrhosis because of the high tissue contrast provided by MRI and the available liver-specific contrast agents. Contrast enhanced MRI is now regarded as the best non invasive imaging modality. However, even with liver-specific contrast enhanced MRI, there is a diagnostic problem for small HCC lesions (< 10 mm) as well as in the differentiation from other non-malignant nodules. Large HCC lesions are well-recognized on conventional MRI by their rapid enhancement in the arterial phase and their contrast agent wash-out in the portal-venous phase. Small HCC is less typical on conventional MRI, and differentiation of atypical nodules in the cirrhotic liver is challenging[27-31].

Xu *et al*[27,28] found that ADC values were not useful in cirrhotic livers, because cirrhotic parenchyma and solid benign lesions have low ADC values. They cannot be differentiated from lesions with malignant diffusion restriction because of the considerable overlap among their ADC values. Necrosis and vascularization within HCC also alter diffusion, often seen as a false increase in the ADC values.

Zech *et al*[29] reported a higher sensitivity for DWI compared to conventional MRI in the detection of HCC in the cirrhotic liver (98% for DWI *vs* 83%-85% for MRI). Vandecaveye *et al*[30] concluded that DWI provided higher sensitivity and positive predictive value for the detection of HCC < 20 mm compared to conventional contrast enhanced MRI (sensitivity and specificity 91.2% and 82.9% *vs* 67.6% and 61.6%, positive predictive value 81.6% and 59.0%, respectively). DWI did not show significantly better results than conventional MRI in detecting HCC > 20 mm. These findings can be explained by the better contrast-to-noise ratio and background suppression of normal liver parenchyma and vascular or bile structures in DWI, which make small lesions more visible, especially when they are in close vicinity to vessels or bile ducts. DWI provides a high negative predictive value on the presence or absence of HCC and reduces the rate of unnecessary invasive diagnostic procedures and follow-up.

Detection of liver metastases

Several studies have demonstrated the usefulness of DWI in the detection of liver metastases. They compared DWI to unenhanced and dynamic liver specific contrast enhanced MRI (Table 2).

Coenegrachts *et al*[20] showed that lesion conspicuity of hemangiomas and metastases is significantly higher with respiratory triggered DWI at low b-values compared to conventional unenhanced MRI imaging. This is due to an excellent lesion to liver contrast and suppression of background signals from vessels.

Koh *et al*[32] compared the diagnostic accuracy of DWI and mangafodipir trisodium (MnDPDP)-enhanced MRI alone and in combination in the detection of colorectal liver metastases. They found that a combination of MnDPDP MRI and DWI resulted in the highest diagnostic accuracy (0.94-0.96 *vs* 0.88-0.92 for MnDPDP alone and 0.83-0.90 for DWI alone) with an increased sensitivity, but no loss of specificity. DWI alone is not useful because the sequence is very susceptible to motion artifacts, which obscure lesions and make images difficult to interpret. This is especially the case in the left lobe of the liver. They also stated that experience is needed to interpret DWI correctly, mainly because of the large numbers of artifacts on the images[33].

Parikh *et al*[34] reported a significantly higher overall lesion detection rate for breath-hold or respiratory triggered DWI than for conventional T2-weighted MRI (88% *vs* 70%). Bruegel *et al*[35] compared respiratory DWI-EPI with T2-TSE. They found a sensitivity and specificity for T2-TSE MRI of 45%-62% for unenhanced MRI and 88%-91% for DWI-EPI for lesions > 10 mm. When considering only small metastases < 10 mm, the differences between DWI and conventional MRI with and without contrast are even more pronounced: a sensitivity of 85% for DWI-EPI and 26%-44% for T2-TSE. Lesion detection on T2-TSE is hindered by low lesion to liver contrast and by the interfering bright signal from intrahepatic vessels. Lesion conspicuity with DWI is excellent and limitation of the DWI sequence is predominantly referred to lesion characterization rather than to lesion detectability.

Table 2 Performance of DWI and conventional MRI in the detection of liver metastases *n* (%)

Study	Sensitivity	Specificity	Accuracy	PPV	NPV
Vandecaveye *et al*[30]					
> 20 mm					
B600 SI ratio	100	81.8	94.9	93.3	100
T2-CE MRI	96.4	81.8	92.3	93.1	90.0
< 20 mm					
B600SI ratio	91.2	82.9	86.7	81.6	91.9
T2-CE MRI	67.6	61.0	64.0	59.0	69.4
Koh *et al*[32][1]					
MnDPDP MRI	81.3	93.0	88-92		
DWI 0, 150, 500 BH	78.3	95.0	83-90		
MnDPDP MRI and DWI	92.2	97.0	94-96		
DWI RT	88-91				
T2 MRI	45-62				
Nasu *et al*[36]					
DWI RT (0, 500)	82	94			
SPIO MRI	66	90			

[1]In this study, 2 observers reviewed the images. The given values in sensitivity, specificity and diagnostic accuracy refer to the separate results of both observers. PPV: Positive predictive value; NPV: Negative predictive value.

Nasu *et al*[36] assessed the diagnostic accuracy of respiratory triggered DWI in combination with unenhanced MRI *vs* superparamagnetic iron oxide (SPIO)-enhanced imaging. On the basis of a receiver operator characteristic analysis (ROC), averaged over 3 observers, they found a sensitivity and specificity for SPIO-enhanced images of 66% and 90% and for DWI 82% and 94%, respectively.

Predicting response to therapy of primary and secondary liver malignancies by DWI

Tumor responses to chemotherapy and radiation therapy are conventionally assessed by measurement of percentage reduction in tumor size after chemotherapy. However, tumor size measurement on CT or MRI is insensitive to early treatment changes. Theoretically, DWI is sensitive to microenvironmental changes in tumors that occur after treatment. Studies on the predictive value of DWI in primary cancer demonstrated a strong negative correlation between mean pre-treatment ADC values and percentage size reduction of tumors after chemotherapy and chemoradiation. High pretreatment ADC values in tumors were associated with a poor response to chemotherapy[37,38].

Koh *et al*[37] showed that high pre-treatment ADC values in colorectal liver metastases were predictive of a poor response to oxaliplatin and 5-fluorouracil-based chemotherapy. They determined with ROC that a mean pretreatment ADC150-500 (ADC map with b-values 150 s/mm^2 and 500 s/mm^2) of 1.69 × 10^{-3} mm^2/s had 60% sensitivity and 100% specificity for identification of non-responding metastatic lesions. They found also a significant linear regression relation between mean ADC150-500 and percentage in tumor size reduction

after treatment. Responding tumors showed a significant increase in ADC values at the end of the treatment. Non-responding tumors and liver parenchyma did not show significant changes in ADC values. Cui *et al*[38] analyzed 87 liver metastases of colorectal and gastric origin in 23 patients. They also found significant lower ADC values in responding tumors than in non-responding ones. ADC increased in responding metastases, but not in non-responding ones. They found a weak correlation between tumor size reduction and pretreatment ADC values. The theoretical background for these findings is that higher ADC values are observed in necrotic tissue, and in tissue with loss of cell membrane integrity. When these changes are present before chemotherapy, it may indicate a more aggressive phenotype. Necrotic regions within a tumor are usually poorly perfused, resulting in less delivery of chemotherapeutic agents to these areas. Necrotic regions areas are also exposed to a more hypoxic and acidic environment, which diminishes the effect of chemotherapy. Necrosis in hepatic metastases is present in almost half of the cases. A possible explanation for non-responding tumors with lower ADC values may be the fact that necrosis is not always associated with high ADC values, especially in the case of coagulation necrosis without cell lysis or liquefaction. The increase in ADC values at the end of the treatment suggests a change from a more cellular pretreatment to a less cellular or necrotic phenotype.

Only one study assessed DWI in HCC treatment with sorafenib. Schraml *et al*[39] showed that ADC values with sorafenib, an angiogenesis inhibitor for treatment of HCC, actually showed a decrease instead of an increase. This may be a result of ischemia, induced by inhibition of angiogenesis. The extracellular volume is decreasing, leading to lower ADC values during treatment. They also often observed hemorrhage within the tumors (55%), which may contribute to a decrease in ADC. However, progression of HCC more than 3 mo after therapy was related to a decrease in ADC values. Only conventional MRI could differentiate between hemorrhage and tumor progression. Pre-treatment HCC had high ADC values, because of rich vascularization of the tumors. ADC changes early after chemotherapy seem to reflect the underlying mechanisms in tumor necrosis, most probably hemorrhagic, induced by the novel targeted agent sorafenib early after therapy and may indicate tumor reactivation in the later follow-up period.

DWI after locoregional treatment for liver tumors

Locoregional therapy for liver tumors is used in patients who are not eligible for surgery. The most commonly used local ablative therapies are radiofrequency ablation (RFA) and transcatheter arterial chemoembolization (TACE). The success of these procedures is determined by the rate of ablation site recurrences (ASR), i.e. tumor recurrence as result of incomplete ablation. Close and careful follow-up is needed in patients who underwent treatment by RFA and TACE to detect ASR at an early stage. Unfortunately, diagnostic management remains an issue in these patients, because of difficulties in differentiating ASR from non-tumoral tissue changes after thermal therapy. Since DWI can provide information about molecular tissue characteristics, it may have an additional value in the evaluation and follow-up of local ablative therapies in patients with liver tumors.

There is one study which evaluated the time-related diffusion alterations after hepatic RFA with regard to potential diagnostic information for the detection of ASR. Schraml *et al*[40] reviewed 54 oncological patients treated by RFA for liver metastases from different origins. The ablation zone did not show significant alterations at different time points. Measurement of the ADC value of the entire ablation zone was not suitable for the detection of ASR, because locally changing ADC values were masked by the heterogeneous appearance of the entire ablation zone. Peripheral zones should be analyzed separately. An important technical limitation of ADC measurements after RFA is that the limited spatial resolution does not allow exact ROI positioning in the narrow peripheral rim. Viable tumors after RFA appeared as hyper-intense, and necrotic regions were recognized as hypointense areas on DWI. ASR showed significantly lower ADC values than the ablation zone and normal liver parenchyma (1.02×10^{-3} mm^2/s *vs* 1.31×10^{-3} mm^2/s). Suspected areas on DWI were more easily identified and analyzed in conjunction to conventional MR. Signal alterations in the periphery, especially ones with lower ADC values should raise suspicion on ASR. Edema, inflammation, fibrosis and necrosis are associated with higher ADC values. DWI together with conventional imaging is a promising tool in the evaluation of the post-RFA liver and may contribute to the detection of ASR.

The use of DWI after TACE in HCC has recently been investigated. Goshima *et al*[41] reported significant increases in ADC values after TACE, but they varied widely and did not contribute to the accurate diagnosis of tumor necrosis by any cut-off points. Yu *et al*[42] found that DWI added to conventional MRI could increase the sensitivity for determining ASR especially in the case of atypical lesions. However, they also noticed an increase in the number of false positive findings by adding DWI which affected the overall accuracy of MRI. This was caused by perilesional inflammation and arterial reperfusion of the perilesional atrophic area after TACE. ADC measurement was not helpful for distinguishing viable tumors from perilesional nontumorous changes, since there was great overlap between the ADC values of both entities.

CONCLUSION

DWI in the liver is a relative new and increasingly used imaging technique in addition to conventional unenhanced and contrast enhanced MRI. DWI proved to be helpful in the characterization of focal liver lesions, but should always be used in conjunction with traditional MRI since there is great overlap between ADC values of benign and malignant lesions. DWI is useful in the detection of

small HCC in the cirrhotic liver, with higher sensitivity, specificity and positive predictive value compared to conventional contrast enhanced imaging due to better lesion to liver contrast and background suppression of signals arising from vessels and bile ducts. This is also the case for the detection of metastases in the liver. However, it should be noted that DWI images are difficult to interpret since DWI is very sensitive to artifacts. It seems reasonable to use DWI in conjunction to conventional imaging. DWI is not yet commonly used in the follow-up after treatment of liver malignancies. Pre-treatment ADC values in tumors treated with chemotherapy seem to be useful in the prediction and evaluation of the treatment response of primary and secondary liver malignancies. DWI in the follow-up after RFA and TACE shows promising results in the detection of ablation site recurrences, especially in combination with conventional contrast enhanced imaging.

REFERENCES

1 **Bammer R**. Basic principles of diffusion-weighted imaging. *Eur J Radiol* 2003; **45**: 169-184
2 **Naganawa S**, Kawai H, Fukatsu H, Sakurai Y, Aoki I, Miura S, Mimura T, Kanazawa H, Ishigaki T. Diffusion-weighted imaging of the liver: technical challenges and prospects for the future. *Magn Reson Med Sci* 2005; **4**: 175-186
3 **Charles-Edwards EM**, deSouza NM. Diffusion-weighted magnetic resonance imaging and its application to cancer. *Cancer Imaging* 2006; **6**: 135-143
4 **Thoeny HC**, De Keyzer F. Extracranial applications of diffusion-weighted magnetic resonance imaging. *Eur Radiol* 2007; **17**: 1385-1393
5 **Kwee TC**, Takahara T, Ochiai R, Nievelstein RA, Luijten PR. Diffusion-weighted whole-body imaging with background body signal suppression (DWIBS): features and potential applications in oncology. *Eur Radiol* 2008; **18**: 1937-1952
6 **Koh DM**, Takahara T, Imai Y, Collins DJ. Practical aspects of assessing tumors using clinical diffusion-weighted imaging in the body. *Magn Reson Med Sci* 2007; **6**: 211-224
7 **Le Bihan D**, Poupon C, Amadon A, Lethimonnier F. Artifacts and pitfalls in diffusion MRI. *J Magn Reson Imaging* 2006; **24**: 478-488
8 **Kwee TC**, Takahara T, Ochiai R, Katahira K, Van Cauteren M, Imai Y, Nievelstein RA, Luijten PR. Whole-body diffusion-weighted magnetic resonance imaging. *Eur J Radiol* 2009; **70**: 409-417
9 **Ivancevic MK**, Kwee TC, Takahara T, Ogino T, Hussain HK, Liu PS, Chenevert TL. Diffusion-weighted MR imaging of the liver at 3.0 Tesla using TRacking Only Navigator echo (TRON): a feasibility study. *J Magn Reson Imaging* 2009; **30**: 1027-1033
10 **Taouli B**, Sandberg A, Stemmer A, Parikh T, Wong S, Xu J, Lee VS. Diffusion-weighted imaging of the liver: comparison of navigator triggered and breathhold acquisitions. *J Magn Reson Imaging* 2009; **30**: 561-568
11 **Yoshikawa T**, Ohno Y, Kawamitsu H, Ku Y, Seo Y, Zamora CA, Aoyama N, Sugimura K. Abdominal apparent diffusion coefficient measurements: effect of diffusion-weighted image quality and usefulness of anisotropic images. *Magn Reson Imaging* 2008; **26**: 1415-1420
12 **Kwee TC**, Takahara T, Niwa T, Ivancevic MK, Herigault G, Van Cauteren M, Luijten PR. Influence of cardiac motion on diffusion-weighted magnetic resonance imaging of the liver. *MAGMA* 2009; **22**: 319-325
13 **Goshima S**, Kanematsu M, Kondo H, Yokoyama R, Kajita K, Tsuge Y, Watanabe H, Shiratori Y, Onozuka M, Moriyama N. Diffusion-weighted imaging of the liver: optimizing b value for the detection and characterization of benign and malignant hepatic lesions. *J Magn Reson Imaging* 2008; **28**: 691-697
14 **Kandpal H**, Sharma R, Madhusudhan KS, Kapoor KS. Respiratory-triggered versus breath-hold diffusion-weighted MRI of liver lesions: comparison of image quality and apparent diffusion coefficient values. *AJR Am J Roentgenol* 2009; **192**: 915-922
15 **Feuerlein S**, Pauls S, Juchems MS, Stuber T, Hoffmann MH, Brambs HJ, Ernst AS. Pitfalls in abdominal diffusion-weighted imaging: how predictive is restricted water diffusion for malignancy. *AJR Am J Roentgenol* 2009; **193**: 1070-1076
16 **Sandrasegaran K**, Akisik FM, Lin C, Tahir B, Rajan J, Aisen AM. The value of diffusion-weighted imaging in characterizing focal liver masses. *Acad Radiol* 2009; **16**: 1208-1214
17 **Lichy MP**, Aschoff P, Plathow C, Stemmer A, Horger W, Mueller-Horvat C, Steidle G, Horger M, Schafer J, Eschmann SM, Kiefer B, Claussen CD, Pfannenberg C, Schlemmer HP. Tumor detection by diffusion-weighted MRI and ADC-mapping--initial clinical experiences in comparison to PET-CT. *Invest Radiol* 2007; **42**: 605-613
18 **Gourtsoyianni S**, Papanikolaou N, Yarmenitis S, Maris T, Karantanas A, Gourtsoyiannis N. Respiratory gated diffusion-weighted imaging of the liver: value of apparent diffusion coefficient measurements in the differentiation between most commonly encountered benign and malignant focal liver lesions. *Eur Radiol* 2008; **18**: 486-492
19 **Oner AY**, Celik H, Oktar SO, Tali T. Single breath-hold diffusion-weighted MRI of the liver with parallel imaging: initial experience. *Clin Radiol* 2006; **61**: 959-965
20 **Coenegrachts K**, Delanote J, Ter Beek L, Haspeslagh M, Bipat S, Stoker J, Van Kerkhove F, Steyaert L, Rigauts H, Casselman JW. Improved focal liver lesion detection: comparison of single-shot diffusion-weighted echoplanar and single-shot T2 weighted turbo spin echo techniques. *Br J Radiol* 2007; **80**: 524-531
21 **Low RN**, Gurney J. Diffusion-weighted MRI (DWI) in the oncology patient: value of breathhold DWI compared to unenhanced and gadolinium-enhanced MRI. *J Magn Reson Imaging* 2007; **25**: 848-858
22 **Asbach P**, Hein PA, Stemmer A, Wagner M, Huppertz A, Hamm B, Taupitz M, Klessen C. Free-breathing echo-planar imaging based diffusion-weighted magnetic resonance imaging of the liver with prospective acquisition correction. *J Comput Assist Tomogr* 2008; **32**: 372-378
23 **Demir OI**, Obuz F, Sağol O, Dicle O. Contribution of diffusion-weighted MRI to the differential diagnosis of hepatic masses. *Diagn Interv Radiol* 2007; **13**: 81-86
24 **Bruegel M**, Holzapfel K, Gaa J, Woertler K, Waldt S, Kiefer B, Stemmer A, Ganter C, Rummeny EJ. Characterization of focal liver lesions by ADC measurements using a respiratory triggered diffusion-weighted single-shot echo-planar MR imaging technique. *Eur Radiol* 2008; **18**: 477-485
25 **Holzapfel K**, Bruegel M, Eiber M, Ganter C, Schuster T, Heinrich P, Rummeny EJ, Gaa J. Characterization of small (</=10mm) focal liver lesions: Value of respiratory-triggered echo-planar diffusion-weighted MR imaging. *Eur J Radiol* 2009; Epub ahead of print
26 **Coenegrachts K**, Matos C, ter Beek L, Metens T, Haspeslagh M, Bipat S, Stoker J, Rigauts H. Focal liver lesion detection and characterization: comparison of non-contrast enhanced and SPIO-enhanced diffusion-weighted single-shot spin echo echo planar and turbo spin echo T2-weighted imaging. *Eur J Radiol* 2009; **72**: 432-439
27 **Xu H**, Li X, Xie JX, Yang ZH, Wang B. Diffusion-weighted magnetic resonance imaging of focal hepatic nodules in an experimental hepatocellular carcinoma rat model. *Acad Radiol* 2007; **14**: 279-286

28 **Xu PJ**, Yan FH, Wang JH, Lin J, Ji Y. Added value of breathhold diffusion-weighted MRI in detection of small hepatocellular carcinoma lesions compared with dynamic contrast-enhanced MRI alone using receiver operating characteristic curve analysis. *J Magn Reson Imaging* 2009; **29**: 341-349

29 **Zech CJ**, Reiser MF, Herrmann KA. Imaging of hepatocellular carcinoma by computed tomography and magnetic resonance imaging: state of the art. *Dig Dis* 2009; **27**: 114-124

30 **Vandecaveye V**, De Keyzer F, Verslype C, Op de Beeck K, Komuta M, Topal B, Roebben I, Bielen D, Roskams T, Nevens F, Dymarkowski S. Diffusion-weighted MRI provides additional value to conventional dynamic contrast-enhanced MRI for detection of hepatocellular carcinoma. *Eur Radiol* 2009; **19**: 2456-2466

31 **Willatt JM**, Hussain HK, Adusumilli S, Marrero JA. MR Imaging of hepatocellular carcinoma in the cirrhotic liver: challenges and controversies. *Radiology* 2008; **247**: 311-330

32 **Koh DM**, Brown G, Riddell AM, Scurr E, Collins DJ, Allen SD, Chau I, Cunningham D, deSouza NM, Leach MO, Husband JE. Detection of colorectal hepatic metastases using MnDPDP MR imaging and diffusion-weighted imaging (DWI) alone and in combination. *Eur Radiol* 2008; **18**: 903-910

33 **Koh DM**, Scurr E, Collins DJ, Pirgon A, Kanber B, Karanjia N, Brown G, Leach MO, Husband JE. Colorectal hepatic metastases: quantitative measurements using single-shot echo-planar diffusion-weighted MR imaging. *Eur Radiol* 2006; **16**: 1898-1905

34 **Parikh T**, Drew SJ, Lee VS, Wong S, Hecht EM, Babb JS, Taouli B. Focal liver lesion detection and characterization with diffusion-weighted MR imaging: comparison with standard breath-hold T2-weighted imaging. *Radiology* 2008; **246**: 812-822

35 **Bruegel M**, Rummeny EJ. Hepatic metastases: use of diffusion-weighted echo-planar imaging. *Abdom Imaging* 2009; Epub ahead of print

36 **Nasu K**, Kuroki Y, Nawano S, Kuroki S, Tsukamoto T, Yamamoto S, Motoori K, Ueda T. Hepatic metastases: diffusion-weighted sensitivity-encoding versus SPIO-enhanced MR imaging. *Radiology* 2006; **239**: 122-130

37 **Koh DM**, Scurr E, Collins D, Kanber B, Norman A, Leach MO, Husband JE. Predicting response of colorectal hepatic metastasis: value of pretreatment apparent diffusion coefficients. *AJR Am J Roentgenol* 2007; **188**: 1001-1008

38 **Cui Y**, Zhang XP, Sun YS, Tang L, Shen L. Apparent diffusion coefficient: potential imaging biomarker for prediction and early detection of response to chemotherapy in hepatic metastases. *Radiology* 2008; **248**: 894-900

39 **Schraml C**, Schwenzer NF, Martirosian P, Bitzer M, Lauer U, Claussen CD, Horger M. Diffusion-weighted MRI of advanced hepatocellular carcinoma during sorafenib treatment: initial results. *AJR Am J Roentgenol* 2009; **193**: W301-W307

40 **Schraml C**, Schwenzer NF, Clasen S, Rempp HJ, Martirosian P, Claussen CD, Pereira PL. Navigator respiratory-triggered diffusion-weighted imaging in the follow-up after hepatic radiofrequency ablation-initial results. *J Magn Reson Imaging* 2009; **29**: 1308-1316

41 **Goshima S**, Kanematsu M, Kondo H, Yokoyama R, Tsuge Y, Shiratori Y, Onozuka M, Moriyama N. Evaluating local hepatocellular carcinoma recurrence post-transcatheter arterial chemoembolization: is diffusion-weighted MRI reliable as an indicator? *J Magn Reson Imaging* 2008; **27**: 834-839

42 **Yu JS**, Kim JH, Chung JJ, Kim KW. Added value of diffusion-weighted imaging in the MRI assessment of perilesional tumor recurrence after chemoembolization of hepatocellular carcinomas. *J Magn Reson Imaging* 2009; **30**: 153-160

S- Editor Tian L **L- Editor** Cant MR **E- Editor** Ma WH

World Journal of Gastroenterology

Online Submissions: http://www.wjgnet.com/1007-9327office
wjg@wjgnet.com
doi:10.3748/wjg.v16.i13.1577

World J Gastroenterol 2010 April 7; 16(13): 1577-1586
ISSN 1007-9327 (print)

TOPIC HIGHLIGHT

Paul E Sijens, PhD, Associate Professor, *Series Editor*

Magnetic resonance spectroscopy to study hepatic metabolism in diffuse liver diseases, diabetes and cancer

Pieter C Dagnelie, Susanne Leij-Halfwerk

Pieter C Dagnelie, Susanne Leij-Halfwerk, Department of Epidemiology, Maastricht University, 6200 MD Maastricht, The Netherlands

Author contributions: Dagnelie PC designed the paper, wrote the introduction, discussion and conclusions as well as the sections on liver metabolism in patients with diabetes and patients with a distant malignant tumor, and carried out the final editing of the manuscript; Leij-Halfwerk S co-designed and co-edited the paper and wrote the sections on MRS in diffuse and chronic liver disease, viral hepatitis and HIV, alcohol abuse, and other liver diseases.

Correspondence to: Pieter C Dagnelie, PhD, Department of Epidemiology, Maastricht University, PO Box 616, 6200 MD Maastricht, The Netherlands. dagnelie@epid.unimaas.nl
Telephone: +31-43-3882393 Fax: +31-43-3884128
Received: February 25, 2010 Revised: March 22, 2010
Accepted: March 29, 2010
Published online: April 7, 2010

Abstract

This review provides an overview of the current state of the art of magnetic resonance spectroscopy (MRS) in *in vivo* investigations of diffuse liver disease. So far, MRS of the human liver *in vivo* has mainly been used as a research tool rather than a clinical tool. The liver is particularly suitable for static and dynamic metabolic studies due to its high metabolic activity. Furthermore, its relatively superficial position allows excellent MRS localization, while its large volume allows detection of signals with relatively low intensity. This review describes the application of MRS to study the metabolic consequences of different conditions including diffuse and chronic liver diseases, congenital diseases, diabetes, and the presence of a distant malignancy on hepatic metabolism. In addition, future prospects of MRS are discussed. It is anticipated that future technical developments such as clinical MRS magnets with higher field strength (3 T) and improved delineation of multicomponent signals such as phosphomonoester and phosphodiester using proton decoupling, especially if combined with price reductions for stable isotope tracers, will lead to intensified research into metabolic syndrome, cardiovascular disease, hepato-biliary diseases, as well as non-metastatic liver metabolism in patients with a distant malignant tumor.

Key words: Cancer; Cirrhosis; Diabetes; Diffuse liver disease; Hepatitis; Magnetic resonance spectroscopy

Peer reviewer: Paul E Sijens, PhD, Associate Professor, Radiology, UMCG, Hanzeplein 1, 9713GZ Groningen, The Netherlands

Dagnelie PC, Leij-Halfwerk S. Magnetic resonance spectroscopy to study hepatic metabolism in diffuse liver diseases, diabetes and cancer. *World J Gastroenterol* 2010; 16(13): 1577-1586 Available from: URL: http://www.wjgnet.com/1007-9327/full/v16/i13/1577.htm DOI: http://dx.doi.org/10.3748/wjg.v16.i13.1577

INTRODUCTION

The liver is a particularly suitable and interesting organ for metabolic studies as it plays a central role in intermediary metabolism, has a high metabolic activity with rapid response to metabolic insults, and is profoundly altered in acute and chronic diseases. Magnetic resonance spectroscopy (MRS) has been established as a non-invasive technique to study cellular biochemistry and metabolism, both at high magnetic strengths *in vitro* and in the whole body *in vivo* at field strengths of up to 3 T.

MRS has a number of important advantages over conventional approaches when studying metabolism in diffuse liver disease in humans. The non-invasive character of the technique allows valid assessment of the metabolic profile of many hepatic metabolites *in vivo* which cannot

be accurately measured using invasive biopsy techniques, due to the instability of these compounds and the invasiveness of biopsies. In addition, the non-destructive character of MRS, combined with the large hepatic blood flow, allows repeated measurements over time in the same subject, facilitating long-term longitudinal (observational/intervention) studies as well as short-term dynamic metabolic intervention studies with real-time monitoring of biochemical or metabolic alterations after a meal or an oral or intravenous metabolic challenge by nutrients (sugars, amino acids, lipids), hormones *etc*. Moreover, the technique can be complemented by dynamic stable isotope tracer studies, allowing the simultaneous assessment of hepatic metabolite concentrations by MRS and turnover measurements in plasma. Of note, although challenge techniques are also used in clinical practice for diagnostic purposes, for instance, to diagnose inherited metabolic errors of metabolism, MRS of the human liver *in vivo* has so far mainly been used as a research tool rather than a clinical tool.

However, one limitation of MRS studies is that only compounds present at mmol/L concentrations can be detected, due to the low inherent sensitivity of the MR signal *in vivo*.

The liver is a particularly suitable and interesting organ for metabolic studies for a number of reasons: first, it plays a central role in intermediary metabolism, has a high metabolic activity with a rapid response to metabolic insults, and is profoundly altered in acute and chronic diseases. Second, its superficial location in the right upper abdomen, covered only by a thin layer of skin, adipose tissue and muscle, allows excellent MRS localization using a double-tuned surface coil, by different localization techniques such as chemical shift imaging (spectroscopic imaging, CSI/SI)[1-3] and image-selected *in vivo* spectroscopy (ISIS)[4,5]. Third, the relatively large volume of the liver allows the detection of signals with relatively low intensity in volumes of up to 1 L; of note, for the study of diffuse liver disease, the inherent low spatial resolution of MRS does not play a restrictive role.

Different nuclei such as ^{31}P, ^{1}H, ^{13}C and ^{19}F have been applied in studies of diffuse liver disease. So far, ^{1}H MRS has mainly been applied to detect hepatic lipid levels, ^{31}P MRS to investigate intracellular energy metabolism, phospholipid metabolism and gluconeogenesis, and ^{13}C MRS to study liver lipid and glycogen metabolism. ^{1}H and ^{31}P are naturally abundant isotopes, whereas ^{13}C represents only 1% of total carbon (the majority being ^{12}C). Therefore, in many ^{13}C studies, investigators have infused ^{13}C-labeled compounds to increase the MR signal in dynamic metabolic studies.

The present review provides an overview of the current state of the art of MRS in *in vivo* investigations of diffuse liver disease. First, we discuss publications regarding the application of MRS to study diffuse and chronic liver diseases including cirrhosis, fibrosis and alcoholic liver disease, followed by the application of MRS in congenital diseases and pediatrics. We then discuss the application of MRS to study the metabolic involvement of the liver in diseases, such as diabetes or the presence of a malignant tumor elsewhere in the body. Finally, future prospects including potential clinical applications of MRS are discussed.

From the present review, we excluded T2 and MRS studies on liver iron and fat content as well as *in vitro* applications of MRS in hepato-biliary disease[6,7], as well as MRS studies of focal liver diseases such as secondary liver tumors, lymphomas and adenomas, and transplantation. We also excluded ^{19}F MRS studies of metabolites of fluorinated chemotherapeutic drugs such as 5-FU and capecitabine[8].

MRS IN DIFFUSE AND CHRONIC LIVER DISEASE

Over the last two decades, the usefulness of ^{31}P MRS for the diagnosis of liver disease has been investigated as a non-invasive alternative to liver biopsy, which is still the gold standard and carries significant morbidity[9]. The *in vivo* spectra of the human liver reflect metabolic and biochemical alterations in disease. Several publications on liver functionality have addressed spectral changes related to the underlying liver disease. However, in order to be helpful as a diagnostic tool, MR spectra should provide both sensitive and specific information for different types of liver disease, such as hepatitis, steatosis, fibrosis or cirrhosis.

The ^{31}P MRS spectrum provides information on phosphorylated compounds of hepatic metabolism: alpha-, beta- and gamma peaks of nucleotide triphosphates (NTP), inorganic phosphate (Pi), phosphomonoesters (PME) and phosphodiesters (PDE). The NTP, PME and PDE peaks are multicomponent and individual resonances of their components cannot be distinguished by the majority of techniques currently used. PME reflects components from glucose metabolism (gluconeogenesis and glycolysis) and cell membrane precursors such as phosphoethanolamine (PE) and phosphocholine (PC)[10]. The majority of the NTP resonance contains ATP components; below, we will use ATP and NTP as synonyms, following the nomenclature of the cited publications. The PDE peak contains information on cell membrane breakdown products, such as glycerophosphorylethanolamine (GPE) and glycerophosphorylcholine (GPC), and endoplasmic reticulum[11].

The diagnostic value of ^{31}P MRS for various types of diffuse liver disease has been investigated in several studies. Overall, diffuse liver disease was associated with increasing levels of PME and decreasing levels of PDE. These changes have been attributed to hepatocyte damage, increased phospholipid turnover in hepatocyte membranes, and/or altered glucose metabolism. In general, the magnitude of MRS changes increased significantly with increased disease severity and increased functional impairment.

In one of the earliest reports[12], liver metabolite concentrations were studied in 24 patients with various types of diffuse liver disease as compared to healthy control subjects. The authors reported high PME and low PDE levels in patients with acute viral hepatitis, high PME levels in patients with alcoholic hepatitis, and decreased Pi and Pi/ATP ratios in primary biliary cirrhosis and in some patients with hepatitis[12]. However, they noted that these changes were not present in all patients.

Cox *et al*[1] studied 49 patients with liver disease of varying etiology, including 25 patients with diffuse liver disease such as cirrhosis and non-hepatic malignancies. A non-specific elevation in PME/PDE was observed in the ^{31}P MR spectra of 10 (40%) out of these 25 patients with mixed diffuse liver disease. Even though the spectral pattern did not distinguish between diseases of varying etiologies, there was a linear correlation between increasing PME/PDE and a reduction in plasma albumin concentrations ($P = 0.03$).

Subsequent MRS studies showed elevated PME/NTP levels compared to healthy controls in patient populations with primary biliary cirrhosis[13] and compensated/decompensated cirrhosis of various etiology[14]. Jalan *et al*[13] studied 23 patients with primary biliary cirrhosis of varying functional severity and healthy subjects using ^{31}P MRS. PME/NTP, Pi/NTP, PME/PDE, and PME/Pi ratios were higher and PDE/NTP ratios significantly lower in patients compared with healthy volunteers. Significant correlations were seen between PME/Pi ratios and prognostic indicators such as the Christensen index, the Mayo R value, and the Pugh score.

Taylor-Robinson *et al*[14] compared 14 patients with compensated cirrhosis (Pugh's score $\leqslant$ 7) and 17 with decompensated cirrhosis (Pugh's score $\geqslant$ 8) of various etiology with healthy subjects. Worsening liver function was associated with increased PME/NTP and decreased PDE/NTP ratios. In freeze-clamped tissue, elevated PE and PC, and reduced GPE and GPC mirrored these *in vivo* changes, but no distinction was noted between compensated and decompensated cirrhosis. In contrast, electron microscopy showed that functional decompensation was associated with reduced endoplasmic reticulum (ER) in parenchymal liver disease, but elevated ER in biliary cirrhosis. In a more recent study in only 14 cirrhotic subjects[15], reduced ATP and elevated PME/PDE levels were detected in patients with decompensated cirrhosis only.

The capability of ^{31}P MRS to detect pathological processes was further investigated by comparing *in vivo* MRS results with histological samples. In 38 patients with various types of diffuse liver disease, van Wassenaer-van Hall *et al*[5] showed that the degree of elevation of PME/Ptotal in individual patients was significantly correlated with necrosis, intralobular degeneration, and portal inflammation scorings in liver biopsies[5], but not with fibrosis. However, ^{31}P MRS was not able to classify patients into diagnostic categories, such as fibrosis *vs* cirrhosis, and no diagnostic value of MRS was found with respect to steatosis and cholangitis.

Dezortova *et al*[16] studied 80 patients with liver cirrhosis of different etiology and functional status, described by Child-Pugh score, and a control group of healthy subjects. Patients with both alcoholic and viral etiology had lower absolute PDE and ATP levels than healthy subjects. Patients with alcoholic etiology, but not viral etiology, also had lower Pi levels than controls. Patients with cholestatic disease had elevated PDE levels. Thus, these authors were able to distinguish alcoholic, viral and cholestatic etiologies of liver cirrhosis based on MR spectra.

Noren *et al*[17] studied patients with non-alcoholic fatty liver disease (NAFLD) and none to moderate inflammation ($n = 13$), patients with severe fibrosis or cirrhosis ($n = 16$), and healthy controls. All patients underwent liver biopsy and extensive biochemical evaluation. Absolute concentrations and the anabolic charge (AC), defined as (PME)/[(PME)+(PDE)], were calculated. AC was increased and PDE reduced in the cirrhotic group relative to healthy subjects, whereas NAFLD patients showed values similar to controls. Using a PDE concentration of 10.5 mmol/L as a cut-off value to discriminate between mild, (F0-2) and advanced (F3-4) fibrosis, the sensitivity and specificity of PDE were 81% and 69%, respectively. AC, using a cut-off value of 0.27, showed a sensitivity of 93% and a specificity of 54%. The authors concluded that PDE is a potential marker of liver fibrosis, whereas AC is a potentially clinically useful parameter discriminating mild from advanced fibrosis.

Interestingly, few authors have performed dynamic ^{31}P MRS studies with a metabolic challenge, in contrast with diabetes and cancer (see below). In healthy subjects, it is well known that fructose infusion induces a rapid rise in PME and marked reductions in ATP and Pi[3,18,19]. An early Japanese study[20] evaluated changes in the metabolic state of the liver after an intravenous fructose load (250 mg/kg) in six patients with liver cirrhosis and eight healthy volunteers. The cirrhotic livers did not show the usual increase in PME after the fructose load, suggesting that fructose metabolism in the cirrhotic livers had impediments before the fructose-1-phosphate stage. Furthermore, the spectra of the cirrhotic livers showed a significant drop in Pi, PDE and ATP peak after the fructose challenge. Dufour and colleagues[21] studied nine patients with nonalcoholic cirrhosis. Fructose (250 mg/kg) was injected intravenously, and further spectra were collected sequentially every 6 min for 1 h. PME formation and utilization of Pi were markedly attenuated in cirrhotic patients; these measures correlated with the impairment of liver function as measured by galactose-elimination capacity[21].

In summary, the general observation in cirrhosis and fibrosis is an increase in PME, often combined with reductions in PDE and ATP. Of note, the observed changes were correlated with classical markers such as Pugh score and plasma albumin. However, ^{31}P MRS was not able to classify patients into diagnostic categories, such as fibrosis *vs* cirrhosis, and no diagnostic value of MRS was found with respect to steatosis and cholangitis.

An intravenous fructose load induced a rapid rise in PME and reductions in ATP and Pi.

VIRAL HEPATITIS AND HIV

A study of 26 patients with an acute viral hepatitis A infection showed increased PME/PDE ratios[22]. After 6 wk of recovery, these abnormalities in liver metabolites were restored to normal levels, as reflected by decreasing PME and increasing PDE[22].

Lim and colleagues[9] used ^{31}P MRS to assess disease severity in 48 patients with hepatitis C virus (HCV)-related liver disease. Worse liver function was correlated with an *in vivo* elevation in PME and decrease in PDE. PME/PDE ratios showed an increase from control (0.15), *via* mild disease (0.18) and moderate disease (0.25), to the cirrhosis group (0.38). An 80% sensitivity and specificity was achieved when using a PME/PDE ratio less than or equal to 0.2 to denote mild hepatitis and a corresponding ratio greater than or equal to 0.3 to denote cirrhosis[9]. In a subsequent study[23], the same authors applied ^{31}P MRS to prospectively study 47 patients with biopsy-proven hepatitis C undergoing viral eradication treatment with interferon and ribavirin at 6-mo intervals over a total period of 6-18 mo. In 25 out of 32 patients with virological response to HCV treatment, this was accompanied by decreasing PME/PDE ratios over time, whereas in 15 patients without virological response, PME/PDE ratios increased[23], suggesting that PME and PDE can be used to monitor treatment response to HCV.

Elevated levels of PME were also observed in a study of 75 chronic hepatitis B and C infected patients using ^{1}H-MRS[24]. In addition, compared to healthy control subjects, glutamine/glutamate and glycogen/glucose resonances were increased, whereas lipids were decreased[24]. As in studies using ^{31}P MRS, increases in metabolite levels were correlated with disease severity[24]. In a study in patients with hepatitis C virus infection (HCV, n = 14) and 20 HIV/HCV co-infected individuals[25], a significant increase in glutamine/glutamate and PME, both measured relative to hepatic lipid levels, was observed in both groups when compared with healthy individuals. These changes in metabolite ratios were attributed to an increase in the particular metabolite contents and a decrease in lipid levels. HIV/HCV-infected patients treated with anti-retroviral therapy showed elevated PME and glutamine/glutamate levels and decreased total lipid levels compared to patients not undergoing anti-retroviral treatment[25]. The authors concluded that ^{1}H-MRS could be used to detect even slight alterations in hepatic metabolite ratios in this type of patient.

Orlacchio *et al*[26] also applied ^{1}H-MRS but used the water signal as a reference instead of the lipid signal. These authors studied 23 patients with biopsy-proven precirrhotic HCV-related liver disease, graded by the Ishak fibrosis (F) scoring system. Similar to the previous studies, increasing disease severity correlated with a significant increase in choline-containing compounds and glutamine/glutamate. In contrast, lipid levels in this study were found to be increased in patients relative to healthy subjects[26].

In summary, ^{31}P MRS studies have demonstrated that PME/PDE ratios in viral hepatitis are increased, and normalization of PME/PDE over time correlates with treatment effectiveness. ^{1}H MRS studies showed increased glutamine/glutamate and glycogen/glucose resonances. The observation of either increased or decreased lipid resonances in different studies requires further investigation.

ALCOHOL ABUSE

Although the above data show that different ^{31}P MRS studies have demonstrated elevated PME/NTP levels in patient populations with alcoholic liver disease compared to healthy subjects, there are few reports on the effects of alcohol abuse and alcohol abstinence *per se*. Menon *et al*[27] studied 26 chronic alcohol abusers by ^{31}P MRS 6-12 h after their last alcoholic drink and following abstinence from alcohol. Results showed that in patients with minimal liver injury, recent drinking was associated with a significant elevation in PDE/ATP and a non-significant rise in PME/ATP, and abstinence with normalization of both metabolite ratios. In contrast, in patients with alcoholic cirrhosis, recent drinking was associated with a significant elevation in mean PME/ATP and a non-significant increase in PDE/ATP, whereas abstinence was associated with no significant change in PME/ATP but with a reduction in PDE/ATP. The authors suggested that the changes in PDE/ATP most likely reflected the induction of hepatocyte ER.

In summary, recent alcohol consumption is associated with elevated PME and PDE. In patients with minimal liver injury, both metabolites are normalized during abstinence; in contrast, in patients with cirrhosis, only PDE is normalized during alcohol abstinence.

OTHER LIVER DISEASES

Several studies have been performed on acute poisoning, inherited diseases and pediatrics using ^{31}P MRS. A study in 18 patients after acetaminophen overdose showed that liver metabolites including PME, PDE and ATP, were all dramatically decreased with increasing liver damage expressed as the international normalized ratio (INR) of prothrombin[28]. Repeated MRS measurements in the same patients would be particularly valuable to see whether improvement in liver damage could also be confirmed by ^{31}P MRS.

The presence of hemolysis, elevated liver enzymes and low platelets in pregnant women (HELLP syndrome) can be associated with disturbed hepatic metabolism. To investigate whether or not women with HELLP syndrome have detectable abnormalities of hepatic energetics, Magee *et al*[29] studied seven patients with HELLP syndrome. One pregnancy was later terminated but the other women gave birth to healthy infants. One patient with the most clinically severe HELLP syndrome by laboratory criteria exhibited MR spectra which showed a relative increase in phosphomonoester and an absolute decrease in hepatic

ATP (to 62% of control)[29]. Most patients with HELLP syndrome had normal liver metabolism as assessed by MRS, although these results show that clinically severe HELLP syndrome can be associated with disturbed hepatic metabolism consistent with that seen in hepatic ischemia and/or granulocytic infiltration of the liver.

In ten patients with severe hypothyroidism, prospective ^{31}P MRS measurements before and after thyroid hormone treatment were performed. In contrast with striated muscle, which showed a marked normalization of phosphocreatine/Pi ratios within several weeks of thyroid treatment, no changes in hepatic metabolism during treatment were detected by ^{31}P MRS[30].

In a single patient with amyloid light chain (AL) amyloidosis, hepatic ^{1}H MR spectra were characterized by small line widths, a striking increase in trimethylammonium compounds, and the presence of a further resonance at 3.8 ppm[31]. None of the healthy control subjects showed trimethylammonium levels of comparable intensity[31].

Changes in liver metabolites in inherited liver diseases have been reported using ^{31}P MRS. In a report by Dixon *et al*[32] on an infant with galactosemia, these authors showed increased levels of galactose-1-phosphate in the liver which decreased during diet therapy, paralleling the falling level of galactose-1-phosphate in red blood cells.

Elevated plasma uric acid concentrations (hyperuricemia), which are a characteristic feature in gout patients, may be caused by altered liver fructose metabolism. As hereditary fructose intolerance is known to be associated with hyperuricemia, this concept has been used in ^{31}P MRS studies[33-35]. The effect of a fructose challenge on liver metabolism was studied by ^{31}P MRS in five patients with hereditary fructose intolerance (HFI) and eight heterozygotes for HFI[33]. In patients with HFI, ingestion of small amounts of fructose was followed by an increase in sugar phosphates (PME) and a decrease in Pi in hepatic ^{31}P MR spectra, combined with a rise in plasma uric acid. ^{31}P MRS could be used to diagnose fructose intolerance in heterozygotes. Oral fructose (50 g) also led to sugar phosphate accumulation and Pi depletion in the liver, which was associated with a larger increase in plasma uric acid than in control subjects. The effect of fructose on liver Pi and plasma uric acid was most pronounced in heterozygotes with gout (n = 3). In a subsequent study in 18 additional subjects from different families with familial gout[34], the authors demonstrated a positive association between response in ^{31}P MR spectra (i.e. increase in PME, decrease in Pi) and response in serum uric acid after oral glucose, suggesting ^{31}P MRS as a method for initial screening of this defect.

Limited MRS data are available in the pediatric population. Nevertheless, ^{31}P MR spectra of infants have been compared with adult spectra in an attempt to investigate changes in hepatic metabolism with age[36]. Spectra from three infants showed that PME/ATP levels were markedly higher than in adults, whereas PDE/ATP levels were decreased when compared with adults. Spectral hepatic concentrations of a single adolescent studied were intermediary between the neonates and the adults. The authors hypothesized that this indicated an increased rate of membrane synthesis in the infant livers, and concluded that these differences should be taken into account when comparing studies using varying ages[36].

In summary, a considerable amount of data on the use of MRS for the study of liver metabolism in disease is currently available, although most studies were performed in relatively small groups. Static measurements mainly reveal alterations in relative PME and/or PDE concentrations as compared to healthy controls. In contrast, dynamic applications of the MRS technique to obtain information during a challenge have remained limited to date. Challenge tests will be discussed in more detail in the following sections.

LIVER METABOLISM IN PATIENTS WITH DIABETES

Impairment of hypoglycemic counterregulation, which occurs even in intensively treated type diabetes, has traditionally been attributed to deficits in counterregulatory hormone secretion in type I diabetes, and to impaired hormone sensitivity of target organs in type Ⅱ diabetes. In the normal fed state, the liver takes up glucose for energy production (*via* glycolysis and TCA cycle) and stores excess energy as glycogen, whereas in the fasted state, the liver releases glucose produced from glycogen and *via* gluconeogenesis; in fact, the liver is almost exclusively responsible for endogenous glucose production (EGP). After a glucose load, liver glycogen can be synthesized both directly from glucose (*via* glucose-6P, glucose-1P and UDP-glucose) and indirectly from 3 carbon units (*via* phosphoenolpyruvate-glucose-6P *etc*.). ^{13}C MRS, either at natural abundance or combined with ^{13}C tracer infusion, provides a tool to study glycogen content in the liver and thus, in dynamic studies, net glycogen synthesis and breakdown over time. Moreover, combined with turnover measurements using deuterated glucose tracer infusions and measurement of isotopic enrichment of UDP-glucose using acetaminophen (measured as acetaminophen glucuronide in plasma/urine) allows an estimation of relative contributions of the direct and indirect pathways of glycogen synthesis. Noninvasive sampling of hepatic glutamine pools by oral administration of phenylacetate allows simultaneous estimation of the contribution of pyruvate oxidation to the TCA cycle flux[37].

Over the past decades, ^{13}C MRS studies have significantly contributed to the notion that the liver plays a critical role in the derangements of plasma glucose regulation in both type I and type Ⅱ diabetes. Most MRS studies to date have been performed in diabetes type I. To determine alterations in the direct and indirect pathways of glycogen synthesis in diabetes, Cline and coworkers[37] studied subjects with poorly controlled diabetes type I using a 5 h hyperglycemic-hyperinsulinemic clamp (plasma glucose: 9 mmol/L, insulin: 400 pmol/L) and [1-13C]-glucose. Hepatic pools of UDP-glucose and glutamine

were noninvasively sampled by oral administration of acetaminophen and phenylacetate, respectively. Although total hepatic glycogen synthesis was similar in both groups, the flux through the indirect (gluconeogenic) pathway was found to be proportionately about twice as active in the diabetic subjects compared to the control subjects. Moreover, the relative contribution of pyruvate oxidation to the TCA cycle flux in diabetic subjects was decreased by circa 30%, indicating reduced glycolysis. The abnormalities were not immediately reversed by normalizing intraportal concentrations of glucose, insulin and glucagon, and might contribute to postprandial hyperglycemia.

Hwang *et al*[38] studied poorly controlled diabetes type I patients and weight-matched control subjects during a day in which three isocaloric mixed meals were ingested. Although fasting hepatic glycogen levels were identical in the two groups, the diabetic subjects synthesized less glycogen over the day than healthy subjects. Again, the flux through the gluconeogenic pathway relative to the direct pathway of glycogen synthesis was markedly reduced in diabetic subjects.

Bischof *et al*[39] studied poorly controlled diabetes type I patients (HbA1C: 8.8% and matched non-diabetic subjects (HbA1C: 5.5%) in an experiment over 24 h with 3 isocaloric mixed meals. Over 24 h, the mean plasma glucose concentration was 2.4-fold higher in diabetic subjects. Net liver glycogen synthesis and breakdown were calculated from linear regression of the glycogen concentration time curves from 19:30-22:30, and 22:30-8:00, respectively. Glycogen synthesis was reduced by 74% and glycogen breakdown by 47%, and both were partly but not completely normalized by intensified insulin treatment.

In a subsequent study in long-term well-controlled diabetes type I patients, Bischof *et al*[40], showed that tight glycemic control in diabetes type I patients normalized overall glycogen synthesis and breakdown as well as glucose production. However, the relative contribution of the indirect pathway of glycogen synthesis remained elevated in diabetic subjects, a finding which indicated augmented gluconeogenesis in type I diabetic patients, which would be consistent with experimental models showing increased PEP-carboxykinase and/or reduced glucokinase activity in the liver of diabetic animals.

Also, in 6 to 12-year-old children with diabetes type I [41], the capacity to replenish hepatic glycogen after an overnight fast was at least as good as in age-matched healthy children.

Kishore *et al*[42] compared the hepatic response to hypoglycemia in well-controlled type I diabetes patients and healthy subjects. In the overnight fasted state, diabetes type I patients had decreased hepatic glycogen levels compared to controls. In insulin-induced hypoglycemia, the normal response of glycogenolysis observed in healthy subjects was virtually absent in diabetic subjects.

Type Ⅱ diabetes patients were studied by Magnusson *et al*[43], who compared seven diabetic (mean duration 13 years) and five healthy subjects matched for age and body mass index (BMI) during 23 h of fasting after an initial liquid meal. Oral medication with sulfonylurea agents (n = 5) was discontinued 3 d before the study and insulin treatment (n = 2) was discontinued the evening before the study. Blood glucose levels in the diabetic subjects were consistently higher throughout the experiment. Four hours after the meal, hepatic glycogen levels in diabetic subjects were < 50% of those in control subjects. During the subsequent fasting period, glycogen breakdown was reduced in diabetic subjects; instead, their rate of gluconeogenesis was markedly increased, resulting in a circa 20% overall increase in glucose output compared to healthy subjects.

Krssak and colleagues[44] studied hepatic glycogen synthesis, glycogen breakdown and gluconeogenesis in patients with type Ⅱ diabetes (mean duration 6 years) and age- and weight-matched healthy subjects before and after a mixed meal. Hepatic glycogen concentrations were lower in diabetic patients before and after dinner, and post-meal glycogen synthesis was reduced by circa 44%. Overnight, rates of glycogenolysis were also circa 50% lower in diabetic patients than controls. Endogenous glucose production was elevated in diabetic patients before dinner and remained so for 3 h after dinner; also, the nadir of glucose production was delayed in diabetic patients (240 min *vs* 60-90 min); thereafter, glucose production in patients and controls was similar. At 6-9 h after dinner, gluconeogenesis amounted to 67% of EGP in diabetic patients *vs* 43% in controls.

During a subsequent hyperglycemic-hyperinsulinemic clamp, glycogen synthesis was circa 46% lower in diabetic patients, with a similar contribution from the direct and indirect pathways. Glycogen breakdown was similar, resulting in circa 54% lower net glycogen synthesis. EGP was circa 30% elevated in diabetic patients both before and during the clamp. Hepatocellular lipid content was three times higher in type Ⅱ diabetic patients and negatively correlated with rates of net glycogen synthesis and whole-body glucose uptake during the clamp test (which was circa 37% reduced in diabetic patients)[44]. Petersen *et al*[45] demonstrated that an average weight loss of 8 kg in type Ⅱ diabetic patients over a period of 7 wk led to normalization of plasma glucose concentrations as well as hepatic glycogenolysis, glucose production and gluconeogenesis, indicating marked restoration of hepatic insulin sensitivity. These changes were associated with a reduction in hepatic lipid content from 12% to 3%, whereas muscle lipid content and muscle insulin resistance remained unchanged[45].

In summary, the presence of marked alterations in hepatic glucose and glycogen metabolism in type I and type Ⅱ diabetes has been substantiated by ^{13}C MRS in combination with isotope tracer studies. When compared with non-diabetic humans, both patients with type I and type Ⅱ diabetes exhibit elevated endogenous glucose production by increased gluconeogenesis, combined with reduced glycogen synthesis and breakdown. In type I diabetes, this defect can be partly restored by combined long- and short-term optimized treatment with insulin. In contrast, in type Ⅱ diabetes, increased gluconeogenesis appears to be the main cause of elevated glucose

production and fasting hyperglycemia, and it is normalized by weight reduction.

LIVER METABOLISM IN PATIENTS WITH A DISTANT MALIGNANT TUMOUR

The cancer-bearing state is generally associated with profound alterations in host metabolism. Many patients lose weight due to decreasing fat and muscle mass, a condition known as cancer cachexia, which not only leads to functional decline but is also an important predictor of poor prognosis. Although cancer cachexia is partly caused by decreased appetite, altered metabolism in host organs such as liver and muscle are now thought to play a major role in the pathogenesis of the condition. So far, most studies have concentrated on experimental animal models of cancer cachexia. To further explore the role of altered liver metabolism in the etiology of cancer cachexia in humans, Dagnelie *et al*[46] and Leij-Halfwerk *et al*[47-51] performed a series of studies in patients with advanced lung and breast cancer. Importantly, patients were only included if they were free of liver metastases, as confirmed by CT and/or ultrasound. In all studies, weight-stable and weight-losing cancer patients were compared with healthy subjects. Dietary energy intake was similar in all subjects, and all spectra were acquired in the overnight-fasted state. Since ATP peak areas differed between patients and controls, total phosphorous content of the liver (which was demonstrated to be stable) was used as a reference.

In one study, ATP peak areas were significantly reduced in both weight-stable (WS) and weight-losing (WL) cancer patients[46]; in the second study, the reduction was only statistically significant in WL but not WS cancer patients[47]. During a 90-min infusion of 2.8 mmol/kg per minute of the gluconeogenic amino acid alanine, liver ATP levels decreased in healthy subjects and patients to a similar extent for 60 min; however, from 60-90 min, ATP levels in WS cancer patients and healthy subjects recovered to baseline values despite continued infusion, but further decreased in WL patients, indicating impaired ATP recovery[47]. Intravenous infusion of ATP at 75 μg/kg per minute over 24 h induced complete normalization of liver ATP levels both in WL and WS patients to levels similar to healthy subjects[51].

As shown in Figure 1, baseline PME values in the liver were markedly increased in WL cancer patients relative to WS patients and healthy controls, due to increased glucose cycling and gluconeogenesis as indicated by both the observed downfield alteration of the PME chemical shift[46] and the significant correlation of PME levels with glucose turnover and gluconeogenesis from alanine[49]. Baseline alanine turnover as measured by tracer techniques was elevated in WL cancer patients, but not in WS patients[48]. L-alanine infusion induced a steady 33% rise in PME in healthy subjects (Figure 1). In WS cancer patients, a markedly faster and higher (i.e. 69%) response of PME to alanine infusion was observed, whereas WL patients showed virtually no further rise in PME (7%) relative to their already elevated baseline PME levels (Figure 1)[48].

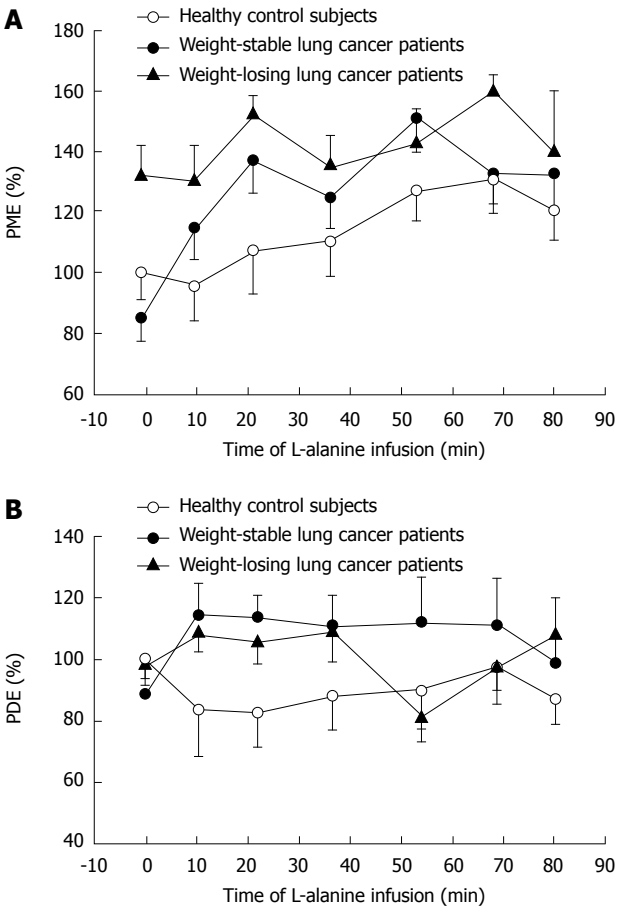

Figure 1 PME (A) and PDE (B) concentrations in the liver of healthy control subjects (*n* = 9) as well as weight-stable (*n* = 10) and weight-losing (*n* = 7) lung cancer patients during a primed-constant infusion of L-alanine (initial priming, 1.4-2.8 mmol/kg; infusion, 2.8 mmol/kg per hour). Curves represent means; bars, SE. Values are expressed as percentage of mean baseline value of healthy subjects (100%). Times during L-alanine infusion are mid-time points of 31P MRS data collection referenced to the start of the L-alanine infusion (0 = baseline). From[50], with permission.

In cancer patients, but not in healthy subjects, the rise in PME levels during alanine infusion was strongly inversely correlated with baseline PME (r = -0.82). Liver intracellular pH increased in the order: healthy < cancer-WS < cancer-WL[46], suggesting that the host liver may have a similar intra-extracellular pH gradient as reported for cancerous tissue[52-55].

In summary, using ^{31}P MRS, marked alterations in hepatic glucose metabolism were demonstrated in the non-metastatic liver of cancer patients, as shown by elevated hepatic concentrations of gluconeogenic intermediates in the overnight-fasted state, as well as during infusion of a gluconeogenic challenge. Of note, the rapid response of the PME peak to alanine infusion demonstrated rapid induction of the gluconeogenic pathway in WS cancer patients, corroborating the power of MRS as a tool to detect enzymatic alterations within the liver.

DISCUSSION

So far, MRS has primarily been used as a research tool.

MRS *in vivo* allows rapid assessment of the metabolic profile and function, including alterations in liver metabolism and physiology under different conditions. Dynamic studies have so far mainly been performed in diabetes and cancer. The limitation of these studies is the relatively high cost of the equipment and, even more, the cost of ^{13}C enriched compounds which are infused to increase hepatic ^{13}C content and to directly monitor the signal increase of ^{13}C in different metabolites above the 1% natural abundance of ^{13}C. As high-field machines become more available in the next decades, it is expected that the application of ^{13}C MRS studies in the liver may continue. However, the possibilities of ^{31}P MRS have by no means been exhausted, as is shown by the dynamic studies demonstrating altered host liver metabolism in patients with a malignant tumor elsewhere in the body. As the studies in cancer and diabetes demonstrate, metabolic challenges such as carbohydrates (like as glucose and fructose), amino acids (such as alanine) and lipids are likely to yield substantial new knowledge in the near future.

Comparing individual papers investigating disease states is difficult as there is no overall standard for representation of data or methods. Interpretation of part of the studies in diffuse liver disease is hampered by the notion that healthy controls were not always matched for age, weight/body mass index (BMI), gender, *etc*.; often, healthy subjects were younger than patients. As it has been shown that these factors may impact the quality of the spectra[56] and concentrations of metabolites[36], attempts should be made to minimize their bias. Many studies showed substantial between-subject variability within patient and control groups, e.g. with regard to PME.

Another important issue is the difference in magnetic field strengths and techniques used in different studies with regard to spatial resolution and differences in repetition times (TR), which lead to T1 weighting. T1 weighting in quantification of metabolites in liver MRS studies has so far been relatively neglected[2]. Each data acquisition step in MRS comprises a brief excitation of nuclei of interest by irradiation with non-ionizing radiofrequency energy, followed by measurement of the signal derived from relaxing nuclei in the tissue of interest. TR is defined as the time between two subsequent radiofrequency pulses. The full information is only derived when the nuclei of interest are allowed sufficient time to fully relax. T1 weighting occurs when a new radiofrequency pulse is administered before full relaxation of the nuclei of interest. Although depending on the pulse angle, a rule of thumb is that the applied TR must be circa 5 times T1 or longer in order to obtain fully relaxed spectra. Sijens *et al*[2], using chemical shift imaging with 1 D phase encoding for localized measurement of ^{31}P metabolites to measure a large liver voxel, showed that, with a pulse angle of 70° at TR 1 s, concentrations of liver metabolites are only 54%-84% of those at full relaxation (TR 50 s). Importantly, T1 relaxation times may change in disease: Dagnelie *et al*[46] showed ATP concentrations in WL-cancer patients to be reduced relative to healthy subjects at TR 5 s and TR 20 s, but not at TR 1 s. In a later study, Leij-Halfwerk *et al*[51] showed that ATP infusion induced an increase in hepatic ATP levels at TR 15 s; however, this was not observed at TR 1 s (Leij-Halfwerk *et al*, 2002, unpublished data). Thus, accurate assessment of changes in metabolite concentrations in different conditions is only possible if TR is chosen to be sufficiently long to allow a large degree of relaxation. As the measured MR signal becomes larger as TR increases, signal to noise ratios will improve, allowing a smaller number of acquisitions per phase encoding step, thereby relatively reducing measurement time. Thus, using 4 phase encoding steps, Sijens *et al*[2] showed the following number of acquisitions and measurement time at TR 1, 5 and 20 s, respectively: 60 (4:08 min), 20 (7:20 min), and 8 acquisitions (13:20 min).

What are the prospects for the clinical application of MRS in diffuse liver disease? For use as a diagnostic tool, not only high sensitivity and specificity at an individual patient levels are essential, but also practicality of application including patient burden and costing. These requests are most likely to be fulfilled in inherited diseases, where marked metabolic alterations are typical, however, for the majority of diseases, other, less invasive tools will remain methods of first choice. However, MRS may be an excellent tool for assessing disease severity and for monitoring disease progress or recuperation, as shown e.g. in diabetes[45] and patients with primary biliary cirrhosis[13].

Finally, altered findings in MRS may predict disease progression, weight loss or survival, and thus assist in the estimation of patients' prognosis. For instance, preliminary analyses (Leij-Halfwerk & Dagnelie, unpublished observations) demonstrated that elevated baseline PME levels in WS cancer patients predicted subsequent weight loss and shorter survival.

CONCLUSION

MRS of diffuse liver disease has given important new insight in a number of diseases, including inherited diseases, hepatitis, steatosis and cirrhosis. Importantly, MRS has also allowed new insights in metabolic derangements in non-liver diseases such as diabetes and non-liver cancer. Based on the progress achieved so far by MRS studies in diabetes, it is anticipated that future technical developments such as clinical MRS magnets with higher field strength (3 T) and improved delineation of multi-component signals such as PME and PDE using proton decoupling, especially if combined with price reductions for stable isotope tracers, will lead to intensified research into metabolic syndrome, cardiovascular disease, hepato-biliary diseases, as well as non-metastatic liver metabolism in patients with a distant malignant tumor.

Of note, there are also potential drawbacks: thus, tightening regulations related to preparing and administering compounds by intravenous infusion or orally threaten to make metabolic research extremely costly (or perhaps even impossible) in the near future: a development which could have dramatic negative consequences for scientific and clinical progress in the field.

Emphasis should be placed on the development of standards of the techniques used in order to be able to compare data and to obtain valid estimates of absolute metabolite concentrations. In order to allow MRS to compete with standards of care, efforts should be made to validate results in larger patient cohorts and to minimize bias in distinguishing diseased states from healthy states.

REFERENCES

1 **Cox IJ**, Menon DK, Sargentoni J, Bryant DJ, Collins AG, Coutts GA, Iles RA, Bell JD, Benjamin IS, Gilbey S. Phosphorus-31 magnetic resonance spectroscopy of the human liver using chemical shift imaging techniques. *J Hepatol* 1992; **14**: 265-275

2 **Sijens PE**, Van Dijk P, Dagnelie PC, Oudkerk M. Non-T1-weighted 31P chemical shift imaging of the human liver. *Magn Reson Imaging* 1995; **13**: 621-628

3 **Terrier F**, Vock P, Cotting J, Ladebeck R, Reichen J, Hentschel D. Effect of intravenous fructose on the P-31 MR spectrum of the liver: dose response in healthy volunteers. *Radiology* 1989; **171**: 557-563

4 **Matson GB**, Twieg DB, Karczmar GS, Lawry TJ, Gober JR, Valenza M, Boska MD, Weiner MW. Application of image-guided surface coil P-31 MR spectroscopy to human liver, heart, and kidney. *Radiology* 1988; **169**: 541-547

5 **van Wassenaer-van Hall HN**, van der Grond J, van Hattum J, Kooijman C, Hoogenraad TU, Mali WP. 31P magnetic resonance spectroscopy of the liver: correlation with standardized serum, clinical, and histological changes in diffuse liver disease. *Hepatology* 1995; **21**: 443-449

6 **Sijens PE**. Parametric exploration of the liver by magnetic resonance methods. *Eur Radiol* 2009; **19**: 2594-2607

7 **Cox IJ**, Sharif A, Cobbold JF, Thomas HC, Taylor-Robinson SD. Current and future applications of in vitro magnetic resonance spectroscopy in hepatobiliary disease. *World J Gastroenterol* 2006; **12**: 4773-4783

8 **Klomp D**, van Laarhoven H, Scheenen T, Kamm Y, Heerschap A. Quantitative 19F MR spectroscopy at 3 T to detect heterogeneous capecitabine metabolism in human liver. *NMR Biomed* 2007; **20**: 485-492

9 **Lim AK**, Patel N, Hamilton G, Hajnal JV, Goldin RD, Taylor-Robinson SD. The relationship of in vivo 31P MR spectroscopy to histology in chronic hepatitis C. *Hepatology* 2003; **37**: 788-794

10 **Bell JD**, Cox IJ, Sargentoni J, Peden CJ, Menon DK, Foster CS, Watanapa P, Iles RA, Urenjak J. A 31P and 1H-NMR investigation in vitro of normal and abnormal human liver. *Biochim Biophys Acta* 1993; **1225**: 71-77

11 **Bailes DR**, Bryant DJ, Bydder GM, Case HA, Collins AG, Cox IJ, Evans PR, Harman RR, Hall AS, Rose MR, Ross BD, Young IR. Localised phosphorus-31 NMR spectroscopy of normal and pathological human organs in vivo using phase encoding techniques. *J Magn Reson* 1987; **74**: 158-170

12 **Oberhaensli R**, Rajagopalan B, Galloway GJ, Taylor DJ, Radda GK. Study of human liver disease with P-31 magnetic resonance spectroscopy. *Gut* 1990; **31**: 463-467

13 **Jalan R**, Sargentoni J, Coutts GA, Bell JD, Rolles K, Burroughs AK, Taylor Robinson SD. Hepatic phosphorus-31 magnetic resonance spectroscopy in primary biliary cirrhosis and its relation to prognostic models. *Gut* 1996; **39**: 141-146

14 **Taylor-Robinson SD**, Sargentoni J, Bell JD, Saeed N, Changani KK, Davidson BR, Rolles K, Burroughs AK, Hodgson HJ, Foster CS, Cox IJ. In vivo and in vitro hepatic 31P magnetic resonance spectroscopy and electron microscopy of the cirrhotic liver. *Liver* 1997; **17**: 198-209

15 **Corbin IR**, Ryner LN, Singh H, Minuk GY. Quantitative hepatic phosphorus-31 magnetic resonance spectroscopy in compensated and decompensated cirrhosis. *Am J Physiol Gastrointest Liver Physiol* 2004; **287**: G379-G384

16 **Dezortova M**, Taimr P, Skoch A, Spicak J, Hajek M. Etiology and functional status of liver cirrhosis by 31P MR spectroscopy. *World J Gastroenterol* 2005; **11**: 6926-6931

17 **Noren B**, Dahlqvist O, Lundberg P, Almer S, Kechagias S, Ekstedt M, Franzén L, Wirell S, Smedby O. Separation of advanced from mild fibrosis in diffuse liver disease using 31P magnetic resonance spectroscopy. *Eur J Radiol* 2008; **66**: 313-320

18 **Oberhaensli RD**, Galloway GJ, Taylor DJ, Bore PJ, Radda GK. Assessment of human liver metabolism by phosphorus-31 magnetic resonance spectroscopy. *Br J Radiol* 1986; **59**: 695-699

19 **Boesch C**, Elsing C, Wegmüller H, Felblinger J, Vock P, Reichen J. Effect of ethanol and fructose on liver metabolism: a dynamic 31Phosphorus magnetic resonance spectroscopy study in normal volunteers. *Magn Reson Imaging* 1997; **15**: 1067-1077

20 **Kachi K**, Araki T, Uchiyama G. [Effect of intravenous fructose load on the P-31 MR spectrum of the cirrhotic liver] *Nippon Igaku Hoshasen Gakkai Zasshi* 1991; **51**: 127-132

21 **Dufour JF**, Stoupis C, Lazeyras F, Vock P, Terrier F, Reichen J. Alterations in hepatic fructose metabolism in cirrhotic patients demonstrated by dynamic 31phosphorus spectroscopy. *Hepatology* 1992; **15**: 835-842

22 **Yamane Y**, Umeda M, O'uchi T, Mitsushima T, Nakata K, Nagataki S. Phosphorus-31 nuclear magnetic resonance in vivo spectroscopy of human liver during hepatitis A virus infection. *Dig Dis Sci* 1994; **39**: 33-38

23 **Lim AK**, Patel N, Hamilton G, Mylvahan K, Kuo YT, Goldin RD, Taylor-Robinson SD. 31P MR spectroscopy in assessment of response to antiviral therapy for hepatitis C virus-related liver disease. *AJR Am J Roentgenol* 2007; **189**: 819-823

24 **Cho SG**, Kim MY, Kim HJ, Kim YS, Choi W, Shin SH, Hong KC, Kim YB, Lee JH, Suh CH. Chronic hepatitis: in vivo proton MR spectroscopic evaluation of the liver and correlation with histopathologic findings. *Radiology* 2001; **221**: 740-746

25 **Tarasów E**, Wiercińska-Drapało A, Jaroszewicz J, Siergiejczyk L, Orzechowska-Bobkiewicz A, Prokopowicz D, Walecki J. Metabolic disturbances in liver 1H MR spectroscopy in HIV and HCV co-infected patients as a potential marker of hepatocyte activation. *Acta Radiol* 2004; **45**: 803-809

26 **Orlacchio A**, Bolacchi F, Angelico M, Mancini A, Cozzolino V, Cadioli M, Simonetti G. In vivo, high-field, 3-Tesla 1H MR spectroscopic assessment of liver fibrosis in HCV-correlated chronic liver disease. *Radiol Med* 2008; **113**: 289-299

27 **Menon DK**, Harris M, Sargentoni J, Taylor-Robinson SD, Cox IJ, Morgan MY. In vivo hepatic 31P magnetic resonance spectroscopy in chronic alcohol abusers. *Gastroenterology* 1995; **108**: 776-788

28 **Dixon RM**, Angus PW, Rajagopalan B, Radda GK. 31P magnetic resonance spectroscopy detects a functional abnormality in liver metabolism after acetaminophen poisoning. *Hepatology* 1992; **16**: 943-948

29 **Magee LA**, Dixon RM, Kemp GJ, Redman CW, Styles P. 31P magnetic resonance spectroscopy of the liver in HELLP syndrome. *Br J Obstet Gynaecol* 1999; **106**: 582-588

30 **Hagspiel KD**, von Weymarn C, McKinnon G, Haldemann R, Marincek B, von Schulthess GK. Effect of hypothyroidism on phosphorus metabolism in muscle and liver: in vivo P-31 MR spectroscopy study. *J Magn Reson Imaging* 1992; **2**: 527-532

31 **Roser W**, Stock KW. 1H MRS of liver and brain in a patient with AL amyloidosis. *Magn Reson Imaging* 1997; **15**: 993-996

32 **Dixon RM**, Ouwerkerk R, Rajagopalan B, Radda GK. 31P magnetic resonance spectroscopy of the liver in an infant with galactosaemia. *MAGMA* 1993; **1**: 119-121

33 **Oberhaensli RD**, Rajagopalan B, Taylor DJ, Radda GK, Collins JE, Leonard JV, Schwarz H, Herschkowitz N. Study

of hereditary fructose intolerance by use of 31P magnetic resonance spectroscopy. *Lancet* 1987; **2**: 931-934
34 **Seegmiller JE**, Dixon RM, Kemp GJ, Angus PW, McAlindon TE, Dieppe P, Rajagopalan B, Radda GK. Fructose-induced aberration of metabolism in familial gout identified by 31P magnetic resonance spectroscopy. *Proc Natl Acad Sci USA* 1990; **87**: 8326-8330
35 **Seegmiller JE**, Dixon RM, Kemp GJ, Angus PW, McAlindon TE, Dieppe P, Rajagopalan B, Radda GK. An aberration of fructose metabolism in familial gout identified by 31P magnetic resonance spectroscopy of the liver. *Trans Assoc Am Physicians* 1990; **103**: 298-306
36 **Iles RA**, Cox IJ, Bell JD, Dubowitz LM, Cowan F, Bryant DJ. 31P magnetic resonance spectroscopy of the human paediatric liver. *NMR Biomed* 1990; **3**: 90-94
37 **Cline GW**, Rothman DL, Magnusson I, Katz LD, Shulman GI. 13C-nuclear magnetic resonance spectroscopy studies of hepatic glucose metabolism in normal subjects and subjects with insulin-dependent diabetes mellitus. *J Clin Invest* 1994; **94**: 2369-2376
38 **Hwang JH**, Perseghin G, Rothman DL, Cline GW, Magnusson I, Petersen KF, Shulman GI. Impaired net hepatic glycogen synthesis in insulin-dependent diabetic subjects during mixed meal ingestion. A 13C nuclear magnetic resonance spectroscopy study. *J Clin Invest* 1995; **95**: 783-787
39 **Bischof MG**, Krssak M, Krebs M, Bernroider E, Stingl H, Waldhäusl W, Roden M. Effects of short-term improvement of insulin treatment and glycemia on hepatic glycogen metabolism in type 1 diabetes. *Diabetes* 2001; **50**: 392-398
40 **Bischof MG**, Bernroider E, Krssak M, Krebs M, Stingl H, Nowotny P, Yu C, Shulman GI, Waldhäusl W, Roden M. Hepatic glycogen metabolism in type 1 diabetes after long-term near normoglycemia. *Diabetes* 2002; **51**: 49-54
41 **Matyka K**, Dixon RM, Mohn A, Rajagopalan B, Shmueli E, Styles P, Dunger DB. Daytime liver glycogen accumulation, measured by 13C magnetic resonance spectroscopy, in young children with Type 1 diabetes mellitus. *Diabet Med* 2001; **18**: 659-662
42 **Kishore P**, Gabriely I, Cui MH, Di Vito J, Gajavelli S, Hwang JH, Shamoon H. Role of hepatic glycogen breakdown in defective counterregulation of hypoglycemia in intensively treated type 1 diabetes. *Diabetes* 2006; **55**: 659-666
43 **Magnusson I**, Rothman DL, Katz LD, Shulman RG, Shulman GI. Increased rate of gluconeogenesis in type II diabetes mellitus. A 13C nuclear magnetic resonance study. *J Clin Invest* 1992; **90**: 1323-1327
44 **Krssak M**, Brehm A, Bernroider E, Anderwald C, Nowotny P, Dalla Man C, Cobelli C, Cline GW, Shulman GI, Waldhäusl W, Roden M. Alterations in postprandial hepatic glycogen metabolism in type 2 diabetes. *Diabetes* 2004; **53**: 3048-3056
45 **Petersen KF**, Dufour S, Befroy D, Lehrke M, Hendler RE, Shulman GI. Reversal of nonalcoholic hepatic steatosis, hepatic insulin resistance, and hyperglycemia by moderate weight reduction in patients with type 2 diabetes. *Diabetes* 2005; **54**: 603-608
46 **Dagnelie PC**, Sijens PE, Kraus DJ, Planting AS, van Dijk P. Abnormal liver metabolism in cancer patients detected by (31)P MR spectroscopy. *NMR Biomed* 1999; **12**: 535-544
47 **Leij-Halfwerk S**, Dagneli PC, Kappert P, Oudkerk M, Sijens PE. Decreased energy and phosphorylation status in the liver of lung cancer patients with weight loss. *J Hepatol* 2000; **32**: 887-892
48 **Leij-Halfwerk S**, Dagnelie PC, van Den Berg JW, Wattimena JD, Hordijk-Luijk CH, Wilson JP. Weight loss and elevated gluconeogenesis from alanine in lung cancer patients. *Am J Clin Nutr* 2000; **71**: 583-589
49 **Leij-Halfwerk S**, Dagnelie PC, Van Den Berg JW, Wilson JH, Sijens PE. Hepatic sugar phosphate levels reflect gluconeogenesis in lung cancer: simultaneous turnover measurements and 31P magnetic resonance spectroscopy in vivo. *Clin Sci* (Lond) 2000; **98**: 167-174
50 **Leij-Halfwerk S**, van den Berg JW, Sijens PE, Wilson JH, Oudkerk M, Dagnelie PC. Altered hepatic gluconeogenesis during L-alanine infusion in weight-losing lung cancer patients as observed by phosphorus magnetic resonance spectroscopy and turnover measurements. *Cancer Res* 2000; **60**: 618-623
51 **Leij-Halfwerk S**, Agteresch HJ, Sijens PE, Dagnelie PC. Adenosine triphosphate infusion increases liver energy status in advanced lung cancer patients: an in vivo 31P magnetic resonance spectroscopy study. *Hepatology* 2002; **35**: 421-424
52 **Stubbs M**, Bhujwalla ZM, Tozer GM, Rodrigues LM, Maxwell RJ, Morgan R, Howe FA, Griffiths JR. An assessment of 31P MRS as a method of measuring pH in rat tumours. *NMR Biomed* 1992; **5**: 351-359
53 **Gerweck LE**, Seetharaman K. Cellular pH gradient in tumor versus normal tissue: potential exploitation for the treatment of cancer. *Cancer Res* 1996; **56**: 1194-1198
54 **Raghunand N**, Gillies RJ. pH and chemotherapy. *Novartis Found Symp* 2001; **240**: 199-211; discussion 265-268
55 **Gerweck LE**, Vijayappa S, Kozin S. Tumor pH controls the in vivo efficacy of weak acid and base chemotherapeutics. *Mol Cancer Ther* 2006; **5**: 1275-1279
56 **Solga SF**, Horska A, Hemker S, Crawford S, Diggs C, Diehl AM, Brancati FL, Clark JM. Hepatic fat and adenosine triphosphate measurement in overweight and obese adults using 1H and 31P magnetic resonance spectroscopy. *Liver Int* 2008; **28**: 675-681

S- Editor Tian L **L- Editor** Webster JR **E- Editor** Ma WH

World Journal of Gastroenterology

Online Submissions: http://www.wjgnet.com/1007-9327office
wjg@wjgnet.com
doi:10.3748/wjg.v16.i13.1587

World J Gastroenterol 2010 April 7; 16(13): 1587-1597
ISSN 1007-9327 (print)

TOPIC HIGHLIGHT

Paul E Sijens, PhD, Associate Professor, *Series Editor*

Liver iron content determination by magnetic resonance imaging

Konstantinos Tziomalos, Vassilios Perifanis

Konstantinos Tziomalos, 1st Propedeutic Department of Internal Medicine, Medical School, Aristotle University of Thessaloniki, AHEPA University Hospital, Thessaloniki 54636, Greece
Vassilios Perifanis, Thalassemia Unit, Hippokration Hospital, Thessaloniki 54642, Greece
Author contributions: Tziomalos K and Perifanis V jointly performed the literature search and wrote this review.
Correspondence to: Vassilios Perifanis, MD, PhD, Consultant in Hematology, 15 Neohoriou street, Thessaloniki 56727, Greece. bperifanis@yahoo.gr
Telephone: +30-2310-631183 Fax: +30-2310-992834
Received: February 3, 2010 Revised: February 25, 2010
Accepted: March 4, 2010
Published online: April 7, 2010

Abstract

Accurate evaluation of iron overload is necessary to establish the diagnosis of hemochromatosis and guide chelation treatment in transfusion-dependent anemia. The liver is the primary site for iron storage in patients with hemochromatosis or transfusion-dependent anemia, therefore, liver iron concentration (LIC) accurately reflects total body iron stores. In the past 20 years, magnetic resonance imaging (MRI) has emerged as a promising method for measuring LIC in a variety of diseases. We review the potential role of MRI in LIC determination in the most important disorders that are characterized by iron overload, that is, thalassemia major, other hemoglobinopathies, acquired anemia, and hemochromatosis. Most studies have been performed in thalassemia major and MRI is currently a widely accepted method for guiding chelation treatment in these patients. However, the lack of correlation between liver and cardiac iron stores suggests that both organs should be evaluated with MRI, since cardiac disease is the leading cause of death in this population. It is also unclear which MRI method is the most accurate since there are no large studies that have directly compared the different available techniques. The role of MRI in the era of genetic diagnosis of hemochromatosis is also debated, whereas data on the accuracy of the method in other hematological and liver diseases are rather limited. However, MRI is a fast, non-invasive and relatively accurate diagnostic tool for assessing LIC, and its use is expected to increase as the role of iron in the pathogenesis of liver disease becomes clearer.

Key words: Thalassemia major; Iron overload; Magnetic resonance imaging; Liver; Hemochromatosis; Desferrioxamine; Deferiprone; Deferasirox; Thalassemia intermedia; Myelodysplastic syndromes

Peer reviewer: Paul E Sijens, PhD, Associate Professor, Radiology, UMCG, Hanzeplein 1, 9713GZ Groningen, The Netherlands

Tziomalos K, Perifanis V. Liver iron content determination by magnetic resonance imaging. *World J Gastroenterol* 2010; 16(13): 1587-1597 Available from: URL: http://www.wjgnet.com/1007-9327/full/v16/i13/1587.htm DOI: http://dx.doi.org/10.3748/wjg.v16.i13.1587

INTRODUCTION

Iron homeostasis in humans depends exclusively on the modulation of iron absorption since iron excretion is passive (by shedding of intestinal and skin cells, and additionally, in women by menstruation), and cannot be actively upregulated[1]. Therefore, patients with excessive iron absorption (hemochromatosis) or with transfusion-dependent congenital or acquired anemia are at increased risk for developing iron overload[1]. Excessive iron is toxic because it generates free radicals and induces oxidative stress[2]. Iron overload can result in the development of diabetes and other endocrinopathies, liver cirrhosis and hepatocellular carcinoma (HCC), cardiomyopathy and

premature death in patients with thalassemia major[3-6] and hemochromatosis[7-10]. In turn, the management of iron overload with chelation therapy in thalassemia major[11-14] and with phlebotomy in hemochromatosis reduces the risk of diabetes, liver and cardiac disease and death[7-9].

The accurate evaluation of iron overload is necessary to establish the diagnosis of hemochromatosis and guide chelation treatment in transfusion-dependent anemia[3,15-17]. Serum ferritin levels are not an accurate measure of total body iron stores, particularly in patients with high iron burden, because concurrent conditions, particularly inflammation and liver disease, increase these levels independently of iron burden[16,18,19]. Serum iron, transferrin, transferrin saturation and transferrin receptor levels are also imprecise markers of body iron stores[18]. The liver is the primary site for iron storage in patients with hemochromatosis or transfusion-dependent anemia, therefore, liver iron concentration (LIC) accurately reflects total body iron stores[1,19,20]. Liver biopsy with measurement of iron concentration by atomic absorption spectroscopy is considered the gold standard for LIC assessment[16]. However, hepatic iron distribution appears to be uneven, particularly when cirrhosis is present, but also in the absence of cirrhosis[21-25]. In addition, liver biopsy is an invasive procedure and complications requiring hospitalization are observed in approximately 0.5% of patients with thalassemia major who undergo liver biopsy, even in experienced centers[26]. The risks of liver biopsy also preclude repeated biopsies, which are necessary in patients with thalassemia major in order to adjust chelation treatment and avoid iron overload and chelation-associated toxicity[3,16,17,19].

It is apparent that there is a pressing need for non-invasive methods that can provide accurate LIC measurements. Superconducting quantum interference devices (SQUIDs) has been used for this purpose, but appear to underestimate LIC and are available in only a few centers[16]. In the past 20 years, magnetic resonance imaging (MRI) has emerged as a promising method for measuring LIC in a variety of diseases. We review the potential role of MRI in LIC determination in the most important disorders characterized by iron overload, namely, thalassemia major, other hemoglobinopathies, acquired anemia, and hemochromatosis.

LITERATURE SEARCH

A literature search (using PubMed) was performed using the following key words: "thalassemia major", "iron overload", "MRI", "liver", "hemochromatosis", "desferrioxamine", "deferiprone", "deferasirox", "thalassemia intermedia", "sickle cell disease", "myelodysplastic syndromes", "bone marrow transplantation", "hepatitis C", "alcoholic liver disease" and "non-alcoholic liver disease" up to 13 January 2010. The authors also manually reviewed the references of retrieved articles for any pertinent material.

MRI METHODS FOR ASSESSING LIC

The measurement of iron overload with MRI is based on the shortening effect of the interaction of iron-containing molecules (particularly ferritin and hemosidirin) with hydrogen nuclei (mainly in water molecules) on T2 relaxation time[19,27,28]. Hepatic iron deposition with MRI can be quantified by measuring the ratio of the signal intensity of the liver and of a reference tissue (mainly paraspinous muscle, which does not develop siderosis)[27,28]. These signal intensity ratios (SIRs) can be derived from either spin-echo (SE) T2-weighted or from gradient recalled-echo (GRE) T2*-weighted sequences[27,28]. Liver siderosis can also be determined by the direct measurement of relaxation time (relaxometry), either T2 [or 1/T2 (R2)] from SE sequences or T2* [or 1/T2* (R2*)] from GRE sequences; it is also possible to measure both R2 and R2* relaxation times (hybrid method)[27,28]. SIR-measuring methods are faster than relaxometry but less sensitive, particularly in patients with severe iron overload[27,28]. In addition, SIR-measuring methods appear to have smaller interscanner reproducibility than do relaxometry methods[29,30]. Among relaxometry methods, R2 acquisition time is longer than R2* acquisition time[30].

MRI IN THALASSEMIA MAJOR

LIC determination

Some early studies have assessed the accuracy of LIC quantification by liver/muscle SIR derived from either GRE or SE sequences[21,31,32]. The correlation between LIC measured in liver biopsy and SIR was stronger when GRE sequences were used[21,31,32]. However, both methods were inaccurate in patients with severe iron overload or liver fibrosis, who represent a sizable percentage of the thalassemia population[21,31,33]. In contrast, the presence of viral hepatitis did not affect the correlation between MRI- and liver-biopsy-based LIC measurements[31]. More recent studies also have reported moderate correlations between SIR and LIC (r = 0.65-0.89)[34-36].

Regarding relaxometry methods, two large studies (n = 80 and n = 106) have reported moderate correlations between liver T2 and T2* measured in 1.5 T scanners with LIC (r = -0.82 and r = -0.81, respectively)[37,38]. The correlation coefficient between liver T2* and LIC was stronger in patients without hepatic fibrosis (-0.93 *vs* -0.68 in patients with liver fibrosis)[38]. Two smaller studies (n = 46 and n = 52, respectively) reported relatively stronger correlations between LIC and liver R2 determined in a 1.5 T and 0.5 T imager, respectively (r = 0.874 and r = 0.94, respectively)[39,40]. Interestingly, the presence of liver fibrosis reduced the accuracy of the method only in the 1.5 T scanner[39,40]. Liver inflammation and chronic hepatitis C virus (HCV) infection also had no effect on the correlation between R2 and LIC in the 0.5 T unit[39,40]. A recent study also has suggested that measuring liver R2* in higher field strength imagers (i.e. 3 T *vs* 1.5 T) yields less accurate measurements, particularly in patients with more severe iron overload[41]. However, the latter studies evaluated patients with different characteristics and their results are not directly comparable[39-41].

Several studies have shown that relaxometry methods are more accurate than SIR-measuring methods for LIC determination[30,36,42,43]. In an early comparative study, liver R2 correlated more strongly with biopsy-determined LIC than liver/paraspinous muscle SIR measured in SE sequences (r = 0.97 and 0.71, respectively)[42]. Moreover, the presence of liver fibrosis or inflammation did not affect the correlation between liver R2 and LIC[42]. Liver/subcutaneous fat SIR did not correlate significantly with LIC[42]. In another early small study (n = 10), liver R2 relaxation time measured with a 0.5 T MRI unit was better correlated with LIC than was R2* relaxation time[43]. In a large study in patients with thalassemia major (n = 57), sickle cell disease (SCD) (n = 34), thalassemia intermedia (n = 6) and other causes of iron overload (aplastic anemia, hemochromatosis and heme-metabolism defects; n = 5), liver R2 and R2* measured with a 1.5 T scanner showed a strong correlation with LIC (r = 0.98 and 0.97, respectively; Figure 1)[30]. R2 showed less variability between imaging slices and better reproducibility between examinations compared with R2*[30]. Combined measurement of R2 and R2* did not improve diagnostic accuracy[30]. We also recently showed in 94 patients with thalassemia major a strong correlation between liver R2, R2* and GRE-derived liver/muscle SIR in a 1.5 T unit[36]. Liver R2 was more accurate than the other methods in patients with more severe iron overload[36]. According to current guidelines for the management of patients with thalassemia major, MRI is a feasible alternative to liver biopsy for determining LIC[16]. The use of R2 sequences and local individual calibration is recommended[16].

LIC and iron overload in other organs in thalassemia major

Myocardial iron-overload-induced heart failure is the cause of death in approximately 60% of patients with thalassemia major[4]. Measurement of cardiac T2* is the currently recommended method for assessing cardiac iron overload[16]. However, several large cross-sectional studies (total, n = 429) have not identified a significant correlation between cardiac and liver T2*[38,44-47]. Only one large study (n = 180) has reported a weak, albeit significant, correlation between liver T2* and cardiac T2* (r = 0.18, $P < 0.05$)[48]. In smaller studies (n = 46 and 38, respectively), liver R2 and R2* did not correlate significantly with cardiac R2 and R2*[39,49,50]. We also found no correlation between myocardial R2* and liver R2, and R2* and GRE-derived liver/muscle SIR in 94 patients[36]. Only a few studies have reported a significant correlation between liver T2 and heart T2[37], or between liver R2* and cardiac R2*[51]; however, the correlation was weak (r = 0.34 and 0.23, respectively)[37,51]. Cardiac iron overload has also been reported in patients with minimal iron deposition in the liver[50-52]. Finally, in a recent large study in 652 patients with thalassemia major, liver T2* was very weakly correlated with cardiac T2* (R^2 = 0.003, P = 0.04)[53]. More importantly, liver T2* was not associated with the development of heart failure or arrhythmia, whereas cardiac T2* predicted heart failure and arrhythmia[53].

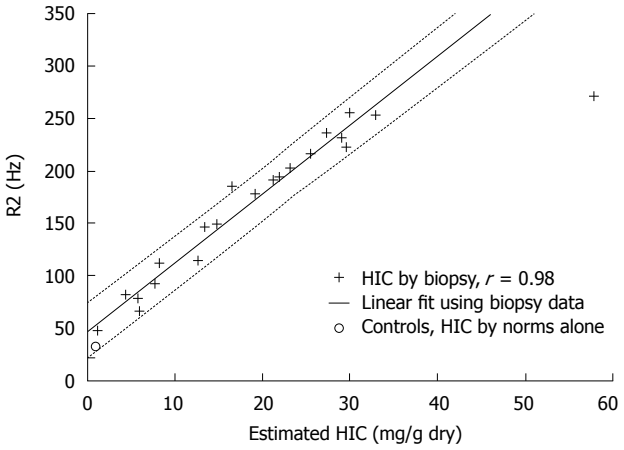

Figure 1 Plot of transverse relaxivity R2 (1/T2) *vs* biopsy-measured LIC in 20 patients (22 biopsies). *R* value was 0.98, and dotted lines indicate 95% prediction intervals for the regression. Average R2 value for 13 healthy controls is shown by "o", plotted using an LIC value estimated from normative data (no biopsy) (reproduced with permission from[30]).

The lack of correlation between liver and cardiac iron load might be explained by different mechanisms of iron uptake in the two organs[28]. In addition, small studies have suggested that iron deposition and chelation-induced clearance of iron from the heart lag behind liver iron changes[50,54]. Moreover, patients receiving treatment with different chelators might experience iron clearance from the liver and heart at different rates[46,55-58]. It appears that desferrioxamine is more or similarly effective than deferiprone in removing iron from the liver, but less effective than the latter in removing iron from the heart[46,55-58]. Deferasirox, another oral chelator, appears to be similarly effective to desferrioxamine in reducing liver iron (assessed with liver biopsy or SQUID) when appropriately dosed[59,60]. In uncontrolled studies, deferasirox also has reduced cardiac iron deposition (assessed with cardiac T2*)[61,62]. These findings suggest that myocardial iron overload should also be monitored closely in patients with thalassemia major[16]. According to recent guidelines for the management of these patients, myocardial iron deposition should be monitored with T2* MRI every year in patients with a poor chelation history, or in those with LIC, who show a non-optimal response to chelation therapy[16].

Endocrine disorders, particularly hypogonadism and diabetes, are frequently observed in patients with thalassemia major[63,64]. However, liver iron load does not appear to predict the extent of iron deposition in the pancreas or the pituitary gland, as assessed by SIR[65-67], T2[68], R2[49] or T2*[69]. However, in the largest study that has assessed the relationship between hepatic and pancreas/pituitary gland iron stores (n = 180), liver T2* correlated weakly, albeit significantly, with pancreas and pituitary gland T2* (r = 0.35 and 0.17, respectively)[48]. Liver T2* also correlated significantly with pituitary gland T2 and pituitary gland/muscle SIR (r = 0.21 and 0.63, respectively)[48]. However, liver T2* was not associated with the presence of endocrine disorders (diabetes, hypothyroidism, hypo-

gonadism and hypoparathyroidism)[48]. No differences in liver iron overload between diabetic and non-diabetic patients were reported in other studies using T2*[69,70] or SIR obtained from SE or GRE sequences[34]. There was also no correlation between liver T2* and insulin resistance or pancreatic β-cell reserve[69]. Only one small study (n = 31) has reported more severe liver iron overload (assessed with liver/paraspinous muscle SIR in GRE sequences) in diabetic patients[66]. Regarding hypogonadotropic hypogonadism, one study of 36 patients has reported no difference in liver/subcutaneous fat SIR between patients with hypogonadotropic hypogonadism and those without pituitary gland dysfunction[67], whereas another larger study (n = 50) has identified low liver T2* as a predictor of the presence of hypogonadism (but not of diabetes)[70]. The apparent lack of association between the iron burden in liver, pancreas and pituitary gland might be partly due to different mechanisms of iron accumulation in these organs[49,65-69]. In addition, pancreatic T2 and R2 are also reduced by the development of fatty degeneration, which might also confound the relationship between liver and pancreatic relaxation times in MRI[49,66,68].

Liver MRI in patients with thalassemia major who have undergone bone marrow transplantation

Allogeneic bone marrow transplantation (BMT) from an HLA-identical donor is a potentially curative treatment for thalassemia major, particularly when pre-transplantation chelation treatment is adequate and there is no portal fibrosis or hepatomegaly[71-74]. In these patients, liver iron overload progressively decreases without phlebotomy but may persist for 4-6 years after BMT in older patients[75,76]. In patients who have undergone BMT for thalassemia major, higher LIC independently predicts progression of liver fibrosis[77]. In these patients, phlebotomy reduces liver iron overload and improves liver and myocardial function[78-80]. Liver MRI has also been used in these patients to assess iron overload[81]. Measurement of liver T2 and T2* with a 1.5 T imager revealed iron overload in four out of eight patients, even though a mean time of 11.3 years had elapsed since BMT, and seven patients had received iron chelation treatment with phlebotomy, desferrioxamine or their combination for a mean 39 mo[81]. In contrast, heart T2 and T2* were normal in all patients[81].

LIC DETERMINATION WITH MRI IN OTHER HEMOGLOBINOPATHIES

Thalassemia intermedia is a diverse group of hemoglobinopathies that are characterized by less severe transfusion dependency and iron overload than in thalassemia major[82,83]. Liver iron overload assessed with measurement of the T2* relaxation time is less pronounced in patients with thalassemia intermedia than in those with thalassemia major[84]. Even though patients with thalassemia intermedia have liver iron overload compared with healthy controls, cardiac T2* does not differ between the former and the latter[84]. In a study of 26 patients with thalassemia intermedia, liver T2 strongly correlated with LIC (r = -0.82, P = 0.0003) but not with heart T2 (r = -0.17, P = 0.41)[37]. Iron overload can develop in patients with thalassemia intermedia who have not been regularly transfused[82,83]. In patients with thalassemia intermedia who received < 10 red blood cell (RBC) units, liver R2 revealed iron overload in two-thirds of the patients, whereas cardiac T2* was normal in all patients[85]. In a very recent study in 49 patients with thalassemia intermedia, liver T2* revealed the presence of hepatic iron overload in 77.5% of patients, even though 44.9% had never been transfused and only 8.2% were being regularly transfused[86]. In contrast, no patient had cardiac iron overload and liver T2* did not correlate with cardiac T2*[86].

Beta thalassemia/hemoglobin E, a frequent hemoglobinopathy in Asia, manifests as thalassemia intermedia in half of the patients and as thalassemia major in the other half[87,88]. Iron overload can develop even in patients who do not require regular transfusions and is due to increased intestinal absorption of iron[87,88]. In a pivotal study in patients with beta thalassemia/hemoglobin E (n = 41), thalassemia major (n = 9) or hereditary hemochromatosis (n = 23), liver R2 strongly correlated with LIC measured in biopsy (r = 0.98, P < 0.0001)[89]. However, R2 variability increased with increasing LIC[89].

Hemoglobin H (Hb H) disease is another frequent hemoglobinopathy in Asia, which results from the deletion of three of the four α-globin genes (deletional Hb H disease) or from deletion of two α-globin genes and a non-deletional mutation of a third α-globin gene (non-deletional Hb H disease). In all cases, there is an excess of β-globin chains that form β_4 tetramers (Hb H)[88,90,91]. The clinical phenotype of Hb H disease is variable and often resembles thalassemia intermedia[88,90,91]. Regular transfusions are infrequently required but iron overload can develop even in never-transfused patients[88,91]. Increased intestinal iron absorption due to hemolysis and ineffective erythropoiesis appears to explain the development of iron overload in these patients[91]. Non-deletional Hb H disease has more severe presentation and more frequently leads to iron overload than does deletional Hb H disease[91,92]. In an early study in 36 non-transfusion-dependent patients with Hb H disease, liver/paraspinous muscle SIR obtained from GRE sequences was more sensitive in detecting iron overload than SIR determined from SE sequences[93]. Liver iron overload was observed in 33/36 patients, whereas iron overload in the heart and pancreas were present in only one and six patients, respectively[93]. In a large study in 114 Chinese patients with Hb H disease, liver/paraspinous muscle SIR measured from GRE sequences revealed liver iron overload in 85% of the patients[92]. Iron overload was present even though only one patient was transfusion-dependent and only eight had received more than five transfusions (median number of transfusions: 5.5; range: 5-20)[92]. Patients with deletional Hb H disease had more severe iron overload than those with non-deletional Hb H disease[92]. In a smaller recent study in 37 patients with Hb H

disease or thalassemia intermedia and serum ferritin levels > 1000 pmol/L, liver T2* was abnormal in most patients (84%)[94]. Log-liver T2* correlated with serum ferritin levels but not with heart, pancreas or pituitary siderosis, as assessed by MRI, or with abnormalities in pancreatic function or the growth hormone axis[94].

Chronic RBC transfusion therapy is increasingly being used in patients with SCD, particularly for the primary or secondary prevention of stroke[95]. However, iron overload frequently develops in patients with SCD who are receiving chronic RBC transfusion therapy[96]. The development of iron overload in these patients increases the risk for hospitalization[97] and death[98], whereas chelation treatment reduces mortality[97]. In a recent study in patients with SCD, thalassemia major or bone marrow failure, liver R2* was strongly correlated with LIC assessed with liver biopsy (r = 0.96-0.98, P < 0.001), regardless of the presence of fibrosis[99]. In another study in 35 patients with SCD, liver T2 was moderately correlated with LIC (r = -0.80, P = 0.00001) but not with heart T2 (r = 0.10, P = 0.56)[37].

LIC DETERMINATION WITH MRI IN OTHER HEMATOLOGICAL DISORDERS

Iron overload frequently develops in patients with myelodysplastic syndromes (MDSs), which can result in abnormal liver function, diabetes and heart failure and increase the risk of death[100-104]. In these patients, treatment with desferrioxamine improves liver, pancreas and pituitary gland function[100,102,105]. Several small studies (n = 10 or 11) have assessed liver iron deposition by measuring liver T2* and have revealed liver iron overload in almost all patients[106-109]. Log liver T2* correlates with RBC units transfused[106,107]. In contrast, myocardial siderosis was present in only 10%-15% of patients and cardiac T2* did not correlate with liver T2*[106,108,109]. Only one study has assessed pancreas and pituitary gland siderosis with MRI in patients with MDS, and has reported no association between liver T2* and pancreas or pituitary gland siderosis, but a correlation between log liver T2* and indices of insulin resistance and reduced beta cell reserve[106]. According to recent guidelines, iron overload should be monitored in patients with MDS, using serum ferritin and transferrin levels, whereas liver MRI is considered useful but not essential[92].

Iron overload is frequently observed in patients who have undergone allogeneic BMT for hematological diseases other than thalassemia major, and results primarily from RBC transfusions[110-112]. Iron overload in these patients appears to be associated with increased risk for infections, veno-occlusive disease, hepatic dysfunction[110,113,114] and death[111,114-118]. Phlebotomy improves liver function in this population[118]. It is recommended that patients who have undergone BMT and have iron overload should be treated with phlebotomy and/or chelation therapy[112]. Liver MRI is a useful tool for quantifying body iron stores in this population[110]. In an early study in 13 children who had undergone autologous BMT, mostly for non-hematological disorders (neuroblastoma in 8 patients), liver iron overload assessed with liver/paraspinous muscle SIR measured in SE sequences was present in 10 patients (77%)[119]. Liver iron overload is correlated with RBC units transfused[119]. Three small studies (n = 32, 19 and 20) have revealed liver iron overload in the majority of patients (97%, 95% and 85%, respectively) who had undergone allogeneic BMT for leukemia, MDS, multiple myeloma, lymphoma, aplastic anemia or myelofibrosis, who had serum ferritin levels greater than the upper limit of the normal range, > 1000 ng/mL or > 1600 pmol/L, respectively[120-122]. Liver iron deposition was assessed by liver/paraspinous muscle SIR measured from GRE sequences[122], R2[121] or T2*[120]. Liver siderosis correlated with RBC units transfused[122]. Patients with more advanced liver siderosis more frequently exhibited elevated transaminases, which normalized in most of them after phlebotomy[122]. However, liver iron deposition did not correlate with heart, pancreas or pituitary siderosis as assessed by MRI, or with abnormalities in pancreatic function or the growth hormone axis[120]. In addition, the duration of post-BMT follow-up, type of graft or conditioning, and the presence of chronic graft-versus-host-disease had no effect on the presence of liver iron overload[121].

Two small case-series (n = 11 and 3, respectively) have evaluated iron overload with MRI in patients with acute leukemia or solid tumors who received multiple RBC transfusions due to chemotherapy-induced anemia[123,124]. Liver/muscle SIR identified liver iron overload in all patients, whereas cardiac T2* was marginally reduced and pancreas/skeletal muscle SIR was normal in all patients[123,124].

LIC DETERMINATION WITH MRI IN NON-HEMATOLOGICAL DISEASES

Hemochromatosis is an autosomal recessive disease with variable penetrance. In most patients, it results from a mutation of the *HFE* gene, which leads to iron overload by increasing intestinal iron absorption and by enhancing iron release from macrophages after phagocytosis of erythrocytes[7,8,15]. In an early study in 20 patients with hemochromatosis and 18 with hematological diseases (mainly MDS), liver/muscle SIR obtained from SE sequences correlated strongly with LIC (r^2 = 0.98)[125]. However, in subsequent studies in patients with suspected hemochromatosis, SIR obtained from GRE sequences has provided a more accurate determination of LIC than from SE sequences[126,127]. In a more recent and larger study in 174 patients with suspected hemochromatosis or with chronic HCV infection, Gandon *et al*[128] have shown that liver/muscle SIR obtained from GRE sequences identifies liver iron overload with high sensitivity and specificity. The severity of hepatic siderosis and the presence of cirrhosis does not affect the accuracy of MRI measurements. The diagnostic accuracy of the technique proposed by Gandon *et al*[128] has been replicated in other studies in patients

with suspected hemochromatosis, chronic HCV infection, or persistent elevation of transaminase levels[129,130]. However, it should be mentioned that this method does not appear to be accurate in assessing LIC in patients with thalassemia major or MDS, who have higher LIC than patients with hemochromatosis[35]. Two smaller studies (n = 11 and 23, respectively) have reported a strong correlation between liver R2 and biopsy-determined LIC in hemochromatosis[89,131]. Some experts consider liver MRI to be the method of choice for documenting iron overload in patients with suspected hemochromatosis[15]. Nevertheless, others argue that MRI has limited sensitivity to detect mild iron overload in patients with suspected hemochromatosis[7].

Besides hemochromatosis, mild to moderate iron overload is also present in some patients with other liver diseases, including chronic hepatitis B or C, alcoholic liver disease and non-alcoholic fatty liver disease[1,132-136]. In chronic hepatitis B or C and alcoholic liver disease, low levels of hepcidin, a protein that regulates iron absorption, may play a role in the development of iron overload[1,132-134,136]. Increased iron uptake from hepatocytes due to upregulation of transferrin receptors might also contribute[136]. In non-alcoholic fatty liver disease, insulin-induced redistribution of intracellular transferrin receptors to the hepatocyte membrane, and downregulation of the iron exporter protein due to the pro-inflammatory state present in these patients, may contribute to the development of liver iron overload[132]. MRI is a sensitive method for evaluating liver iron deposition in patients with chronic HCV infection[128-130]. However, liver biopsy is required in most of these patients to assess the presence of inflammation, fibrosis and cirrhosis.

Increased LIC is frequently observed in patients with non-biliary cirrhosis (not due to hemochromatosis) and can occasionally be severe; in contrast, liver siderosis is rare in biliary cirrhosis[1,23,134]. Liver/paraspinous muscle SIR obtained from SE or GRE sequences has revealed liver iron overload in 40% of cirrhosis patients[137]. However, in studies in patients with cirrhosis of various etiologies in whom liver biopsy had been performed, there was only a moderate correlation between liver/muscle SIR in GRE sequences and histological grading of liver siderosis (r = 0.515, $P < 0.001$)[138]. Moreover, others did not find a difference in liver iron load (assessed with SIR obtained from GRE sequences) between patients with viral hepatitis and cirrhosis[139]. In addition, liver siderosis in either SE or GRE sequences did not increase with the progression of viral hepatitis-induced cirrhosis[140]. Despite these discrepant findings, MRI might be particularly useful when cirrhosis is present because of the risk of bleeding in these patients during liver biopsy and because of the uneven iron distribution in the cirrhotic liver[21-25].

Finally, MRI might be useful for the evaluation of iron stores in porphyria cutanea tarda, a familial or sporadic disease that is characterized by decreased activity of hepatic uroporphyrinogen decarboxylase (UROD), which is frequently associated with iron overload[141]. In these patients, iron inhibits UROD activity, and phlebotomy is the treatment of choice[136,141]. A recent study in 20 patients with porphyria cutanea tarda measured liver/paraspinous muscle SIR from GRE sequences and identified liver iron overload in 11 (55%)[142].

CONCLUSION

MRI is a potentially useful non-invasive method for evaluating liver iron stores in a wide spectrum of hematological and liver diseases. Most studies have been performed in thalassemia major and MRI is currently a widely accepted method for guiding chelation treatment in these patients. However, the lack of correlation between liver and cardiac iron stores suggests that both organs should be evaluated with MRI, since cardiac disease is the leading cause of death in this population. It is also unclear which MRI method is the most accurate because there are no large studies that have directly compared the different techniques. Another issue is the reproducibility of the various methods in different centers. Liver/muscle SIR obtained from GRE sequences[128-130] and liver and heart T2* have been shown to be reproducible in different scanners[143-145] but more data are needed. The role of MRI in the era of genetic diagnosis of hemochromatosis is also debated, whereas data on the accuracy of the method in other hematological and liver diseases are rather limited. However, MRI is a fast non-invasive and relatively accurate diagnostic tool for assessing liver iron content, and its use is expected to increase as the role of iron in the pathogenesis of liver disease becomes clearer.

REFERENCES

1 **Batts KP**. Iron overload syndromes and the liver. *Mod Pathol* 2007; **20** Suppl 1: S31-S39
2 **Hentze MW**, Muckenthaler MU, Andrews NC. Balancing acts: molecular control of mammalian iron metabolism. *Cell* 2004; **117**: 285-297
3 **Rund D**, Rachmilewitz E. Beta-thalassemia. *N Engl J Med* 2005; **353**: 1135-1146
4 **Borgna-Pignatti C**, Rugolotto S, De Stefano P, Zhao H, Cappellini MD, Del Vecchio GC, Romeo MA, Forni GL, Gamberini MR, Ghilardi R, Piga A, Cnaan A. Survival and complications in patients with thalassemia major treated with transfusion and deferoxamine. *Haematologica* 2004; **89**: 1187-1193
5 **Telfer PT**, Prestcott E, Holden S, Walker M, Hoffbrand AV, Wonke B. Hepatic iron concentration combined with long-term monitoring of serum ferritin to predict complications of iron overload in thalassaemia major. *Br J Haematol* 2000; **110**: 971-977
6 **Olivieri NF**, Nathan DG, MacMillan JH, Wayne AS, Liu PP, McGee A, Martin M, Koren G, Cohen AR. Survival in medically treated patients with homozygous beta-thalassemia. *N Engl J Med* 1994; **331**: 574-578
7 **Adams PC**, Barton JC. Haemochromatosis. *Lancet* 2007; **370**: 1855-1860
8 **Pietrangelo A**. Hereditary hemochromatosis--a new look at an old disease. *N Engl J Med* 2004; **350**: 2383-2397
9 **Niederau C**, Fischer R, Pürschel A, Stremmel W, Häussinger D, Strohmeyer G. Long-term survival in patients with hereditary hemochromatosis. *Gastroenterology* 1996; **110**: 1107-1119
10 **Loréal O**, Deugnier Y, Moirand R, Lauvin L, Guyader D,

Jouanolle H, Turlin B, Lescoat G, Brissot P. Liver fibrosis in genetic hemochromatosis. Respective roles of iron and non-iron-related factors in 127 homozygous patients. *J Hepatol* 1992; **16**: 122-127
11 **Brittenham GM**, Griffith PM, Nienhuis AW, McLaren CE, Young NS, Tucker EE, Allen CJ, Farrell DE, Harris JW. Efficacy of deferoxamine in preventing complications of iron overload in patients with thalassemia major. *N Engl J Med* 1994; **331**: 567-573
12 **Ehlers KH**, Giardina PJ, Lesser ML, Engle MA, Hilgartner MW. Prolonged survival in patients with beta-thalassemia major treated with deferoxamine. *J Pediatr* 1991; **118**: 540-545
13 **Aldouri MA**, Wonke B, Hoffbrand AV, Flynn DM, Ward SE, Agnew JE, Hilson AJ. High incidence of cardiomyopathy in beta-thalassaemia patients receiving regular transfusion and iron chelation: reversal by intensified chelation. *Acta Haematol* 1990; **84**: 113-117
14 **Wolfe L**, Olivieri N, Sallan D, Colan S, Rose V, Propper R, Freedman MH, Nathan DG. Prevention of cardiac disease by subcutaneous deferoxamine in patients with thalassemia major. *N Engl J Med* 1985; **312**: 1600-1603
15 **Brissot P**, Troadec MB, Bardou-Jacquet E, Le Lan C, Jouanolle AM, Deugnier Y, Loréal O. Current approach to hemochromatosis. *Blood Rev* 2008; **22**: 195-210
16 **Angelucci E**, Barosi G, Camaschella C, Cappellini MD, Cazzola M, Galanello R, Marchetti M, Piga A, Tura S. Italian Society of Hematology practice guidelines for the management of iron overload in thalassemia major and related disorders. *Haematologica* 2008; **93**: 741-752
17 **Fischer R**, Harmatz PR. Non-invasive assessment of tissue iron overload. *Hematology Am Soc Hematol Educ Program* 2009; 215-221
18 **Kushner JP**, Porter JP, Olivieri NF. Secondary iron overload. Hematology *Am Soc Hematol Educ Program* 2001; 47-61
19 **Brittenham GM**, Badman DG. Noninvasive measurement of iron: report of an NIDDK workshop. *Blood* 2003; **101**: 15-19
20 **Angelucci E**, Brittenham GM, McLaren CE, Ripalti M, Baronciani D, Giardini C, Galimberti M, Polchi P, Lucarelli G. Hepatic iron concentration and total body iron stores in thalassemia major. *N Engl J Med* 2000; **343**: 327-331
21 **Chan YL**, Li CK, Lam CW, Yu SC, Chik KW, To KF, Yeung DK, Howard R, Yuen PM. Liver iron estimation in beta-thalassaemia: comparison of MRI biochemical assay and histological grading. *Clin Radiol* 2001; **56**: 911-916
22 **Emond MJ**, Bronner MP, Carlson TH, Lin M, Labbe RF, Kowdley KV. Quantitative study of the variability of hepatic iron concentrations. *Clin Chem* 1999; **45**: 340-346
23 **Ludwig J**, Hashimoto E, Porayko MK, Moyer TP, Baldus WP. Hemosiderosis in cirrhosis: a study of 447 native livers. *Gastroenterology* 1997; **112**: 882-888
24 **Villeneuve JP**, Bilodeau M, Lepage R, Côté J, Lefebvre M. Variability in hepatic iron concentration measurement from needle-biopsy specimens. *J Hepatol* 1996; **25**: 172-177
25 **Ambu R**, Crisponi G, Sciot R, Van Eyken P, Parodo G, Iannelli S, Marongiu F, Silvagni R, Nurchi V, Costa V. Uneven hepatic iron and phosphorus distribution in beta-thalassemia. *J Hepatol* 1995; **23**: 544-549
26 **Angelucci E**, Baronciani D, Lucarelli G, Baldassarri M, Galimberti M, Giardini C, Martinelli F, Polchi P, Polizzi V, Ripalti M. Needle liver biopsy in thalassaemia: analyses of diagnostic accuracy and safety in 1184 consecutive biopsies. *Br J Haematol* 1995; **89**: 757-761
27 **Argyropoulou MI**, Astrakas L. MRI evaluation of tissue iron burden in patients with beta-thalassaemia major. *Pediatr Radiol* 2007; **37**: 1191-1200; quiz 1308-1309
28 **Wood JC**. Magnetic resonance imaging measurement of iron overload. *Curr Opin Hematol* 2007; **14**: 183-190
29 **Virtanen JM**, Komu ME, Parkkola RK. Quantitative liver iron measurement by magnetic resonance imaging: in vitro and in vivo assessment of the liver to muscle signal intensity and the R2* methods. *Magn Reson Imaging* 2008; **26**: 1175-1182
30 **Wood JC**, Enriquez C, Ghugre N, Tyzka JM, Carson S, Nelson MD, Coates TD. MRI R2 and R2* mapping accurately estimates hepatic iron concentration in transfusion-dependent thalassemia and sickle cell disease patients. *Blood* 2005; **106**: 1460-1465
31 **Angelucci E**, Giovagnoni A, Valeri G, Paci E, Ripalti M, Muretto P, McLaren C, Brittenham GM, Lucarelli G. Limitations of magnetic resonance imaging in measurement of hepatic iron. *Blood* 1997; **90**: 4736-4742
32 **Bonetti MG**, Castriota-Scanderbeg A, Criconia GM, Mazza P, Sacco M, Amurri B, Masi C. Hepatic iron overload in thalassemic patients: proposal and validation of an MRI method of assessment. *Pediatr Radiol* 1996; **26**: 650-656
33 **Perifanis V**, Tziomalos K, Tsatra I, Karyda S, Patsiaoura K, Athanassiou-Metaxa M. Prevalence and severity of liver disease in patients with b thalassemia major. A single-institution fifteen-year experience. *Haematologica* 2005; **90**: 1136-1138
34 **Ooi GC**, Khong PL, Chan GC, Chan KN, Chan KL, Lam W, Ng I, Ha SY. Magnetic resonance screening of iron status in transfusion-dependent beta-thalassaemia patients. *Br J Haematol* 2004; **124**: 385-390
35 **Rose C**, Vandevenne P, Bourgeois E, Cambier N, Ernst O. Liver iron content assessment by routine and simple magnetic resonance imaging procedure in highly transfused patients. *Eur J Haematol* 2006; **77**: 145-149
36 **Christoforidis A**, Perifanis V, Spanos G, Vlachaki E, Economou M, Tsatra I, Athanassiou-Metaxa M. MRI assessment of liver iron content in thalassamic patients with three different protocols: comparisons and correlations. *Eur J Haematol* 2009; **82**: 388-392
37 **Voskaridou E**, Douskou M, Terpos E, Papassotiriou I, Stamoulakatou A, Ourailidis A, Loutradi A, Loukopoulos D. Magnetic resonance imaging in the evaluation of iron overload in patients with beta thalassaemia and sickle cell disease. *Br J Haematol* 2004; **126**: 736-742
38 **Anderson LJ**, Holden S, Davis B, Prescott E, Charrier CC, Bunce NH, Firmin DN, Wonke B, Porter J, Walker JM, Pennell DJ. Cardiovascular T2-star (T2*) magnetic resonance for the early diagnosis of myocardial iron overload. *Eur Heart J* 2001; **22**: 2171-2179
39 **Alexopoulou E**, Stripeli F, Baras P, Seimenis I, Kattamis A, Ladis V, Efstathopoulos E, Brountzos EN, Kelekis AD, Kelekis NL. R2 relaxometry with MRI for the quantification of tissue iron overload in beta-thalassemic patients. *J Magn Reson Imaging* 2006; **23**: 163-170
40 **Papakonstantinou O**, Kostaridou S, Maris T, Gouliamos A, Premetis E, Kouloulias V, Nakopoulou L, Kattamis C. Quantification of liver iron overload by T2 quantitative magnetic resonance imaging in thalassemia: impact of chronic hepatitis C on measurements. *J Pediatr Hematol Oncol* 1999; **21**: 142-148
41 **Storey P**, Thompson AA, Carqueville CL, Wood JC, de Freitas RA, Rigsby CK. R2* imaging of transfusional iron burden at 3T and comparison with 1.5T. *J Magn Reson Imaging* 2007; **25**: 540-547
42 **Papakonstantinou OG**, Maris TG, Kostaridou V, Gouliamos AD, Koutoulas GK, Kalovidouris AE, Papavassiliou GB, Kordas G, Kattamis C, Vlahos LJ. Assessment of liver iron overload by T2-quantitative magnetic resonance imaging: correlation of T2-QMRI measurements with serum ferritin concentration and histologic grading of siderosis. *Magn Reson Imaging* 1995; **13**: 967-977
43 **Gomori JM**, Horev G, Tamary H, Zandback J, Kornreich L, Zaizov R, Freud E, Krief O, Ben-Meir J, Rotem H. Hepatic iron overload: quantitative MR imaging. *Radiology* 1991; **179**: 367-369
44 **Leung AW**, Chu WC, Lam WW, Lee V, Li CK. Magnetic

resonance imaging assessment of cardiac and liver iron load in transfusion dependent patients. *Pediatr Blood Cancer* 2009; **53**: 1054-1059

45 **Maris TG**, Papakonstantinou O, Chatzimanoli V, Papadakis A, Pagonidis K, Papanikolaou N, Karantanas A, Gourtsoyiannis N. Myocardial and liver iron status using a fast T*2 quantitative MRI (T*2qMRI) technique. *Magn Reson Med* 2007; **57**: 742-753

46 **Perifanis V**, Christoforidis A, Vlachaki E, Tsatra I, Spanos G, Athanassiou-Metaxa M. comparison of effects of different long-term iron-chelation regimens on myocardial and hepatic iron concentrations assessed with T2* magnetic resonance imaging in patients with beta-thalassemia major. *Int J Hematol* 2007; **86**: 385-389

47 **Tanner MA**, Galanello R, Dessi C, Westwood MA, Smith GC, Nair SV, Anderson LJ, Walker JM, Pennell DJ. Myocardial iron loading in patients with thalassemia major on deferoxamine chelation. *J Cardiovasc Magn Reson* 2006; **8**: 543-547

48 **Au WY**, Lam WW, Chu WW, Yuen HL, Ling AS, Li RC, Chan HM, Lee HK, Law MF, Liu HS, Liang R, Ha SY. A cross-sectional magnetic resonance imaging assessment of organ specific hemosiderosis in 180 thalassemia major patients in Hong Kong. *Haematologica* 2008; **93**: 784-786

49 **Papakonstantinou O**, Alexopoulou E, Economopoulos N, Benekos O, Kattamis A, Kostaridou S, Ladis V, Efstathopoulos E, Gouliamos A, Kelekis NL. Assessment of iron distribution between liver, spleen, pancreas, bone marrow, and myocardium by means of R2 relaxometry with MRI in patients with beta-thalassemia major. *J Magn Reson Imaging* 2009; **29**: 853-859

50 **Noetzli LJ**, Carson SM, Nord AS, Coates TD, Wood JC. Longitudinal analysis of heart and liver iron in thalassemia major. *Blood* 2008; **112**: 2973-2978

51 **Aessopos A**, Fragodimitri C, Karabatsos F, Hatziliami A, Yousef J, Giakoumis A, Dokou A, Gotsis ED, Berdoukas V, Karagiorga M. Cardiac magnetic resonance imaging R2* assessments and analysis of historical parameters in patients with transfusion-dependent thalassemia. *Haematologica* 2007; **92**: 131-132

52 **Anderson LJ**, Westwood MA, Prescott E, Walker JM, Pennell DJ, Wonke B. Development of thalassaemic iron overload cardiomyopathy despite low liver iron levels and meticulous compliance to desferrioxamine. *Acta Haematol* 2006; **115**: 106-108

53 **Kirk P**, Roughton M, Porter JB, Walker JM, Tanner MA, Patel J, Wu D, Taylor J, Westwood MA, Anderson LJ, Pennell DJ. Cardiac T2* magnetic resonance for prediction of cardiac complications in thalassemia major. *Circulation* 2009; **120**: 1961-1968

54 **Anderson LJ**, Westwood MA, Holden S, Davis B, Prescott E, Wonke B, Porter JB, Walker JM, Pennell DJ. Myocardial iron clearance during reversal of siderotic cardiomyopathy with intravenous desferrioxamine: a prospective study using T2* cardiovascular magnetic resonance. *Br J Haematol* 2004; **127**: 348-355

55 **Anderson LJ**, Wonke B, Prescott E, Holden S, Walker JM, Pennell DJ. Comparison of effects of oral deferiprone and subcutaneous desferrioxamine on myocardial iron concentrations and ventricular function in beta-thalassaemia. *Lancet* 2002; **360**: 516-520

56 **Pepe A**, Lombardi M, Positano V, Cracolici E, Capra M, Malizia R, Prossomariti L, De Marchi D, Midiri M, Maggio A. Evaluation of the efficacy of oral deferiprone in beta-thalassemia major by multislice multiecho T2*. *Eur J Haematol* 2006; **76**: 183-192

57 **Pennell DJ**, Berdoukas V, Karagiorga M, Ladis V, Piga A, Aessopos A, Gotsis ED, Tanner MA, Smith GC, Westwood MA, Wonke B, Galanello R. Randomized controlled trial of deferiprone or deferoxamine in beta-thalassemia major patients with asymptomatic myocardial siderosis. *Blood* 2006; **107**: 3738-3744

58 **Maggio A**, D'Amico G, Morabito A, Capra M, Ciaccio C, Cianciulli P, Di Gregorio F, Garozzo G, Malizia R, Magnano C, Mangiagli A, Quarta G, Rizzo M, D'Ascola DG, Rizzo A, Midiri M. Deferiprone versus deferoxamine in patients with thalassemia major: a randomized clinical trial. *Blood Cells Mol Dis* 2002; **28**: 196-208

59 **Piga A**, Galanello R, Forni GL, Cappellini MD, Origa R, Zappu A, Donato G, Bordone E, Lavagetto A, Zanaboni L, Sechaud R, Hewson N, Ford JM, Opitz H, Alberti D. Randomized phase II trial of deferasirox (Exjade, ICL670), a once-daily, orally-administered iron chelator, in comparison to deferoxamine in thalassemia patients with transfusional iron overload. *Haematologica* 2006; **91**: 873-880

60 **Cappellini MD**, Cohen A, Piga A, Bejaoui M, Perrotta S, Agaoglu L, Aydinok Y, Kattamis A, Kilinc Y, Porter J, Capra M, Galanello R, Fattoum S, Drelichman G, Magnano C, Verissimo M, Athanassiou-Metaxa M, Giardina P, Kourakli-Symeonidis A, Janka-Schaub G, Coates T, Vermylen C, Olivieri N, Thuret I, Opitz H, Ressayre-Djaffer C, Marks P, Alberti D. A phase 3 study of deferasirox (ICL670), a once-daily oral iron chelator, in patients with beta-thalassemia. *Blood* 2006; **107**: 3455-3462

61 **Pathare A**, Taher A, Daar S. Deferasirox (Exjade) significantly improves cardiac T2* in heavily iron-overloaded patients with beta-thalassemia major. *Ann Hematol* 2010; **89**: 405-409

62 **Pennell DJ**, Porter JB, Cappellini MD, El-Beshlawy A, Chan LL, Aydinok Y, Elalfy MS, Sutcharitchan P, Li CK, Ibrahim H, Viprakasit V, Kattamis A, Smith G, Habr D, Domokos G, Roubert B, Taher A. Efficacy of deferasirox in reducing and preventing cardiac iron overload in {beta}-thalassemia. *Blood* 2009; Epub ahead of print

63 **Christoforidis A**, Perifanis V, Tsatra I, Vlachaki E, Athanassiou-Metaxa M. Evolution of OGTT in patients with beta-thalassaemia major in relation to chelation therapy. *Diabetes Res Clin Pract* 2007; **76**: 6-11

64 **Cunningham MJ**, Macklin EA, Neufeld EJ, Cohen AR. Complications of beta-thalassemia major in North America. *Blood* 2004; **104**: 34-39

65 **Christoforidis A**, Haritandi A, Tsitouridis I, Tsatra I, Tsantali H, Karyda S, Dimitriadis AS, Athanassiou-Metaxa M. Correlative study of iron accumulation in liver, myocardium, and pituitary assessed with MRI in young thalassemic patients. *J Pediatr Hematol Oncol* 2006; **28**: 311-315

66 **Papakonstantinou O**, Ladis V, Kostaridou S, Maris T, Berdousi H, Kattamis C, Gourtsoyiannis N. The pancreas in beta-thalassemia major: MR imaging features and correlation with iron stores and glucose disturbances. *Eur Radiol* 2007; **17**: 1535-1543

67 **Argyropoulou MI**, Kiortsis DN, Efremidis SC. MRI of the liver and the pituitary gland in patients with beta-thalassemia major: does hepatic siderosis predict pituitary iron deposition? *Eur Radiol* 2003; **13**: 12-16

68 **Argyropoulou MI**, Kiortsis DN, Astrakas L, Metafratzi Z, Chalissos N, Efremidis SC. Liver, bone marrow, pancreas and pituitary gland iron overload in young and adult thalassemic patients: a T2 relaxometry study. *Eur Radiol* 2007; **17**: 3025-3030

69 **Au WY**, Lam WW, Chu W, Tam S, Wong WK, Liang R, Ha SY. A T2* magnetic resonance imaging study of pancreatic iron overload in thalassemia major. *Haematologica* 2008; **93**: 116-119

70 **Lam WW**, Au WY, Chu WC, Tam S, Ha SY, Pennell DJ. One-stop measurement of iron deposition in the anterior pituitary, liver, and heart in thalassemia patients. *J Magn Reson Imaging* 2008; **28**: 29-33

71 **Di Bartolomeo P**, Santarone S, Di Bartolomeo E, Olioso P, Bavaro P, Papalinetti G, Di Carlo P, Papola F, Nicolucci A, Di Nicola M, Iacone A. Long-term results of survival in

patients with thalassemia major treated with bone marrow transplantation. *Am J Hematol* 2008; **83**: 528-530
72 **Lucarelli G**, Clift RA, Galimberti M, Angelucci E, Giardini C, Baronciani D, Polchi P, Andreani M, Gaziev D, Erer B, Ciaroni A, D'Adamo F, Albertini F, Muretto P. Bone marrow transplantation in adult thalassemic patients. *Blood* 1999; **93**: 1164-1167
73 **Lucarelli G**, Galimberti M, Polchi P, Angelucci E, Baronciani D, Giardini C, Andreani M, Agostinelli F, Albertini F, Clift RA. Marrow transplantation in patients with thalassemia responsive to iron chelation therapy. *N Engl J Med* 1993; **329**: 840-844
74 **Lucarelli G**, Galimberti M, Polchi P, Angelucci E, Baronciani D, Giardini C, Politi P, Durazzi SM, Muretto P, Albertini F. Bone marrow transplantation in patients with thalassemia. *N Engl J Med* 1990; **322**: 417-421
75 **Muretto P**, Del Fiasco S, Angelucci E, De Rosa F, Lucarelli G. Bone marrow transplantation in thalassemia: modifications of hepatic iron overload and associated lesions after long-term engrafting. *Liver* 1994; **14**: 14-24
76 **Lucarelli G**, Angelucci E, Giardini C, Baronciani D, Galimberti M, Polchi P, Bartolucci M, Muretto P, Albertini F. Fate of iron stores in thalassaemia after bone-marrow transplantation. *Lancet* 1993; **342**: 1388-1391
77 **Angelucci E**, Muretto P, Nicolucci A, Baronciani D, Erer B, Gaziev J, Ripalti M, Sodani P, Tomassoni S, Visani G, Lucarelli G. Effects of iron overload and hepatitis C virus positivity in determining progression of liver fibrosis in thalassemia following bone marrow transplantation. *Blood* 2002; **100**: 17-21
78 **Angelucci E**, Muretto P, Lucarelli G, Ripalti M, Baronciani D, Erer B, Galimberti M, Giardini C, Gaziev D, Polchi P. Phlebotomy to reduce iron overload in patients cured of thalassemia by bone marrow transplantation. Italian Cooperative Group for Phlebotomy Treatment of Transplanted Thalassemia Patients. *Blood* 1997; **90**: 994-998
79 **Mariotti E**, Angelucci E, Agostini A, Baronciani D, Sgarbi E, Lucarelli G. Evaluation of cardiac status in iron-loaded thalassaemia patients following bone marrow transplantation: improvement in cardiac function during reduction in body iron burden. *Br J Haematol* 1998; **103**: 916-921
80 **Angelucci E**, Muretto P, Lucarelli G, Ripalti M, Baronciani D, Erer B, Galimberti M, Annibali M, Giardini C, Gaziev D, Rapa S, Polchi P. Treatment of iron overload in the "ex-thalassemic". Report from the phlebotomy program. *Ann N Y Acad Sci* 1998; **850**: 288-293
81 **Mavrogeni S**, Gotsis ED, Berdousi E, Ladis V, Verganelakis D, Toulas P, Cokkinos DV. Myocardial and hepatic T2* magnetic resonance evaluation in ex-thalassemic patients after bone-marrow transplantation. *Int J Cardiovasc Imaging* 2007; **23**: 739-745
82 **Taher A**, Isma'eel H, Cappellini MD. Thalassemia intermedia: revisited. *Blood Cells Mol Dis* 2006; **37**: 12-20
83 **Borgna-Pignatti C**. Modern treatment of thalassaemia intermedia. *Br J Haematol* 2007; **138**: 291-304
84 **Mavrogeni S**, Gotsis E, Ladis V, Berdousis E, Verganelakis D, Toulas P, Cokkinos DV. Magnetic resonance evaluation of liver and myocardial iron deposition in thalassemia intermedia and b-thalassemia major. *Int J Cardiovasc Imaging* 2008; **24**: 849-854
85 **Origa R**, Barella S, Argiolas GM, Bina P, Agus A, Galanello R. No evidence of cardiac iron in 20 never- or minimally-transfused patients with thalassemia intermedia. *Haematologica* 2008; **93**: 1095-1096
86 **Roghi A**, Cappellini MD, Wood JC, Musallam KM, Patrizia P, Fasulo MR, Cesaretti C, Taher AT. Absence of cardiac siderosis despite hepatic iron overload in Italian patients with thalassemia intermedia: an MRI T2* study. *Ann Hematol* 2009; Epub ahead of print
87 **Vichinsky E**. Hemoglobin e syndromes. *Hematology Am Soc Hematol Educ Program* 2007; 79-83
88 **Cohen AR**, Galanello R, Pennell DJ, Cunningham MJ, Vichinsky E. Thalassemia. *Hematology Am Soc Hematol Educ Program* 2004; 14-34
89 **St Pierre TG**, Clark PR, Chua-anusorn W, Fleming AJ, Jeffrey GP, Olynyk JK, Pootrakul P, Robins E, Lindeman R. Noninvasive measurement and imaging of liver iron concentrations using proton magnetic resonance. *Blood* 2005; **105**: 855-861
90 **Fucharoen S**, Viprakasit V. Hb H disease: clinical course and disease modifiers. *Hematology Am Soc Hematol Educ Program* 2009; 26-34
91 **Chui DH**, Fucharoen S, Chan V. Hemoglobin H disease: not necessarily a benign disorder. *Blood* 2003; **101**: 791-800
92 **Chen FE**, Ooi C, Ha SY, Cheung BM, Todd D, Liang R, Chan TK, Chan V. Genetic and clinical features of hemoglobin H disease in Chinese patients. *N Engl J Med* 2000; **343**: 544-550
93 **Ooi GC**, Chen FE, Chan KN, Tsang KW, Wong YH, Liang R, Chan V, Ngan H. Qualitative and quantitative magnetic resonance imaging in haemoglobin H disease: screening for iron overload. *Clin Radiol* 1999; **54**: 98-102
94 **Au WY**, Lam WW, Chu WW, Tam S, Wong WK, Lau J, Yeung YM, Liu HS, Liang R. Organ-specific hemosiderosis and functional correlation in Chinese patients with thalassemia intermedia and hemoglobin H disease. *Ann Hematol* 2009; **88**: 947-950
95 **Stuart MJ**, Nagel RL. Sickle-cell disease. *Lancet* 2004; **364**: 1343-1360
96 **Harmatz P**, Butensky E, Quirolo K, Williams R, Ferrell L, Moyer T, Golden D, Neumayr L, Vichinsky E. Severity of iron overload in patients with sickle cell disease receiving chronic red blood cell transfusion therapy. *Blood* 2000; **96**: 76-79
97 **Fung EB**, Harmatz P, Milet M, Ballas SK, De Castro L, Hagar W, Owen W, Olivieri N, Smith-Whitley K, Darbari D, Wang W, Vichinsky E. Morbidity and mortality in chronically transfused subjects with thalassemia and sickle cell disease: A report from the multi-center study of iron overload. *Am J Hematol* 2007; **82**: 255-265
98 **Ballas SK**. Iron overload is a determinant of morbidity and mortality in adult patients with sickle cell disease. *Semin Hematol* 2001; **38**: 30-36
99 **Hankins JS**, McCarville MB, Loeffler RB, Smeltzer MP, Onciu M, Hoffer FA, Li CS, Wang WC, Ware RE, Hillenbrand CM. R2* magnetic resonance imaging of the liver in patients with iron overload. *Blood* 2009; **113**: 4853-4855
100 **Takatoku M**, Uchiyama T, Okamoto S, Kanakura Y, Sawada K, Tomonaga M, Nakao S, Nakahata T, Harada M, Murate T, Ozawa K. Retrospective nationwide survey of Japanese patients with transfusion-dependent MDS and aplastic anemia highlights the negative impact of iron overload on morbidity/mortality. *Eur J Haematol* 2007; **78**: 487-494
101 **Malcovati L**, Porta MG, Pascutto C, Invernizzi R, Boni M, Travaglino E, Passamonti F, Arcaini L, Maffioli M, Bernasconi P, Lazzarino M, Cazzola M. Prognostic factors and life expectancy in myelodysplastic syndromes classified according to WHO criteria: a basis for clinical decision making. *J Clin Oncol* 2005; **23**: 7594-7603
102 **Jensen PD**, Jensen FT, Christensen T, Nielsen JL, Ellegaard J. Relationship between hepatocellular injury and transfusional iron overload prior to and during iron chelation with desferrioxamine: a study in adult patients with acquired anemias. *Blood* 2003; **101**: 91-96
103 **Schafer AI**, Cheron RG, Dluhy R, Cooper B, Gleason RE, Soeldner JS, Bunn HF. Clinical consequences of acquired transfusional iron overload in adults. *N Engl J Med* 1981; **304**: 319-324
104 **Cazzola M**, Barosi G, Gobbi PG, Invernizzi R, Riccardi A, Ascari E. Natural history of idiopathic refractory sideroblastic anemia. *Blood* 1988; **71**: 305-312
105 **Schafer AI**, Rabinowe S, Le Boff MS, Bridges K, Cheron RG,

Dluhy R. Long-term efficacy of deferoxamine iron chelation therapy in adults with acquired transfusional iron overload. *Arch Intern Med* 1985; **145**: 1217-1221
106 **Au W**, Lam W, Chu W, Tam S, Wong W, Chan H, Law M, Liu H, Liang R. A pilot MRI study of organ specific hemosiderosis and functional correlation in Chinese patients with myelodysplasia and aplastic anemia with raised ferritin levels. *Hematol Oncol* 2008; **26**: 225-228
107 **Di Tucci AA**, Matta G, Deplano S, Gabbas A, Depau C, Derudas D, Caocci G, Agus A, Angelucci E. Myocardial iron overload assessment by T2* magnetic resonance imaging in adult transfusion dependent patients with acquired anemias. *Haematologica* 2008; **93**: 1385-1388
108 **Konen E**, Ghoti H, Goitein O, Winder A, Kushnir T, Eshet Y, Rachmilewitz E. No evidence for myocardial iron overload in multitransfused patients with myelodysplastic syndrome using cardiac magnetic resonance T2 technique. *Am J Hematol* 2007; **82**: 1013-1016
109 **Chacko J**, Pennell DJ, Tanner MA, Hamblin TJ, Wonke B, Levy T, Thomas PW, Killick SB. Myocardial iron loading by magnetic resonance imaging T2* in good prognostic myelodysplastic syndrome patients on long-term blood transfusions. *Br J Haematol* 2007; **138**: 587-593
110 **Majhail NS**, Lazarus HM, Burns LJ. Iron overload in hematopoietic cell transplantation. *Bone Marrow Transplant* 2008; **41**: 997-1003
111 **Altès A**, Remacha AF, Sureda A, Martino R, Briones J, Canals C, Brunet S, Sierra J, Gimferrer E. Iron overload might increase transplant-related mortality in haematopoietic stem cell transplantation. *Bone Marrow Transplant* 2002; **29**: 987-989
112 **Socié G**, Salooja N, Cohen A, Rovelli A, Carreras E, Locasciulli A, Korthof E, Weis J, Levy V, Tichelli A. Nonmalignant late effects after allogeneic stem cell transplantation. *Blood* 2003; **101**: 3373-3385
113 **Pullarkat V**. Objectives of iron chelation therapy in myelodysplastic syndromes: more than meets the eye? *Blood* 2009; **114**: 5251-5255
114 **Pullarkat V**, Blanchard S, Tegtmeier B, Dagis A, Patane K, Ito J, Forman SJ. Iron overload adversely affects outcome of allogeneic hematopoietic cell transplantation. *Bone Marrow Transplant* 2008; **42**: 799-805
115 **Mahindra A**, Bolwell B, Sobecks R, Rybicki L, Pohlman B, Dean R, Andresen S, Sweetenham J, Kalaycio M, Copelan E. Elevated pretransplant ferritin is associated with a lower incidence of chronic graft-versus-host disease and inferior survival after myeloablative allogeneic haematopoietic stem cell transplantation. *Br J Haematol* 2009; **146**: 310-316
116 **Kataoka K**, Nannya Y, Hangaishi A, Imai Y, Chiba S, Takahashi T, Kurokawa M. Influence of pretransplantation serum ferritin on nonrelapse mortality after myeloablative and nonmyeloablative allogeneic hematopoietic stem cell transplantation. *Biol Blood Marrow Transplant* 2009; **15**: 195-204
117 **Armand P**, Kim HT, Cutler CS, Ho VT, Koreth J, Alyea EP, Soiffer RJ, Antin JH. Prognostic impact of elevated pretransplantation serum ferritin in patients undergoing myeloablative stem cell transplantation. *Blood* 2007; **109**: 4586-4588
118 **McKay PJ**, Murphy JA, Cameron S, Burnett AK, Campbell M, Tansey P, Franklin IM. Iron overload and liver dysfunction after allogeneic or autologous bone marrow transplantation. *Bone Marrow Transplant* 1996; **17**: 63-66
119 **Kornreich L**, Horev G, Yaniv I, Stein J, Grunebaum M, Zaizov R. Iron overload following bone marrow transplantation in children: MR findings. *Pediatr Radiol* 1997; **27**: 869-872
120 **Au WY**, Lam WM, Chu WC, Tam S, Wong WK, Pennell DJ, Lie AK, Liang R. A magnetic resonance imaging study of iron overload in hemopoietic stem cell transplant recipients with increased ferritin levels. *Transplant Proc* 2007; **39**: 3369-3374
121 **Majhail NS**, DeFor T, Lazarus HM, Burns LJ. High prevalence of iron overload in adult allogeneic hematopoietic cell transplant survivors. *Biol Blood Marrow Transplant* 2008; **14**: 790-794
122 **Rose C**, Ernst O, Hecquet B, Maboudou P, Renom P, Noel MP, Yakoub-Agha I, Bauters F, Jouet JP. Quantification by magnetic resonance imaging and liver consequences of post-transfusional iron overload alone in long term survivors after allogeneic hematopoietic stem cell transplantation (HSCT). *Haematologica* 2007; **92**: 850-853
123 **Lutz K**, von Komorowski G, Dürken M, Engelhardt R, Dinter DJ. Myocardial iron overload in transfusion-dependent pediatric patients with acute leukemia. *Pediatr Blood Cancer* 2008; **51**: 691-693
124 **Emy PY**, Levin TL, Sheth SS, Ruzal-Shapiro C, Garvin J, Berdon WE. Iron overload in reticuloendothelial systems of pediatric oncology patients who have undergone transfusions: MR observations. *AJR Am J Roentgenol* 1997; **168**: 1011-1015
125 **Jensen PD**, Jensen FT, Christensen T, Ellegaard J. Noninvasive assessment of tissue iron overload in the liver by magnetic resonance imaging. *Br J Haematol* 1994; **87**: 171-184
126 **Bonkovsky HL**, Rubin RB, Cable EE, Davidoff A, Rijcken TH, Stark DD. Hepatic iron concentration: noninvasive estimation by means of MR imaging techniques. *Radiology* 1999; **212**: 227-234
127 **Gandon Y**, Guyader D, Heautot JF, Reda MI, Yaouanq J, Buhé T, Brissot P, Carsin M, Deugnier Y. Hemochromatosis: diagnosis and quantification of liver iron with gradient-echo MR imaging. *Radiology* 1994; **193**: 533-538
128 **Gandon Y**, Olivié D, Guyader D, Aubé C, Oberti F, Sebille V, Deugnier Y. Non-invasive assessment of hepatic iron stores by MRI. *Lancet* 2004; **363**: 357-362
129 **Alústiza JM**, Artetxe J, Castiella A, Agirre C, Emparanza JI, Otazua P, García-Bengoechea M, Barrio J, Mújica F, Recondo JA. MR quantification of hepatic iron concentration. *Radiology* 2004; **230**: 479-484
130 **Ernst O**, Sergent G, Bonvarlet P, Canva-Delcambre V, Paris JC, L'Herminé C. Hepatic iron overload: diagnosis and quantification with MR imaging. *AJR Am J Roentgenol* 1997; **168**: 1205-1208
131 **Kaltwasser JP**, Gottschalk R, Schalk KP, Hartl W. Noninvasive quantitation of liver iron-overload by magnetic resonance imaging. *Br J Haematol* 1990; **74**: 360-363
132 **Lecube A**, Hernández C, Simó R. Glucose abnormalities in non-alcoholic fatty liver disease and chronic hepatitis C virus infection: the role of iron overload. *Diabetes Metab Res Rev* 2009; **25**: 403-410
133 **Isom HC**, McDevitt EI, Moon MS. Elevated hepatic iron: a confounding factor in chronic hepatitis C. *Biochim Biophys Acta* 2009; **1790**: 650-662
134 **Wallace DF**, Subramaniam VN. Co-factors in liver disease: the role of HFE-related hereditary hemochromatosis and iron. *Biochim Biophys Acta* 2009; **1790**: 663-670
135 **Adams PC**, Passmore L, Chakrabarti S, Reboussin DM, Acton RT, Barton JC, McLaren GD, Eckfeldt JH, Dawkins FW, Gordeuk VR, Harris EL, Leiendecker-Foster C, Gossman E, Sholinsky P. Liver diseases in the hemochromatosis and iron overload screening study. *Clin Gastroenterol Hepatol* 2006; **4**: 918-923; quiz 807
136 **Kohgo Y**, Ikuta K, Ohtake T, Torimoto Y, Kato J. Iron overload and cofactors with special reference to alcohol, hepatitis C virus infection and steatosis/insulin resistance. *World J Gastroenterol* 2007; **13**: 4699-4706
137 **Ito K**, Mitchell DG, Gabata T, Hann HW, Kim PN, Fujita T, Awaya H, Honjo K, Matsunaga N. Hepatocellular carcinoma: association with increased iron deposition in the cirrhotic liver at MR imaging. *Radiology* 1999; **212**: 235-240
138 **Kim MJ**, Mitchell DG, Ito K, Kim JH, Pasqualin D, Rubin R. Hepatic iron deposition on magnetic resonance imaging: correlation with inflammatory activity. *J Comput Assist Tomogr* 2002; **26**: 988-993

139 **Kim MJ**, Mitchell DG, Ito K, Hann HW, Park YN, Kim PN. Hepatic iron deposition on MR imaging in patients with chronic liver disease: correlation with serial serum ferritin concentration. *Abdom Imaging* 2001; **26**: 149-156
140 **Ito K**, Mitchell DG, Hann HW, Outwater EK, Kim Y, Fujita T, Okazaki H, Honjo K, Matsunaga N. Progressive viral-induced cirrhosis: serial MR imaging findings and clinical correlation. *Radiology* 1998; **207**: 729-735
141 **Sassa S**. Modern diagnosis and management of the porphyrias. *Br J Haematol* 2006; **135**: 281-292
142 **Dereure O**, Jumez N, Bessis D, Gallix B, Guillot B. Measurement of liver iron content by magnetic resonance imaging in 20 patients with overt porphyria cutanea tarda before phlebotomy therapy: a prospective study. *Acta Derm Venereol* 2008; **88**: 341-345
143 **Tanner MA**, He T, Westwood MA, Firmin DN, Pennell DJ. Multi-center validation of the transferability of the magnetic resonance T2* technique for the quantification of tissue iron. *Haematologica* 2006; **91**: 1388-1391
144 **Westwood MA**, Firmin DN, Gildo M, Renzo G, Stathis G, Markissia K, Vasili B, Pennell DJ. Intercentre reproducibility of magnetic resonance T2* measurements of myocardial iron in thalassaemia. *Int J Cardiovasc Imaging* 2005; **21**: 531-538
145 **Westwood MA**, Anderson LJ, Firmin DN, Gatehouse PD, Lorenz CH, Wonke B, Pennell DJ. Interscanner reproducibility of cardiovascular magnetic resonance T2* measurements of tissue iron in thalassemia. *J Magn Reson Imaging* 2003; **18**: 616-620

S- Editor Tian L **L- Editor** Kerr C **E- Editor** Ma WH

World Journal of Gastroenterology

Online Submissions: http://www.wjgnet.com/1007-9327office
wjg@wjgnet.com
doi:10.3748/wjg.v16.i13.1598

World J Gastroenterol 2010 April 7; 16(13): 1598-1609
ISSN 1007-9327 (print)

TOPIC HIGHLIGHT

Paul E Sijens, PhD, Associate Professor, *Series Editor*

Perfusion magnetic resonance imaging of the liver

Choon Hua Thng, Tong San Koh, David J Collins, Dow Mu Koh

Choon Hua Thng, Tong San Koh, Department of Oncologic Imaging, National Cancer Centre, Singapore 169610, Singapore
David J Collins, Dow Mu Koh, Department of Radiology, Royal Marsden NHS Foundation Trust, Sutton, SM2 5PT, United Kingdom
David J Collins, CR UK-EPSRC Cancer Imaging Centre, Institute of Cancer Research, Sutton, SM2 5PT, United Kingdom
Author contributions: Thng CH researched the subject and drafted the paper; Koh TS, Collins DJ and Koh DM revised, edited and contributed to the final version of the manuscript.
Supported by Singapore Cancer Syndicate (SCS_CS-0072); Biomedical Research Council (BMRC 08/1/31/19/577); CRUK and EPSRC Cancer Imaging Centre in association with the MRC and Department of Health (England) grant C1060/A10334; and NHS funding to the NIHR Biomedical Research Centre (UK)
Correspondence to: Dr. Dow Mu Koh, Department of Radiology, Royal Marsden NHS Foundation Trust, Downs Road, Sutton, Surrey SM2 5PT, United Kingdom. dowmukoh@icr.ac.uk
Telephone: +44-208-6613587 Fax: +44-208-6613901
Received: February 3, 2010 Revised: February 24, 2010
Accepted: March 3, 2010
Published online: April 7, 2010

Abstract

Perfusion magnetic resonance imaging (MRI) studies quantify the microcirculatory status of liver parenchyma and liver lesions, and can be used for the detection of liver metastases, assessing the effectiveness of anti-angiogenic therapy, evaluating tumor viability after anti-cancer therapy or ablation, and diagnosis of liver cirrhosis and its severity. In this review, we discuss the basic concepts of perfusion MRI using tracer kinetic modeling, the common kinetic models applied for analyses, the MR scanning techniques, methods of data processing, and evidence that supports its use from published clinical and research studies. Technical standardization and further studies will help to establish and validate perfusion MRI as a clinical imaging modality.

Key words: Magnetic resonance imaging; Dynamic contrast-enhanced magnetic resonance imaging; Liver; Tracer kinetic modeling

Peer reviewer: Paul E Sijens, PhD, Associate Professor, Radiology, UMCG, Hanzeplein 1, 9713GZ Groningen, The Netherlands

Thng CH, Koh TS, Collins DJ, Koh DM. Perfusion magnetic resonance imaging of the liver. *World J Gastroenterol* 2010; 16(13): 1598-1609 Available from: URL: http://www.wjgnet.com/1007-9327/full/v16/i13/1598.htm DOI: http://dx.doi.org/10.3748/wjg.v16.i13.1598

INTRODUCTION

Perfusion magnetic resonance imaging (MRI) refers to imaging of tissue blood flow (i.e. tissue microcirculation), which is beyond the resolution of the MR scanner to directly visualize. In the liver, perfusion MRI can be applied to measure microcirculation in the liver parenchyma or in tumors. Whilst there are techniques available for direct measurement of blood flow in macroscopic vessels, such as the portal vein and hepatic artery, such as Doppler ultrasound (US), contrast-enhanced US, xenon computed tomography (CT) or phased contrast MR angiography; these are beyond the scope of the current review. Instead, our discussions are primarily focused on dynamic contrast-enhanced (DCE) MRI techniques with tracer kinetic modeling, which allows for the quantitative characterization of parenchymal and tumor microcirculatory alterations in the liver. Selected DCE liver perfusion studies using other imaging modalities are used to illustrate the value of perfusion imaging.

In the liver, conventional characterization of focal liver lesions is reliant on observing the rate and pattern of contrast enhancement assessed visually on DCE scans. The rate and pattern of contrast enhancement reflects the time evolution of the contrast agent within the liver tissue, which occurs as a result of the microcirculatory

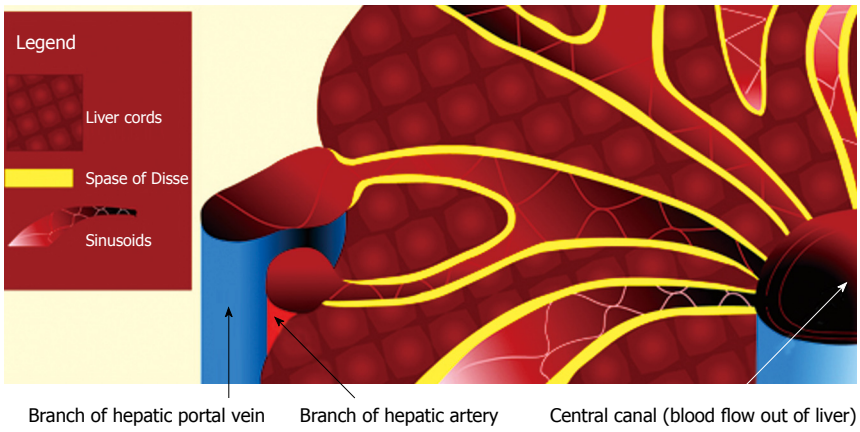

Figure 1 Schematic diagram illustrating the vascular architecture of the liver. Note the dual blood supply into the liver derived from the portal vein and hepatic artery. The vascular inflow is channeled into the hepatic sinusoids, which normally communicate freely with the Space of Disse (yellow). The Space of Disse is an interstitial space that lies between the sinusoids and the liver cords. From the hepatic sinusoids, blood is drained out of the liver *via* branches of the hepatic vein.

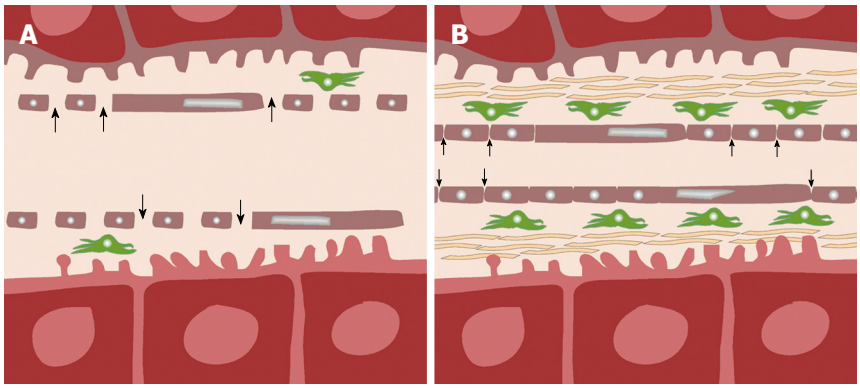

Figure 2 Schematic diagram showing pathophysiological differences between normal (A) and cirrhotic (B) liver. In normal liver (A), normal fenestrae along the hepatic sinusoids allow free passage of blood (arrows) into the Space of Disse, in which, stellate cells (green) are found. In liver cirrhosis (B), there is an increase in the number of stellate cells, associated with deposition of collagenous fibers in the Space of Disse, and loss of fenestrae as the sinusoids become more capillary-like. As a result, transfer of low-molecular-weight compounds (e.g. contrast medium) from the sinusoids into the Space of Disse becomes more impeded (small arrows).

pathophysiological changes. Perfusion MRI could extend the currently used qualitative assessment applied for the differential diagnosis of focal liver lesions, by applying quantitative metrics to describe their vascular behavior.

In the treatment of liver tumors, current therapy for hepatocellular carcinoma (HCC) includes novel anti-angiogenic agents such as sorafenib. As these drugs may have significant clinical effects without causing tumor shrinkage, the microcirculatory characteristics, such as blood flow and tumor capillary permeability, have the potential to be response biomarkers, which allow these drug effects to be confidently assessed. Furthermore, it may also be possible to explore whether the quantitative microcirculatory parameters correlate with drug exposure and whether they can predict response. Quantitative vascular measurements could also be applied to assess the efficacy of local tumor ablation such as by trans-arterial chemo-embolization (TACE), radiofrequency ablation (RFA) or yttrium-90 microsphere embolization.

The early detection of liver metastases remains challenging, but changes in the relative hepatic arterial *vs* portal venous blood supply allow earlier detection of microscopic liver metastases[1]. Likewise, changes in the relative contribution of hepatic arterial and portal blood flow are also observed in patients with liver cirrhosis[2-8].

Central to the assessment of liver perfusion are model-based or model-free methods that analyze the contrast concentration-time curve in focal liver lesions or liver parenchyma, derived from the DCE-MRI images. Although similar concentration-time curves may be obtained using CT and nuclear medicine studies, radiation burden is a practical concern, which becomes even more significant on repeated measurements. The ability of MRI to acquire such information without radiation burden and in a potentially more favorable scan plane (e.g. oblique coronal), to demonstrate the vascular input into the liver, are important advantages.

NORMAL AND ABNORMAL LIVER CIRCULATION

The liver is a highly vascular organ that consists of a series of porous vascular channels (sinusoids with fenestrae) that are predominantly supplied by the portal vein (75%) and supplemented by the hepatic artery (25%)[9]. The two arterial inputs mix in the sinusoids at different time intervals to supply the liver cords. There is a small space (Space of Disse) that separates the sinusoids from the tightly ordered hepatic cords, which comprise two rows of closely apposed hepatocytes. The Space of Disse may be considered as an interstitial space within the liver. However, due to the large size of the fenestrae of the sinusoids, there is usually free exchange of low-molecular-weight compounds (e.g. gadolinium contrast medium) between the vascular space (sinusoids) and the interstitial space (Space of Disse) (Figures 1 and 2)[10].

In cirrhosis, due to sinusoidal capillarization, there is loss of normal fenestrae, due to deposition of basement membrane and new formation of capillary tight junctions along the sinusoids. There is also deposition of fibers by

activated Ito cells (hepatic stellate or antigen presenting cells), which results in enlargement of the Space of Disse. Consequently, transfer of low-molecular-weight gadolinium contrast medium from the vascular sinusoids into the interstitial space becomes increasingly impeded (Figure 2)[11].

In liver metastases and HCC, tumor blood supply is initially derived from proliferation of the sinusoidal cells that become capillarized with loss of fenestrae and formation of basement membrane. This also results in a significant barrier to the free passage of low-molecular-weight contrast medium between the sinusoidal space and interstitial space of the tumor. As the tumor continues to grow, there is recruitment of new vessels directly supplied by the hepatic artery (neoarteriogenesis). This is a prominent feature of HCC but can also be seen in the peritumoral area of liver metastases[12-15]. Such arterialization of the vascular supply is typical of malignant liver tumors.

MRI TECHNIQUE FOR MEASURING HEPATIC PERFUSION

For perfusion MRI of the liver, injection of a low-molecular-weight gadolinium-chelate contrast is necessary, and this is administered through a wide bore (20G or larger) intravenous cannula sited within a large antecubital vein. Contrast medium is injected using a programmable pump injector, which ensures uniform and rapid contrast delivery as a tight bolus. The amount of contrast medium administered is based on body weight. For example, using Gd-DTPA (Magnevist®, Bayer-Schering, Germany), 0.1-0.2 mmol of contrast medium/kg body weight is typically administered. Once the contrast medium is injected, imaging of the liver commences using an MRI sequence that is capable of rapid and repeated measurements, to enable the passage of contrast medium through the liver to be tracked accurately. Liver perfusion imaging is typically performed using T1-weighted MRI sequences. On T1-weighted imaging, liver or tumor perfusion is observed as increasing enhancement as contrast medium passes through the liver or tumor.

With regard to technical details, a T1-weighted 3D spoiled gradient echo technique with variable flip angles is useful. Parallel imaging could be applied to reduce scan time and improve temporal resolution. Compared with 2D imaging sequences, the 3D technique eliminates inaccuracies due to the radiofrequency excitation pulse profile, and also has the advantage of better signal-to-noise ratio. However, the peripheral image sections may still have to be excluded from analysis because they may have unfavorable slice profiles or be degraded by wrap artifacts that result from phase under-sampling. T1 mapping or calibration, a necessary step for quantitative analysis, can be performed using the variable flip angle method described by Wang *et al*[16]. As the gadolinium contrast concentration is inversely proportional to change in the reciprocal of T1, a gadolinium contrast concentration-time curve of the liver or tumor can be generated, which is then used to derive quantitative vascular perfusion indices. Table 1 provides an example of a liver perfusion MRI protocol implemented on a commercial scanner. It is important to note that such an imaging sequence may vary from one imaging platform to another, and it is important to engage the help of an experienced clinical scientist to ensure that the performance of the sequence is optimized. Although some workers have advocated simpler methods of estimating gadolinium concentration by measuring differences in signal intensities before and after contrast arrival in the liver, we would like to caution that the success of this simplified approach might be dependent on the imaging sequence, as well as the range of signal intensity and tracer concentration encountered.

Table 1 Illustrative example of a perfusion MRI sequence performed on a 1.5 T MR platform

MRI platform	Avanto (Siemens, Erlangen, Germany)
Type of pulse sequence	3D FLASH
TR	2.72 ms
TE	1 ms
Partition thickness	8 mm
Slices per slab	10
Matrix	256 × 159
Phase encode direction	Anterior to posterior
Number of averages	1
Sensitivity encoding factor	2
Flip angle before contrast	2° and 14°
Flip angle after contrast	14°
Bandwidth	490 Hz
RF spoiling	Yes
Temporal resolution	1.98 s per slab of 10 slices.
Precontrast scans	10 measurements of each flip angle averaged for calculation of native T1
Gadolinium injection	0.2 mmol/kg at 3 mL/s followed by 20 mL flush
Patient respiration	Quiet breathing
Post contrast scans	A total of 180 consecutive measurements. Inject contrast only when the 20th measurement has been completed
Scan sections to use for processing	Center 6 image sections only

MRI: Magnetic resonance imaging; FLASH: Fast low-angle shot; TR: repetition time; TE: Echo time.

In order to track liver perfusion reliably, MRI of the liver should employ a high temporal resolution technique (i.e. repeated imaging of the same area in the liver about every 4 s), in a scan plane that shows the lesion or area of interest. Ideally, the aorta and the portal vein should be included in the same image sections. Hence, an oblique imaging plane (e.g. oblique coronal) afforded by the MRI technique would be particularly helpful to ensure all these structures are included. The signal intensity changes within these structures, together with the T1 calibration maps, are used to derive the gadolinium contrast concentration-time curves in the liver and tumors. Once the gadolinium contrast concentration-time curve in an area of interest is known, knowledge of the contemporaneous contrast enhancement within the aorta and portal vein allows analytic methods to be applied to extract quantitative or semi-quantitative parameters that describe the vascular

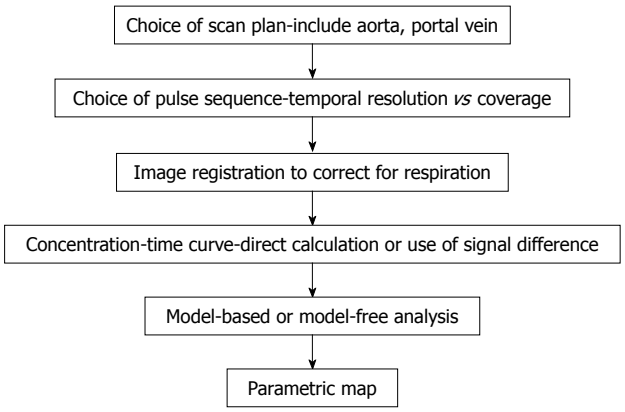

Figure 3 Chart shows workflow involved from data acquisition to obtaining vascular information by perfusion MRI of the liver.

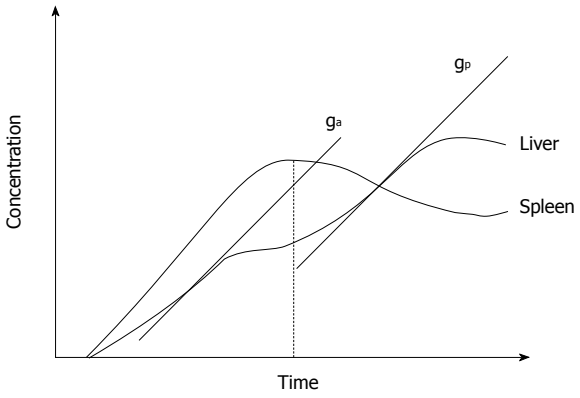

Figure 4 Schematic plot of gadolinium concentration-time curve in liver tissue obtained from a perfusion MRI study. The diagram illustrates how the maximum gradient for arterial perfusion (g_a) and portal perfusion (g_p) are derived (based on Miles *et al*[2]). Note that the peak splenic enhancement is used to define the transition between arterial and portal phase of liver parenchyma enhancement. The maximum slope after the peak splenic enhancement is used to define portal perfusion.

properties. The MR images may also be qualitatively assessed by visual survey for areas of increased enhancement relative to the normal liver parenchyma. However, such comparisons can be subjective. The various approaches to extracting quantitative and/or semi-quantitative liver perfusion data are discussed in the next section.

One of the challenges to acquiring high quality liver perfusion MRI is respiratory motion, which can substantially degrade image quality. It is currently a subject of debate whether to acquire images during breath-hold or quiet respiration. Imaging in quiet respiration is widely performed, which allows rapid uninterrupted image acquisition for high temporal resolution data. However, the images often need to be aligned using image registration techniques, which can be complex, prior to quantitative analysis. Furthermore, respiration can result in through-plane motion and non-linear tissue deformation that cannot be easily overcome. For these reasons, imaging in sequential breath-hold has been advocated as a method to minimize the effects of respiratory motion. Images are acquired during suspended respiration (usually expiration), followed by a short period of normal breathing, after which respiration is again suspended for image acquisition. Imaging during expiration can be monitored by navigator control. Breath-hold imaging minimizes the need for complex image registration, but the main potential disadvantage is decreased temporal sampling because images cannot be acquired continuously. One method which can be used to improve temporal sampling of breath-hold studies is to acquire two datasets (instead of one) during each breath-hold[17]. Single breath-hold studies have also been reported. In single breath-hold studies, patients are required to breath-hold for 40-60 s during which the first passage of gadolinium contrast is observed[18].

EXTRACTING LIVER PERFUSION INFORMATION FROM MRI DATA

Once the MRI data have been acquired, they have to be analyzed in a meaningful way to extract information that describes tissue vascularity. Dynamic MRI data can be processed using a model-free or a model-based approach, with the former being simpler to implement.

Using model-free approaches, semi-quantitative descriptions of liver perfusion can be derived by observing the rate of liver tissue signal change in the arterial and portovenous phases of contrast enhancement. One semi-quantitative description of liver vascularity is the hepatic perfusion index (HPI), which describes the relative contribution of arterial *vs* portovenous flow to the total liver perfusion. The HPI has been investigated using different imaging techniques, and appears to provide biologically meaningful information despite its relative simplicity.

However, the quantitative model-based approach is appealing because it may provide more sophisticated descriptions of tissue vascular properties, by underpinning the data analysis on mathematical assumptions that reflect alterations in the underlying pathophysiology. Both model-free and model-based approaches are being widely investigated; each has provided unique information that has shown to improve liver disease assessment.

A simplified schema which shows the workflow for performing DCE-MRI is shown in Figure 3.

Model-free approaches for vascular quantification

These methods are based on simply observing the MR signal changes that result from the passage of contrast agent through the liver parenchyma or liver tumor, but may not directly relate these to the contemporaneous change in the aorta or portal vein. Disease characterization is based on the fact that the perfused liver or tumor shows enhancement with the arrival of contrast agent and therefore perfusion can be estimated by the rate of tissue enhancement. Hence, most model-free approaches use parameters derived from the initial slope of the tissue signal intensity-time or contrast concentration-time curve (Figure 4).

HPI

One semi-quantitative index that can be calculated using the model-free approach is the HPI. The HPI was first proposed by Miles *et al*[2]. HPI refers to the proportion of hepatic perfusion that is derived from the hepatic artery, and it can be calculated using the following formula: arterial perfusion/arterial perfusion + portal venous perfusion). Miles *et al*[2] have used the time to peak in the splenic enhancement curve to distinguish between the arterial and portal venous phases of the liver. Liver arterial perfusion is then estimated by the maximum slope in the liver enhancement curve before the splenic peak, divided by the peak aortic enhancement (Figure 4). Correspondingly, liver portal venous perfusion is estimated by dividing the maximum slope in the liver enhancement curve after the splenic peak by the peak aortic enhancement (Figure 4).

Blomley *et al*[3] have further refined calculation of portal venous perfusion by removing the contribution of the hepatic artery from the liver contrast concentration-time curve by subtracting from it a scaled splenic contrast concentration-time curve. This is because the spleen is predominantly supplied by the aorta and not by the portal vein. Using the arterially subtracted liver contrast concentration-time curve, the portal venous perfusion is estimated by dividing the maximum slope of the arterially subtracted liver curve by the peak portal enhancement. This more direct method of estimating portal vascular contribution has also been advocated by Tsushima *et al*[19]. However, liver arterial perfusion can be estimated in a similar way as proposed by Miles *et al*[2].

The key advantage of using model-free approaches is that they are relatively easy to derive and do not require complex computation.

Understanding tracer kinetic modeling for perfusion MRI

Applying tracer kinetic modeling enables quantitative vascular information to be extracted from temporally sampled MRI data, when the passage of contrast medium through the liver parenchyma or tumor is observed over time. Generally, an assumption is made that the imaged voxel contains a supplying impermeable artery that leads to a permeable capillary that leaks tracer (gadolinium contrast) into the interstitial space (Figure 5). The tracer is cleared from the voxel *via* an impermeable vein. However, the vessels and the interstitial space are beyond the resolution of the MRI scanner to directly image. What is measured by the MRI scanner is the average concentration of the tracer at any one time (reflected by the measured signal intensity) within the image voxel, which changes as contrast medium courses through.

Tracer kinetic modeling uses mathematical curve fitting to describe the tissue contrast concentration-time curves. If the contrast concentration-time curve of the vascular supply is known (arterial input function), subsequent mathematical operations by convolution or deconvolution allow quantitative vascular parameters to be derived that best fit the tumor or tissue contrast concentration-time curves. Such an approach could be applied to tumor and non-tumor tissues, although the mathematical and pathophysiological assumptions may be different for each. Using one particular kinetic model (e.g. distributed parameter model), quantitative parameters such as hepatic arterial flow, portal venous flow, fraction of total flow contributed by hepatic artery, capillary permeability-surface area product (PS), percentage of intravascular space (v_1), percentage of interstitial space (v_2), and mean transit time (MTT) are derived. However, depending on the mathematical model applied and physiological assumptions made, variants of such quantitative parameters are obtained. Hence, when applying tracer kinetic modeling to clinical studies, it is important to state the choice of kinetic model employed at the outset. Currently, there is no consensus as to which kinetic model is best suited to evaluate the liver, and development of an international consensus in this area would be welcomed.

It has been observed that a hypervascular tumor (usually a tumor with a larger vascular space relative to the interstitial space) shows a pattern of rapid arterial enhancement followed by washout, whereas a hypovascular tumor (usually a tumor with a larger interstitial space relative to the vascular space) shows progressive enhancement. These observations could also be explained by considering tracer kinetic modeling.

A hypervascular tumor is predominantly supplied directly by hepatic arterial neovessels. As the intravascular space is relatively larger than the interstitial space, the average concentration imaged by the voxel predominantly reflects changes in the intravascular space. In such lesions, there is rapid and strong enhancement in the arterial phase. However, in the equilibrium phase, the contrast redistributes to the interstitium and the rest of the body. This reduces the concentration of tracer in the tumor vascular space and is visualized as contrast wash-out within the voxel.

A hypovascular tumor may be supplied by the hepatic artery and the portal vein. As the interstitial space is relatively larger than the intravascular space, the averaged contrast medium concentration within the image voxel predominantly reflects changes in the interstitial space. Hence, there is faint enhancement in the arterial phase as contrast agent diffuses into the relatively large interstitial space. With continued blood flow in the portal venous phase, more contrast medium diffuses outwards and the concentration in the interstitium increases. In the equilibrium phase, although the tracer concentration in the vascular space has reduced due to redistribution to the rest of the body, it is still higher than the concentration in the tumor interstitium. Hence, there may even be a net efflux of contrast medium into the interstitium in the equilibrium phase, and such a tumor may demonstrate a pattern of progressive enhancement.

Clearly, the above explanations could be simplistic, as other measurement factors determine the degree of tumor enhancement. Nevertheless, these descriptions

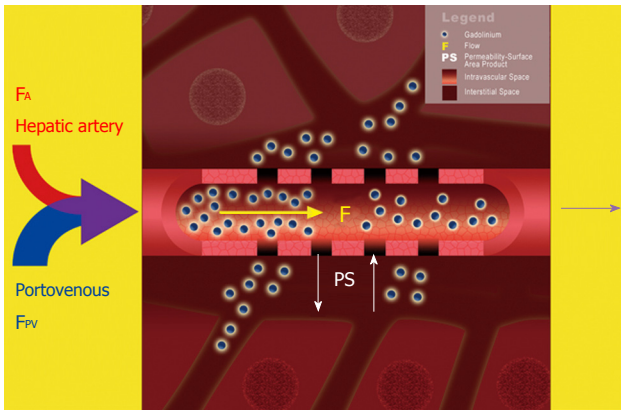

Figure 5 Schematic diagram illustrating a dual-input dual-compartment tracer kinetic model. Dual blood supply carrying gadolinium contrast molecules (blue spheres) from the hepatic artery (F_A) and portal vein (F_{PV}) enters the hepatic sinusoids (intravascular space). From here, the contrast molecules can leak outwards into the Space of Disse (interstitial space). Using a dual-input, dual compartment tracer kinetic model allows the estimation of intravascular properties (e.g. blood flow, F), as well as characteristics of the interstitial space (e.g. PS).

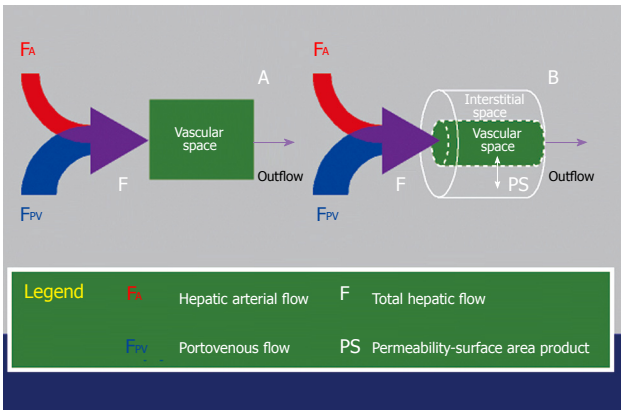

Figure 6 Schematic diagram illustrating the key difference between a single-compartment model (A) and a dual-compartment tracer kinetic model (B). Using a single-compartment model, only the vascular compartment is considered and kinetic properties related to this (e.g. blood flow, F) can be estimated. The behavior of the normal liver can be approximated by a single-compartment model. Using a dual-compartment model, kinetic properties that describe the interstitial space (e.g. PS) can be quantified in addition. In disease states (e.g. liver cirrhosis and tumors), the vascular behavior of these tissues are better described using a dual-compartment model.

can help us to appreciate how the pathophysiological differences in different disease processes could account for their imaging behavior.

Model-based vascular quantification

Several kinetic models are currently in use for the assessment of liver perfusion. A detailed mathematical analysis of these is beyond the scope of this review. Kinetic models applied to the liver vary according to the physiological assumptions made, and can broadly differ in the following ways.

Single-input *vs* dual-input: Single-input models assume that the vascular input is derived from the hepatic artery only, whereas dual-input models assume that the vascular input is derived from both the hepatic artery and the portal vein. Dual-input models are more physiological, although in tumors, where the blood supply in highly arterialized, assumption of a single vascular input may suffice to approximate the vascular behavior.

Single-compartment *vs* dual-compartment: Single compartment models assume that the contrast is confined to only one compartment (i.e. vascular space), whereas dual compartment models assume that there is dynamic distribution of contrast between two compartments (i.e. the vascular space and the interstitial space). Single-compartment models are computationally simpler and could be applied as an approximation for the normal liver, because the Space of Disse communicates freely with the sinusoids. Dual-compartment models are computationally more demanding but may give a better reflection of the microcirculation of the diseased liver, resulting from tumor or cirrhosis[4,20] (Figure 6).

Conventional compartment (CC) model *vs* distributed parameter (DP) model: In several kinetic models, the assumption is made that there is instantaneous mixing or equilibrium of the contrast medium along the entire course of a vessel. We term these as CC models. One example of a CC model is Toft's model[21]. Another approach takes into account a concentration gradient within the vascular space. This approach is called the DP model. CC models are simpler to implement and computationally easier to solve but make more assumptions about the microcirculation. By comparison, DP models are more complex, which attempts to make fewer assumptions about the microcirculation, but are computationally more intensive and require higher temporal resolution data to derive meaningful results.

Derived microcirculatory parameters: Generally, dual compartment models are necessary to extract parameters that describe the interstitial space, e.g. v_2, PS and extraction fraction (EF) using the DP model; or extracellular extravascular volume using the Toft's model. Such parameters cannot be derived using a single-compartment model. Single compartment models allow for estimates of blood flow, volume of distribution and mean transit time.

Clearly, the choice of the kinetic model depends on many factors including local expertise, available software to perform the perfusion analysis, understanding of the disease pathophysiology, MRI measurement technique applied, and the quality (spatial and temporal resolution) of the MRI data. At the time of writing, only a few commercial softwares are available to undertake such analyses, and many research groups are therefore reliant on self-scripted software for data evaluation. Not surprisingly, this has led to disparate efforts in developing analysis tools, which are often institution-specific and non-standardized. The lack of standardization in the methodologies applied

Table 2 Examples of the types of tracer kinetic models that have been applied for perfusion MRI of the liver

Study	Diseases	Comment
Single-input, single compartment, CC model		
Scharf *et al*[48]	Preclinical study in pigs	Experimental model of normal liver in pigs. Only arterial input from hepatic artery taken into account. Such a model may lack physiological realism, especially when there is substantial vascular input contribution from the portal vein
Single-input, dual-compartment, DP model		
Sahani *et al*[30]	HCC	Single input assumed because majority of vascular input to HCC is derived from hepatic artery. Dual-compartment model used to probe interstitial space and PS, which can be substantial in tumors. DP model implemented as standard on General Electric (GE) perfusion software 2.0 used for analysis
Dual-input, single-compartment, CC model		
Materne *et al*[45-47]	Normal and cirrhotic livers	Assumption of single compartment based on understanding that the fenestra in the sinusoids of liver are extremely porous and allows free exchange of low-molecular-weight contrast tracers between the vascular and the sinusoidal interstitial space. To simplify calculations, assumption was made that there was instantaneous mixing of contrast medium from the dual input[6,7,27,45-47,49] within the single compartment. In this way, quantitative parameters such as arterial perfusion, portal venous perfusion, MTT and volume of distribution (Ve) could be derived. Cuenod *et al*[27,49] applied a deconvolution technique to fit these parameters, and variants of such a model were also used by Funabasam *et al*[50] and Miyazaki *et al*[51]
Cuenod *et al*[27,49]	Metastatic disease	
Dual-input, dual-compartment, DP model		
Koh *et al*[4,20]	Metastases, HCC and cirrhosis	The DP model applies a concentration gradient within the vascular space. Parameters derived include, arterial flow, portal venous flow, fractional arterial flow, permeability, fractional intravascular space, fractional interstitial space, MTT, contrast arrival time. A dual-input dual-compartment approximation of the DP model is used commercially (CT Perfusion 3.0; General Electric, Milwaukee, USA) and was also adopted by Chen *et al*[42,52,53] in perfusion studies of the liver

CC: Conventional compartment; HCC: Hepatocellular carcinoma; DP: Distributed parameter; MTT: Mean transit time; CT: Computed tomography.

for data analysis is an acknowledged issue by researchers in the field, and there is fortunately increasing international efforts towards the harmonization and standardization of imaging acquisition and data analysis. Such developments are paramount for the wider clinical adoption of the technique and institution-vendor partnerships are being developed to address such challenges.

Some of the kinetic modeling approaches that have been applied in the published literature are summarized in Table 2.

CLINICAL APPLICATIONS OF PERFUSION MRI IN THE LIVER

Liver metastases

Model-free approach: Several studies have demonstrated the potential of perfusion imaging to detect changes in the liver of patients at risk of liver metastases. Totman *et al*[22] have shown that there is a difference in the portal perfusion index (PPI) between patients with and without cancer. Leggett *et al*[1] have observed that the HPI is elevated in patients with overt metastases compared with those without metastases. In another study, Tsushima *et al*[23] have found that the normal looking liver in a patient with liver metastases shows a reduction in the PPI, which suggests that there is potential for using liver perfusion studies to detect microscopic metastases. These cross-sectional imaging observations have been corroborated by nuclear scintigraphy studies[24,25]. Despite the reported relationship between high HPI and low PPI with increased likelihood of liver micrometastases in patients with cancer, few studies have had longitudinal follow-up to validate the subsequent development of macroscopic liver metastases. For example, in the study by Leggett *et al*[1], follow-up data were only available in eight patients, of which three who subsequently developed macroscopic liver metastases showed decreased portal perfusion. Although there is great potential to use liver perfusion studies to detect or predict microscopic liver metastases, more work involving longitudinal studies is required to establish its clinical role (Figure 7).

Meijerink *et al*[26] have found functional liver perfusion maps to be helpful supplements to the routine radiological diagnosis of liver metastases. Compared with routine four-phase CT, total-liver-volume CT perfusion studies with calculation of the HPI increased the sensitivity of metastases detection to 89.2% from 78.4% and specificity to 82.6% from 78.3%. Four out of a total of 37 metastases were detected with the help of perfusion maps. Perfusion CT maps increase the conspicuity of metastatic disease because of the increased perfusion at the tumor rims, which makes liver metastases appear larger, thus facilitating the detection of smaller lesions.

Model-based approach: There have been few studies using a model-based approach for evaluating liver metastases. Cuenod *et al*[27] have applied a dual-input single-compartment model in rats and have observed that the presence of micrometastases in an apparently macroscopically normal liver resulted in a 34% decrease in portal blood flow and a 25% increase in the MTT for blood to pass through the liver. The changes were similar for macrometastases but more marked.

Koh *et al*[20] have employed a dual-input dual-compartment DP model in three patients with liver metastases for a technical validation study. Using the particular model, they found that the normal liver had near zero interstitial space volume and PS (which may be explained by the

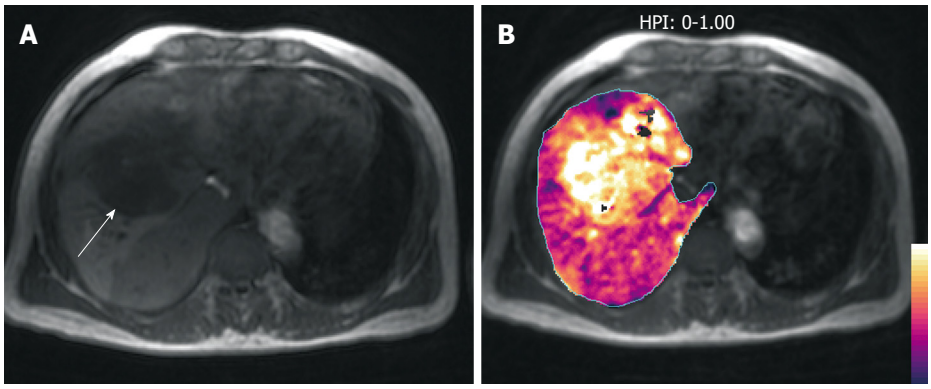

Figure 7 A middle-aged man with colorectal liver metastases to the liver. A: T1-weighted axial MR image demonstrates a hypointense liver metastasis in the right liver lobe (arrow); B: HPI map (calculated by the method described by Miles *et al*[2]) overlaid on the T1-weighted image shows increased HPI within the metastasis, typical of malignant disease.

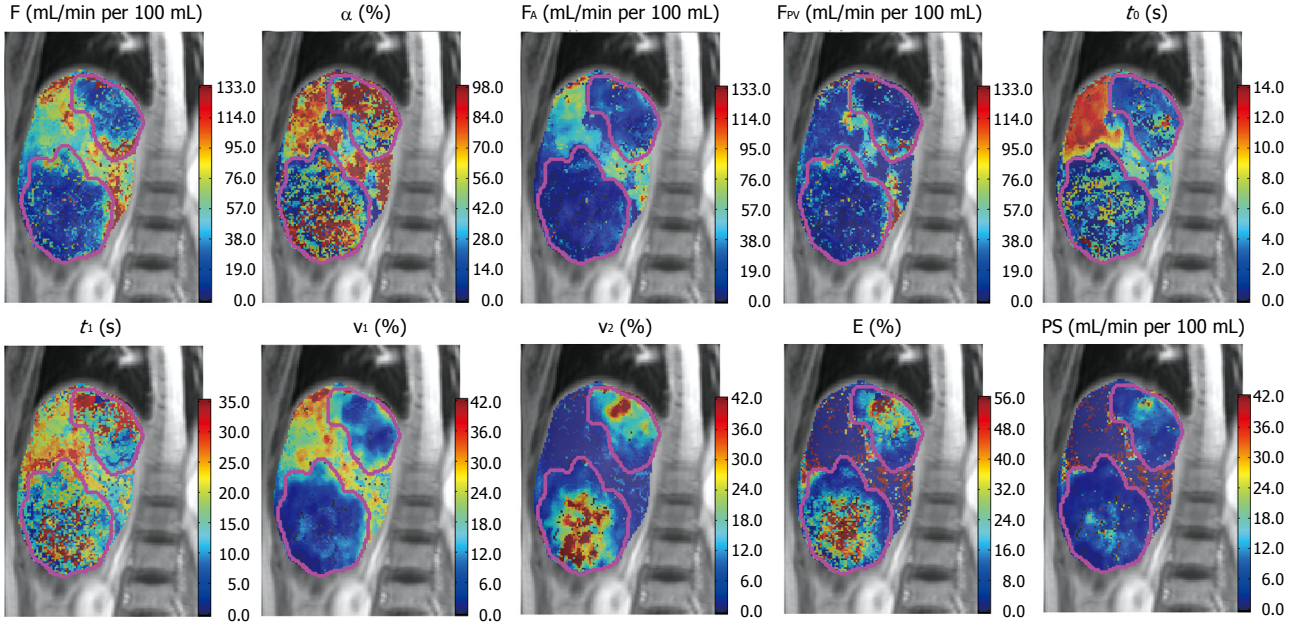

Figure 8 Parameteric maps of a patient with colorectal metastases derived from a dual-input, dual-compartment, DP tracer kinetic model. F (blood flow), α (arterial fraction, or % hepatic arterial flow from total hepatic blood flow), F_A (hepatic arterial blood flow), F_{PV} (hepatic portal venous blood flow), t_0 (contrast arrival time), t_1 (MTT), v_1 (fractional intravascular volume), v_2 (fractional interstitial volume), E (extraction fraction), PS (permeability-surface area product). Note that in the two liver metastases demonstrated (outlined in pink), the lesions were characterized by lower total blood flow, but higher arterial fraction and fractional interstitial volume.

large fenestrae allowing free contrast medium exchange between the Space of Disse and the liver sinusoids), and that liver metastases have a non-zero and finite interstitial space volume and PS. Using this quantitative technique, there is an increase in the arterial fraction (arterial flow/sum of arterial and portal flow) to the metastases, although the portal flow remains significant (Figure 8). These observations of the difference in kinetic modeling behavior between the normal liver and liver metastases are supported by histopathological observations reported by Liu and Matsui[12]. Thus, the dual-input dual-compartment DP model appears to have the potential to characterize microcirculatory pathophysiology but larger studies are required to confirm the initial findings.

HCC

Model-free approach: Abdullah *et al*[28] have studied the differences between colorectal metastases and HCC and have found no significant difference in HPI between the two malignant entities. However, there is an increase in arterial flow, portal flow, and total blood flow in HCC compared to colorectal metastases. The distribution volume is also observed to be higher in HCC.

Model-based approach: Fournier *et al*[29] have applied the dual-input single-compartment model in a rat HCC model and have found that HCC is characterized by higher arterial flow and lower portal flow.

Sahani *et al*[30] have employed a single-input dual-compartment DP model in patients with HCC and have found that blood flow, blood volume and PS are higher in well-differentiated HCC compared with moderately or poorly differentiated HCC, which suggests that such vascular quantification could yield information on tumor grade.

Koh *et al*[4] have used the dual-input dual-compartment DP model in four patients with HCC and have measured the fractional interstitial space and associated extravasation parameters (PS and extraction ratio). HCC is characterized by increased arterial flow, increased total blood flow,

as well as early contrast agent arrival time. The early arrival of contrast agent is postulated to be related to arteriogenesis and direct tumor supply by branches of the hepatic artery. Tumor vascularity (fractional intravascular volume) was higher for two out of four patients. Portal venous flow decreased but remained significant. The derived microcirculatory parameters were supported by histopathological findings of arteriogenesis in HCC[15,31]. Together with other imaging modalities such as diffusion-weighted MRI, MR perfusion imaging has the potential to contribute significantly to the multi-parameteric functional assessment of the liver to improve the diagnosis and characterization of HCC[32].

Assessment of treatment response

Anti-angiogenic agents have emerged as a class of anti-tumor agents that target tumor vasculature. The rationale of anti-angiogenic therapy is based on the observation that tumors require new blood vessels for growth and survival. Based on the diffusion distances of oxygen and nutrients, tumor cells cannot survive if they are further than 2 mm from a blood vessel. Thus, effective anti-angiogenic therapy acts by depriving a growing tumor of its nutrients, and can thus curb the growth of the primary tumor as well as its metastasis.

However, current methods of assessing efficacy of chemotherapy, such as the Response Evaluation Criteria in Solid Tumors (RECIST), are based on observing a decrease in tumor size[33]. Effective anti-angiogenic therapy often manifests as lack of tumor growth rather than decrease in tumor size because the therapy is not cytotoxic. Hence, there is a need for a reliable response biomarker to assess the efficacy of such therapy.

The challenge for a reliable response biomarker holds true for HCC that is treated by local tumor ablation. Ablated tumor differs from viable tumor in its blood supply. Previous international consensus conferences have recommended that the RECIST criteria be modified for HCC to assess only the viable tumor[34-36]. Viable tumor is defined as tumor that shows enhancement in the arterial phase. Thus, MR perfusion imaging also has the potential to provide valuable functional information that can be used to distinguish viable tumor from necrosis in HCC[37].

Model-free approach: Wang *et al*[38] have analyzed the arterial uptake slope in MR liver perfusion studies of patients with HCC treated with thalidomide. They have found that there was a greater decrease in the peak enhancement, maximum enhancement, and slope of enhancement in patients without disease progression compared to those who progressed on treatment. Miyazaki *et al*[39] have applied HPI to assess the efficacy of anti-angiogenic therapy in patients with liver metastases and have found a median 15% decrease in HPI at 28 d after anti-angiogenic treatment in patients who responded to treatment. In another study, Meijerink *et al*[40] have evaluated liver HPI and have found that HPI decreased in liver tumor treated with combination anti-angiogenic therapy with AZD2171 and gefitinib. However, most of these studies involved relatively small numbers of patients, and more studies are therefore required to establish whether MR liver perfusion indices can serve as a reliable response biomarker for anti-angiogenic drug therapy.

Meijerink *et al*[41] also have evaluated HPI for assessing local recurrence in liver metastases treated with RFA. The authors have found that an increase in HPI parallels disease recurrence detection by ^{18}fluorodeoxyglucose positron emission tomography.

Model-based approach: There are few published studies that have applied a model-based approach for the evaluation of treatment response in hepatic malignancy. Chen *et al*[42] have studied the effects of transarterial chemoembolization using a dual-input dual-compartment DP model and have found that the hepatic arterial fraction, hepatic arterial perfusion, and hepatic blood volume are significantly reduced by effective embolization. These indices could also help to indicate the presence of viable tumor. The potential of using model-based approaches for assessing the effects of anti-angiogenic or antivascular treatment is currently being investigated (Figure 9).

Cirrhosis

Model-free approach: Increase in hepatic arterial perfusion and decrease in portal venous perfusion have been reported in perfusion scintigraphy studies in patients with liver cirrhosis[43]. Miles *et al*[2] and Blomley *et al*[3] also have found an increase in HPI and decreased PPI respectively in cirrhotic liver.

Model-based approach: Guan *et al*[44] have applied a dual-input dual-compartment DP model in rats treated with diethylnitrosamine. As diethylnitrosamine induces a continuum of hepatitis, hepatic fibrosis and eventually cirrhosis, a gradual increase in hepatic arterial flow and MTT are observed across these groups, accompanied by a corresponding gradual decrease in blood volume and blood flow.

Koh *et al*[4] have utilized a dual-input dual-compartment DP model and have found that cirrhotic livers return a measurable fractional interstitial space, whereas normal liver shows a near-zero fractional interstitial space. In another study, Hashimoto *et al*[5] have applied a dual-input dual-compartment DP model and have found that the hepatic arterial fraction increases with the extent of fibrosis and cirrhosis.

The use of a single-compartment kinetic model has also been found to be useful for the assessment of liver cirrhosis.

Annet *et al*[6] have investigated a dual-input single-compartment CC model and have found that the microcirculatory parameters derived from such a technique correlate with the severity of cirrhosis and portal pressure. The measured portal pressure, a reflection of the degree of portal hypertension, is correlated with the calculated portal fraction, portal perfusion and MTT. Furthermore, the severity of cirrhosis as assessed by Child-Pugh class has been found to correlate with portal fraction, portal

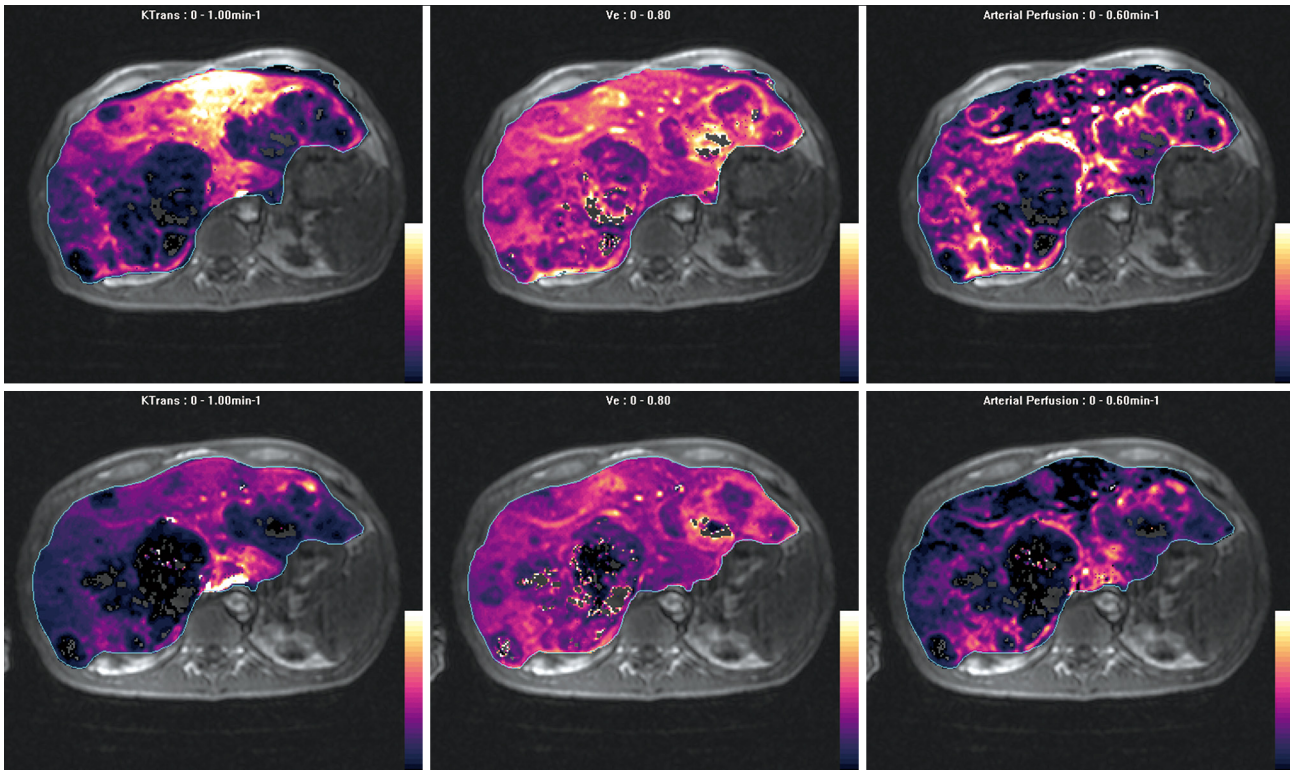

Figure 9 Parametric maps of efflux constant (Ktrans), extravascular extracellular space (Ve) and arterial perfusion fraction before (top row) and after (bottom row) anti-angiogenic therapy obtained using a dual-input, single-compartment, conventional compartment model (after Materne *et al*[46]). Note multiple metastases in the liver, which are largely hypovascular but show increased arterial perfusion at the edge of the lesions. The metastases also show moderate Ve. After treatment with anti-angiogenic drug, arterial perfusion is reduced at the tumor rims, also with a decrease in tumor Ve. The Ktrans in the left lobe of the liver is also decreased, which may reflect drug effects on microscopic disease.

perfusion, arterial perfusion and MTT. Cirrhotic livers have shown an increase in arterial perfusion, decrease in portal perfusion, decrease in total blood flow, and an increase in MTT.

These findings can be corroborated with other published studies. In an earlier study by Van Beers *et al*[7], a cutoff threshold of 22.6 s for the MTT in the liver enabled the diagnosis of liver cirrhosis to be made with a sensitivity and specificity of 81%. In another study, Hagiwara *et al*[8] have used a dual-input single-compartment CC model and have found that there was an increase in the arterial blood flow, arterial fraction, distribution volume, and MTT in patients with advanced hepatic fibrosis. Receiver operating curve analysis has shown that the MTT, distribution volume and arterial flow are good predictive parameters with an area under the receiver operating characteristic curves that ranges from 0.791 to 0.824, and reported sensitivity of 76.9%-84.6% and specificity of 71.4%-78.5%. Thus, MR liver perfusion appears to be a promising method for the non-invasive diagnosis of liver cirrhosis and for assessing the severity of the condition.

CONCLUSION

MR liver perfusion imaging provides functional information about the microcirculation of liver parenchyma and focal liver lesions and appears to be a promising technique for evaluating liver metastases and HCC; for assessing the efficacy of anti-angiogenic or local tumor ablation therapy; and for diagnosing cirrhosis and assessing its severity. However, standardization of imaging acquisition and analysis techniques need to be actively addressed for the technique to be widely adopted.

ACKNOWLEDGMENTS

The authors would like to acknowledge Mr. Septian Hartono (National Cancer Centre, Singapore) and Dr. Keiko Miyazaki (Institute of Cancer Research, UK) for their valuable assistance in the preparation of the manuscript.

REFERENCES

1 **Leggett DA**, Kelley BB, Bunce IH, Miles KA. Colorectal cancer: diagnostic potential of CT measurements of hepatic perfusion and implications for contrast enhancement protocols. *Radiology* 1997; **205**: 716-720
2 **Miles KA**, Hayball MP, Dixon AK. Functional images of hepatic perfusion obtained with dynamic CT. *Radiology* 1993; **188**: 405-411
3 **Blomley MJ**, Coulden R, Dawson P, Kormano M, Donlan P, Bufkin C, Lipton MJ. Liver perfusion studied with ultrafast CT. *J Comput Assist Tomogr* 1995; **19**: 424-433
4 **Koh TS**, Thng CH, Hartono S, Lee PS, Choo SP, Poon DY, Toh HC, Bisdas S. Dynamic contrast-enhanced CT imaging of hepatocellular carcinoma in cirrhosis: feasibility of a prolonged dual-phase imaging protocol with tracer kinetics

modeling. *Eur Radiol* 2009; **19**: 1184-1196
5 **Hashimoto K**, Murakami T, Dono K, Hori M, Kim T, Kudo M, Marubashi S, Miyamoto A, Takeda Y, Nagano H, Umeshita K, Nakamura H, Monden M. Assessment of the severity of liver disease and fibrotic change: the usefulness of hepatic CT perfusion imaging. *Oncol Rep* 2006; **16**: 677-683
6 **Annet L**, Materne R, Danse E, Jamart J, Horsmans Y, Van Beers BE. Hepatic flow parameters measured with MR imaging and Doppler US: correlations with degree of cirrhosis and portal hypertension. *Radiology* 2003; **229**: 409-414
7 **Van Beers BE**, Leconte I, Materne R, Smith AM, Jamart J, Horsmans Y. Hepatic perfusion parameters in chronic liver disease: dynamic CT measurements correlated with disease severity. *AJR Am J Roentgenol* 2001; **176**: 667-673
8 **Hagiwara M**, Rusinek H, Lee VS, Losada M, Bannan MA, Krinsky GA, Taouli B. Advanced liver fibrosis: diagnosis with 3D whole-liver perfusion MR imaging--initial experience. *Radiology* 2008; **246**: 926-934
9 **Chiandussi L**, Greco F, Sardi G, Vaccarino A, Ferraris CM, Curti B. Estimation of hepatic arterial and portal venous blood flow by direct catheterization of the vena porta through the umbilical cord in man. Preliminary results. *Acta Hepatosplenol* 1968; **15**: 166-171
10 **Pandharipande PV**, Krinsky GA, Rusinek H, Lee VS. Perfusion imaging of the liver: current challenges and future goals. *Radiology* 2005; **234**: 661-673
11 **Villeneuve JP**, Dagenais M, Huet PM, Roy A, Lapointe R, Marleau D. The hepatic microcirculation in the isolated perfused human liver. *Hepatology* 1996; **23**: 24-31
12 **Liu Y**, Matsui O. Changes of intratumoral microvessels and blood perfusion during establishment of hepatic metastases in mice. *Radiology* 2007; **243**: 386-395
13 **Terayama N**, Terada T, Nakanuma Y. An immunohistochemical study of tumour vessels in metastatic liver cancers and the surrounding liver tissue. *Histopathology* 1996; **29**: 37-43
14 **Nakanuma Y**, Terada T, Terasaki S, Ueda K, Nonomura A, Kawahara E, Matsui O. 'Atypical adenomatous hyperplasia' in liver cirrhosis: low-grade hepatocellular carcinoma or borderline lesion? *Histopathology* 1990; **17**: 27-35
15 **Hayashi M**, Matsui O, Ueda K, Kawamori Y, Gabata T, Kadoya M. Progression to hypervascular hepatocellular carcinoma: correlation with intranodular blood supply evaluated with CT during intraarterial injection of contrast material. *Radiology* 2002; **225**: 143-149
16 **Wang HZ**, Riederer SJ, Lee JN. Optimizing the precision in T1 relaxation estimation using limited flip angles. *Magn Reson Med* 1987; **5**: 399-416
17 **Orton MR**, Miyazaki K, Koh DM, Collins DJ, Hawkes DJ, Atkinson D, Leach MO. Optimizing functional parameter accuracy for breath-hold DCE-MRI of liver tumours. *Phys Med Biol* 2009; **54**: 2197-2215
18 **Jackson A**, Haroon H, Zhu XP, Li KL, Thacker NA, Jayson G. Breath-hold perfusion and permeability mapping of hepatic malignancies using magnetic resonance imaging and a first-pass leakage profile model. *NMR Biomed* 2002; **15**: 164-173
19 **Tsushima Y**, Blomley MJ, Kusano S, Endo K. Measuring portal venous perfusion with contrast-enhanced CT: comparison of direct and indirect methods. *Acad Radiol* 2002; **9**: 276-282
20 **Koh TS**, Thng CH, Lee PS, Hartono S, Rumpel H, Goh BC, Bisdas S. Hepatic metastases: in vivo assessment of perfusion parameters at dynamic contrast-enhanced MR imaging with dual-input two-compartment tracer kinetics model. *Radiology* 2008; **249**: 307-320
21 **Tofts PS**, Brix G, Buckley DL, Evelhoch JL, Henderson E, Knopp MV, Larsson HB, Lee TY, Mayr NA, Parker GJ, Port RE, Taylor J, Weisskoff RM. Estimating kinetic parameters from dynamic contrast-enhanced T(1)-weighted MRI of a diffusable tracer: standardized quantities and symbols. *J Magn Reson Imaging* 1999; **10**: 223-232
22 **Totman JJ**, O'gorman RL, Kane PA, Karani JB. Comparison of the hepatic perfusion index measured with gadolinium-enhanced volumetric MRI in controls and in patients with colorectal cancer. *Br J Radiol* 2005; **78**: 105-109
23 **Tsushima Y**, Blomley MJ, Yokoyama H, Kusano S, Endo K. Does the presence of distant and local malignancy alter parenchymal perfusion in apparently disease-free areas of the liver? *Dig Dis Sci* 2001; **46**: 2113-2119
24 **Warren HW**, Gallagher H, Hemingway DM, Angerson WJ, Bessent RG, Wotherspoon H, McArdle CS, Cooke TG. Prospective assessment of the hepatic perfusion index in patients with colorectal cancer. *Br J Surg* 1998; **85**: 1708-1712
25 **Ballantyne KC**, Charnley RM, Perkins AC, Pye G, Whalley DR, Wastie ML, Hardcastle JD. Hepatic perfusion index in the diagnosis of overt metastatic colorectal cancer. *Nucl Med Commun* 1990; **11**: 23-28
26 **Meijerink MR**, van Waesberghe JH, van der Weide L, van den Tol P, Meijer S, van Kuijk C. Total-liver-volume perfusion CT using 3-D image fusion to improve detection and characterization of liver metastases. *Eur Radiol* 2008; **18**: 2345-2354
27 **Cuenod C**, Leconte I, Siauve N, Resten A, Dromain C, Poulet B, Frouin F, Clément O, Frija G. Early changes in liver perfusion caused by occult metastases in rats: detection with quantitative CT. *Radiology* 2001; **218**: 556-561
28 **Abdullah SS**, Pialat JB, Wiart M, Duboeuf F, Mabrut JY, Bancel B, Rode A, Ducerf C, Baulieux J, Berthezene Y. Characterization of hepatocellular carcinoma and colorectal liver metastasis by means of perfusion MRI. *J Magn Reson Imaging* 2008; **28**: 390-395
29 **Fournier LS**, Cuenod CA, de Bazelaire C, Siauve N, Rosty C, Tran PL, Frija G, Clement O. Early modifications of hepatic perfusion measured by functional CT in a rat model of hepatocellular carcinoma using a blood pool contrast agent. *Eur Radiol* 2004; **14**: 2125-2133
30 **Sahani DV**, Holalkere NS, Mueller PR, Zhu AX. Advanced hepatocellular carcinoma: CT perfusion of liver and tumor tissue--initial experience. *Radiology* 2007; **243**: 736-743
31 **Matsui O**, Kadoya M, Kameyama T, Yoshikawa J, Takashima T, Nakanuma Y, Unoura M, Kobayashi K, Izumi R, Ida M. Benign and malignant nodules in cirrhotic livers: distinction based on blood supply. *Radiology* 1991; **178**: 493-497
32 **Sijens PE**. Parametric exploration of the liver by magnetic resonance methods. *Eur Radiol* 2009; **19**: 2594-2607
33 **Eisenhauer EA**, Therasse P, Bogaerts J, Schwartz LH, Sargent D, Ford R, Dancey J, Arbuck S, Gwyther S, Mooney M, Rubinstein L, Shankar L, Dodd L, Kaplan R, Lacombe D, Verweij J. New response evaluation criteria in solid tumours: revised RECIST guideline (version 1.1). *Eur J Cancer* 2009; **45**: 228-247
34 **Llovet JM**, Di Bisceglie AM, Bruix J, Kramer BS, Lencioni R, Zhu AX, Sherman M, Schwartz M, Lotze M, Talwalkar J, Gores GJ. Design and endpoints of clinical trials in hepatocellular carcinoma. *J Natl Cancer Inst* 2008; **100**: 698-711
35 **Bruix J**, Sherman M. Management of hepatocellular carcinoma. *Hepatology* 2005; **42**: 1208-1236
36 **Bruix J**, Sherman M, Llovet JM, Beaugrand M, Lencioni R, Burroughs AK, Christensen E, Pagliaro L, Colombo M, Rodés J. Clinical management of hepatocellular carcinoma. Conclusions of the Barcelona-2000 EASL conference. European Association for the Study of the Liver. *J Hepatol* 2001; **35**: 421-430
37 **Prokop M**. CT and MR to assess the response of liver tumors to hepatic perfusion. *Recent Results Cancer Res* 1998; **147**: 136-154
38 **Wang J**, Chen LT, Tsang YM, Liu TW, Shih TT. Dynamic contrast-enhanced MRI analysis of perfusion changes in advanced hepatocellular carcinoma treated with an antiangiogenic agent: a preliminary study. *AJR Am J Roentgenol* 2004; **183**: 713-719
39 **Miyazaki K**, Collins DJ, Walker-Samuel S, Taylor JN,

Padhani AR, Leach MO, Koh DM. Quantitative mapping of hepatic perfusion index using MR imaging: a potential reproducible tool for assessing tumour response to treatment with the antiangiogenic compound BIBF 1120, a potent triple angiokinase inhibitor. *Eur Radiol* 2008; **18**: 1414-1421

40 **Meijerink MR**, van Cruijsen H, Hoekman K, Kater M, van Schaik C, van Waesberghe JH, Giaccone G, Manoliu RA. The use of perfusion CT for the evaluation of therapy combining AZD2171 with gefitinib in cancer patients. *Eur Radiol* 2007; **17**: 1700-1713

41 **Meijerink MR**, van Waesberghe JH, van der Weide L, van den Tol P, Meijer S, Comans EF, Golding RP, van Kuijk C. Early detection of local RFA site recurrence using total liver volume perfusion CT initial experience. *Acad Radiol* 2009; **16**: 1215-1222

42 **Chen G**, Ma DQ, He W, Zhang BF, Zhao LQ. Computed tomography perfusion in evaluating the therapeutic effect of transarterial chemoembolization for hepatocellular carcinoma. *World J Gastroenterol* 2008; **14**: 5738-5743

43 **Bolton RP**, Mairiang EO, Parkin A, Ware F, Robinson P, Losowsky MS. Dynamic liver scanning in cirrhosis. *Nucl Med Commun* 1988; **9**: 235-247

44 **Guan S**, Zhao WD, Zhou KR, Peng WJ, Mao J, Tang F. CT perfusion at early stage of hepatic diffuse disease. *World J Gastroenterol* 2005; **11**: 3465-3467

45 **Materne R**, Annet L, Dechambre S, Sempoux C, Smith AM, Corot C, Horsmans Y, Van Beers BE. Dynamic computed tomography with low- and high-molecular-mass contrast agents to assess microvascular permeability modifications in a model of liver fibrosis. *Clin Sci* (Lond) 2002; **103**: 213-216

46 **Materne R**, Van Beers BE, Smith AM, Leconte I, Jamart J, Dehoux JP, Keyeux A, Horsmans Y. Non-invasive quantification of liver perfusion with dynamic computed tomography and a dual-input one-compartmental model. *Clin Sci* (Lond) 2000; **99**: 517-525

47 **Materne R**, Smith AM, Peeters F, Dehoux JP, Keyeux A, Horsmans Y, Van Beers BE. Assessment of hepatic perfusion parameters with dynamic MRI. *Magn Reson Med* 2002; **47**: 135-142

48 **Scharf J**, Zapletal C, Hess T, Hoffmann U, Mehrabi A, Mihm D, Hoffmann V, Brix G, Kraus T, Richter GM, Klar E. Assessment of hepatic perfusion in pigs by pharmacokinetic analysis of dynamic MR images. *J Magn Reson Imaging* 1999; **9**: 568-572

49 **Cuenod CA**, Leconte I, Siauve N, Frouin F, Dromain C, Clément O, Frija G. Deconvolution technique for measuring tissue perfusion by dynamic CT: application to normal and metastatic liver. *Acad Radiol* 2002; **9** Suppl 1: S205-S211

50 **Funabasama S**, Tsushima Y, Sanada S, Inoue K.[J]Hepatic perfusion CT imaging analyzed by the dual-input one-compartment model] *Nippon Hoshasen Gijutsu Gakkai Zasshi* 2003; **59**: 1548-1554

51 **Miyazaki S**, Murase K, Yoshikawa T, Morimoto S, Ohno Y, Sugimura K. A quantitative method for estimating hepatic blood flow using a dual-input single-compartment model. *Br J Radiol* 2008; **81**: 790-800

52 **Lee TY**, Purdie TG, Stewart E. CT imaging of angiogenesis. *Q J Nucl Med* 2003; **47**: 171-187

53 **St Lawrence KS**, Lee TY. An adiabatic approximation to the tissue homogeneity model for water exchange in the brain: I. Theoretical derivation. *J Cereb Blood Flow Metab* 1998; **18**: 1365-1377

S- Editor Tian L **L- Editor** Kerr C **E- Editor** Ma WH

World Journal of Gastroenterology

Online Submissions: http://www.wjgnet.com/1007-9327office
wjg@wjgnet.com
doi:10.3748/wjg.v16.i13.1610

World J Gastroenterol 2010 April 7; 16(13): 1610-1621
ISSN 1007-9327 (print)

REVIEW

Techniques for colorectal anastomosis

Yik-Hong Ho, Mohamed Ahmed Tawfik Ashour

Yik-Hong Ho, Mohamed Ahmed Tawfik Ashour, Discipline of Surgery, School of Medicine, James Cook University, Townsville, QLD 4811, Australia
Author contributions: Ho YH and Ashour MAT contributed equally to this review.
Correspondence to: Yik-Hong Ho, MD, FRCSEd, FRCS (Glasc.), FRACS, FICS, Professor and Head of Surgery, Discipline of Surgery, School of Medicine, James Cook University, Clinical School 1MB52, Angus Smith Dr, Douglas, Townsville, QLD 4811, Australia. yikhong.ho@jcu.edu.au
Telephone: +61-7-47961417 Fax: +61-7-47961401
Received: December 15, 2009 Revised: January 20, 2010
Accepted: January 27, 2010
Published online: April 7, 2010

Abstract

Colorectal anastomotic leak remains one of the most feared post-operative complications, particularly after anterior resection of the rectum with, the shift from abdomino-peritoneal resections to total mesorectal excision and primary anastomosis. The literature fails to demonstrate superiority of stapled over hand-sewn techniques in colorectal anastomosis, regardless of the level of anastomosis, although a high stricture rate was noted in the former technique. Thus, improvements in safety aspects of anastomosis and alternatives to hand-sewn and stapled techniques are being sought. Here, we review alternative anastomotic techniques used to fashion bowel anastomosis. Compression anastomosis using compression anastomotic clips, endoluminal compression anastomotic rings, AKA-2, biofragmental anastomotic rings, or Magnamosis all involve the concept of creating a sutureless end-to-end anastomosis by compressing two bowel ends together, leading to a simultaneous necrosis and healing process that joins the two lumens. Staple line reinforcement is a new approach that reduce the drawbacks of staplers used in colorectal practice, i.e. leakage, bleeding, misfiring, and inadequate tissue approximation. Various non-absorbable, semi or fully absorbable materials are now available. Two other techniques can provide alternative anastomotic support to the suture line: a colorectal drain and a polyester stent, which can be utilized in ultra-low rectal excision and can negate the formation of a defunctioning stoma. Doxycycline coated sutures have been used to overcome the post-operative weakness in anastomosis secondary to rapid matrix degradation mediated by matrix metalloproteinase. Another novel technique, the electric welding system, showed promising results in construction of a safe, neat, smooth sutureless bowel anastomosis. Various anastomotic techniques have been shown to be comparable to the standard techniques of suturing and stapling. However, most of these alternatives need to be accepted and optimized for future use.

Key words: Alternative anastomosis; Compression anastomotic clip; Compression anastomotic ring; Biofragmental anastomotic ring; AKA-2; Magnamosis (magnetic anastomosis); Matrix metallo-proteinase; Sutureless

Peer reviewer: Antonio Basoli, Professor, General Surgery "Paride Stefanini", Università di Roma-Sapienza, Viale del Policlinico 155, Roma 00161, Italy

Ho YH, Ashour MAT. Techniques for colorectal anastomosis. *World J Gastroenterol* 2010; 16(13): 1610-1621 Available from: URL: http://www.wjgnet.com/1007-9327/full/v16/i13/1610.htm
DOI: http://dx.doi.org/10.3748/wjg.v16.i13.1610

INTRODUCTION

Since the first reports of laparoscopic colectomy in the 1990's, this technique has matured into a well-developed mode of therapy. It has introduced the colorectal surgical world to the advantages, and the unique perspectives and concerns of minimal access surgery. Colorectal anastomotic leakage remains one of the most feared post-operative complications, particularly after anterior resection of the rectum, with the shift from abdomino-peritoneal resections to total mesorectal excision and primary

anastomosis. It is also associated with a higher local recurrence rate and lower long-term survival. Moreover, long-term functional outcome might be adversely affected by anastomotic leakage[1-4]. The importance of surgical technique is underscored by the wide variations of anastomotic leakage rates among surgeons. The frequency of anastomotic leakage ranges from 1% to 24%[5-7]. The rate of leakage is generally considered to be higher for elective rectal anastomosis (12% to 19%) than for colonic anastomosis (11%)[8-10].

PHYSIOLOGY OF GASTROINTESTINAL HEALING

Better appreciation of the principles of intestinal healing will lead to a better adoption of techniques to overcome the risk factors inherent to the laparoscopic approach and hence anastomotic dehiscence. The environment for wound healing is substantially different in an anastomosis, due to the presence of shear stress (secondary to intraluminal bulk transit and peristalsis), as well as the presence of aerobic and anaerobic bacteria.

The process of intestinal anastomotic healing can be arbitrarily divided into an acute inflammatory (lag) phase, a proliferative phase, and, finally, a remodeling or maturation phase. Collagen is the single most important molecule for determining intestinal wall strength, which makes its metabolism of particular interest for understanding anastomotic healing. After surgery, degradation of mature collagen begins in the first 24 h and predominates for the first four days. This is caused by the upregulation of matrix metalloproteinases (MMPs), which are an important class of enzymes involved in collagen metabolism. *In vivo* use of MMP inhibitors has been found to increase the strength of intestinal anastomoses by up to 48% at postoperative day three, which suggests that these enzymes are important in determining the risk of leakage. By postoperative day seven, collagen synthesis takes over, especially proximal to the anastomosis. After five to six weeks, there is no significant increase in the amount of collagen in a healing wound or anastomosis, though turnover and, thus synthesis, are extensive. The strength of the scar continues to increase progressively with time. The orientation and the cross-linking between collagen fibers maintain the tensile strength of the tissues[11,12].

Bursting pressure is used as a quantitative measure to grade the strength of an anastomosis *in vivo*. This pressure has been found to increase rapidly in the early postoperative period, reaching 60% of the strength of the surrounding bowel by three to four days and 100% by 1 wk[11]. In 1887, Halsted[13] discovered that the submucosa provides the GI tract with the majority of its tensile strength. The bulk of collagen is contained within this layer, along with blood vessels, lymphatics, and nerve fibers. Type I collagen predominates (68%), followed by type Ⅲ collagen (20%), and type V collagen (12%). The serosa is a thin layer of connective tissue that covers the muscularis propria. When creating an anastomosis, direct apposition of this layer minimizes the risk of leakage[14,15]. During the first postoperative days, anastomotic strength is limited, and hence the risk of wound failure is greatest, as collagen breakdown increases. Early anastomotic strength is therefore dependent on the suture- or staple-holding capacity of existing collagen, until a large amount of new collagen can be synthesized by both fibroblasts and smooth muscle cells. Postoperatively, anastomosis will be weak for one or two days until this occurs[16-19].

FASHIONING ANASTOMOSES

Over the past two decades, numerous different materials have been used to join one bowel end to another, including catgut, stainless steel, and newer monofilamentous and absorbable sutures. In the past 30 years, stapling devices have been embraced enthusiastically by the surgical community[11]. However, the choice of either technique in fashioning anastomoses is a matter of controversy among various schools[18].

Apart from inert substances, most foreign materials will evoke an inflammatory reaction in the human body and surgical sutures are no exception. It is now known that silk has the ability to evoke an inflammatory reaction that can persist for weeks after implantation. Substances such as polypropylene (Prolene), catgut, and polyglycolic acid (Dexon) evoke a milder response. There is little difference between absorbable and nonabsorbable sutures with respect to the strength of the anastomosis[11].

STAPLING

Surgical stapling devices were first introduced by Hültl, Humer (Budapest) in 1908; but their use has grown since the introduction of new and reliable disposable instruments in the past 30 years[11]. However despite comparable results in terms of mortality, anastomotic dehiscence, and wound infection, the rate of stricture at the anastomotic site is considerably higher with staples than with sutures: 8% *vs* 2%, respectively, for colorectal anastomosis[20].

Lim *et al*[21] confirmed the presence of foreign body reaction in stapled human GI anastomoses. The source of the foreign materials eliciting this reaction was the stapler cartridges.

The literature fails to demonstrate superiority of stapled over hand-sewn techniques in colorectal anastomosis, regardless of the level of anastomosis, although a high stricture rate was noted with the former technique.

The use of staplers for intraperitoneal anastomosis has been questioned[20]; Matos systematically reviewed (Cochrane Database) nine studies involving 1233 patients (622 stapled and 611 hand-sewn) and found that overall leaks were 13% *vs* 13.4%, clinical 6.3% *vs* 7.1%, radiological 7.8% *vs* 7.2%. There was insufficient evidence to demonstrate superiority of either technique[20]. The decision over which technique to use must be judged on the basis of previous experience, clinical circumstances, and available resources. Another systematic review showed that both techniques (stapler *vs* Hand-sewn) are effective,

and the choice may be based on personal preference[22]. Other prospective and randomized trials have shown different results. No significance intergroup difference was found in regard to time for anastomosis construction or occurrence of complications in colorectal anastomosis[23]. In addition, the routine use of stapling instruments for infraperitoneal colorectal anastomosis could not be recommended because of a higher incidence of mishaps and strictures, even though the operation took less time to perform and anastomotic leakage occurred less often[24].

Therefore, there is an ongoing search for an ideal method of anastomosis that would not only lower the incidence of dangerous complications, but also avoid the need for a defunctioning colostomy or ileostomy. Based on the aforementioned data, there is still controversy between surgeons.

It is therefore necessary to review all relevant studies and trials to resolve this issue. Multi-center, well-designed, randomized controlled trials are required to build a link between new technology and practice. As technology advances, the use of newer techniques should allow improvements in the quality of patient care.

COMPRESSION ANASTOMOSIS

Connecting sections of the intestine after the surgical removal of a diseased portion has been the subject of research and invention since the 19th century. The goal has been to find a method to eliminate the leakage associated with anastomosis. The principle of compression anastomosis consists of two opposing rings trapping the cut ends of the transected bowel with subsequent ischemia and eventual sloughing of the trapped bowel, thus releasing the rings into the fecal stream[25]. Despite its technical safety, it was not accepted[26].

The idea of compression anastomosis was first reported in 1826 by Denan, who conceived a sutureless bowel anastomosis that encompassed the inverting technique proposed by Lembert. The idea was to compress two bowel walls together and cause a simultaneous necrosis and healing process leading to the joining of the two lumens. In 1892, Murphy introduced a mechanical device known as "Murphy's button" that was used for years[27].

It comprises a pair of metal rings that hold circular segments of intestine together under continuous pressure; the rings are expelled several days after surgery. However, its clinical success was limited and the results were mediocre. Moreover, it was a metallic foreign body that remained in the lumen of the bowel for several days until it was spontaneously discharged from the body with the necrotic tissues[28].

In the 1980s a device comprising two magnetic rings was used for intestinal anastomosis, but this concept was not further pursued[29].

In 1984, Kanshin *et al*[30] developed the AKA-2 device (Seidel Medipool, Munich, Germany) for colorectal surgery. In 1985, Hardy *et al*[31] introduced the Valtrac biofragmentable anastomotic ring (BAR) (Davis and Geck/Cyanamid, Danbury, CT). Numerous publications, including prospective randomized controlled trials (RCTs), reported that the BAR was safe and efficacious in both emergency and elective surgery[31-39]. Both devices adopted the concept of compression anastomosis, and incorporated some of the basic features of Murphy's button. However, in contrast to the BAR, the AKA-2 ring is not absorbable and it is usually disconnected from the anastomosis after four to six days. In addition, it was made exclusively for transanal application[40].

Years later a novel device for performing compression anastomosis using the shape memory alloy (SMA) of nickel-titanium was introduced. The device is available both as a clip (Compression Anastomosis Clip or CAC, NiTi Medical Technologies, Netanya, Israel), and as a ring (Compression Anastomosis Ring or CAR, NiTi Medical Technologies). After approximately one week, the entire device, together with the necrosed tissue, detaches and is naturally expelled from the body[41-44]. A summary of the four main types of compression devices is presented in Table 1.

CLASSIFICATION OF DIFFERENT COMPRESSION DEVICES

Valtrac™ BAR

Valtrac™ BAR is composed of two segments containing absorbable polyglycolic acid (87.5%) and barium sulfate (12.5%). It comes in a size range (25, 28, 31, and 34 mm). The two components interdigitate on a central frame; a 6-mm gap is seen between the scalloped edges of the BAR in the open position, and a 1.5-mm, 2-mm, or 2.5-mm gap is made in the fully closed position to accommodate different thicknesses of bowel wall. This also limits the amount of tissue necrosis[45].

Each ring is securely placed into the cut bowel ends with the aid of a purse-string suture, and the device snapped shut. Between two and three weeks after the operation, the BAR rings fragment and are passed into the stool. This results in the production of a sutureless, inverted, serosa-to-serosa intestinal anastomosis[46]. The BAR has been used for construction of various types of anastomosis, including procedures involving the upper and lower GI tract. Prior to the development of the transanal applicator, early studies often excluded patients with low rectal anastomosis[47].

In a randomized control trail comparing BAR with stapling devices in extra-peritoneal mid-rectal anastomosis, surgeons did not consider the use of BAR to be more difficult than a stapled anastomosis. The time required to create a BAR anastomosis was slightly shorter than the time needed for a stapled anastomosis, although this was not statistically significant. The overall operating time, intraoperative blood loss, and postoperative complication rates were similar with both anastomotic techniques[48]. Correspondingly, there were no statistical differences in the complication rates between the BAR and a sutured anastomosis in elective and emergency procedures[48].

Table 1 Characteristics of the four main compression devices

	BAR	AKA-2	CAC	EndoCAR[27]
Absorbable	Yes	No	No	No
Application	Laparoscopy, laparoscopy, transanal	Transanal	Laparotomy, laparoscopy, hand-assisted lap	Laparotomy, laparoscopy, hand-assisted lap
Internal Lumen	11-20	25, 28, 31	8	One ring size (27 mm) replaces a number of competitive sizes (25-34 mm)
Average time to expulsion (d)	14-21	4-6	7	7-10
Type of surgery				
Elective/emergency	Yes/yes	Yes/yes	Yes/no	Yes/no
Foreign body reaction	No	Possible to metal pins	No	No
Tissue healing	Extensive fibrosis/may cause stricture	Extensive fibrosis/may cause stricture	Primary intention/no strictures reported	Primary intention/no strictures reported (recovery of multi-layer lumen structure)
Anastomotic index	Lumen capacity depends upon standardized ring size		Full lumen capacity within 8-12 wk	
Efficacy	Safe and secure and can be applied to achieve multiple anastomosis (in case requiring rapidity and security)			
Learning curve[1]	Technically difficult than the other three devices		Technically simple after education	
Cost[2]	About $600	NA	About $3	NA (however higher than conventional staples)
Tissue thickness accommodation	Selecting ring size to be compatible with diameter and thickness of bowel wall	Same as BAR	Only one size, shape memory alloy that accommodates varies tissue thickness. Unique thermo-mechanical properties and super elasticity	
Type of anastomosis	End-to-end, end-to-side, side-to-side		Side-to-side	End-to-end
Site of anastomosis	Suitable for intestinal, colonic and rectal anastomosis	Distal colon and rectal only	Intestinal, colonic and rectal anastomosis	

[1]Galizia *et al*[47] described a learning curve of nine patients for BAR anastomosis. A meta-analysis of over 500 cases in North America, Europe and Israel, 75% of surgeons rated the CAR[27] device to be very easy or easy to use[83]; [2]Cost-effectives depend upon a number of factors namely learning curve and post operative morbidity. However, as multiple staplers are used for construction of most colonic/rectal anastomosis, there might be a cost advantage for compression devices. BAR: Biofragmentable anastomotic ring; CAC: Compression anastomotic clip.

An initial study with large animal models (300 dogs and 31 pigs) presented a randomized analysis of 28 pigs, comparing sutured, stapled and BAR anastomosis. They found the "Burst" pressure at day 0 was highest with the BAR and equal at days seven and 16 in all three types of anastomosis. The authors stated that the BAR anastomoses were performed more easily and quickly than the other two anastomoses. Microscopic examination also revealed the least amount of tissue necrosis for the BAR anastomosis[46].

In 1987, Hardy *et al*[49] published results of the first 27 patients who had colorectal anastomoses using the BAR device. They reported no difficulties and all patients tolerated a regular diet before fragmentation of the rings.

In the 1990s, the device gained popularity and a number of prospective studies confirmed that the results with the device were satisfactory, although there were reports of intraoperative problems, such as failure of the purse-string suture, incorrect estimation of the diameter of the colon lumen, subsequent mucosal tears, and failure of the device to lock. Many of these might simply have been because of the operator's learning curve[33,50-53].

Based on the previously mentioned studies, possible limitations of the device include: (1) Failure of purse string sutures; (2) Incorrect estimation of colon lumen diameter; (3) Subsequent mucosal tears; (4) Failure of the device to lock (the bowel might be contused by closing maneuver from outside the gut); (5) Excessive snapping pressure could shatter the friable device; (6) fragmentation delay; (7) possibility of postoperative tenesmus and frequent stool passage before excretion of fragments; (8) bulky and uncomfortable device to deploy; and (9) potential risk of relative obstruction due to smaller inner diameter of the ring.

AKA-2

In 1984, Kanshin *et al*[30] developed the AKA-2 device (Seidel, Medipool) to address the transanal approach for compression anastomosis. The AKA-2 is composed of two rings: a base ring, which includes metal pins and metal springs, attached on a plastic ring (the "distal ring"), and a proximal plastic ring (the "proximal ring"). The rings are applied with a transanal applicator. The AKA-2 works on a similar principle to that of endoanal stapling devices, though the bowel edges are pressed together with intraluminal rings and held in place by metal pins. Circular blades cut the central cuff of bowel, and the metal pins ensure constant compression on the inverted bowel edges. The two plastic rings and the compressed resection margins separate from the anastomosis after four to six days and are expelled with the feces[46]. The technique had an advantage in that it created a good lumen size for stool passage.

There is only one report in English of the use of this device[40]; the majority of the literature being in Russian or German. A prospective audit presented the results of

442 patients undergoing colorectal surgery for benign and cancerous disease. There was a 5.4% overall complication rate, with 11 patients (2.5%) developing clinical features of an anastomotic leak, which is relatively low compared to other series using various anastomotic techniques[48,49,54,55]. Fourteen of the 442 patients died (3.2%), of which three cases were related to anastomotic leak (0.7%). Among 442 patients who underwent AKA-2 anastomosis only two patients developed a stricture[40].

The authors maintain that the advantage of this device is that it produces a good size lumen for the passage of feces. The plastic ring sizes are 25, 28, and 31 mm, respectively. In addition, necrosis of inverted resection margins is the only biological factor leading to the rejection of the plastic rings, which is an advantage in cases with delayed healing. However, early device exclusion raised the possibility of higher leak rate, as it is concurrent with the maximal breaking strength of anastomosis[46].

Compression anastomotic clip

Nitinol[60] (Nickel Titanium Naval Ordinance Laboratory), an alloy of nickel and titanium, is a temperature-dependent, shape-memory alloy (SMA) that has been used in the formation of compression anastomoses[56]. The metal is shaped under high temperatures, and when it is ice cooled (to less than 0℃), it loses its rigidity and becomes flexible. At or above room temperature, it resumes its preset configuration. It has been used mostly for vascular prostheses, orthodontic braces, and for internal fixation of bone fractures for its inherent advantage of controlled compression with a constant force[46].

The Nitinol CAC device (Niti Medical Technologies) has been approved by the food and drug administration (FDA) for use in GI surgery[41]. The device consists of a double-ring that, in the open and flexible state (at 0℃), has a diameter of 30 mm and an opening angle of 30 degrees. At body temperature, the rings return to their closed configuration and hold bowel tissue under a constant compressive force, regardless of the thickness of intervening tissue. This leads to ischemia of the entrapped bowel wall and the formation of a compression anastomosis. The internal diameter of the rings is 8 mm, and is pierced by a 5-mm blade built into the applicator to restore bowel continuity in the early period. The device is elastic, pliable, and easy to manipulate[46].

Initial reports on both animal and human studies using the CAC device to create a side-to-side anastomosis in upper and lower GI tracts revealed no signs of anastomotic stricture or leakage, with formation of a uniform, completely re-epithelialized anastomotic line[41]. There were no reported postoperative complications, and colonoscopic examination at six months demonstrated a satisfactory anastomosis[43].

The safety of this device has been documented in numerous animal studies[41,57], and the safety of the alloy has been demonstrated by its extensive uses in other medical procedures. The CAC was considered to be safe, simple, and effective in colon surgery in a study that evaluated the thermo-mechanical properties of the device[58].

In line with this conclusion, a randomized control trial studied the clinical effects of using the CAC device in small intestinal anastomosis proximal to the ileocecal valve. CAC anastomosis was performed in 33 out of 66 patients, with the other 33 patients being used as a control group for whom a stapled anastomosis was constructed. The main indication was gastric cancer in both groups. Anastomosis was fashioned to reconstruct a Roux-en-Y loop, entero-entrostomy, Billroth Ⅱ gastro-jejunostomy, and gastro-jejunostomy. The authors found no post-operative complications whatsoever in terms of leakage, obstruction, bleeding, or stenosis after six months of follow-up[59].

Clinical trials for SMA of nickel-titanium in intestinal anastomosis are scarce, and all of the clinical reports are of CAC from a single center that included only elective cases performed both by laparotomy and laparoscopically[42-44]. None of the patients who underwent surgery with CAC had a protective stoma. None of the patients reported so far in published clinical studies experienced a clinical leak and initial experience with a laparoscopic technique had similar results, thus precluding the learning curve among surgeons.

The consensus among the published studies was that microscopic examination of the CAC anastomosis showed minimal inflammation and no foreign body reaction, with very little scar tissue at the anastomotic line.

The specific advantages of the CAC include a one sized clip with a wide external diameter, preprogrammed round shape negating the need to forcefully close the rings and therefore diminish the risk of shattering the device. It exerts constant compression of the bowel ends, regardless of the intervening tissue thickness; coils exert a constant stress plateau at about 400 Mpa. The result is a smooth homogenous anastomosis formed by the gradual controlled necrosis of the tissue, limited by the coil perimeter while the external edges become sealed[46]. A drawback of this device is the need for suture closure of the insertion incisions made in the bowel wall.

Endoluminal compression anastomotic ring, EndoCAR[27]

The endoluminal compression anastomotic ring, EndoCAR[27] (spectrum of the shape memory alloy of nickel-titanium), utilizes two separate synthetic rings that are mounted on an instrument very similar to a circular stapler. An anvil containing one ring is fixed to the proximal bowel end, and the instrument with the other ring is inserted trans-anally for a rectal anastomosis. When engaged, the rings are locked together by Nitinol springs that exert the desired constant controlled pressure force (7.7 Newtons or 1.65 Pounds), and a circular knife resects the access tissue. As in the side-to-side device, a simultaneous necrosis-healing process takes place, and at the completion of this process (seven to ten days), the

Table 2 Compression anastomosis: clinical experience and complications

Study	Device	Emergency/elective	Anastomotic leakage	Obstruction	Stricture
Bubrick *et al*[34]	BAR	0/395	12 (3.2%)	18 (5%)	-
Cahill *et al*[35]	BAR	0/101	2 (2%)	4 (4%)	-
Corman *et al*[36]	BAR	0/222	6 (2.7%)	9 (4%)	2 (0.9%)
Gullichsen *et al*[37]	BAR	-	-	13 (16%)	-
Seow-Choen *et al*[39]	BAR	-	0	0	2 (10%)
Di Castro *et al*[49]	BAR	90/424	17	0	4 (1%)
Thiede *et al*[33]	BAR	0/1360	34 (2.5%)	-	-
Pahlman *et al*[38]	BAR	24/26	2 (4%)	3 (6%)	-
Ghitulescu *et al*[53]	BAR	23/136	7 (4.2%)	13 (7.9%)	3 (1.8%)
Kim *et al*[45]	BAR	101/515	5 (0.8%)	13 (2.1%)	1 (0.5%)
Wullstein *et al*[40]	AKA-2	70/372	11 (2.5%)	-	2 (0.5%)
Nudelman *et al*[43]	CAC	0/5	0	0	0
Nudelman *et al*[42]	CAC	0/30	0	0	0
Nudelamn *et al*[44]	CAC	0/10	0	0	0
Liu *et al*[59]	CAC	0/33	0	0	0

device is detached and expelled naturally. Furthermore, the longitudinally orientated metal prongs further fixate both bowel ends and prevent tissue slippage from axial movements. An advantage of this contemporary device is that there is no anastomotic-scarred lip inside lumen and a safe applier removal without fishtailing[60].

Two separate studies looked at bursting strength in a porcine model. Kopelman *et al*[57] measured a mean bursting strength of 247.7 mmHg (range 100-300 mmHg) in nine animals at time zero (immediately after the excision of the fashioned anastomosis). Furthermore Stewart *et al*[61] revealed a significantly higher bursting pressure after compression anastomosis in comparison with a conventional double stapling technique (103, 75.3 mmHg *vs* 3, 23 mmHg, respectively). Four of the nine compression anastomoses failed at the anastomotic line whereas nine of nine stapled anastomoses failed at the staple line (Fishers' exact test, $P < 0.01$). Bursting pressures measured at two weeks after the anastomosis revealed equal pressures (266, 32.2 mmHg and 230, 87.5 mmHg, respectively). Compression therefore seems to be capable of overcoming anastomotic weakness during the 'classical' lag-phase and to result in equal strength after detachment of the ring[62].

Kopelman *et al*[57] looked at the anastomotic index (ratio of the mean bowel diameter 5 cm proximal and distal to the anastomosis and on antero-lateral and posterior view), which was 0.81 (0.60-0.92) at two months.

An early clinical trial was performed in Israel using the EndoCAR[27] device to construct a left-side anastomosis. Four patients were enrolled. No device related complications were noted in these patients and no anastomotic leak reported (unpublished data). Based upon that experience, a pilot study was started in May 2007 in Uppsala (Sweden) and in Leuven (Belgium) to obtain clinical data in a consecutive group of 40 patients[62]. The recruited patients had either malignant or benign (diverticular) disease requiring resection with a high colorectal anastomosis (between 10 and 15 cm from the anal verge). Preliminary results from that pilot study showed that of the first ten patients, nine underwent high anterior resection, and left colectomy was performed on one patient. No leak age occurred in this first group of patients. No other data is available yet.

These promising results demonstrate that this device could be a revolutionary invention in colorectal practice; however, there are still doubts regarding its efficacy in low/ultralow rectal anastomoses. The location of the ring above the pelvic floor could induce persistent anal sensation (urge) and it is still unknown whether a spontaneous evacuation will occur in diverted patients.

Magnamosis

Controlled magnetic approaches have shown promise in biliary and vascular anastomoses (although the latter involves permanent implantation). A specially designed self-orienting device has been put into a trial to test the hypothesis of creating a magnetically mediated intestinal anastomosis using a temporary device that is expelled some time after creating the desired compression-necrosis effect (Department of Surgery, University of California, San Francisco)[63].

Two topologies were evaluated; namely the uniform and the gradient compression device. The study was conducted on 16 pigs with the creation of a side-to-side anastomosis. Half of these were created with the uniform device and the rest with the gradient. They also created hand-sewn and stapled side-to-side anastomosis for comparison. Devices were designed with surface fields of approximately 3000 Gauss (G). Preliminary experimentation had revealed that combinations of 3000/6000 G and 6000/6000 G uniformly caused necrosis and perforation within 48 h independent of device geometry. The results were promising, with the creation of successful patent anastomosis using the magnetic devices and no leaks reported[63].

The mechanical integrity of the magnetic anastomoses was not statistically significantly different from stapled or hand-sewn; however, there was a trend toward greater strength with the gradient type device and earlier patency. No evidence of stenosis was reported[63].

Table 2 presents the past clinical experience with

Table 3 List of reinforcement materials[64]

	Material	Stapler type	Company
Non-absorbable	ePTFE	Linear	W.L. Gore, Elkton, MD, USA
Semi-absorbable	Bovine pericardium (peristrips dry)	Circular linear	Synovis Life Technologies, Inc.
	Porcine small bowel (surgisis)	Linear	Cook Biotech Inc.
Absorbable	Polyglycolic acid:trimethylene carbonate (seamguard bioabsorbable)	Linear circular	W.L. Gore & Associates, Inc.
	Cellulose (Xcell)	Linear	Xylos Corp.
	Knitted calcium alginate (foreseal)	Linear	Laboratoires Brothier, Nanterre, France

compression anastomosis devices and their related complications.

BUTTRESSING OF INTESTINAL ANASTOMOSIS

Many staple devices are commercially available, however all the different types and models have inherent drawbacks that contribute to post-operative complications. Complications such as enteric leakage, bleeding, inadequate tissue approximation, and misfiring (technical failures) have been reported. However, complications related to colorectal anastomosis are the most devastating in terms of morbidity and mortality[64].

A new approach to reduce this is to use staple line reinforcement materials. Gastrointestinal reinforcement is well known, but its application in colorectal surgery is relatively new[65]. The application of buttressing materials is thought to moderate the tension of the stapler line because it acts as a neutralization plate. It reinforces the stapler line by sealing the gaps between staples and narrowing the spaces, thus reducing tearing of tissues, bleeding, and leakage[64]. Reinforcement materials can be applied exogenously to the staple line or incorporated into it. The material is composed of two regions, one that secures it to the stapler prior to activation, and is later discarded, and the other forms the seal. It has an adhesive surface and is readily packed in a sterile manner[65].

Reinforcement material can be non-absorbable, semi- or fully-absorbable. Studies have shown diminished incidence of leakage and stapler line failure in gastrointestinal and pulmonary surgery. Although all types of materials seem equally adequate in reducing staple line complications, the material itself can cause problems[65]. Therefore, the choice of material must be considered from a safety point of view, although there seems to be advantages of absorbable material over the other two types.

The effects of the materials in colorectal anastomosis have been tested in a small clinical pilot study by Franklin *et al*[66,67] using bio-absorbable seamguard (BSG) with a linear stapler. Published data revealed no bleeding, or apparent bleeding, at the staple line.

Several reports support the theoretical benefits of reinforcement materials in increasing the burst pressure[68-71]. It was also hypothesized that buttressing of stapler line can have a positive effect on tumor recurrence[66]. Although published studies showed a decrease in complications with these materials, no previous studies have shown significant results for reducing bleeding or leak rates at the stapler line. Thus, further research and investigations are required. Table 3 refers to the list of materials used as staple line adjuncts.

Non-absorbable materials

ePTFE: ePTFE is a very easy and quickly employed material composed of non-absorbable expanded polytetrafluoroethylene. It is constructed like a sleeve that can be slid over both arms of the stapling device negating the need for additional fixing to the stapler before firing. After firing, the material is released from the arms by pulling a ripcord. The potential benefits of this material include a low host response and biocompatibility. There are no reports of strip erosion or migration with this material, which evokes a minimal tissue inflammatory reaction. It provides thick tissue coverage for an extended period of time with no extra handling time required for its preparation and use. Its application suits open and laparoscopic procedures[72,73].

Semiabsorbable material

Bovine pericardium: This material is composed of bovine pericardium (peristrips dry). It is temporarily attached to the stapler with gel (which is applied to inner surface of both stapler arms), after which the stapler is positioned and locked over the strips. It can be applied on linear, as well as circular, staplers. The material is then incorporated by the host tissue after firing the stapler. Apart from increasing the burst pressure, this material demands relatively more handling time than other materials. However, it has the potential of to reduce the time required to stop staple line bleeding. Possible limitations include a high risk of animal source contamination, resulting in an inflammatory reaction to the xenomaterial (non-biocompatible). This makes it prone to erosion and migration[64]. Recently, its combination with Veritas technology results in remodeling of the material into indistinguishable host tissue.

Porcine small intestinal submucosa: This is a completely resorbable, acellular xenograft composed of

porcine small animal submucosa. It is suitable for anastomotic and non-anastomotic staplers. A potential advantage is that it provides a bioscaffold for tissue growth, inducing submucosal regeneration and also achieving an increase in burst pressure[74,75]. However, its efficacy in human staple-line reinforcement is undocumented.

Absorbable material

Polyglycolic acid:trimethylene carbonate: This is a synthetic fiber web that is composed of polyglycolic acid: trimethylene carbonate Maxon polymer. It is formed like a sleeve to be fitted over the stapler arms and released by pulling the suture that holds the sleeve in place. It can also be affixed as discs onto circular-type staplers. The material is strongly biocompatible, simple and easy to apply on the stapler and is non antigenic. It maintains its strength for four to six weeks and is fully resorbed after six months (hydrolytic and enzymatic reactions lead to the breakdown of the material)[76,77]. Overall, it minimizes staple-line bleeding, leakage, and operative time[78-80].

Cellulose: Cellulose (XylosT M Surgical Reinforcing Material. Xcell SDMC surgical film) was originally developed as a wound dressing. This dry sterile material is composed of a microbially-derived cellulose matrix having multilayered, three-dimensional structures. The cellulose is produced by *Acetobacter xylinum* bacteria and is processed into a resorbable form. Research is in progress to evaluate and construct it as a possible staple line reinforcing material in GI surgery[81].

Knitted calcium alginate: This material is composed of polysaccharidic polyglycuronates biopolymers (highly purified fractions from calcium alginates), originating from seaweeds. The device consists of preformed coated knitted bio-absorbable sheets held into the form of sleeves (one cartridge device, one anvil device) sized to fit snugly onto the forks of the surgical stapler. When applied to wet surfaces, the material becomes highly conformable and acquires bio-adhesive and sealant properties. It contains no additives or preservatives, and therefore no presoaking or rinsing is required as a preparatory step. The device is easy to handle and simple to apply, eliciting minimal foreign body response[82]. However, clinical trials are scarce.

OTHER FORMS OF ANASTOMOTIC SUPPORT

C-seal (polyganics)

The colorectal drain (C-seal) is applied with a circular stapler. It is a single use tubular device, closed at one end and composed of biodegradable synthetic material. It is a thin walled tube with an approximate diameter of 3 cm and an approximate length of 20 cm. This drain works as a shield covering the newly formed anastomosis, preventing contact between the bowel contents and the anastomosis. Degradation process starts gradually, and the material is expelled from the bowel after approximately 10-15 d. Its theoretical benefits lie in the ability to protect a low rectal anastomosis, preventing leakage. It can also be used as a staple line adjunct. It is microbiologically safe and is completely expelled after two weeks, negating the use of a protective defunctioning stoma in low rectal excision[83].

Polyester stent

Most recently, covered intraluminal stents have been successfully introduced to manage anastomotic leaks after esophagectomy and gastric bypass operations.

A randomized control trial in a large animal model addressed this issue in stapled colorectal anastomosis. The study found that placement of a covered polyester stent across a colorectal anastomosis prevents leak-related complications and supports healing of an anastomotic leak[84].

It consists of a polyflex self-expandable covered plastic stent (25 mm proximal flare and 12 cm long) and a delivery system. The outer layer is composed of braided polyester and the inner layer is silicone (no gaps in this layer). It is applied through a standard flexible colonoscope using a guide wire and a delivery system, and is deployed under fluoroscopic control after reconstruction of the end-to-end anastomosis. The components of the material allow it to adapt elastically to the lumen wall, exerting a well-balanced radial force. The silicone membrane provides a reliable leak occlusion, preventing ingrowth of granulation tissue; hence allowing stent repositioning or removal. Similarly to C-Seal, it negates the need for a diverting stoma in low rectal excision. However, the main disadvantage for the future of these types of stents is migration[84].

NOVEL TECHNIQUES

Doxycycline coated sutures

Experimental studies revealed that the strength of an intestinal anastomosis diminishes postoperatively reaching a nadir on the third postoperative day. This is mediated by the increased activity of MMP, causing local matrix degradation in the tissue surrounding the sutures. This activity is higher still in concurrent bacterial peritonitis, with subsequently greater deterioration of anastomotic strength. Several experimental studies showed that MMP inhibitors administered systemically alleviate postoperative weakening of intestinal anastomoses. Other studies have shown the beneficial effects of treatment with systemic MMP inhibitors, e.g. doxycycline, most notably on the critical third postoperative day[85-87].

Potent MMP inhibitors administered systemically can cause joint stiffness, swelling[88], and other toxic reactions[89]. Additionally, there are concerns about detrimental effects of broad-spectrum hydroxamate MMP inhibitors on secondary healing of cutaneous wounds[90], although these types of MMP inhibitors can increase tensile strength of primary skin wounds[91]. The less

potent MMP inhibitor doxycycline does not appear to delay wound closure[92]. Due to adverse systemic effects, local delivery of an MMP inhibitor in humans would be advantageous over systemic administration[93].

This hypothesis was studied by Pasternak *et al*[93] in 2008. They implemented a novel method for coating sutures with a cross-linked fibrinogen film and then bound the MMP inhibitor (doxycycline) into this film. The sutures were then used in a standard rat model for evaluating mechanical properties of colonic anastomosis three days after surgery. The breaking strength of the anastomosis was higher with the doxycycline-coated sutures than with the controls. This might inspire further studies involving pharmacological manipulation of intestinal healing by local drug delivery[93].

Electric "Welding" of soft tissues

Experience of the application of electric surgery for cutting tissues and hemostasis is about one hundred years long. It has been established that under certain conditions, it is possible to join incisions in different organs and soft tissues by a method based on heating the joint zone by a high-frequency current. Electric welding to join incisions of live tissues and organs during surgery was applied for the first time by the team of researchers of the E.O. Paton Electric Welding Institute of NASU in cooperation with the scientists and specialists of the experimental department of the Institute of Surgery and Transplantology (IS&T) of AMSU with participation of International Association (Welding) and financial support of CSMG Company, USA[94].

They developed a novel welding system that includes a power unit comprising a power source (High frequency coagulator) with an adaptive automatic control system and special software, bipolar welding tools (forceps, clamps and laparoscopes) connected to a power source, and special assembly devices. The control system is based on feedbacks. The tissue layers being joined are brought into contact over their surface layers by means of the welding tool. The surgeon clamps the tissue to be welded by the electrodes of the tool and switches on the welding current source. Upon completion of the process (i.e. thermal denaturation of albumin molecules), control program power is turned off. Clamped tissue is then released and process repeated until complete wound closure[94].

The device has been tested in multiple experimental trials and on more than 2000 patients in the clinics and hospitals of Kiev, Ukraine. The author maintains that the advantage of the device is in the formation of an attractive, neat, smooth thin welded anastomosis. In addition, it is a fumeless and odorless technology, causing no burns to surrounding tissues. The report demonstrates a reduction of blood loss and no organ deformation or stenosis. It also shortens the average operative time (20-40 min)[94].

CONCLUSION

Although alternatives to the conventional methods have been sought, many have been abandoned by the surgical community.

Compression anastomosis, although existing for decades, has not gained worldwide popularity. This concept seems to be difficult for surgeons to accept, as it includes relying on a device to create an anastomosis and letting it be spontaneously discharged from the body. Reinstitution of this concept using new technology, such as Nitinol, could be a potential replacement for the current available techniques. Controlled magnetic anastomosis is no exception to this. It is a promising novel technique for creation of a side-to-side anastomosis but requires to be optimized for future use.

The theoretical benefits of colorectal seals and the polyester stents as adjuncts to creating an end-to-end anastomosis could alleviate the need for a defunctioning stoma for lower rectal tumor resections. This is another concept that needs to be accepted and subjected to further research to optimize its use. In line with this, staple line reinforcement is an effective technique for reducing perioperative complications in stapled resection and anastomoses, with absorbable materials having a considerable advantage over semi or non-absorbable material(s). However, there has been little experience with absorbable staple line reinforcement materials.

A contemporary and sophisticated technique, such as electric tissue welding shows a promising future in modern surgical techniques. It is a revolutionary technique that still needs acceptance and research, utilizing greater patient samples in colorectal surgical practice.

Finally, overcoming the postoperative anastomotic weakness due to over activity of matrix metalloproteinases, and hence the risk of dehiscence, using doxycycline coated sutures should also be explored.

In summary, these various techniques fulfill the requirements of creating a safe anastomosis (overcoming the lag-phase, increasing the bursting pressure, and decreasing the rate of leakage, bleeding and stricture). They revealed great differences in avoiding dramatic complications that can occur with the conventional methods; an outcome that every colorectal surgeon would advocate. Surgeons need to widen their scope of practice, and further trials and research are required to overcome "dogmas" in traditional colorectal practice. Keeping abreast of technological advances is considered vital in every surgeons training and daily practice; failure to do so could lead to reduced quality of patient care.

REFERENCES

1 **Fowler DL**, White SA. Laparoscopy-assisted sigmoid resection. *Surg Laparosc Endosc* 1991; **1**: 183-188
2 **Phillips EH**, Franklin M, Carroll BJ, Fallas MJ, Ramos R, Rosenthal D. Laparoscopic colectomy. *Ann Surg* 1992; **216**: 703-707
3 **Jacobs M**, Verdeja JC, Goldstein HS. Minimally invasive colon resection (laparoscopic colectomy). *Surg Laparosc Endosc* 1991; **1**: 144-150
4 **Fleshman JW**, Nelson H, Peters WR, Kim HC, Larach S, Boorse RR, Ambroze W, Leggett P, Bleday R, Stryker S,

Christenson B, Wexner S, Senagore A, Rattner D, Sutton J, Fine AP. Early results of laparoscopic surgery for colorectal cancer. Retrospective analysis of 372 patients treated by Clinical Outcomes of Surgical Therapy (COST) Study Group. *Dis Colon Rectum* 1996; **39**: S53-S58
5 **Matthiessen P**, Hallböök O, Rutegård J, Simert G, Sjödahl R. Defunctioning stoma reduces symptomatic anastomotic leakage after low anterior resection of the rectum for cancer: a randomized multicenter trial. *Ann Surg* 2007; **246**: 207-214
6 **Enker WE**, Merchant N, Cohen AM, Lanouette NM, Swallow C, Guillem J, Paty P, Minsky B, Weyrauch K, Quan SH. Safety and efficacy of low anterior resection for rectal cancer: 681 consecutive cases from a specialty service. *Ann Surg* 1999; **230**: 544-552; discussion 552-554
7 **Matthiessen P**, Hallböök O, Andersson M, Rutegård J, Sjödahl R. Risk factors for anastomotic leakage after anterior resection of the rectum. *Colorectal Dis* 2004; **6**: 462-469
8 **Fielding LP**, Stewart-Brown S, Blesovsky L, Kearney G. Anastomotic integrity after operations for large-bowel cancer: a multicentre study. *Br Med J* 1980; **281**: 411-414
9 **Karanjia ND**, Corder AP, Bearn P, Heald RJ. Leakage from stapled low anastomosis after total mesorectal excision for carcinoma of the rectum. *Br J Surg* 1994; **81**: 1224-1226
10 **Pakkastie TE**, Luukkonen PE, Järvinen HJ. Anastomotic leakage after anterior resection of the rectum. *Eur J Surg* 1994; **160**: 293-297; discussion 299-300
11 **Mortensen NJ**, Ashraf S. Chapter 29 Intestinal Anastomosis In Section 5 Gastrointestinal Tract and Abdomen. September 2008. Available from: URL: http://www.acssurgery.com/acs/Chapters/CH0529.htm
12 **Syk I**, Agren MS, Adawi D, Jeppsson B. Inhibition of matrix metalloproteinases enhances breaking strength of colonic anastomoses in an experimental model. *Br J Surg* 2001; **88**: 228-234
13 **Halsted WS**. Circular suture of the intestine: an experimental study. *Am J Med Sci* 1887; **94**: 436-461
14 **de Hingh IH**, de Man BM, Lomme RM, van Goor H, Hendriks T. Colonic anastomotic strength and matrix metalloproteinase activity in an experimental model of bacterial peritonitis. *Br J Surg* 2003; **90**: 981-988
15 **Martens MF**, Hendriks T. Postoperative changes in collagen synthesis in intestinal anastomoses of the rat: differences between small and large bowel. *Gut* 1991; **32**: 1482-1487
16 **Hesp FL**, Hendriks T, Lubbers EJ, deBoer HH. Wound healing in the intestinal wall. A comparison between experimental ileal and colonic anastomoses. *Dis Colon Rectum* 1984; **27**: 99-104
17 **Khoury GA**, Waxman BP. Large bowel anastomoses. I. The healing process and sutured anastomoses. A review. *Br J Surg* 1983; **70**: 61-63
18 **Bissett IP**. Ileocolic anastomosis. *Br J Surg* 2007; **94**: 1447-1448
19 **Wise L**, McAlister W, Stein T, Schuck P. Studies on the healing of anastomoses of small and large intestines. *Surg Gynecol Obstet* 1975; **141**: 190-194
20 **Lustosa SA**, Matos D, Atallah AN, Castro AA. Stapled versus handsewn methods for colorectal anastomosis surgery. *Cochrane Database Syst Rev* 2001; CD003144
21 **Lim CB**, Goldin RD, Darzi A, Hanna GB. Characterization of materials eliciting foreign body reaction in stapled human gastrointestinal anastomoses. *Br J Surg* 2008; **95**: 1044-1050
22 **MacRae HM**, McLeod RS. Handsewn vs. stapled anastomoses in colon and rectal surgery: a meta-analysis. *Dis Colon Rectum* 1998; **41**: 180-189
23 **Cajozzo M**, Compagno G, DiTora P, Spallitta SI, Bazan P. Advantages and disadvantages of mechanical vs. manual anastomosis in colorectal surgery. A prospective study. *Acta Chir Scand* 1990; **156**: 167-169
24 **Fingerhut A**, Hay JM, Elhadad A, Lacaine F, Flamant Y. Supraperitoneal colorectal anastomosis: hand-sewn versus circular staples--a controlled clinical trial. French Associations for Surgical Research. *Surgery* 1995; **118**: 479-485
25 **Hardy KJ**. A view of the development of intestinal suture. Part II. Principles and techniques. *Aust N Z J Surg* 1990; **60**: 377-384
26 **Booth CC**. What has technology done to gastroenterology? *Gut* 1985; **26**: 1088-1094
27 **Murphy JB**. Cholecysto-intestinal, gastro-intestinal, entero-intestinal anastomosis, and approximation without sutures. *Med Rec N Y* 1892; **42**: 665-676
28 **Classic articles in colonic and rectal surgery**. Nicholas Senn 1844-1908. Enterorrhaphy; its history, technique and present status. *Dis Colon Rectum* 1985; **28**: 59-68
29 **Jansen A**, Keeman JN, Davies GA, Klopper PJ. Early experiences with magnetic rings in resection of the distal colon. *Neth J Surg* 1980; **32**: 20-27
30 **Kanshin NN**, Lytkin MI, Knysh VI, Klur VIu, Khamidov AI. [First experience with application of compression anastomoses with the apparatus AKA-2 in operations on the large intestine] *Vestn Khir Im I I Grek* 1984; **132**: 52-57
31 **Hardy TG Jr**, Pace WG, Maney JW, Katz AR, Kaganov AL. A biofragmentable ring for sutureless bowel anastomosis. An experimental study. *Dis Colon Rectum* 1985; **28**: 484-490
32 **Ye F**, Lin JJ. [Clinical application of biofragmentable anastomosis ring for intestinal anastomosis] *Zhejiang Daxue Xuebao Yixueban* 2006; **35**: 668-672
33 **Thiede A**, Geiger D, Dietz UA, Debus ES, Engemann R, Lexer GC, Lünstedt B, Mokros W. Overview on compression anastomoses: biofragmentable anastomosis ring multicenter prospective trial of 1666 anastomoses. *World J Surg* 1998; **22**: 78-86; discussion 87
34 **Bubrick MP**, Corman ML, Cahill CJ, Hardy TG Jr, Nance FC, Shatney CH. Prospective, randomized trial of the biofragmentable anastomosis ring. The BAR Investigational Group. *Am J Surg* 1991; **161**: 136-142; discussion 142-143
35 **Cahill CJ**, Betzler M, Gruwez JA, Jeekel J, Patel JC, Zederfeldt B. Sutureless large bowel anastomosis: European experience with the biofragmentable anastomosis ring. *Br J Surg* 1989; **76**: 344-347
36 **Corman ML**, Prager ED, Hardy TG Jr, Bubrick MP. Comparison of the Valtrac biofragmentable anastomosis ring with conventional suture and stapled anastomosis in colon surgery. Results of a prospective, randomized clinical trial. *Dis Colon Rectum* 1989; **32**: 183-187
37 **Gullichsen R**, Ovaska J, Rantala A, Havia T. Small bowel anastomosis with the biofragmentable anastomosis ring and manual suture: a prospective, randomized study. *World J Surg* 1992; **16**: 1006-1009
38 **Pahlman L**, Ejerblad S, Graf W, Kader F, Kressner U, Lindmark G, Raab Y. Randomized trial of a biofragmentable bowel anastomosis ring in high-risk colonic resection. *Br J Surg* 1997; **84**: 1291-1294
39 **Seow-Choen F**, Eu KW. Circular staplers versus the biofragmentable ring for colorectal anastomosis: a prospective randomized study. *Br J Surg* 1994; **81**: 1790-1791
40 **Wullstein C**, Gross E. Compression anastomosis (AKA-2) in colorectal surgery: results in 442 consecutive patients. *Br J Surg* 2000; **87**: 1071-1075
41 **Nudelman IL**, Fuko VV, Morgenstern S, Giler S, Lelcuk S. Gastrointestinal anastomosis with the nickel-titanium double ring. *World J Surg* 2000; **24**: 874-877
42 **Nudelman I**, Fuko V, Waserberg N, Niv Y, Rubin M, Szold A, Lelcuk S. Colonic anastomosis performed with a memory-shaped device. *Am J Surg* 2005; **190**: 434-438
43 **Nudelman I**, Fuko V, Rubin M, Lelcuk S. A nickel-titanium memory-shape device for colonic anastomosis in laparoscopic surgery. *Surg Endosc* 2004; **18**: 1085-1089
44 **Nudelman IL**, Fuko V, Greif F, Lelcuk S. Colonic anastomosis with the nickel-titanium temperature-dependent memory-shape device. *Am J Surg* 2002; **183**: 697-701
45 **Kim SH**, Choi HJ, Park KJ, Kim JM, Kim KH, Kim MC, Kim YH, Cho SH, Jung GJ. Sutureless intestinal anastomosis with

the biofragmentable anastomosis ring: experience of 632 anastomoses in a single institute. *Dis Colon Rectum* 2005; **48**: 2127-2132
46 **Aggarwal R**, Darzi A. Compression anastomoses revisited. *J Am Coll Surg* 2005; **201**: 965-971
47 **Choi HJ**, Kim HH, Jung GJ, Kim SS. Intestinal anastomosis by use of the biofragmentable anastomotic ring: is it safe and efficacious in emergency operations as well? *Dis Colon Rectum* 1998; **41**: 1281-1286
48 **Galizia G**, Lieto E, Castellano P, Pelosio L, Imperatore V, Canfora F, Pignatelli C. Comparison between the biofragmentable anastomosis ring and stapled anastomoses in the extraperitoneal rectum: a prospective, randomized study. *Int J Colorectal Dis* 1999; **14**: 286-290
49 **Hardy TG Jr**, Aguilar PS, Stewart WR, Katz AR, Maney JW, Costanzo JT, Pace WG. Initial clinical experience with a biofragmentable ring for sutureless bowel anastomosis. *Dis Colon Rectum* 1987; **30**: 55-61
50 **Di Castro A**, Biancari F, Brocato R, Adami EA, Truosolo B, Massi G. Intestinal anastomosis with the biofragmentable anastomosis ring. *Am J Surg* 1998; **176**: 472-474
51 **Chen TC**, Ding KC, Yang MJ, Chang CP. New device for biofragmentable anastomotic ring in low anterior resection. *Dis Colon Rectum* 1994; **37**: 834-836
52 **Forde KA**, McLarty AJ, Tsai J, Ghalili K, Delany HM. Murphy's Button revisited. Clinical experience with the biofragmentable anastomotic ring. *Ann Surg* 1993; **217**: 78-81
53 **Ghitulescu GA**, Morin N, Jetty P, Belliveau P. Revisiting the biofragmentable anastomotic ring: is it safe in colonic surgery? *Can J Surg* 2003; **46**: 92-98
54 **Detry RJ**, Kartheuser A, Delriviere L, Saba J, Kestens PJ. Use of the circular stapler in 1000 consecutive colorectal anastomoses: experience of one surgical team. *Surgery* 1995; **117**: 140-145
55 **Hansen O**, Schwenk W, Hucke HP, Stock W. Colorectal stapled anastomoses. Experiences and results. *Dis Colon Rectum* 1996; **39**: 30-36
56 **Barras CD**, Myers KA. Nitinol - its use in vascular surgery and other applications. *Eur J Vasc Endovasc Surg* 2000; **19**: 564-569
57 **Kopelman D**, Lelcuk S, Sayfan J, Matter I, Willenz EP, Zaidenstein L, Hatoum OA, Kimmel B, Szold A. End-to-end compression anastomosis of the rectum: a pig model. *World J Surg* 2007; **31**: 532-537
58 **Song C**, Frank T, Cuschieri A. Shape memory alloy clip for compression colonic anastomosis. *J Biomech Eng* 2005; **127**: 351-354
59 **Liu PC**, Jiang ZW, Zhu XL, Wang ZM, Diao YQ, Li N, Li JS. Compression anastomosis clip for gastrointestinal anastomosis. *World J Gastroenterol* 2008; **14**: 4938-4942
60 **Szold A**. New concepts for a compression anastomosis: superelastic clips and rings. *Minim Invasive Ther Allied Technol* 2008; **17**: 168-171
61 **Stewart D**, Hunt S, Pierce R, Dongli Mao, Frisella M, Cook K, Starcher B, Fleshman J. Validation of the NITI Endoluminal Compression Anastomosis Ring (EndoCAR) device and comparison to the traditional circular stapled colorectal anastomosis in a porcine model. *Surg Innov* 2007; **14**: 252-260
62 **D'Hoore A**, Hompes D, Folkesson J, Penninckx F, PAhlman L. Circular 'superelastic' compression anastomosis: from the animal lab to clinical practice. *Minim Invasive Ther Allied Technol* 2008; **17**: 172-175
63 **Jamshidi R**, Stephenson JT, Clay JG, Pichakron KO, Harrison MR. Magnamosis: magnetic compression anastomosis with comparison to suture and staple techniques. *J Pediatr Surg* 2009; **44**: 222-228
64 **Yo LS**, Consten EC, Quarles van Ufford HM, Gooszen HG, Gagner M. Buttressing of the staple line in gastrointestinal anastomoses: overview of new technology designed to reduce perioperative complications. *Dig Surg* 2006; **23**: 283-291
65 **Cheragwandi A**, Nieuwenhuis DH, Gagner M, Consten EC. An update of available innovative staple line reinforcement materials in colorectal surgery. *Surg Technol Int* 2008; **17**: 131-137
66 **Franklin ME Jr**, Ramila GP, Treviño JM, González JJ, Russek K, Glass JL, Kim G. The use of bioabsorbable staple line reinforcement for circular stapler (BSG "Seamguard") in colorectal surgery: initial experience. *Surg Laparosc Endosc Percutan Tech* 2006; **16**: 411-415
67 **Franklin ME Jr**, Berghoff KE, Arellano PP, Trevino JM, Abrego-Medina D. Safety and efficacy of the use of bioabsorbable seamguard in colorectal surgery at the Texas endosurgery institute. *Surg Laparosc Endosc Percutan Tech* 2005; **15**: 9-13
68 **Arnold W**, Shikora SA. A comparison of burst pressure between buttressed versus non-buttressed staple-lines in an animal model. *Obes Surg* 2005; **15**: 164-171
69 **Hagerman GF**, Gaertner WB, Ruth GR, Potter ML, Karulf RE. Bovine pericardium buttress reinforces colorectal anastomoses in a canine model. *Dis Colon Rectum* 2007; **50**: 1053-1060
70 **Morton JM**, Lucktong TA, Trasti S, Farrell TM. Bovine pericardium buttress limits recanalization of the uncut Roux-en-Y in a porcine model. *J Gastrointest Surg* 2004; **8**: 127-131
71 **Pinheiro JS**, Correa JL, Cohen RV, Novaes JA, Schiavon CA. Staple line reinforcement with new biomaterial increased burst strength pressure: an animal study. *Surg Obes Relat Dis* 2006; **2**: 397-399, discussion 400
72 **Murray KD**, Ho CH, Hsia JY, Little AG. The influence of pulmonary staple line reinforcement on air leaks. *Chest* 2002; **122**: 2146-2149
73 **Vaughn CC**, Vaughn PL, Vaughn CC 3rd, Sawyer P, Manning M, Anderson D, Roseman L, Herbst TJ. Tissue response to biomaterials used for staple-line reinforcement in lung resection: a comparison between expanded polytetrafluoroethylene and bovine pericardium. *Eur J Cardiothorac Surg* 1998; **13**: 259-265
74 **Kini S**, Gagner M, de Csepel J, Gentileschi P, Dakin G. A biodegradeable membrane from porcine intestinal submucosa to reinforce the gastrojejunostomy in laparoscopic Roux-en-Y gastric bypass: preliminary report. *Obes Surg* 2001; **11**: 469-473
75 **de la Fuente SG**, Gottfried MR, Lawson DC, Harris MB, Mantyh CR, Pappas TN. Evaluation of porcine-derived small intestine submucosa as a biodegradable graft for gastrointestinal healing. *J Gastrointest Surg* 2003; **7**: 96-101
76 **Van Winkle W Jr**, Hastings JC. Considerations in the choice of suture material for various tissues. *Surg Gynecol Obstet* 1972; **135**: 113-126
77 **Kangas J**, Paasimaa S, Mäkelä P, Leppilahti J, Törmälä P, Waris T, Ashammakhi N. Comparison of strength properties of poly-L/D-lactide (PLDLA) 96/4 and polyglyconate (Maxon) sutures: in vitro, in the subcutis, and in the achilles tendon of rabbits. *J Biomed Mater Res* 2001; **58**: 121-126
78 **Katz AR**, Mukherjee DP, Kaganov AL, Gordon S. A new synthetic monofilament absorbable suture made from polytrimethylene carbonate. *Surg Gynecol Obstet* 1985; **161**: 213-222
79 **Metz SA**, Chegini N, Masterson BJ. In vivo and in vitro degradation of monofilament absorbable sutures, PDS and Maxon. *Biomaterials* 1990; **11**: 41-45
80 **Farrar DF**, Gillson RK. Hydrolytic degradation of polyglyconate B: the relationship between degradation time, strength and molecular weight. *Biomaterials* 2002; **23**: 3905-3912
81 **Frankel VH**, Serafica GC, Damien CJ. Development and testing of a novel biosynthesized XCell for treating chronic wounds. *Surg Technol Int* 2004; **12**: 27-33
82 **Thomas P**, Massard G, Porte H, Doddoli C, Ducrocq X, Conti M. A new bioabsorbable sleeve for lung staple-line reinforcement (FOREseal): report of a three-center phase II clinical trial. *Eur J Cardiothorac Surg* 2006; **29**: 880-885

83 **The manufacture's IFU (information for use) literature.** Available from: URL: http://www.polyganics.com; http://www.nitisurgical.com/colonring.htm

84 **Tsereteli Z**, Sporn E, Geiger TM, Cleveland D, Frazier S, Rawlings A, Bachman SL, Miedema BW, Thaler K. Placement of a covered polyester stent prevents complications from a colorectal anastomotic leak and supports healing: randomized controlled trial in a large animal model. *Surgery* 2008; **144**: 786-792

85 **Syk I**, Agren MS, Adawi D, Jeppsson B. Inhibition of matrix metalloproteinases enhances breaking strength of colonic anastomoses in an experimental model. *Br J Surg* 2001; **88**: 228-234

86 **Agren MS**, Andersen TL, Mirastschijski U, Syk I, Schiødt CB, Surve V, Lindebjerg J, Delaissé JM. Action of matrix metalloproteinases at restricted sites in colon anastomosis repair: an immunohistochemical and biochemical study. *Surgery* 2006; **140**: 72-82

87 **Siemonsma MA**, de Hingh IH, de Man BM, Lomme RM, Verhofstad AA, Hendriks T. Doxycycline improves wound strength after intestinal anastomosis in the rat. *Surgery* 2003; **133**: 268-276

88 **Renkiewicz R**, Qiu L, Lesch C, Sun X, Devalaraja R, Cody T, Kaldjian E, Welgus H, Baragi V. Broad-spectrum matrix metalloproteinase inhibitor marimastat-induced musculoskeletal side effects in rats. *Arthritis Rheum* 2003; **48**: 1742-1749

89 **Peterson JT**. Matrix metalloproteinase inhibitor development and the remodeling of drug discovery. *Heart Fail Rev* 2004; **9**: 63-79

90 **Mirastschijski U**, Haaksma CJ, Tomasek JJ, Agren MS. Matrix metalloproteinase inhibitor GM 6001 attenuates keratinocyte migration, contraction and myofibroblast formation in skin wounds. *Exp Cell Res* 2004; **299**: 465-475

91 **Witte MB**, Thornton FJ, Kiyama T, Efron DT, Schulz GS, Moldawer LL, Barbul A. Metalloproteinase inhibitors and wound healing: a novel enhancer of wound strength. *Surgery* 1998; **124**: 464-470

92 **Hebda PA**, Whaley D, Kim HG, Wells A. Absence of inhibition of cutaneous wound healing in mice by oral doxycycline. *Wound Repair Regen* 2003; **11**: 373-379

93 **Pasternak B**, Rehn M, Andersen L, Agren MS, Heegaard AM, Tengvall P, Aspenberg P. Doxycycline-coated sutures improve mechanical strength of intestinal anastomoses. *Int J Colorectal Dis* 2008; **23**: 271-276

94 **Paton BE**. Electric welding of soft tissues in surgery "The Paton Welding Journal", number: 9. 2004r. Available from: URL: http://www.iaw.com.ua/english/publications/

95 **Kaidar-Person O**, Rosenthal RJ, Wexner SD, Szomstein S, Person B. Compression anastomosis: history and clinical considerations. *Am J Surg* 2008; **195**: 818-826

S- Editor Wang JL **L- Editor** Stewart GJ **E- Editor** Ma WH

World Journal of Gastroenterology

Online Submissions: http://www.wjgnet.com/1007-9327office
wjg@wjgnet.com
doi:10.3748/wjg.v16.i13.1622

World J Gastroenterol 2010 April 7; 16(13): 1622-1630
ISSN 1007-9327 (print)

ORIGINAL ARTICLE

Therapeutic effect of *Streptococcus thermophilus* CRL 1190-fermented milk on chronic gastritis

Cecilia Rodríguez, Marta Medici, Fernanda Mozzi, Graciela Font de Valdez

Cecilia Rodríguez, Marta Medici, Fernanda Mozzi, Graciela Font de Valdez, Centro de Referencia para Lactobacilos (CERELA)-CONICET, Chacabuco 145, San Miguel de Tucumán, 4000, Tucumán, Argentina
Graciela Font de Valdez, Cátedra Microbiología Superior, Facultad de Bioquímica, Química y Farmacia, Universidad Nacional de Tucumán, Ayacucho 491, San Miguel de Tucumán, 4000, Tucumán, Argentina
Author contributions: Rodríguez C, Medici M, Mozzi F and Font de Valdez G were involved in the design of the study; Rodríguez C and Medici M performed the laboratory assays; Rodríguez C, Mozzi F and Font de Valdez G were involved in the writing of the article.
Supported by CONICET, ANPCyT (project BID 1728 OC/AR PICTR 20801) and CIUNT, Argentina
Correspondence to: Graciela Font de Valdez, Professor, Centro de Referencia para Lactobacilos (CERELA)-CONICET, Chacabuco 145, San Miguel de Tucumán, 4000, Tucumán, Argentina. gfont@cerela.org.ar
Telephone: +54-381-4310465 Fax: +54-381-4005600
Received: November 3, 2009 Revised: November 13, 2009
Accepted: November 20, 2009
Published online: April 7, 2010

Abstract

AIM: To investigate the potential therapeutic effect of exopolysaccharide (EPS)-producing *Streptococcus thermophilus* (*S. thermophilus*) CRL 1190 fermented milk on chronic gastritis in Balb/c mice.

METHODS: Balb/c mice were fed with the fermented milk for 7 d after inducing gastritis with acetyl-salicylic acid (ASA, 400 mg/kg body weight per day for 10 d). Omeprazole was included in this study as a positive therapeutic control. The gastric inflammatory activity was evaluated from gastric histology and inflammation score, number of interleukin-10 (IL-10), interferon-γ (INFγ) and tumor necrosis factor-α (TNF-α) cytokine-producing cells in the gastric mucosa, and thickness of the mucus layer.

RESULTS: Animals receiving treatment with the EPS-producing *S. thermophilus* CRL 1190 fermented milk showed a conserved gastric mucosa structure similar to that of healthy animals. Inflammation scores of the fermented milk-treated mice were lower than those of mice in the gastritis group (0.2 ± 0.03 *vs* 2.0 ± 0.6, $P < 0.05$). A marked decrease in INFγ$^+$ (15 ± 1.0 *vs* 28 ± 1.2, $P < 0.05$) and TNF-α$^+$ (16 ± 3.0 *vs* 33 ± 3.0, $P < 0.05$) cells and an increase in IL-10$^+$ (28 ± 1.5 *vs* 14 ± 1.3, $P < 0.05$) cells compared to the gastritis group, was observed. Also, an increase in the thickness of the mucus gel layer (2.2 ± 0.6 *vs* 1.0 ± 0.3; 5.1 ± 0.8 *vs* 1.5 ± 0.4 in the corpus and antrum mucosa, respectively, $P < 0.05$) compared with the gastritis group was noted. A milk suspension of the purified EPS from *S. thermophilus* CRL1190 was also effective as therapy for gastritis.

CONCLUSION: This study suggests that fermented milk with *S. thermophilus* CRL 1190 and/or its EPS could be used in novel functional foods as an alternative natural therapy for chronic gastritis induced by ASA.

Key words: Lactic acid bacteria; Probiotics; Gastritis; *Streptococcus thermophilus*; Exopolysaccharides

Peer reviewer: Shashi Bala, PhD, Post doctoral Associate, Department of Medicine, LRB 270L, 364 Plantation street, UMass Medical School, Worcester, MA 01605, United States

Rodríguez C, Medici M, Mozzi F, Font de Valdez G. Therapeutic effect of *Streptococcus thermophilus* CRL 1190-fermented milk on chronic gastritis. *World J Gastroenterol* 2010; 16(13): 1622-1630 Available from: URL: http://www.wjgnet.com/1007-9327/full/v16/i13/1622.htm DOI: http://dx.doi.org/10.3748/wjg.v16.i13.1622

INTRODUCTION

Gastritis is a common disorder where discontinuity of the gastric mucosa is observed. It is caused by several factors,

such as alcohol, stress, infection with *Helicobacter pylori* (*H. pylori*)[1-3], resulting in an imbalance between offensive acid-pepsin secretion and defensive mucosal factors like mucin secretion and cell shedding[4]. Non-steroidal anti-inflammatory drugs (NSAIDs) such as acetyl-salicylic acid (ASA) are used worldwide as anti-inflammatory and analgesic agents in the treatment of chronic diseases such as rheumatoid arthritis and osteoarthritis[5] as well as for the prevention of cardiovascular diseases. However, gastrointestinal injury is a serious adverse effect of NSAIDs producing a broad range of toxic effects mainly in the stomach[6], the toxicity of ASA being attributed to direct damage of mucosal cells[7]. Furthermore, ASA affects various mucosal defense lines such as bicarbonate secretion, mucus synthesis, decrease of mucosal blood flow[8,9] with amplification of the inflammatory process by expression of pro-inflammatory cytokines[10].

Among the most conventional drugs employed for the treatment of gastritis are proton-pump inhibitors such as omeprazole (OM)[11]; however, most of these drugs also produce undesirable side effects and drug interactions[12].

Probiotics are "live microorganisms which when consumed in adequate numbers confer a health benefit on the host[13]". Probiotic foods containing lactic acid bacteria (LAB) have been used in the treatment of various gastrointestinal disorders, such as gastric ulcers and inflammation related to *H. pylori* infection, gastrointestinal infections or antibiotic-associated diarrhea[14-16], providing beneficial effects to the host by modulating immune functions, e.g. systemic cytokine production[17]. The mucosal immune system is functionally divided into sites where foreign antigens are taken up and meet immune cells to initiate the immune response through a network of signals among different cell populations. This cell network is highly integrated by cytokine production, and finely regulated by the selective expression of cytokine receptors. The T-helper (Th) cell subsets and cytokine patterns determine the nature of the immune response[18].

Some LAB strains secrete exocellular carbohydrate polymers named exopolysaccharides (EPS). A large diversity of EPS from LAB strains exists regarding their chemical characteristics, yield, technological and functional properties[19-21]. EPS play an important role in the dairy industry mainly in yogurt production and certain kinds of cheeses such as reduced-fat cheddar and mozzarella[22], improving the textural, melting and sensory characteristics of the products. The health-promoting effects ascribed to probiotic strains or foods arise not only from the bacteria themselves but also from the metabolites produced during fermentation.

EPS from LAB have been claimed to participate in various regulatory processes such as immunomodulatory, cholesterol-lowering and anti-ulcer activities[23,24]. In previous work[25], we demonstrated that Balb/c mice fed a fermented milk with the EPS-producing *S. thermophilus* CRL 1190 was efficient in gastritis prevention through the modulation of the immune response and maintenance of the mucus layer. The present study addressed the potential therapeutic application of fermented milk prepared using the EPS-producing *S. thermophilus* CRL 1190 strain for the treatment of ASA-associated chronic gastritis.

MATERIALS AND METHODS

Strain, culture conditions and preparation of the fermented milk

S. thermophilus CRL 1190 {EPS$^+$ and producing also capsular EPS, CPS$^+$; [Centro de Referencia para Lactobacilos (CERELA) culture collection, Tucumán, Argentina]} was used in this study. This strain was previously selected for the physicochemical properties of its polysaccharide[20], for displaying no secondary effects such as bacterial translocation (liver and spleen), and for its effectiveness in preventing gastritis induced by ASA[25]. The strain was cultured (10 mL/L inoculum) in LAPTg broth (peptone, 15 g/L; tryptone, 10 g/L; yeast extract, 10 g/L; glucose, 10 g/L; and tween 80, 1 mL/L) and sub-cultured at least twice in reconstituted skim milk (RSM, 100 g/L) just prior to experimental use. The strain was maintained at -20℃ in RSM containing 100 mL/L glycerol, 10 g/L glucose, and 5 g/L yeast extract.

Fermented milk was prepared in sterile RSM (sterilized at 115℃ for 20 min and cooled down to 37℃) using a 10 mL/L inoculum of an active culture of the EPS$^+$ strain *S. thermophilus* CRL 1190 (named FM 1190), incubated at 37℃ for 16 h and maintained at 4℃ prior to experimental use. Non-fermented milk was used as a control.

Animals

Six week-old Balb/c male mice (25-30 g) were obtained from a closed colony kept at the animal facilities of CERELA and maintained in a room with a 12-h light/dark cycle at 20 ± 2℃. Animals were individually housed in cages (20 cm × 30 cm × 15 cm) with litter tray (20 cm × 30 cm × 6 cm) and allowed to have free access to conventional balanced diet and water *ad libitum*. All mice received no food for 24 h before the assays but had free access to water. Animal protocols were approved by the Ethical Committee for animal care of CERELA.

Experimental protocol

Chronic gastritis was induced following the protocol previously standardized in our laboratory[25]. Oral administration of ASA (BAYER®) supplied in the drinking water given at an approximate daily dose of 400 mg/kg per day for 10 d induced chronic gastritis in Balb/c mice (gastritis group, G). The administered dose was twice the analgesic dose for mice and was applied to induce gastritis in a short experimental time period. Healthy mice (H) received drinking water without ASA during the same experimental period (negative control group).

To evaluate the therapeutic effect of FM 1190 on the chronic gastritis model, animals were randomly divided into 6 groups (n = 5 each): (1) H group: received drinking water without ASA for 10 d; (2) G group: received ASA for 10 d as described above; (3) FM 1190 group: received

FM with the EPS-producing strain CRL 1190 for 7 d after gastritis induction. FM 1190 was administered *ad libitum* at an approximate dose of 10^8 cfu/mL; daily fermented milk consumption was monitored and intake was set at 5 mL/d; (4) Omeprazole (OM) group: received OM (used as positive control in ASA-induced gastric lesions) at a daily dose of 30 mg/kg per day[26] for 7 d after gastritis induction; (5) Milk group (M): received non-fermented milk for 7 d after gastritis induction; and (6) Water group (W): received water for 7 d after gastritis induction (used as negative control).

To determine whether the EPS produced by *S. thermophilus* CRL 1190 (EPS 1190) had an anti-gastritis effect, the polymer was isolated from 16-h milk cultures grown at 37℃ by using a deproteinization/precipitation technique with 200 g/L (final concentration) trichloroacetic acid, and ethanol (ratio 1:3)[20], was further purified as described previously[19], and freeze-dried and stored at 4℃ until use. The EPS 1190 was resuspended in RSM (M-EPS 1190) or in water (W-EPS 1190) and administered to mice intragastrically at a dose of 4 mg/kg per day for 7 d after gastritis induction. The administered EPS amount was calculated based on the EPS quantity received by the animals when they were fed with FM 1190.

After the experimental period (day 11 for groups 1 and 2, and day 18 for the remaining groups), mice were sacrificed by cervical dislocation and weighed. Stomachs were aseptically removed, weighed and rinsed several times with saline solution and used for the assays described below.

Histopathological evaluation of gastric samples

Stomachs were fixed in 10% paraformaldehyde in 0.1 mol/L phosphate-buffered saline (PBS) pH 7.0 and embedded in paraffin following the Sainte-Marie technique[27]. Three serial paraffin sections (4 μm) of each sample were cut from each specimen and stained with hematoxylin-eosin followed by light microscopy examination (Leica DM LS2, Wetzlar, Germany). The pathologic characteristics and degree of inflammation of the gastric mucosa were assessed according to the updated Sydney system[28] by microscopic observation without knowledge of the experimental groups and expressed as follows: normal appearance of scattered mononuclear cells in the lamina propria (same degree as healthy control mice): none = score 0; mild infiltration of mononuclear cells in the lamina propria and the submucosa, and no erosion in the epithelium: mild = score 1; moderate infiltration of mononuclear cells in the lamina propria and the submucosa, and no erosion in the epithelium: moderate = score 2; and severe infiltration of mononuclear cells in the lamina propria and the submucosa, and erosion in some parts of the epithelium: severe = score 3.

Determination of the number of IL-10, INF-γ, and TNF-α-producing cells in gastric mucosa by indirect immunofluorescence assay

Histological slices of the antral and corpus regions of the stomach, processed as described earlier, were deparaffinized and rehydrated in a graded series of ethanol. After incubation at room temperature for 30 min in 10 g/L blocking solution of bovine serum albumin (Sigma Chemical Co.), histological slices were incubated at 37℃ for 60 min with rabbit anti-mouse IL-10 or INF-γ (Peprotech Inc., NJ, USA) or TNF-α (eBioscience, San Diego, CA, USA) polyclonal antibodies. Then, sections were washed twice with saline solution and treated with a 1/10 dilution of a goat anti-rabbit antibody conjugated with fluorescein isothiocyanate (FITC) (Jackson Immuno Research Inc., PA, USA) at 37℃ for 45 min; washed again with saline solution and examined with a fluorescent light microscope (Leica DM LS2). Results were expressed as the number of IL-10, INF-γ and TNF-α-producing cells (fluorescent cells) per 10 fields (magnification × 1000)[29]. Data were obtained by counting 30 fields from 3 histological slices for each animal group.

Mucus layer determined by periodic acid-Schiff staining

The mucus layer was identified by periodic acid-Schiff (PAS) staining[30]. Briefly, after deparaffinization and rehydration, tissue sections were oxidized in 10 mL/L periodic acid for 5 min. Then they were rinsed in distilled water and stained with Schiff's reagent for 10 min. After a second washing with distilled water, tissue sections were counterstained with hematoxylin and rinsed in running tap water. Finally, they were dehydrated, cleared and mounted. Sections were viewed under a microscope (Leica M LS2) and the thickness of the mucus-secreting layer in the corpus and antrum mucosa was assessed with an image analyzer (× 1000) and the ratio of the mucus gel layer thickness to that of the lamina propria mucosa was calculated as a percentage.

Statistical analysis

Experimental data were expressed as mean ± SD and statistically evaluated by analysis of variance (ANOVA) with the SPSS software. Multiple group data were analyzed using one-way ANOVA and the Tukey multiple comparison test. Differences were considered statistically significant at $P < 0.05$.

RESULTS

Body weight and stomach weight

No significant changes in body weight or stomach weight were found during the entire experimental period in animals of any group other than those of the FM 1190 and M-EPS 1190 groups, which showed an increase (between 30%-40% with respect to H and G, respectively) in the stomach weight at the end of the experimental period (data not shown). No correlation between stomach weight and induced gastritis was found.

Histopathological evaluation of gastric samples

Mice subjected to oral administration of ASA at doses of 400 mg/kg per day for 10 d (gastritis group, G) showed moderate infiltration with scattered lymphocytes and

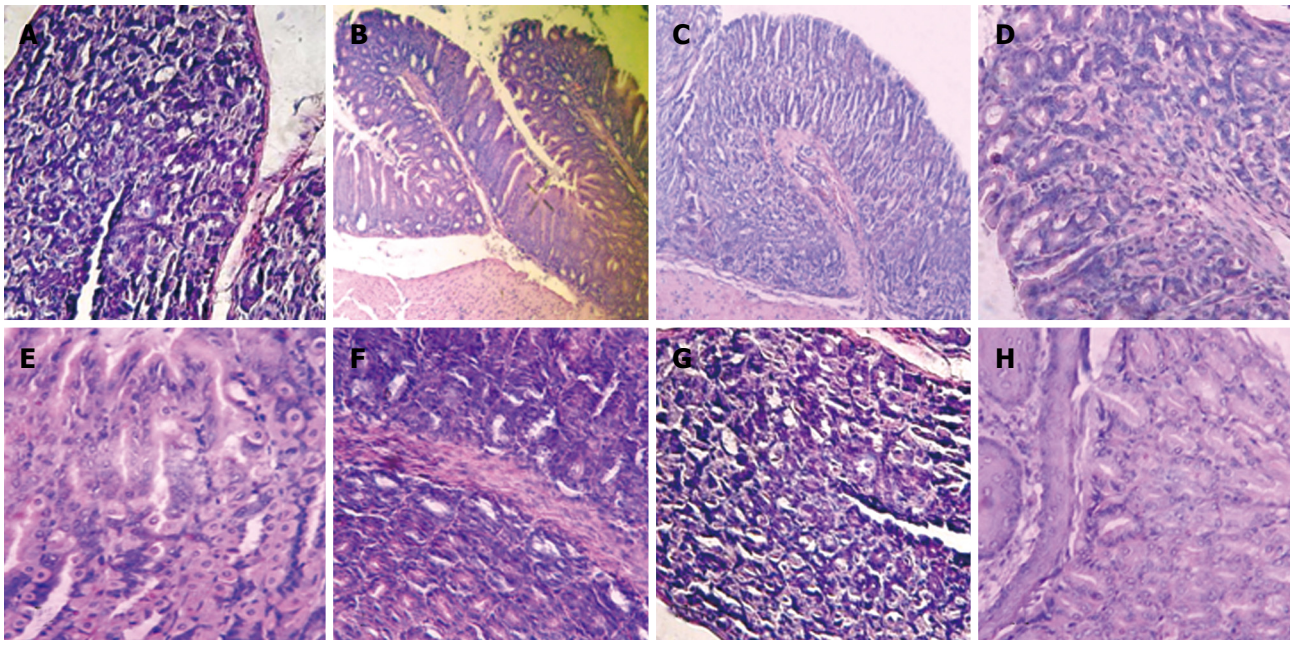

Figure 1 Histological micrographs of mice stomachs. A: H (Healthy) group; B: G (Gastritis) group; C: FM 1190 group (fermented milk with *Streptococcus thermophilus* CRL 1190); D: OM (omeprazole) group; E: M (Milk) group; F: W (Water) group; G: M-EPS 1190 group (EPS produced by *S. thermophilus* CRL 1190 resuspended in milk) showed conserved histological structures; and H: W-EPS 1190 group (EPS produced by *Strep. thermophilus* CRL 1190 resuspended in water) displayed chronic inflammatory infiltrations in the mucosa surface (Hematoxylin & eosin, light microscope, × 100).

macrophages in the surface of the mucosa and folds of mucosa, in the direction of the submucosa, without formation of lymphoid follicles, and predominance in the gastric corpus region (Figure 1B). The induced lesions were classified as superficial chronic gastritis with inflammation score = 2 (Figure 2). No significant increase in polymorphonuclear infiltration in the normal gastric mucosa was observed. Healthy animals (group H) showed an absence of gastritis (Figure 1A). Interestingly, the stomachs from animals treated with FM 1190 and M-EPS 1190 displayed no leukocyte infiltration in the gastric mucosa immediately after treatment (day 18) (Figure 1C and G). Similar stomach structures of mice therapeutically treated with OM (Figure 1D) were observed, showing lower inflammatory scores than the gastritis group (0.2 ± 0.02 *vs* 2.2 ± 0.4, $P < 0.05$, Figure 2). In contrast, the animals treated with milk, water and W-EPS 1190 showed high inflammation scores (1.8 ± 0.5, 2.0 ± 0.5, 1.7 ± 0.4, respectively, $P < 0.05$), compared to those of the gastritis group.

Determination of the number of regulatory and pro-inflammatory cytokine-producing cells in the gastric mucosa

The stomachs from group G mice showed a significant decrease in the regulatory cytokine-producing cells (IL-10$^+$: 14 ± 1.3 *vs* 22 ± 1.7, $P < 0.05$) and an increase in the pro-inflammatory cytokine-producing cells (INFγ$^+$: 28 ± 1.2 *vs* 14 ± 1.0 and TNF-α$^+$: 33 ± 3.0 *vs* 15 ± 2.0, $P < 0.05$) with respect to healthy animals (Figure 3A-C).

The therapeutic administration of FM 1190 to mice regulated the gastric inflammatory process, significantly

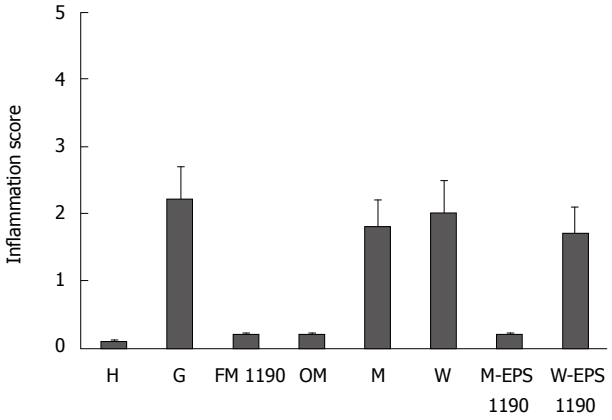

Figure 2 Inflammation score of stomachs in different groups (mean ± SD).

decreasing the number of pro-inflammatory cytokine-producing cells (INFγ$^+$: 15 ± 1.0 *vs* 28 ± 1.2, $P < 0.05$ and TNF-α$^+$ 16 ± 3.0 *vs* 33 ± 3.0, $P < 0.05$) and increasing the regulatory cytokine-producing cells (IL-10$^+$: 28 ± 1.5 *vs* 14 ± 1.3, $P < 0.05$), as compared to the G group. Furthermore, the number of cytokine-producing cells were similar to those of OM and H groups showing IL-10$^+$ values slightly higher than these 2 groups (28 ± 1.5 *vs* 20 ± 2.9; 28 ± 1.5 *vs* 22 ± 1.7, respectively, $P < 0.05$). In contrast, a significant decrease in the number of IL-10$^+$ cells and an increase in the number of both pro-inflammatory cytokine-producing cells (INFγ$^+$- and TNF-α$^+$) similar to those of the G group (Figure 3) were found in the M and W groups, used as controls.

M-EPS 1190 but not W-EPS 1190 was able to modulate the induced gastritis in a similar way to FM

1190, showing a decrease in the number of pro-inflammatory cytokine-producing cells (INFγ$^+$: 15 ± 2.0 *vs* 28 ± 1.2, $P < 0.05$ and TNF-α$^+$: 20 ± 2.6 *vs* 33 ± 3.0, $P < 0.05$) and an increase in the regulatory cytokine-producing cells (IL-10$^+$: 21 ± 2.1 *vs* 14 ± 1.3, $P < 0.05$), as compared to the G group (Figure 3).

A correlation between the histopathological structure and the number of regulatory and pro-inflammatory cytokine producing-cells was observed for all groups.

Mucus layer determined by PAS staining

The thickness ratio in the corpus and antrum mucosa, and representative photomicrographs of PAS-stained corpus mucosa from control (H), gastritis (G) and different therapeutic groups (FM 1190, OM, M and W) are shown in Figure 4A and B. The animals treated with ASA (G group) displayed a disruption in the protective mucus layer and exhibited a significant decrease of 80%-85% in the thickness of the mucus gel layer in both the corpus and antrum gastric regions as compared to healthy animals (corpus: 1.07 ± 0.3 *vs* 5.4 ± 1.0; antrum: 1.47 ± 0.4 *vs* 10.0 ± 1.3, $P < 0.05$).

In general, the different treatments for gastritis revealed a marked depletion (approximately 80%) in the mucus layer with concomitant reduction in the volume of PAS-positive intramucosal mucus in either the corpus or antrum mucosa of animals of most groups compared to the H group. A different behavior was observed in animals of group FM 1190, which showed a decrease of 49%-59% in the mucus layer of the antrum and corpus mucosa, compared with healthy animals (2.2 ± 0.6 *vs* 5.4 ± 1.0; 5.1 ± 0.8 *vs* 10.0 ± 1.3, respectively, $P < 0.05$). However, an increase in the thickness of the mucus gel layer as compared to animals displaying gastritis (G group) was observed (2.2 ± 0.6 *vs* 1.0 ± 0.3; 5.1 ± 0.8 *vs* 1.5 ± 0.4, in corpus and antrum mucosa respectively, $P < 0.05$). The volume of intramucosal mucus was maintained compared to the G group, suggesting that FM 1190 was able to protect the stomach mucosal barrier.

Mice treated with M-EPS 1190 showed an increase in the thickness of the mucus gel layer compared to animals with gastritis (2.1 ± 0.5 *vs* 1.0 ± 0.3; 5.0 ± 0.75 *vs* 1.5 ± 0.4, in corpus and antrum mucosa, respectively, $P < 0.05$) and was similar to the FM 1190 group.

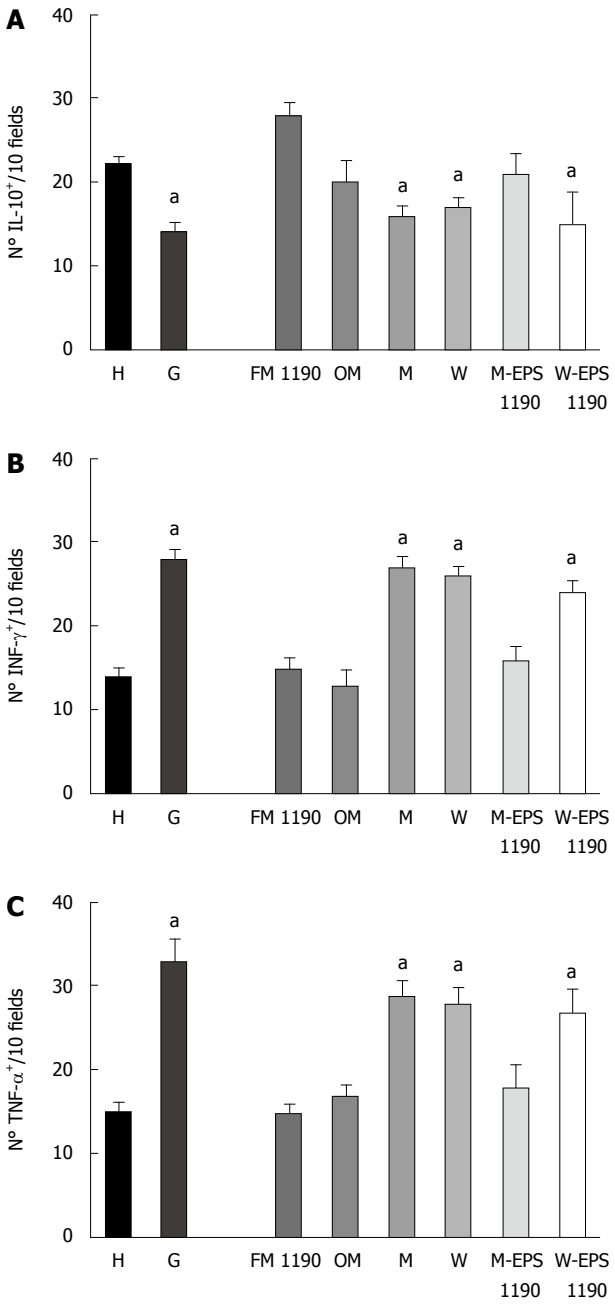

Figure 3 Number of (A) IL-10-, (B) INF-γ- and (C) TNF-α-producing cells on histological slices of stomachs of mice of different groups. Results are presented as means of 3 determinations and are expressed as the number of IL-10-, INF-γ- and TNF-α-producing cells per 10 fields (magnification × 100). $^aP < 0.05$ compared to the controls.

DISCUSSION

It has been demonstrated previously that ASA administration to mice caused chronic inflammation of the gastric mucosa[25]. Mononuclear cell infiltration, an increase in the number of pro-inflammatory cytokine-producing cells, a decrease in the regulatory cytokine-producing cells, and depletion of both the mucus gel layer and volume of intramucosal mucus were observed. The use of probiotics has been proposed to ameliorate different gastrointestinal tract disorders including inflammatory bowel diseases, diarrhea, pancreatitis, irritable bowel syndrome and colorectal cancer[31,32]; however, little attention has been paid to gastric disease. Uchida and Kurakazu[33] reported that yogurt LG21 significantly inhibited the formation of acute gastric lesions caused by HCl in rats; the beneficial effect being dose-dependent. Recently, Liu *et al*[34] reported that continuously feeding LAB-fermented soy-skim milk to rats for 28 d inhibited acute gastric lesions induced by ethanol and pylorus ligation in a dose-dependent manner, and improved prostaglandin E2 and superoxide dismutase activities. In addition, some authors have demonstrated the anti-ulcer properties of LAB-fermented milks on *H. pylori*-induced gastric lesions[14,35]. Based on the multiple functional effects of probiotics on the gastrointestinal

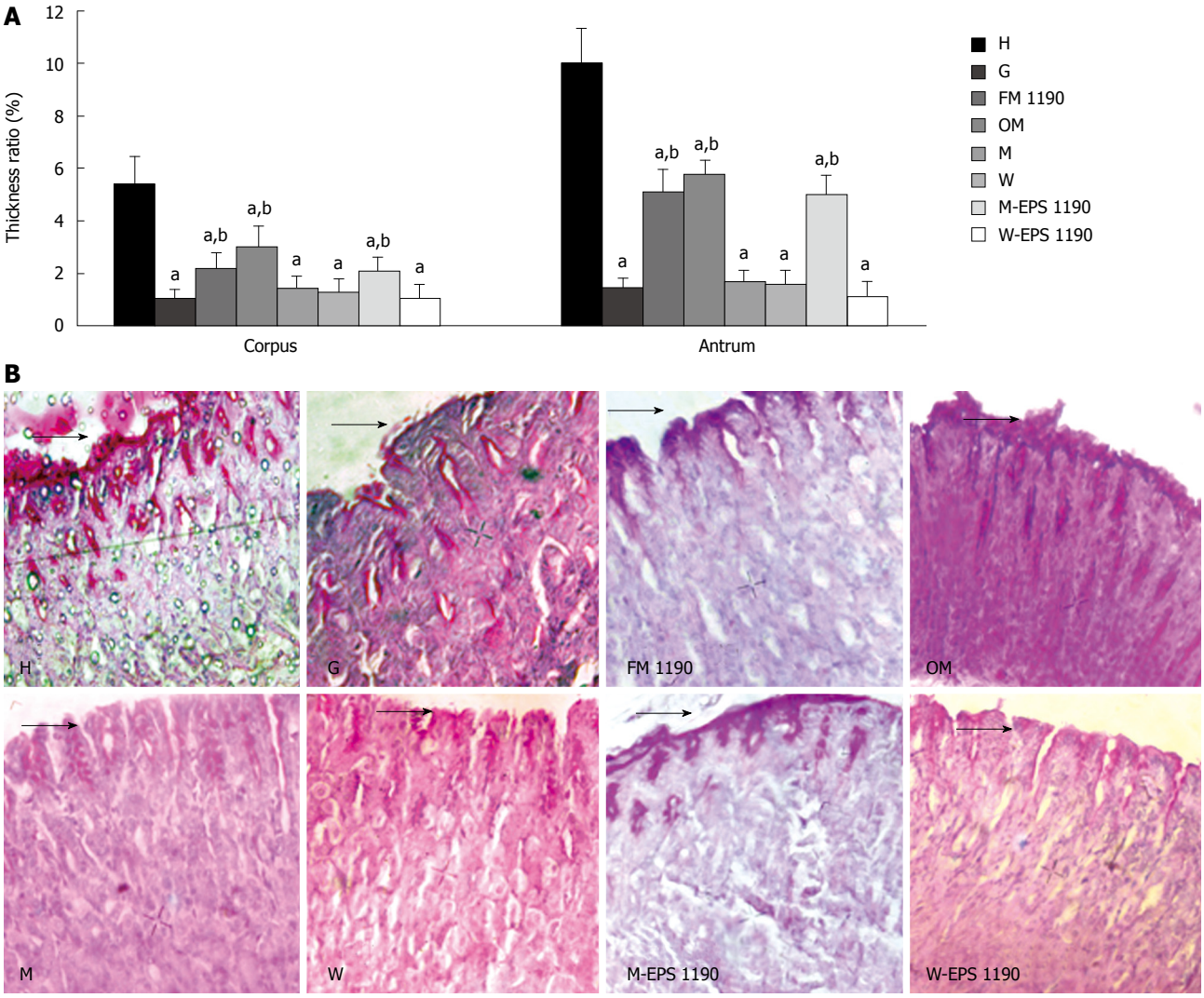

Figure 4 Periodic acid-Schiff (PAS)-positive mucus on the mice gastric mucosa. A: Thickness ratio of the mucus gel layer to the lamina propria mucosa in corpus and antrum mucosa. B: Representative photomicrographs of corpus mucosa from the various groups. Sections were stained using PAS reagent. Values represent mean ± SE of the mean for 5 mice. $^{a}P < 0.05$ compared to the healthy group (H), $^{b}P < 0.05$ compared to the gastritis group (G). Original magnification: × 400. Arrows indicate thickness of mucus layer.

tract, we have previously studied the capability of 2 EPS-producing LAB strains to protect the gastric mucosa from challenges produced by ASA; only the strain *S. thermophilus* CRL 1190 successfully prevented gastric damage by modulation of inflammation with significant preservation of the mucus gel layer[25]. *S. thermophilus* CRL 1190 produces a slime heteropolysaccharide of high molecular mass (MM) composed of D-glucose and D-galactose (molar ratio 1.0:1.5) as well as CPS in milk cultures[20]. In this work, we evaluated the therapeutic effect of milk fermented with *S. thermophilus* CRL 1190 on ASA-induced chronic gastritis. The therapeutic administration of FM 1190 showed a marked ($P < 0.05$) immunomodulatory effect when comparing the pro-inflammatory cytokine-producing cells (TNF-α^{+} and INF-γ^{+}) of healthy animals, as a result of inhibition of IL-10 on Th1[36]. Similar immunological modulation of the preventive effect of *S. thermophilus* CRL 1190 on chronic gastritis was observed in our previous work. Bibiloni *et al*[37] demonstrated that the Th1 cell response could be modulated by probiotic bacteria in pathological processes such as inflammatory bowel disease or colon cancer[38]. Th1 cytokines such as INF-γ and TNF-α, released by lymphocytes and macrophages that infiltrate the gastric mucosa are associated with immune activation and tissue injury. TNF-α has been shown to be a crucial mediator of NSAID-induced gastric mucosal damage[39]. In contrast, IL-10 (Th2 type cytokine) suppresses the differentiation and effector functions of Th1 cells and the production of pro-inflammatory cytokines by dendritic cells and macrophages, thus maintaining immune homeostasis[40]. The proton pump inhibitor drugs used clinically, such as omeprazole, exert an anti-inflammatory action beyond strong acid suppression[41]. It has been reported that omeprazole regulates the cytokine profile in *H. pylori*-infected patients with duodenal ulcer disease by suppressing cytokine synthesis of the Th1 cells[42]. In our study, this drug was used as a positive control in the treatment of ASA-induced gastritis, and it displayed similar therapeutic effectiveness to FM 1190, though the fermented milk displayed slightly higher

numbers of regulatory cytokine-producing cells (IL-10$^+$) than did omeprazole. On the other hand, this drug has diverse adverse effects such as diarrhea, abdominal pain, cutaneous reactions, decreased bone density and microscopic colitis[43,44] as well as drug interactions[45]. Thus, the use of FM 1190 as a therapeutic agent constitutes a safe and nutritional alternative for gastritis treatment.

Myeloperoxidase activity as a neutrophil infiltration marker in gastric tissue was assayed but it could not be used as an inflammatory parameter in the chronic gastritis model as the values obtained were similar to that of the healthy groups (data not shown).

Milk alone, water, omeprazole or the prepared fermented milk did not cause any damage *per se* on the gastric mucosa of healthy animals.

To determine if the therapeutic effect obtained after administration of FM 1190 resulted from the presence of its EPS, the produced biopolymer was isolated, purified and resuspended in milk or water, and assayed for its potential therapeutic effect. As previously observed[25], only the EPS dissolved in milk (M-EPS 1190) displayed a similar behavior to the fermented milk with respect to the cytokine profile and the histological structures, suggesting that EPS-milk protein interactions play a major role in the immune response modulation and consequently, in the therapeutic effect observed. Whey proteins have been reported to possess biological functions including immunomodulatory activities[46] in addition to their nutritional value. Rosaneli *et al*[47] reported the protective effect of bovine milk whey protein concentrate on the ulcerative lesions caused by administration of indomethacin. Moreover, the gastro-protective effect of α-lactoalbumin, one of the major whey proteins, against gastric injury induced by ethanol was demonstrated by enhancing the gastric defense mechanisms such as mucin synthesis and secretion in mucus-producing cells[48-50].

The mucus gel layer is an important defense barrier, covering gastric epithelial cells and holding bicarbonate ions to neutralize hydrogen ions that diffuse back into the gastric mucosa. However, this layer is frequently disrupted by acid, pepsin, alcohol, and other injurious agents in the gastric lumen resulting in damage to gastric epithelial cells[51]. The mucus gel layer thickness in the mouse gastric mucosa as well as the volume of intramucosal PAS-positive mucus were evaluated, as a continuous supply of mucus from the intramucosa is important to preserve the surface gel layer. Therapeutic administration of FM 1190 and M-EPS 1190 increased the thickness of the mucus gel layer in both corpus and antrum mucosa without reducing intramucosal mucus. Thus, the activation of mucin synthesis by FM 1190 and M-EPS 1190 led to the increase in the mucus gel layer and a stable mucus supply from the intramucosa. The stimulation of mucus metabolism contributes to the gastroprotective action. *L. rhamnosus* GG, a probiotic EPS-producing strain widely used in dairy products, is able to increase the mucus layer thickness in the gastric glandular mucosa[29]. Also, it has been observed that the fungal polysaccharide from *Ganoderma lucidum* reinstated the gastric mucus levels[52].

Nagaoka *et al*[53] reported anti-ulcer effects of EPS produced by bifidobacteria, *Lactobacilli* and *Streptococci* strains, which were attributed to the high rhamnose content (> 60%) of the polysaccharides. Conversely, the fermented milk with the EPS-producing strain *S. thermophilus* CRL 804, which produced an EPS with rhamnose and galactose in its monomer composition[20], did not show any anti-gastritis effect in contrast to the EPS 1190 that contained galactose and glucose and displayed a gastroprotective effect. Sengül *et al*[54] showed that a high MM EPS produced by the probiotic strain *L. delbrueckii* subsp. *bulgaricus* B3 significantly ameliorated experimental colitis in rats. Gao *et al*[52,55] found that treatment of acetic acid-induced ulcers in rats with high MM polysaccharide from *Ganoderma lucidum* suppressed or restored the decreased gastric mucus levels, increased gastric prostaglandin concentrations and partly suppressed the TNF-α gene. In addition, a high MM pectin polysaccharide from Chinese herbs has shown to be a potent anti-ulcer compound in experimental HCl-ethanol induced ulcers[56]. Moreover, a high MM-homopolysaccharide from marine microalga *Gyrodinium impudicum* strain KG03 presented immunostimulatory effects, enhancing the tumoricidal activities of macrophages and natural killer cells *in vivo*[57]. In this case, the beneficial effect was attributed to the sulfate groups present in the polymer, which also contained galactose and uronic acids. In our work, the anti-gastritis effect observed for FM 1190 may be ascribed to the large polymer size of EPS 1190, independently of its monomer composition. In addition, it was recently demonstrated[58] that EPS 1190 was partially degraded when the polymer was submitted to the harsh conditions of an *in vitro* gastric system, indicating that this polymer may still exert its beneficial properties *in vivo*.

The present findings indicate that the milk fermented with *S. thermophilus* CRL 1190 and/or its EPS was effective in the therapeutic treatment of chronic gastritis by modulating the immune response of the mice and by increasing the thickness of the gastric mucus gel layer. Thus, the application of this fermented milk and/or its EPS constitutes a potential natural alternative for the prevention and treatment of ASA-associated gastric damage.

COMMENTS

Background

Gastritis is a common disorder where there is discontinuity in the gastric mucosa. It is caused by several factors including the intensive consumption of anti-inflammatory drugs such as acetyl-salicylic acid (ASA), commonly used in the treatment of chronic diseases and prevention of cardiovascular pathologies. The conventional drugs employed as therapies against gastritis often produce undesirable side effects. The administration of specific probiotics provides a new therapy against gastric disease.

Research frontiers

Gastritis affects 80% of the worldwide population according to data of the Worldwide Health Organization. The use of probiotics has been proposed to ameliorate different gastrointestinal tract disorders such as inflammatory bowel disease, diarrhea, irritable bowel syndrome, *etc.*; however, little attention has been

paid to gastric disease. Thus, the authors decided to investigate the therapeutic effect of milk fermented with exopolysaccharide (EPS)-producing *S. thermophilus* CRL 1190 and its polymer on chronic gastritis induced by aspirin in mice.

Innovations and breakthroughs

This research demonstrates for the first time the therapeutic effect of the fermented milk with the polymer-producing strain *S. thermophilus* CRL 1190 and/or its EPS on chronic gastritis induced by ASA in mice. Both the fermented milk and the EPS were able to modulate the immune response in mice and increased the thickness of the gastric mucus gel layer. Furthermore, the therapeutic effectiveness observed was similar to omeprazole®, a commercial drug commonly employed in the treatment of gastritis.

Applications

The fermented milk with the EPS-producing strain *S. thermophilus* CRL 1190 and/or its EPS constitutes a potential natural alternative for the prevention and treatment of ASA-associated gastric damage.

Terminology

EPS are carbohydrate polymers naturally produced by certain bacteria, alga, yeasts and fungi. These polymers are extensively used in several industries mainly due to their thickening, texturizing, and gelifying properties.

Peer review

The research is a well carried out study.

REFERENCES

1 **Bienia A**, Sodolski W, Luchowska E. The effect of chronic alcohol abuse on gastric and duodenal mucosa. *Ann Univ Mariae Curie Sklodowska Med* 2002; **57**: 570-582
2 **Gamboa-Dominguez A**, Ubbelohde T, Saqui-Salces M, Romano-Mazzoti L, Cervantes M, Domínguez-Fonseca C, de la Luz Estreber M, Ruíz-Palacios GM. Salt and stress synergize H. pylori-induced gastric lesions, cell proliferation, and p21 expression in Mongolian gerbils. *Dig Dis Sci* 2007; **52**: 1517-1526
3 **Beck PL**, Xavier R, Lu N, Nanda NN, Dinauer M, Podolsky DK, Seed B. Mechanisms of NSAID-induced gastrointestinal injury defined using mutant mice. *Gastroenterology* 2000; **119**: 699-705
4 **Goel RK**, Bhattacharya SK. Gastroduodenal mucosal defence and mucosal protective agents. *Indian J Exp Biol* 1991; **29**: 701-714
5 **Moskowitz RW**. The appropriate use of NSAIDs in arthritic conditions. *Am J Orthop* (Belle Mead NJ) 1996; **25**: 4-6
6 **Voutilainen M**, Sokka T, Juhola M, Farkkilä M, Hannonen P. Nonsteroidal anti-inflammatory drug-associated upper gastrointestinal lesions in rheumatoid arthritis patients. Relationships to gastric histology, Helicobacter pylori infection, and other risk factors for peptic ulcer. *Scand J Gastroenterol* 1998; **33**: 811-816
7 **Konturek JW**, Dembinski A, Stoll R, Domschke W, Konturek SJ. Mucosal adaptation to aspirin induced gastric damage in humans. Studies on blood flow, gastric mucosal growth, and neutrophil activation. *Gut* 1994; **35**: 1197-1204
8 **Wallace JL**. Nonsteroidal anti-inflammatory drugs and gastroenteropathy: the second hundred years. *Gastroenterology* 1997; **112**: 1000-1016
9 **Ashley SW**, Sonnenschein LA, Cheung LY. Focal gastric mucosal blood flow at the site of aspirin-induced ulceration. *Am J Surg* 1985; **149**: 53-59
10 **Lamarque D**. [Pathogenesis of gastroduodenal lesions induced by non-steroidal anti-inflammatory drugs] *Gastroenterol Clin Biol* 2004; **28** Spec No 3: C18-C26
11 **Scheiman JM**, Behler EM, Loeffler KM, Elta GH. Omeprazole ameliorates aspirin-induced gastroduodenal injury. *Dig Dis Sci* 1994; **39**: 97-103
12 **Prakash A**, Faulds D. Rabeprazole. *Drugs* 1998; **55**: 261-267; discussion 268
13 **FAO/WHO**. 2001. Report on joint FAO/WHO expert consultation on evaluation of health and nutritional properties of probiotics in food including powder milk with live lactic acid bacteria. Available from: URL: http://www.fao.org./es/ESN/Probio/probio.htm
14 **Sgouras D**, Maragkoudakis P, Petraki K, Martinez-Gonzalez B, Eriotou E, Michopoulos S, Kalantzopoulos G, Tsakalidou E, Mentis A. In vitro and in vivo inhibition of Helicobacter pylori by Lactobacillus casei strain Shirota. *Appl Environ Microbiol* 2004; **70**: 518-526
15 **Lam EK**, Woo PC, Cho CH. Probiotics and gastrointestinal disorders. *Pharmacology Online* 2005; **1**: 88–147
16 **Collado MC**, Isolauri E, Salminen S, Sanz Y. The impact of probiotic on gut health. *Curr Drug Metab* 2009; **10**: 68-78
17 **Borchers AT**, Selmi C, Meyers FJ, Keen CL, Gershwin ME. Probiotics and immunity. *J Gastroenterol* 2009; **44**: 26-46
18 **Perdigón G**, Maldonado-Galdeano C, de Moreno de LeBlanc A, Vinderola CG, Medici M, Bibas Bonet ME. Immunomodulation of mucosal immune response by probiotics. *Curr Trends Immunol* 2004; **6**: 69-85
19 **Vaningelgem F**, Zamfir M, Mozzi F, Adriany T, Vancanneyt M, Swings J, De Vuyst L. Biodiversity of exopolysaccharides produced by Streptococcus thermophilus strains is reflected in their production and their molecular and functional characteristics. *Appl Environ Microbiol* 2004; **70**: 900-912
20 **Mozzi F**, Vaningelgem F, Hébert EM, Van der Meulen R, Foulquié Moreno MR, Font de Valdez G, De Vuyst L. Diversity of heteropolysaccharide-producing lactic acid bacterium strains and their biopolymers. *Appl Environ Microbiol* 2006; **72**: 4431-4435
21 **Ruas-Madiedo P**, de los Reyes-Gavilán CG. Invited review: methods for the screening, isolation, and characterization of exopolysaccharides produced by lactic acid bacteria. *J Dairy Sci* 2005; **88**: 843-856
22 **Hassan AN**, Awad S. Application of exopolysaccharide-producing cultures in reduced-fat Cheddar cheese: cryo-scanning electron microscopy observations. *J Dairy Sci* 2005; **88**: 4214-4220
23 **Ruas-Madiedo P**, Hugenholtz J, Zoon P. An overview of the functionality of exopolysaccharides produced by lactic acid bacteria. *Int Dairy J* 2002; **12**: 163-171
24 **Welman AD**, Maddox IS. Exopolysaccharides from lactic acid bacteria: perspectives and challenges. *Trends Biotechnol* 2003; **21**: 269-274
25 **Rodríguez C**, Medici M, Rodríguez AV, Mozzi F, Font de Valdez G. Prevention of chronic gastritis by fermented milks made with exopolysaccharide-producing Streptococcus thermophilus strains. *J Dairy Sci* 2009; **92**: 2423-2434
26 **Watanabe K**, Murakami K, Sato R, Kashimura K, Miura M, Ootsu S, Miyajima H, Nasu M, Okimoto T, Kodama M, Fujioka T. Effect of sucralfate on antibiotic therapy for Helicobacter pylori infection in mice. *Antimicrob Agents Chemother* 2004; **48**: 4582-4588
27 **Saint-Marie G**. A paraffin embedding technique for studies employing immunofluorescence. *J Histochem Cytochem* 1962; **10**: 250-256
28 **Dixon MF**, Genta RM, Yardley JH, Correa P. Classification and grading of gastritis. The updated Sydney System. International Workshop on the Histopathology of Gastritis, Houston 1994. *Am J Surg Pathol* 1996; **20**: 1161-1181
29 **Vinderola G**, Matar C, Perdigón G. Milk fermentation products of L. helveticus R389 activate calcineurin as a signal to promote gut mucosal immunity. *BMC Immunol* 2007; **8**: 19
30 **Lam EK**, Tai EK, Koo MW, Wong HP, Wu WK, Yu L, So WH, Woo PC, Cho CH. Enhancement of gastric mucosal integrity by Lactobacillus rhamnosus GG. *Life Sci* 2007; **80**: 2128-2136
31 **Penner R**, Fedorak RN, Madsen KL. Probiotics and nutraceuticals: non-medicinal treatments of gastrointestinal diseases. *Curr Opin Pharmacol* 2005; **5**: 596-603
32 **Chen LL**, Wang XH, Cui Y, Lian GH, Zhang J, Ouyang CH, Lu FG. Therapeutic effects of four strains of probiotics on experimental colitis in mice. *World J Gastroenterol* 2009; **15**: 321-327
33 **Uchida M**, Kurakazu K. Yogurt containing Lactobacillus

gasseri OLL2716 exerts gastroprotective action against [correction of agaisnt] acute gastric lesion and antral ulcer in rats. *J Pharmacol Sci* 2004; **96**: 84-90
34 **Liu CF**, Hu CL, Chiang SS, Tseng KC, Yu RC, Pan TM. Beneficial Preventive Effects of Gastric Mucosal Lesion for Soy-Skim Milk Fermented by Lactic Acid Bacteria. *J Agric Food Chem* 2009; Epub ahead of print
35 **Miki K**, Urita Y, Ishikawa F, Iino T, Shibahara-Sone H, Akahoshi R, Mizusawa S, Nose A, Nozaki D, Hirano K, Nonaka C, Yokokura T. Effect of Bifidobacterium bifidum fermented milk on Helicobacter pylori and serum pepsinogen levels in humans. *J Dairy Sci* 2007; **90**: 2630-2640
36 **Kidd P**. Th1/Th2 balance: the hypothesis, its limitations, and implications for health and disease. *Altern Med Rev* 2003; **8**: 223-246
37 **Bibiloni R**, Fedorak RN, Tannock GW, Madsen KL, Gionchetti P, Campieri M, De Simone C, Sartor RB. VSL#3 probiotic-mixture induces remission in patients with active ulcerative colitis. *Am J Gastroenterol* 2005; **100**: 1539-1546
38 **de Moreno de Leblanc A**, Perdigón G. Yogurt feeding inhibits promotion and progression of experimental colo-rectal cancer. *Med Sci Monit* 2004; **10**: BR96-BR104
39 **Santucci L**, Fiorucci S, Giansanti M, Brunori PM, Di Matteo FM, Morelli A. Pentoxifylline prevents indomethacin induced acute gastric mucosal damage in rats: role of tumour necrosis factor alpha. *Gut* 1994; **35**: 909-915
40 **Maynard CL**, Weaver CT. Diversity in the contribution of interleukin-10 to T-cell-mediated immune regulation. *Immunol Rev* 2008; **226**: 219-233
41 **Kuroda M**, Yoshida N, Ichikawa H, Takagi T, Okuda T, Naito Y, Okanoue T, Yoshikawa T. Lansoprazole, a proton pump inhibitor, reduces the severity of indomethacin-induced rat enteritis. *Int J Mol Med* 2006; **17**: 89-93
42 **Kountouras J**, Boura P, Lygidakis NJ. Omeprazole and regulation of cytokine profile in Helicobacter pylori-infected patients with duodenal ulcer disease. *Hepatogastroenterology* 2000; **47**: 1301-1304
43 **Kirkpantur A**, Altun B, Arici M, Turgan C. Proton pump inhibitor omeprazole use is associated with low bone mineral density in maintenance haemodialysis patients. *Int J Clin Pract* 2009; **63**: 261-268
44 **Wilcox GM**, Mattia AR. Microscopic colitis associated with omeprazole and esomeprazole exposure. *J Clin Gastroenterol* 2009; **43**: 551-553
45 **Ibáñez A**, Alcalá M, García J, Puche E. [Drug-drug interactions in patients from an internal medicine service] *Farm Hosp* 2008; **32**: 293-297
46 **Shah NP**. Effects of milk-derived bioactives: an overview. *Br J Nutr* 2000; **84** Suppl 1: S3-S10
47 **Rosaneli CF**, Bighetti AE, Antônio MA, Carvalho JE, Sgarbieri VC. Protective effect of bovine milk whey protein concentrate on the ulcerative lesions caused by subcutaneous administration of indomethacin. *J Med Food* 2004; **7**: 309-314
48 **Matsumoto H**, Shimokawa Y, Ushida Y, Toida T, Hayasawa H. New biological function of bovine alpha-lactalbumin: protective effect against ethanol- and stress-induced gastric mucosal injury in rats. *Biosci Biotechnol Biochem* 2001; **65**: 1104-1111
49 **Ushida Y**, Shimokawa Y, Matsumoto H, Toida T, Hayasawa H. Effects of bovine alpha-lactalbumin on gastric defense mechanisms in naive rats. *Biosci Biotechnol Biochem* 2003; **67**: 577-583
50 **Ushida Y**, Shimokawa Y, Toida T, Matsui H, Takase M. Bovine alpha-lactalbumin stimulates mucus metabolism in gastric mucosa. *J Dairy Sci* 2007; **90**: 541-546
51 **Clamp JR**, Ene D. The gastric mucosal barrier. *Methods Find Exp Clin Pharmacol* 1989; **11** Suppl 1: 19-25
52 **Gao Y**, Zhou S, Wen J, Huang M, Xu A. Mechanism of the antiulcerogenic effect of Ganoderma lucidum polysaccharides on indomethacin-induced lesions in the rat. *Life Sci* 2002; **72**: 731-745
53 **Nagaoka M**, Hashimoto S, Watanabe T, Yokokura T, Mori Y. Anti-ulcer effects of lactic acid bacteria and their cell wall polysaccharides. *Biol Pharm Bull* 1994; **17**: 1012-1017
54 **Şengül M**, Aslím B, Uçar G, Yücel N, IsiK S, Bozkurt H, Sakaogullari Z, Atalay F. Effects of exopolysaccharide-producing probiotic strains on experimental colitis in rats. *Dis Colon Rectum* 2005; **49**: 250-258
55 **Gao Y**, Tang W, Gao H, Chan E, Lan J, Zhou S. Ganoderma lucidum polysaccharide fractions accelerate healing of acetic acid-induced ulcers in rats. *J Med Food* 2004; **7**: 417-421
56 **Yamada H**. [Structure and pharmacological activity of pectic polysaccharides from the roots of Bupleurum falcatum L.] *Nippon Yakurigaku Zasshi* 1995; **106**: 229-237
57 **Yim JH**, Son E, Pyo S, Lee HK. Novel sulfated polysaccharide derived from red-tide microalga Gyrodinium impudicum strain KG03 with immunostimulating activity in vivo. *Mar Biotechnol* (NY) 2005; **7**: 331-338
58 **Mozzi F**, Gerbino E, Font de Valdez G, Torino MI. Functionality of exopolysaccharides produced by lactic acid bacteria in an in vitro gastric system. *J Appl Microbiol* 2009; **107**: 56-64

S- Editor Wang YR **L- Editor** Cant MR **E- Editor** Ma WH

World Journal of Gastroenterology

Online Submissions: http://www.wjgnet.com/1007-9327office
wjg@wjgnet.com
doi:10.3748/wjg.v16.i13.1631

World J Gastroenterol 2010 April 7; 16(13): 1631-1638
ISSN 1007-9327 (print)

ORIGINAL ARTICLE

Effects of thymidine phosphorylase on tumor aggressiveness and 5-fluorouracil sensitivity in cholangiocarcinoma

Jongkonnee Thanasai, Temduang Limpaiboon, Patcharee Jearanaikoon, Banchob Sripa, Chawalit Pairojkul, Srisurang Tantimavanich, Masanao Miwa

Jongkonnee Thanasai, Department of Clinical Microbiology, Faculty of Medical Technology, Mahidol University, Bangkok 10700, Thailand; Department of Clinical Chemistry, Centre for Research and Development of Medical Diagnostic Laboratories, Faculty of Associated Medical Sciences, Khon Kaen University, Khon Kaen 40002, Thailand
Temduang Limpaiboon, Patcharee Jearanaikoon, Department of Clinical Chemistry, Centre for Research and Development of Medical Diagnostic Laboratories, Faculty of Associated Medical Sciences, Khon Kaen University, Khon Kaen 40002, Thailand
Banchob Sripa, Chawalit Pairojkul, Department of Pathology, Liver Fluke and Cholangiocarcinoma Research Center, Faculty of Medicine, Khon Kaen University, Khon Kaen 40002, Thailand
Srisurang Tantimavanich, Department of Clinical Microbiology, Faculty of Medical Technology, Mahidol University, Bangkok 10700, Thailand
Masanao Miwa, Nagahama Institute of Bio-Science and Technology, 1266 Tamura-cho, Nagahama, Shiga 526-0829, Japan
Author contributions: Thanasai J and Limpaiboon T contributed equally to this work; Thanasai J, Limpaiboon T, Jearanaikoon P and Miwa M designed the research, analyzed data and wrote the paper; Thanasai J performed the research; Sripa B, Pairojkul C and Tantimavanich S contributed cell lines, analyzed and interpreted data; Limpaiboon T and Miwa M revised and approved the article.
Supported by The Thailand Research Fund through The Royal Golden Jubilee PhD Program Grant No. PHD/0037/2544 for Thanasai J and Limpaiboon T and grants-in-aid from the Centre for Research and Development of Medical Diagnostic Laboratories, Faculty of Associated Medical Sciences, Khon Kaen University, Thailand, and from the Ministry of Education, Sports, Science, Culture and Technology, Japan
Correspondence to: Dr. Temduang Limpaiboon, Department of Clinical Chemistry, Centre for Research and Development of Medical Diagnostic Laboratories, Faculty of Associated Medical Sciences, Khon Kaen University, Khon Kaen 40002, Thailand. temduang@kku.ac.th
Telephone: +66-43-362028 Fax: +66-43-202088
Received: October 26, 2009 Revised: November 30, 2009
Accepted: December 6, 2009
Published online: April 7, 2010

Abstract

AIM: To evaluate the role of thymidine phosphorylase (TP) in cholangiocarcinoma using small interfering RNA (siRNA).

METHODS: A human cholangiocarcinoma-derived cell line KKU-M139, which has a naturally high level of endogenous TP, had TP expression transiently knocked down using siRNA. Cell growth, migration, *in vitro* angiogenesis, apoptosis, and cytotoxicity were assayed in TP knockdown and wild-type cell lines.

RESULTS: TP mRNA and protein expression were decreased by 87.1% ± 0.49% and 72.5% ± 3.2%, respectively, compared with control cells. Inhibition of TP significantly decreased migration of KKU-M139, and suppressed migration and tube formation of human umbilical vein endothelial cells. siRNA also reduced the ability of TP to resist hypoxia-induced apoptosis, while suppression of TP reduced the sensitivity of KKU-M139 to 5-fluorouracil.

CONCLUSION: Inhibition of TP may be beneficial in decreasing angiogenesis-dependent growth and migration of cholangiocarcinoma but may diminish the response to 5-fluorouracil chemotherapy.

Key words: Liver fluke; Cholangiocarcinoma; Thymidine phosphorylase; 5-fluorouracil; siRNA; Tumor aggressiveness; Cell migration

Peer reviewers: Gianfranco D Alpini, PhD, Professor, VA Research Scholar Award Recipient, Professor, Medicine and Systems Biology and Translation Medicine, Dr. Nicholas C Hightower Centennial Chair of Gastroenterology, Central Texas Veterans Health Care System, The Texas A & M University System Health Science Center College of Medicine, Medical

Research Building, 702 SW H.K. Dodgen Loop, Temple, TX, 76504, United States; Xian-Ming Chen, MD, Associate Professor, Department of Medical Microbiology and Immunology, Creighton University, 2500 California Plaza, Omaha, NE 68178, United States

Thanasai J, Limpaiboon T, Jearanaikoon P, Sripa B, Pairojkul C, Tantimavanich S, Miwa M. Effects of thymidine phosphorylase on tumor aggressiveness and 5-fluorouracil sensitivity in cholangiocarcinoma. *World J Gastroenterol* 2010; 16(13): 1631-1638 Available from: URL: http://www.wjgnet.com/1007-9327/full/v16/i13/1631.htm DOI: http://dx.doi.org/10.3748/wjg.v16.i13.1631

INTRODUCTION

Cholangiocarcinoma is a common hepatobiliary malignancy among the Northeastern Thai population and it is an important public health problem because the incidence and fatality rates are high[1,2]. Liver fluke (*Opisthorchis viverrini*) infection is a risk factor for cholangiocarcinoma, which accounts for about 89% of all liver cancer cases in Khon Kaen province, where the liver fluke is highly endemic and the incidence of cholangiocarcinoma is the highest in the world (97.4 per 100 000 males and 39 per 100 000 females)[1]. A number of different genes have been implicated in carcinogenesis of cholangiocarcinoma, e.g. *p53*[3], *MDM2*[3], *hMLH1* and *hMSH2*[4,5], and TFF[6]. We previously demonstrated the high prevalence of thymidine phosphorylase (TP) gene amplification (53.8%; 35 of 65 cases) in cholangiocarcinoma tumor tissues, suggesting that *TP* may play an important role in carcinogenesis of liver fluke-related cholangiocarcinoma[7].

TP (EC 2.4.2.4) is located in chromosomal region 22q13.33 and encodes a protein that catalyzes the reversible phosphorolysis of thymidine, deoxyuridine, and their analogs to their respective bases and 2-deoxyribose-1-phosphate, which is then dephosphorylated to 2-deoxy-D-ribose[8]. TP has been proposed to function in DNA synthesis, cell growth, chemotaxis stimulation in endothelial cells *in vitro*, and to enhance angiogenesis *in vivo*[9,10]. TP is abnormally expressed in certain cancers of the gastrointestinal tract e.g. pancreatic cancers[11], colon carcinomas[12], gallbladder adenocarcinomas[13], and intrahepatic cholangiocarcinoma[14]. Interestingly, TP expression was found to be elevated from 10- to 260-fold in nearly all biopsies examined from carcinomas of the stomach, colon, ovary, and bladder when compared to non-neoplastic regions of these organs[15,16]. Nevertheless, how TP expression is up-regulated in human tumors remains unclear.

During the past few years the utility of RNA interference (RNAi) and post-transcriptional gene silencing has significantly advanced the study of the effects of loss of individual gene functions. Therefore, we investigated the functions and roles of TP in carcinogenesis of liver fluke-related cholangiocarcinoma using small interfering RNA (siRNA) to suppress TP expression. Understanding the functions of TP involved in cholangiocarcinoma will help us elucidate the molecular mechanisms of cholangiocarcinogenesis and thus could potentially provide important strategies for prevention, early diagnosis, and early treatment to reduce the cancer incidence and increase cholangiocarcinoma patient survival.

MATERIALS AND METHODS

Cell lines and culture condition

The KKU-M139 cell line was established from the primary tumor of a 53-year-old Thai woman with squamous cell type cholangiocarcinoma. It was selected for this work after prior screening of TP expression in 5 cholangiocarcinoma-derived cell lines (data not shown). KKU-M139 was maintained in RPMI-1640 medium containing 100 IU/mL penicillin, 100 μg/mL streptomycin, and 100 mL/L heat-inactivated fetal bovine serum (FBS) as a complete medium. The human umbilical vein endothelial cells (HUVECs) isolation procedure followed the protocol of Jaffe *et al*[17]. HUVECs were maintained in M199 medium containing 100 U/mL penicillin, 100 μg/mL streptomycin, 50 mL/L pooled human serum, and 300 mL/L heat-inactivated FBS. Culturing was carried out at 37℃ in a humidified 50 mL/L CO_2 incubator. Confluent HUVEC monolayers (passages 2-4) were used in the assays.

Transient knockdown of TP using siRNA

siRNA sequences against human TP were designed and synthesized by Stealth RNAi (Invitrogen, Carlsbad, CA, USA). The siRNA sequences were 5'-AUAGACUCCA GCUUAUCCAAGGUGC-3' (sense) and 5'-GCACCU UGGAUAAGCUGGAGUCUAU-3' (antisense). A non-related control siRNA that lacked identity with known gene targets was used as a control for non sequence-specific effects. TP siRNA or control siRNA (20 pmol) was transiently transfected into 1×10^5 KKU-M139 using OligofectAMINE (Invitrogen) according to the manufacturer's instructions. Briefly, siRNA:OligofectAMINE complexes were mixed gently in Opti-MEM I reduced-serum medium and incubated for 20 min at room temperature. Then 200 μL of the complex mixture was added to cells growing in a 35-mm Petri dish containing 800 μL Opti-MEM I and mixed gently. After 24 h incubation at 37℃ in a 50 mL/L CO_2 incubator, the complexes were replaced by complete medium. Cells were incubated further for 24 h and gene function assays performed within 72 h post-transfection. The intensity of TP expression, either mRNA or protein, was analyzed using ImageJ software version 1.32j (NIH, Bethesda, MD, USA). To determine the knockdown efficiency, the density of TP expression was normalized with its corresponding β-actin for mRNA or α-tubulin for protein. The normalized intensity was compared between TP siRNA-transfected cells (*TP*-deficient cells) and control siRNA-transfected cells (control cells).

Reverse transcription and semi-quantitative polymerase chain reaction

Total RNA from the KKU-M139 cell line was reverse transcribed using Omniscript reverse transcriptase (QIA-

gen, Hilden, Germany). The forward and reverse primer sequences of TP were 5'-GGCATGGATCTGGAGGAGAC-3' and 5'-CTCTGACCCACGATACAGCA-3', respectively. The forward and reverse primer sequences for β-actin as control were 5'-ACTGGGACGACATGGAGAAA-3' and 5'-ATAGCACAGCCTGGATAGCA-3', respectively. Polymerase chain reaction (PCR) amplification was carried out in a final volume of 20 μL containing first-strand cDNA, 10 pmol of each primer, 5 U Taq polymerase in 1 × Taq buffer (67 mmol/L Tris-HCl, 16.6 mmol/L ammonium sulfate, and 10 mL/L Tween 20), 2.5 mmol/L $MgCl_2$, and 0.2 mmol/L dNTPs. The amplification was initiated by incubation at 94℃ for 5 min followed by 40 cycles of denaturation at 94℃ for 30 s, annealing at 59℃ (for TP) or 60℃ (for β-actin) for 30 s, and extension at 72℃ for 30 s, with a final 10-min extension at 72℃. PCR products were separated on a 20 g/L agarose gel containing 100 ng/mL ethidium bromide. Gels were visualized and photographed on a UV Transilluminator.

Western blot analysis

Total protein was separated on 10% SDS-PAGE then transferred onto a nitrocellulose membrane and blocked with TBST buffer (20 mmol/L Tris-HCl, 150 mmol/L NaCl, 0.5 mL/L Tween 20) plus 50 g/L skim milk. The membrane was probed with anti-TP (Taiho Pharmaceutical Co., Ltd. Japan) or anti-α-tubulin (Zymed Laboratories Inc., San Francisco, CA, USA) as a control at a dilution of 1:1000 in TBST followed by a dilution of 1:2000 of a horseradish peroxidase-conjugated secondary antibody. Immunopositive bands were detected with freshly prepared ECL chemiluminescent solution (Amersham Biosciences, Buckinghamshire, England) and visualized by exposure to X-ray film.

Cell growth assay

To evaluate the cellular growth rates, 1×10^4 wild-type, TP-deficient, or control cells were seeded in 6-well cell culture plates and grown in complete medium at 37℃ in a 50 mL/L CO_2 incubator. The cells were counted in triplicate every day for up to 6 d following a trypan blue dye exclusion assay. The population doubling time was calculated from the exponential growth phase.

Migration assays

The migration of HUVECs stimulated by TP-expressing KKU-M139 cells was evaluated by a 2-chamber assay using a 96-well modified Chemotaxicell chamber (Kurabo, Japan) with an 8-μm pore size membrane. In brief, 100 μL total protein of wild-type, TP-deficient or control cells (PBS alone as a negative control) was added to the lower chamber. HUVECs (1×10^5 resuspended in 60 μL PBS) were placed in the upper chamber then incubated at 37℃ in a 50 mL/L CO_2 incubator for 4 h. The number of cells that moved through the pores toward the attractant-that is, TP protein produced by KKU-M139 cells-and settled on the bottom chamber was counted using trypan blue staining. The assays were performed in triplicate. The migration assay for KKU-M139 cells was carried out using the same protocol, but the lower chamber contained 100 μL of a complete medium as a chemoattractant. RPMI-1640 medium containing 10 mL/L FBS served as a negative control. Wild-type, TP-deficient or control cells (1×10^5 in suspension in 60 μL fresh RPMI-1640) were placed in the upper chamber.

In vitro angiogenesis assay

The HUVEC tube-like structure was determined using the Endothelial Tube Formation Assay (Cell Biolabs Inc., Sandiego, CA, USA) according to the manufacturer's protocol. In brief, HUVECs were harvested and resuspended in M199 culture medium containing 100 mL/L FBS and angiogenesis mediators, i.e. serum of endometriosis patients as a positive control, total protein from KKU-M139 cells before and after treatment with *TP*-siRNA. Cell suspension (150 μL, 1.5×10^4 cells) was layered on the 50 μL of solidified extracellular matrix (ECM) gel in each 96-well plate, and the plate was incubated at 37℃ for 18 h to allow the HUVECs to reorganize into a 3-dimensional tubular structure. The tube-like structures were stained with Calcein AM fluorescent dye, and examined and captured under a fluorescence microscope (Olympus CKX41, Tokyo, Japan). The tube length was quantified using ImageJ (NIH, Bethesda, MD, USA) and represented as total tube length (μm) for 3 photographic fields per experimental condition. Each treatment was performed in duplicate, and the set of experiments was repeated twice independently.

TUNEL apoptosis assay

The DeadEnd™ Colorimetric TUNEL System (Promega, Madison, WI, USA) was used to detect apoptosis in cultured cell lines. In brief, cells grown in a 35-mm petri-dish were exposed to hypoxic conditions for 48 h. Cells were allowed to undergo apoptosis at 37℃ in a humidified 50 mL/L CO_2 incubator for 12 h. Treated cells were fixed with 40 g/L buffered formaldehyde, permeabilized by 2 mL/L Triton X-100, and equilibrated with Equilibration buffer (Promega). The cells were incubated with recombinant terminal deoxynucleotidyl transferase (rTdT) reaction mix, containing biotinylated nucleotides, inside a humidified chamber at 37℃ for 1 h to allow end-labeling of the fragmented DNA of apoptotic cells to occur. The reactions were terminated by addition of 2 × SSC buffer, and endogenous peroxidases were blocked with 3 mL/L H_2O_2. To detect the incorporated biotinylated nucleotides, streptavidin-horseradish peroxidase solution (Promega) in PBS was used. A total of 100 μL diaminobenzidine chromogen was added to each plate and developed until a light brown background occurred. Cells stained brown was counted per total number of cells in the 100 × power field of inverted microscope. The assays were performed in duplicate, and the experiment was repeated at least 3 times.

MTS cytotoxicity assay

To determine the concentration of 5-fluorouracil that

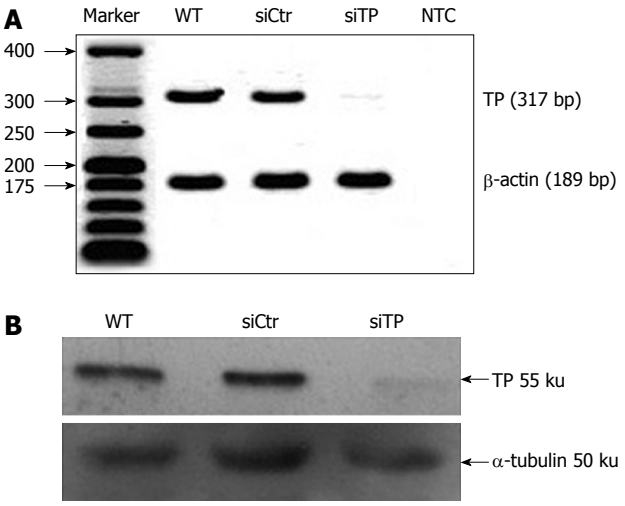

Figure 1 Small interfering RNA (siRNA) significantly reduced thymidine phosphorylase (TP) mRNA analyzed by semi-quantitative polymerase chain reaction (A) and protein (B) analyzed by Western blot of TP-deficient (siTP) cells compared with wild-type (WT) and control (siCtr) cells. For negative control (NTC), no cDNA was present in the reaction.

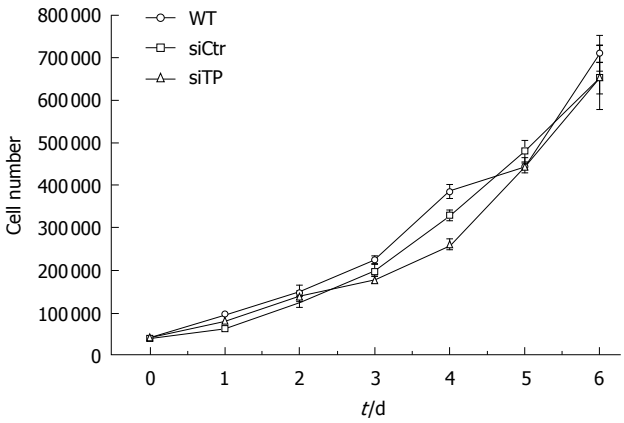

Figure 2 Kinetic growth curves of KKU-M139 WT, control (siCtr), and TP-deficient (siTP) cells. The doubling time of TP-deficient cells was not significantly different from that of WT or control cells.

inhibited cell proliferation by 50% (IC_{50}), the MTS assay (Promega) was used according to the manufacturer's instructions. Briefly, at one day post-transfection, 100 μL of cell suspension (1×10^5 cells/mL) was added to each well of a 96-well flat-bottom culture plate then incubated at 37℃ in a humidified 50 mL/L CO_2 incubator. After 24 h incubation, 100 μL medium containing various concentrations of 5-fluorouracil or fresh medium for untreated controls was added to each well for 48 h. The culture medium containing dead cells was then removed, and 100 μL of medium containing 20 μL MTS solution (317 μg/mL) was added to each well for 2 h to allow living cells to catalyze the MTS to a colored formazan product which was measured at 490 nm using a microplate reader (Tecan Austria GmbH, Salzburg, Austria). The assays were performed in duplicate, and the experiment was repeated twice.

Statistical analysis

Values are presented as mean ± SD. The statistical significance of the data was analyzed by one-way ANOVA using SPSS statistical software version 10.0 for Windows (SPSS Inc, Chicago, IL, USA). $P < 0.05$ was considered statistically significant.

RESULTS

TP is not a pivotal factor for tumor cell proliferation in cholangiocarcinoma

After TP-siRNA transfection, expression of *TP* mRNA (Figure 1A) and protein (Figure 1B) was suppressed by 87.1% ± 0.49% and 72.5% ± 3.2%, respectively, compared with control cells. To evaluate TP function on the proliferation of KKU-M139, the cell growth assay was performed. The population doubling time calculated from exponential growth phase (day 1-day 4) of wild-type, TP-deficient, and control cells was 25.7 ± 4.7, 29.7 ± 2.4, and 29.6 ± 6 h ($n = 4$), respectively (Figure 2). Doubling time of TP-deficient cells was not significantly different from that of wild-type or control cells.

TP-siRNA decreases TP-induced migration of HUVECs and KKU-M139

Angiogenesis, which is crucial for the development and progression of various cancers, requires migration and proliferation of endothelial cells in order to form the vasculature. Therefore, we tested the ability of TP to activate migration of endothelial cells using a 2-chamber assay. Migration of HUVECs toward total protein of TP-deficient cells was similar to that of PBS (Figure 3A). Use of total protein of TP-expressing KKU-M139 cells as a chemoattractant induced the migration of HUVECs by more than 2-fold relative to PBS ($P < 0.05$). Migration of cancer cells is important for invasion and metastasis. We investigated the migration of wild-type, TP-deficient, and control cells directed to 100 mL/L FBS as a chemoattractant. Migration towards 100 mL/L FBS of TP-deficient cells was significantly reduced by 2.4-fold compared with wild-type ($P < 0.001$) and 1.8-fold compared with control cells ($P < 0.01$) (Figure 3B).

TP-siRNA attenuates TP-induced tube formation of HUVECs

To assess the effect of TP on the formation of blood vessels, we analyzed the ability of TP produced from KKU-M139 to induce HUVECs to form tube structures using an ECM gel angiogenesis assay. Tube-like structures were formed by HUVECs activated by serum of endometriosis patients as a positive control (Figure 4A) but not by the PBS as a negative control (Figure 4B). HUVECs exhibited significant tube formation when total protein from wild-type KKU-M139 cells (Figure 4E and F), which endogenously express TP, was added ($P < 0.001$ *vs* PBS). Pre-treatment of KKU-M139 cells with TP-siRNA (Figure 4D) to suppress TP expression reduced tube formation of HUVECs compared with control cells (Figure 4C) (*P*

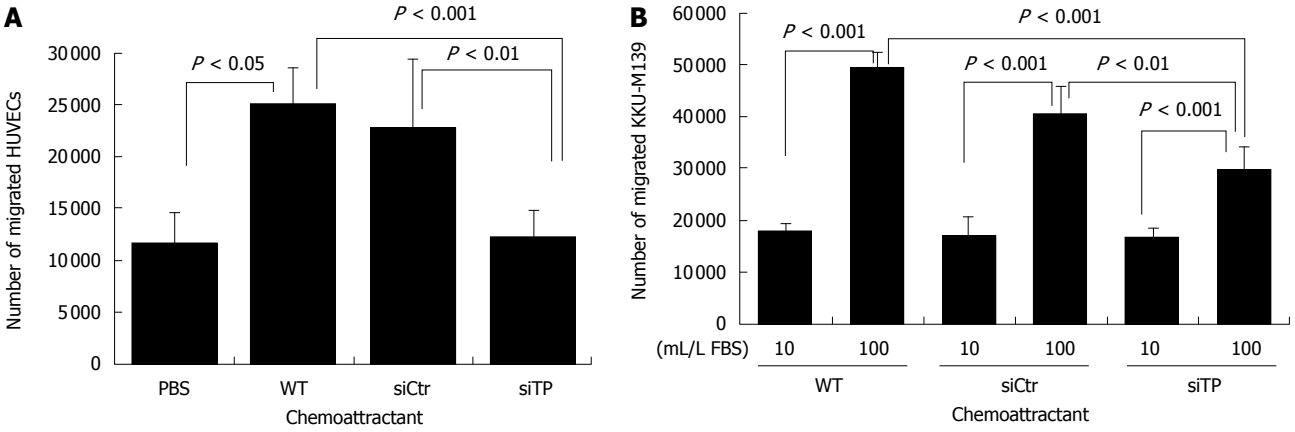

Figure 3 Knockdown of TP reduces migration of HUVECs and KKU-M139. A: Migration of HUVECs toward protein produced from TP-deficient cells (siTP) was similar to that of PBS, and 2-fold less than that of wild-type (WT); B: TP-deficient KKU-M139 cells are less migratory in response to FBS compared with wild-type, and control.

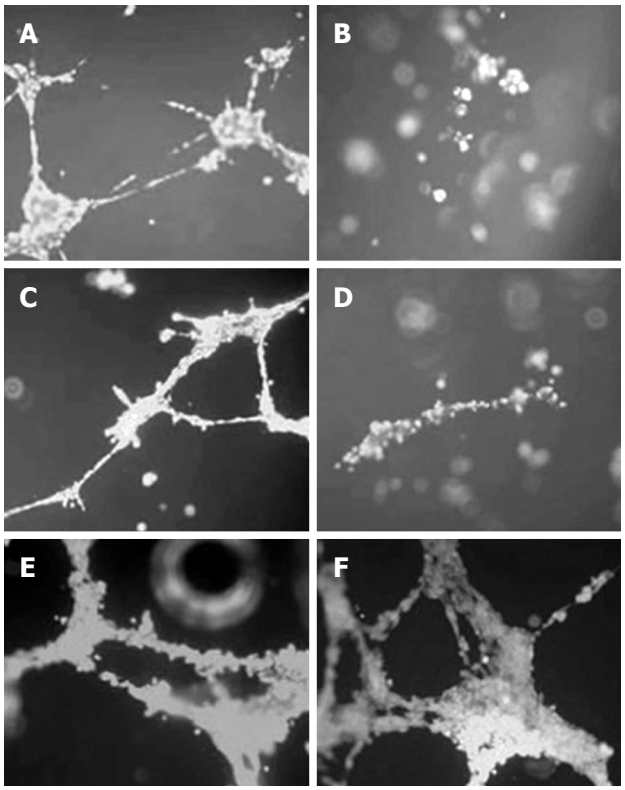

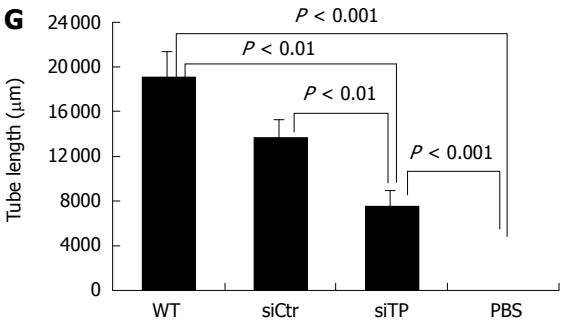

Figure 4 Knockdown of TP decreases the formation of tube-like structures in an ECM gel angiogenesis assay. Serum of endometriosis patients was used as a positive control (A), and PBS as a negative control (B). Total protein of control (siCtr) (C), TP-deficient (siTP) (D), or WT cells (E and F) were assayed. The tube length was quantified (G).

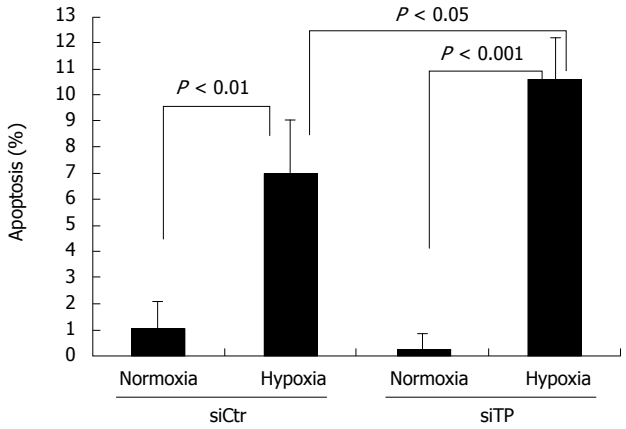

Figure 5 Knockdown of TP leads to increased cell death under hypoxic conditions. TP-deficient (siTP) or control (siCtr) cells were exposed to normoxic or hypoxic conditions for 48 h. Apoptosis was measured with the TUNEL assay.

< 0.01) or wild-type cells ($P < 0.01$) as shown in Figure 4G.

Reduced TP expression decreases resistance to hypoxia-induced apoptosis of KKU-M139

TP was reported to confer resistance to apoptosis induced by hypoxia. Under hypoxic conditions, the TP-deficient cells exhibited significantly more cell death than did the control cells ($P < 0.05$). Thus, TP seems to confer resistance to hypoxia-induced apoptosis in control cells. For both control and TP-deficient cells, the percent apoptosis under normoxic conditions was less than that under hypoxic conditions ($P < 0.01$ and $P < 0.001$, respectively). Anti-apoptotic activity of KKU-M139 under 48 h hypoxic conditions was suppressed by TP knockdown (Figure 5).

TP-siRNA decreases the sensitivity of KKU-M139 cells to 5-fluorouracil

5-fluorouracil is a commonly used chemotherapeutic drug for cholangiocarcinoma, and TP is needed for 5-fluorouracil activation. To determine to what extent TP contributes to the cytotoxic effect of 5-fluorouracil, cells were

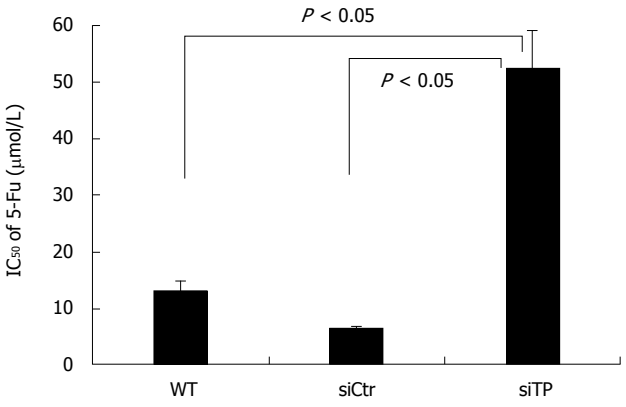

Figure 6 Effects of TP-siRNA on 5-fluorouracil (5-Fu) cytotoxicity of KKU-M139. KKU-M139 WT, control (siCtr), and TP-deficient (siTP) cells were incubated with various concentrations of 5-fluorouracil for 48 h. Sensitivity of the cells to 5-fluorouracil was then determined with a MTS cytotoxicity assay.

exposed to a range of concentrations of 5-fluorouracil in the presence or absence of siRNA against TP. The IC_{50} of control and wild-type cells were 6.4 ± 0.36 and 13 ± 1.70 μmol/L 5-fluorouracil, respectively. As expected, TP-deficient cells required 52.3 ± 6.8 μmol/L 5-fluorouracil, an 8.2-fold increase over that in control cells ($P < 0.05$), to inhibit cell proliferation by 50% (Figure 6).

DISCUSSION

We previously reported that 35 of 65 (53.8%) liver fluke-related cholangiocarcinoma cases exhibited TP amplification, suggesting that TP may contribute to the pathogenesis of cholangiocarcinoma[7]. Here, we report that TP confers resistance to apoptosis, induces migration of a cholangiocarcinoma-derived cell line, and mediates migration and tube formation of HUVECs. However, TP is essential for activation of 5-fluorouracil, a commonly used anti-cancer drug for treatment of cholangiocarcinoma. In fact, TP amplification and overexpression have been reported for various solid tumors that exhibited invasion, metastasis, angiogenesis, and poor prognosis, including cholangiocarcinoma[13-16,18,19]. In this study, transfection with TP-siRNA suppressed TP mRNA expression by approximately 87% and protein expression by 72% (Figure 1), indicating effective gene silencing. The population doubling time of TP-deficient cells was not significantly different from that of wild-type or control cells (Figure 2), suggesting that TP is not a pivotal factor for tumor cell proliferation in cholangiocarcinoma.

Increased TP expression has been shown to increase invasiveness of KB epidermoid carcinoma cells compared with control cells[20]. Migration is an important characteristic of metastatic cancer cells. TP-expressing KKU-M139 also exhibited greater migration than TP knockdown cells (Figure 3B). Nakajima *et al*[21] determined the molecular basis for induction of invasive activity by TP. They suggested that TP and 2-deoxy-D-ribose induces the expression, secretion, and activity of matrix metalloprotease-9 (MMP-9) that subsequently confers invasiveness on cancer cells, but the exact mechanism by which TP and one of its degradation products, 2-deoxy-D-ribose, enhance MMP-9-mediated invasive activity is not known. The expression level of TP was reported to significantly correlate with that of the invasion-related genes MMP-1, MMP-7, and MMP-9[22]. Taken together, these data indicate that TP enhances the invasion of tumor cells through the induction of invasion-related genes in cholangiocarcinoma.

The study by Hotchkiss *et al*[23] demonstrated that TP-expressing cells mediated HUVEC migration via the intracellular metabolism of thymidine by TP and the subsequent extracellular release of 2-deoxy-D-ribose, which formed a chemotactic gradient. Later, they proved that both TP and 2-deoxy-D-ribose stimulated HUVEC migration by increasing cell surface expression of the integrins $\alpha_5\beta_1$ and $\alpha_v\beta_3$ to form focal adhesions. Integrins bind to the ECM and directly activate focal adhesion kinase signaling pathways, mediating cell attachment and migration[24]. KKU-M139, which endogenously expresses TP, also strongly induced HUVEC migration, an early step in angiogenesis. Our study showed that TP-expressing KKU-M139 could stimulate the migration and formation of tube-like structures of HUVECs to a much greater degree than TP-silenced KKU-M139 (Figure 3A and 4). In addition, 2-deoxy-D-ribose can mediate an oxidative stress mechanism and upregulate other angiogenic factors[25]. Attracted endothelial cells proliferate upon stimulation by growth factors released from cancer cells and subsequently form new blood vessels. Suppression of TP-mediated migration and angiogenesis of HUVECs by TP-siRNA thus can be explained by the fact that TP and its product, 2-deoxy-D-ribose, could not exert their effect on cell migration and tube formation. Chemically synthesized TP inhibitor (TPI) has been demonstrated to suppress tumor growth by increasing the proportion of apoptotic cells and probably by inhibiting angiogenesis; TPI completely suppressed angiogenesis by TP-cDNA transfected KB cells[26]. 2-deoxy-L-ribose, the stereoisomer of 2-deoxy-D-ribose, is also a TPI, as shown by the ability of 2-deoxy-L-ribose to inhibit 2-deoxy-D-ribose-mediated angiogenesis and metastasis of tumor cells expressing TP[20,27]. Our study also demonstrated that TP-siRNA was able to act as TP suppressor or inhibitor.

Resistance to apoptosis is a key process in tumor formation. 2-deoxy-D-ribose was found to be involved in a hypoxia-induced apoptotic pathway. 2-deoxy-D-ribose inhibited hypoxia-induced phosphorylation of p38 mitogen-activated protein kinase but not c-jun NH_2-terminal kinase/stress-activated protein kinase in human leukemia HL-60 cells[28]. In addition, 2-deoxy-D-ribose and thymine partially prevented hypoxia-induced apoptosis[29]. 2-deoxy-D-ribose may be an important energy source under hypoxic conditions[30]. The ability of TP-siRNA to increase the proportion of apoptotic KKU-M139 cells (Figure 5) was most likely attributable to an inhibition of TP pathways, however, further studies are needed to de-

termine the exact role of TP in these tumor phenotypes.

The enzymatic activity of TP is also indispensable for the activation of prodrug 5'-deoxy-5-fluorouridine (5'-DFUR) to active 5-fluorouracil and fluorodeoxyuridine in tumors. The sensitivity of TP cDNA-transfected MCF-7 breast cancer cells to 5'-DFUR was increased approximately 20-fold compared to the parent cells or cells with control vector alone, and sensitivity to 5-fluorouracil was also somewhat increased[31]. The sensitivity of a TP-transfected SMMC-7721 hepatocellular carcinoma cell line to 5'-DFUR was also significantly enhanced; however, endothelial cell migration was also promoted at the same time[32]. We demonstrated that TP-siRNA was able to suppress TP expression *in vitro* and that this treatment impaired the therapeutic efficacy of 5-fluorouracil in KKU-M139 (Figure 6), indicating that TP enzyme activity is needed for 5-fluorouracil activation.

In conclusion, we found that TP plays a dual role in development and therapy of cholangiocarcinoma. TP confers apoptotic resistance and migration of a cholangiocarcinoma-derived cell line, and also induces migration and tube formation of HUVECs. On the other hand, TP is essential for the therapeutic efficacy of 5-fluorouracil chemotherapy. It may be useful to examine the expression level of TP in tumors of early stage cholangiocarcinoma patients to select those likely to respond well to 5-fluorouracil. However, most cholangiocarcinoma patients are diagnosed at a late stage, and there are several chemotherapeutic drugs of choice in addition to 5-fluorouracil for cholangiocarcinoma. Inhibition of TP activity may be helpful in decreasing tumor aggressiveness i.e. migration, angiogenesis and anti-apoptosis, and improving the poor prognosis of cancer patients who show high TP expression.

ACKNOWLEDGMENTS

The authors thank the Liver Fluke and Cholangiocarcinoma Research Center, Faculty of Medicine, Khon Kaen University, for contributing the cholangiocarcinoma cell lines in this study. We thank the Taiho Pharmaceutical Co., Ltd. (Japan) for the gift of mouse antibody against human TP.

COMMENTS

Background

Liver fluke-related cholangiocarcinoma is the most common hepatobiliary malignancy found in Northeast Thailand. Amplification of thymidine phosphorylase (TP) copy number was found in most cholangiocarcinoma patients suggesting that it has a significant role in tumor progression.

Research frontiers

TP catalyzes the reversible phosphorolysis of thymidine, deoxyuridine, and their analogs to their respective bases and 2-deoxyribose-1-phosphate which is then dephosphorylated to 2-deoxy-D-ribose. TP is abnormally expressed in certain cancers of the gastrointestinal tract including cholangiocarcinoma. However, how TP expression is upregulated in human tumors remains unclear. In this study, the authors investigated the roles of TP in liver fluke-related cholangiocarcinoma using RNA interference to suppress TP expression.

Innovations and breakthroughs

Suppression of TP not only reduces angiogenesis, resistance to apoptosis, and tumor migration but also diminishes chemosensitivity to 5-fluorouracil in cholangiocarcinoma.

Applications

Because of its significance in tumor aggressiveness and 5-fluorouracil sensitivity, TP expression may be used as a prognostic and predictive marker as well as targeted therapy in cholangiocarcinoma.

Peer review

The *TP* gene is aberrantly expressed in different human malignancies including cholangiocarcinoma. In the current manuscript submitted by Thanasai *et al*, the authors made several interesting observations. This article reports the effects of TP expression on tumor migration and 5-fluorouracil sensitivity in cholangiocarcinoma cells, as well as tumor cell-induced angiogenesis of endothelial cells *in vitro*.

REFERENCES

1 **Vatanasapt V**, Sriamporn S, Vatanasapt P. Cancer control in Thailand. *Jpn J Clin Oncol* 2002; **32** Suppl: S82-S91
2 **Uttaravichien T**, Bhudhisawasdi V, Pairojkul C, Pugkhem A. Intrahepatic cholangiocarcinoma in Thailand. *J Hepatobiliary Pancreat Surg* 1999; **6**: 128-135
3 **Horie S**, Endo K, Kawasaki H, Terada T. Overexpression of MDM2 protein in intrahepatic cholangiocarcinoma: relationship with p53 overexpression, Ki-67 labeling, and clinicopathological features. *Virchows Arch* 2000; **437**: 25-30
4 **Limpaiboon T**, Khaenam P, Chinnasri P, Soonklang M, Jearanaikoon P, Sripa B, Pairojkul C, Bhudhisawasdi V. Promoter hypermethylation is a major event of hMLH1 gene inactivation in liver fluke related cholangiocarcinoma. *Cancer Lett* 2005; **217**: 213-219
5 **Limpaiboon T**, Krissadarak K, Sripa B, Jearanaikoon P, Bhuhisawasdi V, Chau-in S, Romphruk A, Pairojkul C. Microsatellite alterations in liver fluke related cholangiocarcinoma are associated with poor prognosis. *Cancer Lett* 2002; **181**: 215-222
6 **Muenphon K**, Limpaiboon T, Jearanaikoon P, Pairojkul C, Sripa B, Bhudhisawasdi V. Amplification of chromosome 21q22.3 harboring trefoil factor family genes in liver fluke related cholangiocarcinoma is associated with poor prognosis. *World J Gastroenterol* 2006; **12**: 4143-4148
7 **Thanasai J**, Limpaiboon T, Jearanaikoon P, Bhudhisawasdi V, Khuntikeo N, Sripa B, Miwa M. Amplification of D22S283 as a favorable prognostic indicator in liver fluke related cholangiocarcinoma. *World J Gastroenterol* 2006; **12**: 4338-4344
8 **Brown NS**, Bicknell R. Thymidine phosphorylase, 2-deoxy-D-ribose and angiogenesis. *Biochem J* 1998; **334** (Pt 1): 1-8
9 **Akiyama S**, Furukawa T, Sumizawa T, Takebayashi Y, Nakajima Y, Shimaoka S, Haraguchi M. The role of thymidine phosphorylase, an angiogenic enzyme, in tumor progression. *Cancer Sci* 2004; **95**: 851-857
10 **Miyadera K**, Sumizawa T, Haraguchi M, Yoshida H, Konstanty W, Yamada Y, Akiyama S. Role of thymidine phosphorylase activity in the angiogenic effect of platelet derived endothelial cell growth factor/thymidine phosphorylase. *Cancer Res* 1995; **55**: 1687-1690
11 **Fujimoto K**, Hosotani R, Wada M, Lee JU, Koshiba T, Miyamoto Y, Tsuji S, Nakajima S, Doi R, Imamura M. Expression of two angiogenic factors, vascular endothelial growth factor and platelet-derived endothelial cell growth factor in human pancreatic cancer, and its relationship to angiogenesis. *Eur J Cancer* 1998; **34**: 1439-1447
12 **Saeki T**, Tanada M, Takashima S, Saeki H, Takiyama W, Nishimoto N, Moriwaki S. Correlation between expression of platelet-derived endothelial cell growth factor (thymidine phosphorylase) and microvessel density in early-stage human colon carcinomas. *Jpn J Clin Oncol* 1997; **27**: 227-230
13 **Giatromanolaki A**, Sivridis E, Simopoulos C, Polychronidis A, Gatter KC, Harris AL, Koukourakis MI. Thymidine phosphorylase expression in gallbladder adenocarcinomas. *Int J*

Surg Pathol 2002; **10**: 181-188
14 **Aishima S**, Taguchi K, Sugimachi K, Asayama Y, Nishi H, Shimada M, Sugimachi K, Tsuneyoshi M. The role of thymidine phosphorylase and thrombospondin-1 in angiogenesis and progression of intrahepatic cholangiocarcinoma. *Int J Surg Pathol* 2002; **10**: 47-56
15 **O'Brien TS**, Fox SB, Dickinson AJ, Turley H, Westwood M, Moghaddam A, Gatter KC, Bicknell R, Harris AL. Expression of the angiogenic factor thymidine phosphorylase/platelet-derived endothelial cell growth factor in primary bladder cancers. *Cancer Res* 1996; **56**: 4799-4804
16 **Hotta T**, Taniguchi K, Kobayashi Y, Johata K, Sahara M, Naka T, Watanabe T, Ochiai M, Tanimura H, Tsubota YT. Increased expression of thymidine phosphorylase in tumor tissue in proportion to TP-expression in primary normal tissue. *Oncol Rep* 2004; **12**: 539-541
17 **Jaffe EA**, Nachman RL, Becker CG, Minick CR. Culture of human endothelial cells derived from umbilical veins. Identification by morphologic and immunologic criteria. *J Clin Invest* 1973; **52**: 2745-2756
18 **Sato J**, Sata M, Nakamura H, Inoue S, Wada T, Takabatake N, Otake K, Tomoike H, Kubota I. Role of thymidine phosphorylase on invasiveness and metastasis in lung adenocarcinoma. *Int J Cancer* 2003; **106**: 863-870
19 **Miwa S**, Soeda J, Miyagawa S. Interrelationship of platelet-derived endothelial cell growth factor, liver macrophages, and tumor microvessel density in patients with cholangiocellular carcinoma. *Hepatogastroenterology* 2005; **52**: 1398-1402
20 **Uchimiya H**, Furukawa T, Okamoto M, Nakajima Y, Matsushita S, Ikeda R, Gotanda T, Haraguchi M, Sumizawa T, Ono M, Kuwano M, Kanzaki T, Akiyama S. Suppression of thymidine phosphorylase-mediated angiogenesis and tumor growth by 2-deoxy-L-ribose. *Cancer Res* 2002; **62**: 2834-2839
21 **Nakajima Y**, Haraguchi M, Furukawa T, Yamamoto M, Nakanishi H, Tatematsu M, Akiyama S. 2-Deoxy-L-ribose inhibits the invasion of thymidine phosphorylase-overexpressing tumors by suppressing matrix metalloproteinase-9. *Int J Cancer* 2006; **119**: 1710-1716
22 **Gotanda T**, Haraguchi M, Tachiwada T, Shinkura R, Koriyama C, Akiba S, Kawahara M, Nishiyama K, Sumizawa T, Furukawa T, Mimata H, Nomura Y, Akiyama S, Nakagawa M. Molecular basis for the involvement of thymidine phosphorylase in cancer invasion. *Int J Mol Med* 2006; **17**: 1085-1091
23 **Hotchkiss KA**, Ashton AW, Klein RS, Lenzi ML, Zhu GH, Schwartz EL. Mechanisms by which tumor cells and monocytes expressing the angiogenic factor thymidine phosphorylase mediate human endothelial cell migration. *Cancer Res* 2003; **63**: 527-533
24 **Hotchkiss KA**, Ashton AW, Schwartz EL. Thymidine phosphorylase and 2-deoxyribose stimulate human endothelial cell migration by specific activation of the integrins alpha 5 beta 1 and alpha V beta 3. *J Biol Chem* 2003; **278**: 19272-19279
25 **Sengupta S**, Sellers LA, Matheson HB, Fan TP. Thymidine phosphorylase induces angiogenesis in vivo and in vitro: an evaluation of possible mechanisms. *Br J Pharmacol* 2003; **139**: 219-231
26 **Matsushita S**, Nitanda T, Furukawa T, Sumizawa T, Tani A, Nishimoto K, Akiba S, Miyadera K, Fukushima M, Yamada Y, Yoshida H, Kanzaki T, Akiyama S. The effect of a thymidine phosphorylase inhibitor on angiogenesis and apoptosis in tumors. *Cancer Res* 1999; **59**: 1911-1916
27 **Nakajima Y**, Gotanda T, Uchimiya H, Furukawa T, Haraguchi M, Ikeda R, Sumizawa T, Yoshida H, Akiyama S. Inhibition of metastasis of tumor cells overexpressing thymidine phosphorylase by 2-deoxy-L-ribose. *Cancer Res* 2004; **64**: 1794-1801
28 **Ikeda R**, Che XF, Ushiyama M, Yamaguchi T, Okumura H, Nakajima Y, Takeda Y, Shibayama Y, Furukawa T, Yamamoto M, Haraguchi M, Sumizawa T, Yamada K, Akiyama S. 2-Deoxy-D-ribose inhibits hypoxia-induced apoptosis by suppressing the phosphorylation of p38 MAPK. *Biochem Biophys Res Commun* 2006; **342**: 280-285
29 **Kitazono M**, Takebayashi Y, Ishitsuka K, Takao S, Tani A, Furukawa T, Miyadera K, Yamada Y, Aikou T, Akiyama S. Prevention of hypoxia-induced apoptosis by the angiogenic factor thymidine phosphorylase. *Biochem Biophys Res Commun* 1998; **253**: 797-803
30 **Malhotra R**, Lin Z, Vincenz C, Brosius FC 3rd. Hypoxia induces apoptosis via two independent pathways in Jurkat cells: differential regulation by glucose. *Am J Physiol Cell Physiol* 2001; **281**: C1596-C1603
31 **Kim R**, Murakami S, Toge T. Effects of introduction of dThdPase cDNA on sensitivity to 5'-deoxy-5-fluorouridine and tumor angiogenesis. *Int J Oncol* 2003; **22**: 835-841
32 **Zhou J**, Xiao YS, Tang ZY, Fan J, Wu ZQ, Zhao Y, Xue Q, Shen ZZ, Liu YK, Ye SL. Transfection of thymidine phosphorylase cDNA to human hepatocellular carcinoma cells enhances sensitivity to fluoropyrimidine but augments endothelial cell migration. *J Cancer Res Clin Oncol* 2005; **131**: 547-551

S- Editor Wang YR **L- Editor** Cant MR **E- Editor** Ma WH

World Journal of Gastroenterology

Online Submissions: http://www.wjgnet.com/1007-9327office
wjg@wjgnet.com
doi:10.3748/wjg.v16.i13.1639

World J Gastroenterol 2010 April 7; 16(13): 1639-1643
ISSN 1007-9327 (print)

BRIEF ARTICLE

Hepatic osteodystrophy and liver cirrhosis

Vedat Goral, Mehmet Simsek, Nuriye Mete

Vedat Goral, Mehmet Simsek, Department of Gastroenterology, Dicle University School of Medicine, 21280 Diyarbakir, Turkey
Nuriye Mete, Department of Biochemistry, Dicle University School of Medicine, 21280 Diyarbakir, Turkey
Author contributions: The main contributor was Goral V; Simsek M followed-up the patients; Mete N performed the laboratory studies.
Correspondence to: Dr. Vedat Goral, Professor, Department of Gastroenterology, Dicle University School of Medicine, 21280 Diyarbakir, Turkey. vegoral@hotmail.com
Telephone: +90-412-2488443 Fax: +90-412-2488443
Received: January 4, 2010 Revised: January 28, 2010
Accepted: February 4, 2010
Published online: April 7, 2010

Abstract

AIM: To investigate the correlation between hepatic osteodystrophy and osteoporosis in patients with liver cirrhosis.

METHODS: Bone mineral density of the patients (n = 55) and that of the control group (n = 30) were measured by dual-energy X-ray absorptiometry. All the women in the study were premenopausal. Deoxypyridinoline, pyridinoline and urinary Ca^{2+} were measured as bone destruction markers, while alkaline phosphatase (ALP), osteocalcin and insulin-like growth factor-1 (IGF-1) were measured as bone formation markers. Furthermore, interleukin-1 (IL-1), IL-6, tumor necrosis factor α (TNF-α), vitamin D3, direct bilirubin, albumin, cortisol and parathyroid hormone (PTH) levels were measured. The independent Student t test and χ^2 test were employed in comparing both groups, and the Pearson correlation test was used to determine associations.

RESULTS: Comparing cirrhosis and control groups, lumbar total T-score (-1.6 ± 1.2 g/cm^2 *vs* -0.25 ± 1.3 g/cm^2, P < 0.001), lumbar total Z-score (-1.2 ± 1.23 g/cm^2 *vs* -0.6 ± 1.3 g/cm^2, P < 0.001), total femur T-score (-0.05 ± 1 g/cm^2 *vs* -0.6 ± 0.9 g/cm^2, P = 0.003) and total femur Z-score (-0.08 ± 1.5 g/cm^2 *vs* 0.7 ± 0.9 g/cm^2, P = 0.003) showed significantly lower values in the cirrhosis group. Blood ALP level (109.2 ± 57 U/L *vs* 62.6 ± 32.5 U/L, P < 0.001), IL-6 level (27.9 ± 51.6 pg/mL *vs* 3.3 ± 3.1 pg/mL, P = 0.01), TNF-α level (42.6 ± 33.2 pg/mL *vs* 25.3 ± 12.3 pg/mL, P = 0.007) and direct bilirubin level (0.9 ± 0.7 mg/dL *vs* 0.3 ± 0.2 mg/dL, P < 0.001) were significantly higher in the cirrhosis group. IGF-1 level (47.7 ± 26.2 ng/mL *vs* 143.4 ± 53.2 ng/mL, P < 0.001), osteocalcin level (1.05 ± 2.5 ng/mL *vs* 7.0 ± 13 ng/mL, P = 0.002) and 24 h urinary Ca^{2+} (169.6 ± 227.2 mg/dL *vs* 287 ± 168.6 mg/dL, P = 0.003) were significantly lower in the cirrhosis group. Urinary deoxypyridinoline/creatinine (9.4 ± 9.9 pmol/μmol *vs* 8.1 ± 5.3 pmol/μmol, P = 0.51), urinary pyridinoline/creatinine (51.3 ± 66.6 pmol/μmol *vs* 29 ± 25.8 pmol/μmol, P = 0.08), blood IL-1 level (3.4 ± 8.8 pg/mL *vs* 1.6 ± 3.5 pg/mL, P = 0.29), vitamin D3 level (18.6 ± 13.3 μg/L *vs* 18.4 ± 8.9 μg/L, P = 0.95), cortisol level (11.1 ± 4.8 μg/dL *vs* 12.6 ± 4.3 μg/dL, P = 0.15) and PTH level (42.7 ± 38 μg/dL *vs* 34.8 ± 10.9 μg/dL, P = 0.27) were not significantly different.

CONCLUSION: Hepatic osteodystrophy is an important complication encountered in patients with liver cirrhosis and all patients should be monitored for hepatic osteodystrophy.

Key words: Liver cirrhosis; Osteoporosis; Hepatic osteodystrophy

Peer reviewers: Evangelos Kalaitzakis, MD, PhD, Associate Professor, Institute of Internal Medicine, Sahlgrenska Academy, University of Gothenburg, Gothenburg 41345, Sweden; Jen-Hwey Chiu, MD, PhD, Professor, Division of General Surgery, Department of Surgery, Taipei-Veterans General Hospital, Taipei 112, Taiwan, China

Goral V, Simsek M, Mete N. Hepatic osteodystrophy and liver cirrhosis. *World J Gastroenterol* 2010; 16(13): 1639-1643 Available from: URL: http://www.wjgnet.com/1007-9327/full/v16/i13/1639.htm DOI: http://dx.doi.org/10.3748/wjg.v16.i13.1639

INTRODUCTION

Liver cirrhosis develops when the liver parenchyma takes a nodular form as a result of fibrosis arising from delayed wound-healing in chronic liver damage. Osteoporosis, characterized by a reduced bone mass and an increase in bone fracturability due to distortion of bone tissue microstructure, is a multifactorial disease and the most common bone disease. Dual energy X-ray absorptiometry is a method of measuring bone mineral density which has been become the standard in many centers and is a highly accurate X-ray method.

It is known that liver diseases may lead to bone disease[1]. Although chronic liver disease is associated with a broad spectrum of bone diseases, the most common type of hepatic osteodystrophy is osteoporosis. If an increase in bone resorption exceeds bone formation, or decreased bone formation is present together with normal bone destruction, then in advanced cases, bone mass will decrease and the risk of fracture will increase[2]. Increased cytokine levels in chronic liver disease and liver cirrhosis contribute to the development of hepatic osteodystrophy. Levels of interleukin-1 (IL-1), IL-6 and tumor necrosis factor α (TNF-α) are higher in patients with alcoholic hepatitis and liver cirrhosis than gender- and age-matched controls[3]. It is thought that a reduction in growth factors, such as insulin, or an excess of growth inhibitors such, as bilirubin, in patients with cirrhosis causes osteoblastic function disorder[4]. Low bone formation and a high resorption rate in chronic liver disease patients results in osteoporosis. It has been shown that serum osteocalcin decreases depending on reduction of osteoblast function. A decrease in serum osteocalcin levels and an increase in deoxypyridinoline (DPD) level can be explained by lower bone turnover[4-7].

Osteopenia is more frequent than osteomalacia in the primary biliary cirrhosis (PBC)-associated metabolic bone diseases in patients in North America[8]. Osteoclastic activity may be increased in premenopausal PBC women. In these people there is a disorder in the formation of new bone. Calcium and vitamin D metabolism is often normal in anicteric PBC patients[8]. Osteoporosis is a common complication of cholestatic liver disease. In primary sclerosing cholangitis (PSC), the cause of osteoporosis is multifactorial. The pathophysiological mechanism of osteoporosis has not been identified clearly yet[9,10].

The aim of this study was to establish the osteoporosis risk in liver cirrhosis, and to investigate the role of IL-1, IL-6, TNF-α, osteocalcin, insulin-like growth factor-1 (IGF-1), alkaline phosphatase (ALP), parathyroid hormone (PTH), cortisol and 25(OH)D3 in bone metabolism, and to investigate urinary DPD, pyridinoline and Ca^{2+} levels, which are biochemical markers of bone cycling.

MATERIALS AND METHODS

Our study comprised a cohort of 85 patients, 55 men and 30 premenopausal women (older than 18 years) with liver cirrhosis, and a control group (15 men and 15 women). The etiology was 37 hepatitis B, 10 cryptogenic, 2 PBC, 2 cardiac, 2 hepatitis C and 2 Wilson diseases in the patients with liver cirrhosis. The diagnosis of liver cirrhosis was done by biochemical and serological tests, abdominal ultrasonography, upper gastrointestinal endoscopy. Liver biopsy could not performed because of ascites. Twenty-four patients had Child-Pugh stage C (score 11.2), 17 patients had Child-Pugh stage B (score 7.9), 14 patients had Child-Pugh stage A (score 5.6) cirrhosis. Previous diseases, fracture anamnesis, smoking, using of alcohol or coffee were investigated in all cases included in the study. There was no history of diabetes mellitus, hypertension, goitre, early menopause, surgical menopause, hyperparathyroidism or Cushing's syndrome in any of the study subjects, and none. took any drug associated with increased risk of osteoporosis (anticoagulant, oral contraceptive, steroid, thiazide, diuretics, *etc.*).

Height, weight and body mass indexes (BMI) of all cases were calculated. Blood samples were analyzed in the laboratory department. Urea, creatinine, aspartate aminotransferase (AST), alanine aminotransferase (ALT), ALP, gamma glutamyl transpeptidase, Ca^{2+}, P^{+}, bilirubin and albumin levels were measured on an Abbott Aeroset device. Plasma cortisol, thyroid stimulating hormone, free T4, parathyroid hormone (PTH) and alpha-fetoprotein (AFP) levels were determined on a Modulator E 170 autoanalysator by electrochemiluminescence method. IGF-1 was measured on an Immulite 2000 autoanalyser, cytokines (IL-1, IL-6 and TNF-α) on an Immulite 1000 autoanalyser and vitamin D3 on an Agilent 1100 autoanalyser by HPLC.

Hydroxychloric acid was added to 24 h urine for determination of pyridinoline and DPD, markers of bone destruction, by HPLC. Calcium was also determined in 24 h urine. *Clearance* of creatinine was calculated as (24 h urine volume × urine creatinine)/(plasma creatinine × 1440). Bone mineral density measurements were conducted in the triangle of L1-L4 vertebrae and femoral neck, trochanteric major, intertrochanteric region. The results were calculated as g/cm^2. T and Z scores for all subjects were analyzed.

Statistical analysis

Statistical assessment was carried out by SPSS 13.0. The independent Student *t* test and χ^2 test were used for comparing the groups. The Pearson correlation test was used to determine associations.

RESULTS

Seventeen female and 38 male patients with liver cirrhosis and 15 female and 15 male controls were included in the study. There were no significant differences in BMI and gender between the patients and the controls. The mean age of the patients was significantly higher than in the control group (mean, 44.8 years *vs* 34.8 years, Table 1). All the women included in the study were premenopausal, and none took alcohol or coffee. There was no fracture anamnesis. T- and Z-scores were significantly lower in

the cirrhosis group than in controls when bone mineral densities were compared (Table 1). IL-6 and TNF-α were significantly higher in the liver cirrhosis group, but there was no significant difference in IL-1 (Table 1). ALP levels were significantly higher in the cirrhosis group, but IGF-1 and osteocalcin were significantly lower compared to the control group (Table 1). There were no significant differences in DPD/creatinine and pyridinoline/creatinine levels, nor in blood cortisol, PTH and vitamin D levels (Table 1). There were no significant differences in sedimentation rate, AFP and C-reactive protein levels. Prothrombin time and direct biluribin were significantly higher and albumin level significantly lower in the cirrhosis group (Table 1).

Table 1 Clinical features and laboratory test results of the liver cirrhosis and control groups

	Cirrhosis (n = 55)	Control (n = 30)	P-value
Lumbar total T-score (g/cm^2)	-1.6 ± 1.2	-0.25 ± 1.3	< 0.001
Lumbar total Z-score (g/cm^2)	-1.2 ± 1.2	-0.6 ± 1.3	< 0.001
Total femur T-score (g/cm^2)	-0.05 ± 1	0.6 ± 0.9	0.003
Total femur Z-score (g/cm^2)	-0.08 ± 1.5	0.7 ± 0.9	0.003
Age (yr)	44.8 ± 12.9	34.8 ± 8.2	< 0.001
BMI (kg/m^2)	25.5 ± 4.3	25.5 ± 3.7	0.970
IL-1 pg/mL	3.4 ± 8.8	1.6 ± 3.5	0.290
IL-6 pg/mL	27.9 ± 51.6	3.3 ± 3.1	0.010
TNF-α pg/mL	42.6 ± 33.2	25.3 ± 12.3	0.007
AFP (ng/mL)	2.6 ± 16.9	2.6 ± 1.1	0.100
Direct biluribin (mg/dL)	0.3 ± 0.2	0.9 ± 0.7	< 0.001
CRP (mg/L)	5.8 ± 5.9	5.4 ± 11.3	0.800
Osteocalcin (ng/mL)	1.05 ± 2.5	7.0 ± 13	0.002
IGF-1 (ng/mL)	47.7 ± 26.2	143.4 ± 53.2	< 0.001
ALP (IU/L)	109.2 ± 57	62.6 ± 32.5	< 0.001
24 h urinary Ca^{2+} (mg/dL)	169.6 ± 227.2	287 ± 168.6	0.003
Deoxypyridinoline/creatinine (pmol/μmol)	9.4 ± 9.9	8.1 ± 5.3	0.510
pyridinoline/creatinine (pmol/μmol)	51.3 ± 66.6	29 ± 25.8	0.080
Cortisol level μg/dL	11.1 ± 4.8	12.6 ± 4.3	0.150
PTH level μg/dL	42.7 ± 38	34.8 ± 10.9	0.270
Vit D3 level μg/L	18.6 ± 13.3	18.4 ± 8.9	0.950
Albumin (g/dL)	2.5 ± 0.5	4 ± 0.4	0.001
Prothrombin time (s)	17.1 ± 5.2	11.7 ± 1.7	< 0.001
Sedimentation rate (h)	18.8 ± 10.6	11.6 ± 9.6	0.030

BMI: Body mass index; IL: Interleukin; TNF: Tumor necrosis factor; AFP: α-fetoprotein; CRP: C-reactive protein; ALP: Alkaline phosphatase; IGF: Insulin-like growth factor.

DISCUSSION

Hepatic osteodystrophy is an important health problem encountered in patients with liver cirrhosis[1,2]. The reported prevalence of osteoporosis among patients with liver cirrhosis ranges from 20% to 50% depending on patient selection and diagnostic criteria, and the prevalence of fracture ranges from 5% to 20%[9]. In the present study, osteoporosis was found in 37% of patients in accordance with the literature. The fact that all the female patients were premenopausal allowed reliable examination of the effect of liver cirrhosis on osteoporosis. Diamond *et al*[5] found in their 2 separate studies that the prevalence of osteoporosis was 30%-48% in patients with chronic liver disease of different etiologies.

Hepatic osteodystrophy is defined as bone disease associated with chronic liver disease[5,6,11,12]. The mechanism of hepatic osteodystrophy encountered in liver cirrhosis patients has not been clearly determined. Osteoporosis has been reported in patients with cholestatic liver, chronic viral hepatitis, alcoholic liver, hemochromatosis and benign and malignant tumors of the liver[13]. In our study, the prevalence of osteoporosis was determined as 37% from the T-scores in lumbar vertebrae. Lumbar total BMD T-score and Z-score in patients with cirrhosis were significantly lower than those of the control group ($P = 0.003$).

IL-1, IL-6 and TNF-α cytokines are the cytokines most associated with postmenopausal osteoporosis[14]. These cytokines can affect bone metabolism through either increasing osteoclast formation or increasing osteoclast activity. In addition, the cytokines can block osteoblast function directly and increase formation of other cytokines[9]. IL-1, IL-6 and TNF-α levels were higher in patients with alcoholic hepatitis or liver cirrhosis compared to gender- and age-matched controls[13]. The incidence and severity of osteoporosis is increased in patients with chronic hepatitis or intestinal diseases. Inadequate nutrition, use of steroids, and cytokines have roles in this outcome. Pfeilschifter *et al*[15] concluded that these cytokines were strong resorptive agents. In the present study, IL-1, IL-6 and TNF-α levels were higher than those of the control group. It is thought that increased IL-6 and TNF-α levels were effective in promoting hepatic osteodystrophy in our patients with liver cirrhosis.

Menon *et al*[16] have shown that there is a positive correlation between serum bilirubin level and bone destruction ratio. In the present study, increased serum bilirubin levels in patients with osteoporosis concur with studies in the literature. Gillberg *et al*[17] have established that idiopathic osteoporosis exists together with a reduced IGF-1 level. It was thought that reducing growth factors, such as insulin, or increasing bilirubin in cirrhosis patients induces an osteoblastic function disorder[4]. In our study, we found significantly lower IGF-1 levels in the liver cirrhosis group ($P < 0.001$), and direct bilirubin levels were significantly higher ($P < 0.001$).

In recent studies it has been reported that there is no abnormality in Ca^{2+}, phosphorus and vitamin D metabolism in patients with PBS, which was unexpected[18]. However in some studies vitamin D was lower. In our study, in accordance with the literature, vitamin D levels were not higher than the healthy group suggesting that vitamin D metabolism was normal in the liver cirrhosis group.

In another study conducted by Karan *et al*[19], 24 patients with liver cirrhosis developing after hepatitis were compared with 22 healthy controls, and osteocalcin levels were non-significantly lower in the patient group. In the study of Capra *et al*[20], comprising 20 people with cirrhosis and 22 healthy controls, osteocalcin levels in the cirrhosis group were lower than in the control group,

whereas plasma calcitonin levels in the cirrhosis group were higher than in the control group[20].

In most studies, ALP levels in chronic liver patients were elevated, including the study of Karan *et al*[19]. It is necessary to measure enzyme function of osteoblasts (bone ALP) for diagnosis of osteoporosis. If liver-gallbladder disorders can be excluded, serum total ALP levels only can be used as an index of bone formation. In contrast, bone specific isoenzyme of ALP (BAP) is inside the osteoblast membrane and if osteoblast activation exists it is excreted into the circulation. Thus, measurement of BAP is more accurate and is affected less by non-bone pathologies.

Low bone formation and a high resorption ratio in chronic liver patients results in osteoporosis. It has been shown that serum osteocalcin decreases with reduction in osteoblast function. A reduction in serum osteocalcin and an increase in urine DPD can be explained by lower bone turnover[4-7]. Monegal *et al*[21] have established that serum osteocalcin in patients with PBC is low. They emphasized that this was associates with a reduction in bone formation. Guañabens *et al*[22] have found that the volume of bone decreases because of a reduction in bone formation in PBC.

Osteoclastic activity may be increased in premenopausal women with PBC. In these patients there is a disorder in formation of new bone. Calcium and vitamin D metabolism in anicteric patients with PBC is often normal[9]. Osteoporosis is a common complication of cholestatic liver disease. The causes of osteoporosis in PSC are multifactorial. The pathophysiological mechanism of osteoporosis has not been identified clearly yet[10].

In the present study, we investigated osteocalcin and ALP as measures of bone formation. Osteocalcin levels were lower than those of the control group ($P = 0.002$), whereas ALP levels were higher ($P < 0.001$). Lower osteocalcin levels exhibit lower osteoblastic activity. A higher ALP level, which is a bone formation marker, can be associated with cholestasis, while lower serum osteocalcin levels may be associated with a reduction in bone formation. Urine 24 h calcium levels in the liver cirrhosis patients were significantly reduced, and could be associated with inadequate nutrition in these patients, or might indicate that osteoclastic activity did not increase, or even decrease, to reduce bone formation.

PTH stimulates both bone resorption and bone formation, but it is known that if it remains at a high level, osteoclasts are stimulated, whereas osteoblasts are inhibited. Some authors have been reported that hepatocellular dysfunction increases serum PTH levels, while some authors reported no change or even a reduction[23]. In addition to the studies reporting that serum PTH levels in liver cirrhosis patients are higher than that of controls, there exists some studies indicating that the PTH level is lower[23]. In the present study, although there was an increase in PTH levels in the liver cirrhosis group, it was not statistically significant.

Urinary DPD/creatinine and pyridinoline/creatinine level were non-significantly increased in the cirrhosis patients. This finding suggests there may be more bone resorption than normal. Both insulin and IGF-1 have an influence on osteoblast function and contribute to bone formation. IGF-1 levels in the cirrhosis group were significantly lower in the study. This implied that IGF-1 reduction is an important factor in progression to hepatic osteodystrophy. There is an increase in the urinary hydroxyproline/creatinine ratio especially in advanced stages of liver cirrhosis[20]. The urinary deoxypyroline/creatinine ratio and serum bone ALP levels increase in osteoporosis developing from hepatitis C virus-associated liver cirrhosis[4]. Increased activity of the osteoprotegerin system can be associated with increased TNF-α and IL-6 levels[24,25].

In conclusion, metabolic bone diseases are important complications of chronic liver diseases. The bone mineral density of patients with liver cirrhosis is reduced. A decreased osteocalcin level in patients with liver cirrhosis means reduced bone formation, which, in turn, may contribute to development of osteoporosis. Increased TNF-α and IL-6 levels in patients with cirrhosis may contribute to the development of hepatic osteodystrophy. Decreased IGF-1 levels in patients with liver cirrhosis may contribute to the development of osteoporosis. Early scanning for osteoporosis in patients with liver cirrhosis will reduce the risk of morbidity and mortality. As advanced hepatic osteodystrophy is difficult to treat and adversely affects both the quality of life and the long-term prognosis of patients with chronic liver disease, special care is required in order to prevent the development of clinical bone disease in individuals with advanced hepatic disease.

COMMENTS

Background

Liver cirrhosis develops when the liver parenchyma takes a nodular form as a result of fibrosis arising from delayed wound-healing in chronic liver damage. Osteoporosis, characterized by a reduced bone mass and an increase in bone fracturability due to distortion of bone tissue microstructure, is a multifactorial disease and the most common bone disease. In North America, osteopenia is more frequent than osteomalacia in patients with metabolic bone diseases associated with primary biliary cirrhosis. In primary sclerosing cholangitis, the causes of osteoporosis are multifactorial. The pathophysiological mechanism of osteoporosis has not been identified clearly yet.

Research frontiers

Metabolic bone diseases are important complications of chronic liver diseases. Increased cytokine levels in chronic liver disease and in cirrhosis contributes to the development of hepatic osteodystrophy. This study compared bone mineral density and cytokines in patients with liver cirrhosis and controls.

Innovations and breakthroughs

Cytokines have a role in hepatic osteodystrophy. Screening and treatment of symptoms are very useful for patients with liver cirrhosis.

Applications

Early diagnosis of osteoporosis by scanning in patients with liver cirrhosis will reduce the risk of morbidity and mortality. Therefore life quality will be better in patients with liver cirrhosis.

Peer review

The manuscript investigated the correlation between hepatic osteodystrophy and osteoporosis by comparing 55 patients with liver cirrhosis and 30 healthy controls and there are several comments and suggestions. This is an interesting study as the pathogenesis of hepatic osteodystrophy has not been studied extensively.

REFERENCES

1 **Van den Bogaerde JB**, Beynon HLC. Musculoskeletal problems in liver disease. In: McIntyre B, editor. Oxford textbook of hepatology. 2nd ed. Oxford: OUP, 1998: 54, 842-845
2 **Chen CC**, Wang SS, Jeng FS, Lee SD. Metabolic bone disease of liver cirrhosis: is it parallel to the clinical severity of cirrhosis? *J Gastroenterol Hepatol* 1996; **11**: 417-421
3 **Khoruts A**, Stahnke L, McClain CJ, Logan G, Allen JI. Circulating tumor necrosis factor, interleukin-1 and interleukin-6 concentrations in chronic alcoholic patients. *Hepatology* 1991; **13**: 267-276
4 **Gallego-Rojo FJ**, Gonzalez-Calvin JL, Muñoz-Torres M, Mundi JL, Fernandez-Perez R, Rodrigo-Moreno D. Bone mineral density, serum insulin-like growth factor I, and bone turnover markers in viral cirrhosis. *Hepatology* 1998; **28**: 695-699
5 **Diamond TH**, Stiel D, Lunzer M, McDowall D, Eckstein RP, Posen S. Hepatic osteodystrophy. Static and dynamic bone histomorphometry and serum bone Gla-protein in 80 patients with chronic liver disease. *Gastroenterology* 1989; **96**: 213-221
6 **Bonkovsky HL**, Hawkins M, Steinberg K, Hersh T, Galambos JT, Henderson JM, Millikan WJ, Galloway JR. Prevalence and prediction of osteopenia in chronic liver disease. *Hepatology* 1990; **12**: 273-280
7 **Hodgson SF**, Dickson ER, Wahner HW, Johnson KA, Mann KG, Riggs BL. Bone loss and reduced osteoblast function in primary biliary cirrhosis. *Ann Intern Med* 1985; **103**: 855-860
8 **Parés A**, Guañabens N. Osteoporosis in primary biliary cirrhosis: pathogenesis and treatment. *Clin Liver Dis* 2008; **12**: 407-424; x
9 **Raisz LG**. Pathogenesis of osteoporosis: concepts, conflicts, and prospects. *J Clin Invest* 2005; **115**: 3318-3325
10 **Rouillard S**, Lane NE. Hepatic osteodystrophy. *Hepatology* 2001; **33**: 301-307
11 **Idilman R**, de Maria N, Uzunalimoglu O, van Thiel DH. Hepatic osteodystrophy: a review. *Hepatogastroenterology* 1997; **44**: 574-581
12 **Dempster DW**, Lindsay R. Pathogenesis of osteoporosis. *Lancet* 1993; **341**: 797-801
13 **Chen CC**, Wang SS, Jeng FS, Lee SD. Metabolic bone disease of liver cirrhosis: is it parallel to the clinical severity of cirrhosis? *J Gastroenterol Hepatol* 1996; **11**: 417-421
14 **Ambrogini E**, Toraldo G, Marcocci C. Post-menopausal osteoporosis: is it an autoimmune disease? *J Endocrinol Invest* 2005; **28**: 43-47
15 **Pfeilschifter J**. Role of cytokines in postmenopausal bone loss. *Curr Osteoporos Rep* 2003; **1**: 53-58
16 **Menon KV**, Angulo P, Weston S, Dickson ER, Lindor KD. Bone disease in primary biliary cirrhosis: independent indicators and rate of progression. *J Hepatol* 2001; **35**: 316-323
17 **Gillberg P**, Olofsson H, Mallmin H, Blum WF, Ljunghall S, Nilsson AG. Bone mineral density in femoral neck is positively correlated to circulating insulin-like growth factor (IGF)-I and IGF-binding protein (IGFBP)-3 in Swedish men. *Calcif Tissue Int* 2002; **70**: 22-29
18 **Hodgson SF**, Dickson ER, Eastell R, Eriksen EF, Bryant SC, Riggs BL. Rates of cancellous bone remodeling and turnover in osteopenia associated with primary biliary cirrhosis. *Bone* 1993; **14**: 819-827
19 **Karan MA**, Erten N, Tascioglu C, Karan A, Sindel D, Dilsen G. Osteodystrophy in posthepatitic cirrhosis. *Yonsei Med J* 2001; **42**: 547-552
20 **Capra F**, Casaril M, Gabrielli GB, Stanzial A, Ferrari S, Gandini G, Falezza G, Corrocher R. Plasma osteocalcin levels in liver cirrhosis. *Ital J Gastroenterol* 1991; **23**: 124-127
21 **Monegal A**, Navasa M, Guañabens N, Peris P, Pons F, Martinez de Osaba MJ, Rimola A, Rodés J, Muñoz-Gómez J. Osteoporosis and bone mineral metabolism disorders in cirrhotic patients referred for orthotopic liver transplantation. *Calcif Tissue Int* 1997; **60**: 148-154
22 **Guañabens N**, Parés A, Mariñoso L, Brancós MA, Piera C, Serrano S, Rivera F, Rodés J. Factors influencing the development of metabolic bone disease in primary biliary cirrhosis. *Am J Gastroenterol* 1990; **85**: 1356-1362
23 **Kirch W**, Höfig M, Ledendecker T, Schmidt-Gayk H. Parathyroid hormone and cirrhosis of the liver. *J Clin Endocrinol Metab* 1990; **71**: 1561-1566
24 **Gallego-Rojo FJ**, Gonzalez-Calvin JL, Muñoz-Torres M, Mundi JL, Fernandez-Perez R, Rodrigo-Moreno D. Bone mineral density, serum insulin-like growth factor I, and bone turnover markers in viral cirrhosis. *Hepatology* 1998; **28**: 695-699
25 **Nagano T**, Yamamoto K, Matsumoto S, Okamoto R, Tagashira M, Ibuki N, Matsumura S, Yabushita K, Okano N, Tsuji T. Cytokine profile in the liver of primary biliary cirrhosis. *J Clin Immunol* 1999; **19**: 422-427

S- Editor Wang JL **L- Editor** Cant MR **E- Editor** Ma WH

World Journal of Gastroenterology

Online Submissions: http://www.wjgnet.com/1007-9327office
wjg@wjgnet.com
doi:10.3748/wjg.v16.i13.1644

World J Gastroenterol 2010 April 7; 16(13): 1644-1648
ISSN 1007-9327 (print)

BRIEF ARTICLE

Clinicopathological significance and prognostic value of LRP16 expression in colorectal carcinoma

Hong-Qing Xi, Po Zhao, Wei-Dong Han

Hong-Qing Xi, Po Zhao, Department of Pathology, Chinese People's Liberation Army General Hospital, Beijing 100853, China
Wei-Dong Han, Department of Molecular Biology, Institute of Basic Medicine, Chinese People's Liberation Army General Hospital, Beijing 100853, China
Author contributions: Xi HQ performed the research and wrote the manuscript; Zhao P designed the research and was also involved in editing the manuscript; Han WD provided some reagents and analytical tools.
Supported by (in part) Grant from the Ministry of Science and Technology of China, No. 2010 CB912802
Correspondence to: Dr. Po Zhao, Department of Pathology, Chinese People's Liberation Army General Hospital, 28 Fuxing Road, Beijing 100853, China. zhaopo@301hospital.com.cn
Telephone: +86-10-66937736 Fax: +86-10-68181689
Received: December 28, 2009 Revised: February 1, 2010
Accepted: February 8, 2010
Published online: April 7, 2010

Abstract

AIM: To explore the expression of leukemia related protein 16 (LRP16) in colorectal carcinoma, and analyze its correlation with clinicopathologic features and prognosis.

METHODS: Immunohistochemistry for LRP16 was performed in 201 cases of colorectal carcinoma and 60 cases of distal normal mucosa. Medical records were reviewed and clinicopathological analysis was performed.

RESULTS: LRP16 expression was detected in 117 of 201 cases of the colorectal carcinoma and in 21 cases of 60 distal normal mucosa. The expression of LRP16 in carcinoma was significantly higher than that in normal mucosa (χ^2 = 9.999, P = 0.002). LRP16 protein expression was found in 43.3% (52/120) of carcinoma at stage Ⅰ and Ⅱ, and 80.2% (65/81) of carcinoma at stage Ⅲ and Ⅳ (χ^2 =27.088, P = 0.001). Correlation between LRP16 expression and clinicopathological factors was significant in differentiation (P = 0.010), tumor size (P = 0.001), infiltrative depth (P = 0.000) and distant metastasis (P = 0.027). The difference of median survival time between cancer patients with LRP16 expression (38.0 mo) and those without was statistically significant (105.0 mo, Log rank = 41.455, P = 0.001). The multivariate survival analysis revealed that LRP16 expression was correlated significantly (Cox's regression: P = 0.001, relative risk = 2.082) with shortened survival in the patients with colorectal cancer.

CONCLUSION: The expression of LRP16 is related to the degree of differentiation, invasiveness, metastasis and prognosis of colorectal carcinoma.

Key words: Colorectal neoplasms; Immunohistochemistry; Leukemia related protein 16; Prognosis; Clinicopathology

Peer reviewers: Dr. John B Schofield, MB, BS, MRCP, FRCP, Department of Cellular Pathology, Preston Hall, Maidstone, Kent, ME20 7NH, United Kingdom; Dr. Lucia Ricci Vitiani, Department of Hematology, Oncology and Molecular Medicine, Istituto Superiore di Sanità, Viale Regina Elena, 299, Rome 00161, Italy

Xi HQ, Zhao P, Han WD. Clinicopathological significance and prognostic value of LRP16 expression in colorectal carcinoma. *World J Gastroenterol* 2010; 16(13): 1644-1648 Available from: URL: http://www.wjgnet.com/1007-9327/full/v16/i13/1644.htm DOI: http://dx.doi.org/10.3748/wjg.v16.i13.1644

INTRODUCTION

Leukemia related protein 16 (LRP16), which was originally recognized and isolated from human lymphocytes in 1999, was identified as an estrogen-responsive gene. It

localizes on chromosome 11q12.1 and encodes nuclear factor[1-5]. It expresses in testicle, ovaries, mucosa of colon, prostate, small intestine, spleen, thymus[2,3] and gastric carcinoma[6]. LRP16 is also an estrogen receptor α (ERα) coactivator. Its expression level is strongly dependent on the estrogen activities. It is involved in estrogen signaling pathway and can strengthen the ERα responsive gene activation.

Colorectal carcinoma is a major cause of cancer-related morbidity and mortality. In the Western countries, it is the second leading cause of death from cancer[7]. The incidence of colorectal cancer has increased in China recently, therefore, some new molecular markers are necessary to raise the efficiency of tumor diagnosis and to predict prognosis of the patients or even for therapeutic application. It has been reported that ER is identified in colorectal cancer[8-10]. However, no immunohistochemical and clinicopathological studies of LRP16 have been performed in colorectal carcinoma. Here, we investigated the expression of LRP16 in colorectal cancer specimens and normal mucosa by an immunohistochemistry (IHC)-based technique and analyzed the relationship between LRP16 expression and the clinicopathological features of Chinese patients with colorectal cancer.

MATERIALS AND METHODS

Patients and specimens

A series of 201 consecutive colorectal carcinoma patients who were treated surgically in Chinese People's Liberation Army General Hospital (Beijing, China) between August 1999 and September 2003 and 60 cases with distal normal mucosa were recruited in this study. There were 127 men and 74 women with ages ranging from 20 to 81 years (median, 62 years; mean, 57.8 years). The carcinomas were located in the cecum (n = 9), ascending colon (n = 29), transverse colon (n = 14), descending colon (n = 9), sigmoid colon (n = 48) and rectum (n = 92). Of these patients, 24 were grade Ⅰ, 110 grade Ⅱ and 67 grade Ⅲ, according to histological grading; and 48 were stage Ⅰ, 72 were stage Ⅱ, 70 were stage Ⅲ and 11 were stage Ⅳ, according to clinical TNM stage revised by International Union Against Cancer in 2003. All the patients were followed up for survival. During the follow-up period from the date of surgery until April 30, 2009, 126 patients died and 75 were alive (median survival time, 51 mo, range, 0.10-115 mo).

Histological examination

The resected specimens were fixed in 10% formalin. The gross appearance and the size of tumor were recorded. Patients' medical records and histopathology of each specimen were reviewed. The tissues (cancer and normal) were cut into 5-mm slices, embedded in paraffin for histological and immunohistochemical examinations. Each paraffin block was cut at 4 μmol/L in thickness, and sections were mounted onto adhesive-coated slides. Slides were deparaffinized in xylene twice for 10 min and rehydrated through descending concentration of ethanol. Antigen retrieval was performed in 0.01 mol/L citrate buffer (pH 6.0) by microwave oven for 2 min and 30 s at 100℃. Endogenous peroxidase activity was blocked with 0.3% hydrogen peroxidase for 15 min. After washing with phosphate-buffered saline (PBS), the sections with primary polyclonal rabbit antibody to human LRP16 (recognized and isolated in 1999 by Department of Molecular Biology of our hospital) that was diluted 1:1000 in blocking solution were incubated at 4℃ overnight, in a humidified chamber. After washing three times with PBS, the sections incubated for 30 min with biotinylated secondary antibody (polyperoxidase-anti-mouse/rabbit IgG, Zymed) then washed again with PBS. 3,3'-Diaminobenzidine was used as the chromogen. Sections were then counterstained with hematoxylin for 1 min, raised in water, dehydrated in ascending concentrations of ethanol followed by clearance with xylene, and cover slipped permanently for light microscopy. Normal ovary tissue was used as a positive control, whereas the primary antibody was replaced by PBS as a negative control.

Evaluation of score

Immunohistochemically stained slides were reviewed by two investigators independently who were blinded to all clinical data. Slides were analyzed under light microscopy using manual methods. Staining was graded for intensity of staining (0, negative; 1, weak; 2, moderate; 3, strong) and percentage of cells stained (0, < 5%; 1, 6%-25%; 2, 26%-50%; 3, > 50%). The final score was determined by the combined staining score (extent + intensity). Score 0 was defined as negative expression (-), scores 1-3 as weak staining pattern (+), and 4-6 as strong expression (++).

Statistical analysis

Statistical analysis was performed using SPSS 13.0 software (SPSS Inc., Chicago, Illinois). The χ^2 test was used to examine the various clinicopathological characteristics and LRP16 expression. Cumulative survival curves were drawn by the Kaplan-Meier method. The difference between the curves was analyzed by the Log-rank test. Multivariate survival analysis was based on Cox proportional hazard model. $P < 0.05$ was considered statistically significant.

RESULTS

Pattern of LRP16 expression in colorectal carcinoma and normal mucosa

LRP16 staining was performed in 201 colorectal cancer patients and 60 cases of normal tissues by IHC.The result showed that in cancer tissues, LRP16 staining was negative (-) in 41.8% (84/201) cases, weak positive (+) in 21.4% (43/201) cases and strong positive (++) in 36.8% (74/201) cases; whereas in normal mucosas, LRP16 was negative in 65% (39/60) cases, weak positive in 13.3% (8/60) and strong positive in 21.7% (13/60) cases. As a whole, LRP16 expression was detected in 58.2%

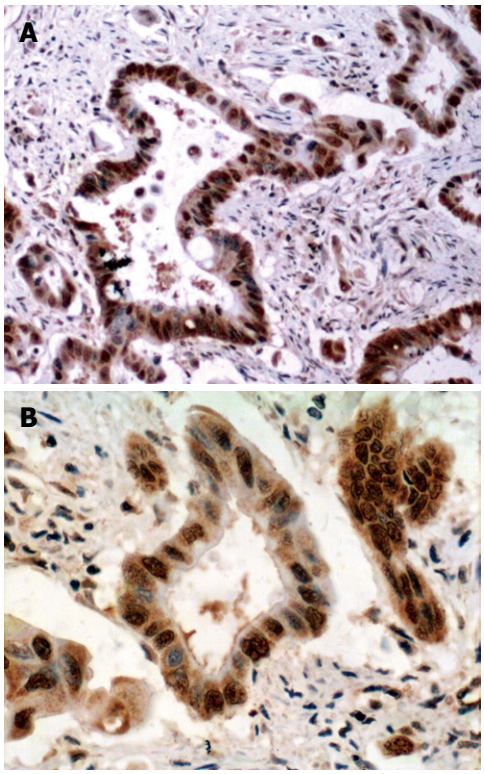

Figure 1 Positive leukemia related protein 16 (LRP16) expression in colorectal adenocarcinoma. The final score was 6, including 3 scores (strong) related to intensity of staining and 3 scores (> 50%) related to extent of staining. Thus it was defined as strong staining pattern (++). A: Immunohistochemistry (IHC), × 100; B: IHC, × 400.

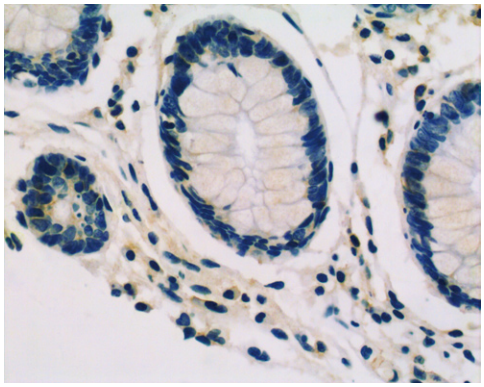

Figure 2 Negative LRP16 expression in normal colorectal mucosa (IHC, × 400). The final score was 0, including 0 score (negative) related to intensity of staining, and 0 scores (< 5%) related to extent of staining. Thus it was defined as negative expression (-).

(117/201) colorectal carcinoma, and in 35% (21/60) distal normal mucosa (Figures 1 and 2). The expression of LRP16 protein was found in cell nucleus or both cell nucleus and cytoplasm. The difference of LRP16 expression between colorectal cancer and normal mucosa was statistically significant ($\chi^2 = 9.998$, $P = 0.002$).

Correlation of LRP16 expression and clinicopathological features in colorectal cancer

Upon clinicopathological analysis, more LRP16 expression was present in bigger tumors ($P = 0.001$). When comparing the LRP16 status with clinicopathological variables, we found significant positive correlations between LRP16 expression and degree of differentiation ($P = 0.010$), depth of invasion ($P = 0.001$), lymph node metastasis ($P = 0.001$) and distant metastasis ($P = 0.027$). The level of LRP16 in cases of low TNM stage (Ⅰ + Ⅱ) was lower than that of high stage (Ⅲ + Ⅳ) ($\chi^2 = 27.088$, $P = 0.001$) (Table 1).

Table 1 Correlation between LRP16 expression and clinicopathological factors in colorectal cancer *n* (%)

Variables	LRP16		Statistical value
	Positive group (*n* = 197)	Negative group (*n* = 139)	
Gender			
Male	78 (61.4)	49 (38.6)	$\chi^2 = 1.460^a$
Female	39 (52.7)	35 (47.3)	$P = 0.227$
Age (yr)			
< 45	20 (64.5)	11 (35.5)	$\chi^2 = 0.640^a$
45 ≤ *n* < 60	36 (58.0)	26 (42.0)	$P = 0.726$
≥ 60	61 (56.5)	47 (43.5)	
Tumor size (cm)			
d < 5	68 (50.0)	68 (50.0)	$\chi^2 = 13.604^a$
5 ≤ d < 10	42 (72.4)	16 (27.6)	$P = 0.001$
d ≥ 10	7 (100.0)	0 (0.0)	
Tumor location			
Cecum	5 (55.6)	4 (44.4)	$\chi^2 = 6.027^a$
Ascending colon	22 (75.9)	7 (24.1)	$P = 0.304$
Transverse colon	8 (57.1)	6 (42.9)	
Descending colon	6 (66.7)	3 (33.3)	
Sigmoid colon	29 (60.4)	19 (39.6)	
Rectum	47 (51.1)	45 (48.9)	
Histologic differentiation			
Well differentiated	12 (50.0)	12 (50.0)	$\chi^2 = 9.210^a$
Moderately differentiated	56 (50.9)	54 (49.1)	$P = 0.010$
Poorly differentiated	49 (73.1)	18 (226.9)	
Depth of invasion, T stage			
T1	2 (28.6)	5 (71.4)	$\chi^2 = 25.470^a$
T2	25 (36.8)	43 (63.2)	$P = 0.001$
T3	79 (69.9)	34 (30.1)	
T4	11 (84.6)	2 (15.4)	
Lymph node metastasis			
LN = 0	58 (45.3)	70 (54.7)	$\chi^2 = 24.735^a$
LN = 1-3	43 (78.2)	12 (21.8)	$P = 0.001$
LN > 3	16 (88.9)	2 (11.1)	
Distant metastasis			
Negative	107 (56.3)	83 (43.7)	$\chi^2 = 5.115^a$
Positive	10 (90.9)	1 (9.1)	$P = 0.027$
TNM stage			
Ⅰ-Ⅱ	52 (43.3)	68 (57.7)	$\chi^2 = 27.088^a$
Ⅲ-Ⅳ	65 (80.2)	16 (19.8)	$P = 0.001$

[a]$P < 0.05$, statistically significant. LRP16: Leukemia related protein 16.

Relationship between LRP16 expression and overall survival of colorectal cancer patients

All 201 patients were followed up for survival to assess LRP16 expression as a prognostic factor. Kaplan-Meier survival curves and Log-rank test demonstrated that LRP16 positive cases showed a significantly shortened median survival time (38.0 mo) in comparison with other patients (105.0 mo) (Log rank = 41.455, $P = 0.001$) (Figure 3).

Table 2 Cox regression analysis of prognostic factors in colorectal carcinoma

Prognostic variables	B	SE	Wald value	*P* value	RR
Gender	0.261	0.197	1.756	0.185	1.298
Age (yr)	0.191	0.124	2.366	0.124	1.211
Tumor location	0.071	0.060	1.338	0.239	1.074
Histologic differentiation	0.747	0.162	21.128	0.001	2.110
Tumor size	0.123	0.188	0.433	0.510	1.131
Depth of invasion	0.508	0.199	6.523	0.011	1.661
Lymph node metastasis	0.060	0.206	0.085	0.771	1.062
Distant metastasis	1.450	0.526	7.589	0.006	4.264
TNM stage	0.717	0.236	9.236	0.002	2.049
LRP16 expression	0.741	0.225	10.868	0.001	2.099

B: Partial regression coefficient; RR: Relative risk. $P < 0.05$, statistically significant.

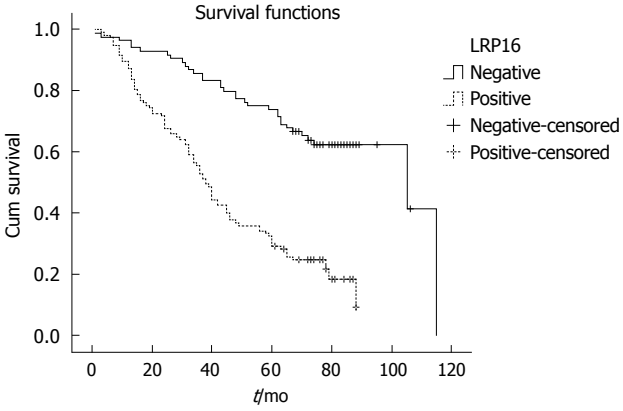

Figure 3 Cumulative survival according to LRP16 expression in colorectal cancer patients. The Kaplan-Meier plot of colorectal carcinoma patients (n = 201) demonstrates a significantly lower survival with LRP16 positive expression, P = 0.001.

The overall 5-year survival rate of the LRP16 negative patients (71.4%) was higher than that of the LRP16 positive group (29.1%). LRP16 expression appeared as a significant independent prognostic factor (P = 0.001) with a relative risk of 2.082 (confidence interval, 1.3-3.2) in the multivariate survival analysis of the patients. Other independent prognostic factors in multivariate survival analysis included tumor shape, degree of differentiation, depth of invasion and distant metastasis (Table 2).

DISCUSSION

LRP16 was originally recognized and isolated from human lymphocytes in 1999[1]. It was identified as an estrogen responsive gene[1-5]. The expression of LRP16 was found in different tissues in varying degrees, including ovary, testicle, prostate, small intestine, spleen, thymus and stomach[2-3,6]. Furthermore, LRP16 is overexpressed in tumors, compared with their matched normal tissues[2]. Some studies have indicated that LRP16 may play an important role in the carcinogenesis and progression of hormone-dependent breast cancer[5,11]. Overexpression of LRP16 significantly stimulated MCF-7 cell proliferation by promoting G1/S transition[4]. The suppression of the endogenous LRP16 in ERα-positive MCF-7 cells not only inhibits cell growth but also significantly attenuates the cellular estrogen-responsive proliferation ability and sensitizes tumor cells to radiation[11-13]. However, some authors thought that expression of LRP16 in ERα-negative cells had no effect on proliferation[11]. The expression of *LRP16* gene was dependent on the estrogen activities[14,15], LRP16 was also involved in estrogen signaling and could strengthen the ERα-responsive gene activation, therefore, it is also considered as an ERα coactivator[11]. Previous studies have demonstrated that ERα/PR status, tumor size and auxiliary lymph node metathesis were closely correlated with LRP16 overexpression[16]. ER includes two subtypes, ERα and ERβ. They have been identified in colorectal cancer tissue and normal mucosa[8-10]. It was also reported that the ER expression level of carcinoma was higher than that of non-cancerous colon tissues[10]. Activation of ER signaling pathway plays an important role in multi-tissue development[17-20]. Therefore, we propose that LRP16, a coactivator of ERα, may display an important function in the carcinogenesis and progression of colorectal cancer as in breast cancer.

Although the detailed molecular mechanism involved in this process is unclear, our study have potentially clinical benefits. LRP16 expression that could be detected by IHC may be a useful molecular marker to predict the prognosis in colorectal carcinoma patients. Moreover, LRP16 and ERα could inter-regulate each other, as LRP16 is an ERα coactivator. This study raises the possibility that anti-estrogen therapy could be used in the patients with high LRP16 expression. This information may help us individualize patient care (e.g. progression and prognosis of patients after operation). In this study, LRP16 expression was commonly up-regulated in colorectal carcinoma and was associated with shortened survival time of the patients in univariate and multivariate analyses. However, further investigations and clinicopathological correlation are necessary.

ACKNOWLEDGMENTS

We thank all colleagues from the Department of Molecular Biology, Chinese People's Liberation Army General Hospital, for their help and supports in this study.

COMMENTS

Background

Colorectal cancer is a major cause of cancer–related morbidity and mortality. In the Western world it is the second leading cause of death from cancer. The evidence of colorectal cancer has increased recently in China. Although this disease is curable by surgical interventions together with chemotherapy and radiation in its early stages, the patients are often asymptomatic before the metastasis occurred. Therefore, effective screening and preventive strategies for colorectal cancer are necessary to enhance our capability to predict the clinical outcome of the disease.

Research frontiers

Leukemia related protein 16 (*LRP16*) gene plays an important role in the

carcinogenesis and progression of hormone-dependent breast cancer. *LRP16* expression was also reported to be associated with invasion, metastasis and prognosis of gastric carcinoma. But no comprehensive description of LRP16 protein expression in colorectal cancer has been reported. In this study, the authors investigated the expression patterns of LRP16 protein in human colorectal cancers and compared the clinical and pathological variables including survival time of the patients.

Innovations and breakthroughs

To date, only limited data on LRP16 protein expression in solid tumors are available. This study is believed to be the first trial for verifying the relationship between LRP16 expression and clinicopathological factors of colorectal carcinoma.

Applications

The authors presented some evidences to show a significant association between high LRP16 expression in colorectal cancer and early disease progression or the disease related death, and they believe that the LRP16 expression status detected by immunohistochemistry (IHC) may be a molecular marker to predict the prognosis of colorectal carcinoma patients.

Peer review

In this paper the authors have analyzed by IHC the expression of LRP16 protein in 201 cases of colorectal carcinoma and 60 cases of distal normal mucosae and they have correlated the expression of this marker with the degree of differentiation, invasiveness, metastasis and prognosis of colorectal carcinoma. The study is well performed and the results are quite interesting, and are potentially helpful for clinical application, the quality of the research and presentation, including photomicrographs and figures, is high, the discussion is clear and well written.

REFERENCES

1 **Yu L**, Han WD, Lou FD, Wang QS, Zhao Y, Caligiuri MA. Cloning of leukemia associated gene LRP16 in acute myeloid leukemia. *Junyi Jinxiu Xueyuan Xuebao* 2000; **21**: 81-84

2 **Han WD**, Yu L, Lou FD, Wang QS, Zhao Y, Shi ZJ, Jiao HY, Zhou JJ. Cloning and Expression Characterization of the Full Length cDNA for a Novel Leukemia-associated Gene LRP16. *Zhongguo Shengwu Huaxue Yu Fenzi Shengwu Xuebao* 2001; **17**: 209-214

3 **Han WD**, Lou FD, Yu L, Wang QS, Han XP, Li JX. SAGE pattern of LRP16 gene and its expression in normal blood and leukemic cells. *Junyi Jinxiu Xueyuan Xuebao* 2002; **23**: 161-163

4 **Han WD**, Mu YM, Lu XC, Xu ZM, Li JX, Yu L, Song HJ, Li M, Lu JM, Pan CY. Estrogen stimulates human breast cancer MCF-7 cell proliferation by up-regulation of LRP16 mRNA via activation of estrogen receptor-alpha. *Zhonghua Neifenmi Daixie Zazhi* 2004; **20**: 165-168

5 **Han WD**, Mu YM, Lu XC, Xu ZM, Li XJ, Yu L, Song HJ, Li M, Lu JM, Zhao YL, Pan CY. Up-regulation of LRP16 mRNA by 17beta-estradiol through activation of estrogen receptor alpha (ERalpha), but not ERbeta, and promotion of human breast cancer MCF-7 cell proliferation: a preliminary report. *Endocr Relat Cancer* 2003; **10**: 217-224

6 **Li YZ**, Zhao P, Han WD. Clinicopathological significance of LRP16 protein in 336 gastric carcinoma patients. *World J Gastroenterol* 2009; **15**: 4833-4837

7 **Compton CC**. Colorectal carcinoma: diagnostic, prognostic, and molecular features. *Mod Pathol* 2003; **16**: 376-388

8 **Jiang H**, Teng R, Wang Q, Zhang X, Wang H, Wang Z, Cao J, Teng L. Transcriptional analysis of estrogen receptor alpha variant mRNAs in colorectal cancers and their matched normal colorectal tissues. *J Steroid Biochem Mol Biol* 2008; **112**: 20-24

9 **Di Leo A**, Messa C, Cavallini A, Linsalata M. Estrogens and colorectal cancer. *Curr Drug Targets Immune Endocr Metabol Disord* 2001; **1**: 1-12

10 **Zhou ZW**, Wan DS, Wang GQ, Pan ZZ, Lu HP, Gao JH, Ding PR. [Expression of estrogen receptor and progesterone receptor in colorectal cancer: a quantitative study] *Ai Zheng* 2004; **23**: 851-854

11 **Han WD**, Zhao YL, Meng YG, Zang L, Wu ZQ, Li Q, Si YL, Huang K, Ba JM, Morinaga H, Nomura M, Mu YM. Estrogenically regulated LRP16 interacts with estrogen receptor alpha and enhances the receptor's transcriptional activity. *Endocr Relat Cancer* 2007; **14**: 741-753

12 **Han WD**, Zhao YL, Li Q, Mu YM, Li X, Song HJ, Lu ZQ. Inhibition of proliferation of human breast cancer MCF-7 cells by small interference RNA against LRP16 gene. *Chin J Cancer Res* 2004; **16**: 239-245

13 **Han WD**, Yang D, Li Q, Zhao XL, Ma L, Mu YM. Improvement of radiation sensitivity by inhibiting expression of the human LRP16 gene in tumor cells. *Junyi Jinxiu Xueyuan Xuebao* 2005; **26**: 183-185

14 **Zhao YL**, Han WD, Li Q, Mu YM, Lu XC, Yu L, Song HJ, Li X, Lu JM, Pan CY. Mechanism of transcriptional regulation of LRP16 gene expression by 17-beta estradiol in MCF-7 human breast cancer cells. *J Mol Endocrinol* 2005; **34**: 77-89

15 **Lu XC**, Lou FD, Han WD, Zhu XD, Mu YM, Xu ZM, Yu L. [Analysis of LRP16 gene promoter activity] *Zhongguo Shiyan Xueyexue Zazhi* 2006; **14**: 146-149

16 **Liao DX**, Han WD, Zhao YL, Pu YD, Mu YM, Luo CH, Li XH. [Expression and clinical significance of LRP16 gene in human breast cancer] *Ai Zheng* 2006; **25**: 866-870

17 **Gerits N,** Kostenko S, Moens U. In vivo functions of mitogen-activated protein kinases: conclusions from knock-in and knock-out mice. *Transgenic Res* 2007; **16**: 281-314

18 **Morissette M**, Jourdain S, Al Sweidi S, Menniti FS, Ramirez AD, Di Paolo T. Role of estrogen receptors in neuroprotection by estradiol against MPTP toxicity. *Neuropharmacology* 2007; **52**: 1509-1520

19 **Zaitsu M**, Narita S, Lambert KC, Grady JJ, Estes DM, Curran EM, Brooks EG, Watson CS, Goldblum RM, Midoro-Horiuti T. Estradiol activates mast cells via a non-genomic estrogen receptor-alpha and calcium influx. *Mol Immunol* 2007; **44**: 1977-1985

20 **Morales LB**, Loo KK, Liu HB, Peterson C, Tiwari-Woodruff S, Voskuhl RR. Treatment with an estrogen receptor alpha ligand is neuroprotective in experimental autoimmune encephalomyelitis. *J Neurosci* 2006; **26**: 6823-6833

S- Editor Wang JL **L- Editor** Ma JY **E- Editor** Zheng XM

World Journal of Gastroenterology

Online Submissions: http://www.wjgnet.com/1007-9327office
wjg@wjgnet.com
doi:10.3748/wjg.v16.i13.1649

World J Gastroenterol 2010 April 7; 16(13): 1649-1654
ISSN 1007-9327 (print)

BRIEF ARTICLE

Long-term efficacy of perioperative chemoradiotherapy on esophageal squamous cell carcinoma

Jin Lv, Xiu-Feng Cao, Bin Zhu, Lv Ji, Lei Tao, Dong-Dong Wang

Jin Lv, Xiu-Feng Cao, Bin Zhu, Lv Ji, Lei Tao, Dong-Dong Wang, Department of Surgery, Oncology Center, Affiliated Nanjing First Hospital of Nanjing Medical University and Oncology Center of Nanjing Medical University, Nanjing 210006, Jiangsu Province, China

Author contributions: Lv J participated in the design of the study, analysis and interpretation of data, manuscript writing, statistical analysis of the data, and revision of the manuscript; Cao XF substantially contributed to the conception and design of the study, fund acquisition, administration and materials support; Zhu B, Ji L, Tao L and Wang DD provided supportive contributions.

Correspondence to: Xiu-Feng Cao, Professor, Department of Surgery, Oncology Center, Affiliated Nanjing First Hospital of Nanjing Medical University and Oncology Center of Nanjing Medical University, 68 Changle Road, Nanjing 210006, Jiangsu Province, China. cxf551101@sina.com
Telephone: +86-25-52887061 Fax: +86-25-52269924

Received: December 8, 2009 Revised: December 31, 2009
Accepted: January 7, 2010
Published online: April 7, 2010

Abstract

AIM: To investigate the role of perioperative chemoradiotherapy (CRT) in the treatment of locally advanced thoracic esophageal squamous cell carcinoma (ESCC).

METHODS: Using preoperative computed tomography (CT)-based staging criteria, 238 patients with ESCC (stage Ⅱ-Ⅲ) were enrolled in this prospective study between January 1997 and June 2004. With informed consent, patients were randomized into 3 groups: preoperative CRT (80 cases), postoperative CRT (78 cases) and surgery alone (S) (80 cases). The 1-, 3-, 5- and 10-year survival were followed up. Progression-free survival (PFS) was chosen as the primary endpoint by treatment arm measured from study entry until documented progression of disease or death from any cause. The secondary endpoint was overall survival (OS) determined as the time (in months) between the date of therapy and the date of death. Other objectives were surgical and adjuvant therapy complications.

RESULTS: With median follow-up of 45 mo for all the enrolled patients, significant differences in the 1-, 3-, 5-, 10-year OS (91.3%, 63.5%, 43.5%, 24.5% *vs* 91%, 62.8%, 42.3%, 24.4% *vs* 87.5%, 51.3%, 33.8%, 12.5%, $P = 0.0176$) and PFS (89.3%, 61.3%, 37.5%, 18.1% *vs* 89.1%, 61.1%, 37.2%, 17.8% *vs* 84.5%, 49.3%, 25.9%, 6.2%, $P = 0.0151$) were detected among the 3 arms. There were no significant differences in OS and PFS between the preoperative CRT and postoperative CRT arm ($P > 0.05$). For the patients who had radical resection, significant differences in median PFS (48 mo *vs* 61 mo *vs* 39.5 mo, $P = 0.0331$) and median OS (56.5 mo *vs* 72 mo *vs* 41.5 mo, $P = 0.0153$) were detected among the 3 arms, but there were no significant differences in OS and PFS between the preoperative CRT and postoperative CRT arm ($P > 0.05$). The local recurrence rates in the preoperative CRT, postoperative CRT group and S group were 11.3%, 14.1% and 35%, respectively ($P < 0.05$). No significant differences were detected among the 3 groups when comparing complications but tended to be in favor of the postoperative CRT and S groups ($P > 0.05$). Toxicities of CRT in the preoperative or postoperative CRT arms were mostly moderate, and could be quickly alleviated by adequate therapy.

CONCLUSION: Rational application of preoperative or postoperative CRT can provide a benefit in PFS and OS in patients with locally advanced ESCC.

Key words: Esophageal cancer; Surgery; Esophagectomy; Chemotherapy; Radiation therapy

Peer reviewers: Marco Giuseppe Patti, MD, Professor of Surgery, Director, Center for Esophageal Diseases, University of Chicago Pritzker School of Medicine, 5841 S. Maryland Avenue, MC 5095, Room G 201, Chicago, IL 60637, United States; Luis Grande, Professor, Department of Surgery, Hospital del Mar, Passeig Marítim 25-29, Barcelona 08003, Spain

Lv J, Cao XF, Zhu B, Ji L, Tao L, Wang DD. Long-term efficacy

of perioperative chemoradiotherapy on esophageal squamous cell carcinoma. *World J Gastroenterol* 2010; 16(13): 1649-1654 Available from: URL: http://www.wjgnet.com/1007-9327/full/v16/i13/1649.htm DOI: http://dx.doi.org/10.3748/wjg.v16.i13.1649

INTRODUCTION

Esophageal squamous cell carcinoma (ESCC) is one of the common malignancies and the seventh leading cause of cancer-related deaths in the world[1]. The 5-year survival rate is only 15%-20% in patients with locally advanced esophageal cancer[2]. Treatment failure mainly results from recurrence or metastasis. A standardized comprehensive treatment is still under development. Radiotherapy can control local-regional esophageal cancer and chemotherapy has both local and systemic antineoplastic activity. With increasing enthusiasm for multidisciplinary treatment modalities to improve outcome, a commonly employed treatment approach for esophageal cancer is chemoradiotherapy (CRT) in addition to surgical resection[3]. Preoperative CRT had been applied to patients with esophageal carcinoma in an effort to reduce the relapse rate and improve survival. Many studies have demonstrated the effectiveness of neoadjuvant CRT[4-9]. In contrast to data available on preoperative CRT, although a number of trials compared adjuvant chemotherapy or radiotherapy with surgery alone, there are almost no randomized trials comparing adjuvant CRT with surgery alone. The only exception is a trial that compared surgery alone with surgery and adjuvant CRT for patients with resectable cancers of the stomach and gastroesophageal junction[10]. Although the results suggest that resection followed by concurrent CRT should be considered for patients with adenocarcinoma of the stomach and the gastroesophageal junction, the question remains whether postoperative CRT can improve overall survival in patients with ESCC.

To our knowledge, as yet no study is available to determine the best sequencing of CRT and surgery. To resolve this deficiency, the present prospective study was conducted in our center from January 1997 to June 2004.

MATERIALS AND METHODS

Patients

Two hundred and seventy one patients with ESCC were diagnosed by endoscopic biopsy and histopathology between January 1997 and June 2004 in our center. According to the preoperative computed tomography (CT) staging criteria, 238 patients with stage Ⅱ-Ⅲ thoracic ESCC were enrolled in this prospective study. The CT staging criteria were as follows: Stage Ⅰ, the tumor was limited to the esophageal lumen or the thickness of the esophageal wall varied between 3 and 5 mm; Stage Ⅱ, the thickness exceeded 5 mm but there was no invasion of the mediastinum or distant metastasis; Stage Ⅲ, the tumor invaded the adjacent mediastinal structure; and Stage Ⅳ, there was distant metastasis. All patients gave informed consent prior to their inclusion in the study. The form had been reviewed by the appropriate ethics committee and had been developed and was administered in accordance with the ethical standards laid down in an appropriate version of the 1964 Declaration of Helsinki. The enrolled patients were randomized into 3 groups: preoperative CRT, postoperative CRT, and surgery alone (S). The randomization method was based on random numerals produced by computer. Characteristics of the preoperative patients are shown in Table 1.

Table 1 Characteristics of the preoperative patients (n = 238)

	Pre-CRT (n = 80)	Post-CRT (n = 78)	S (n = 80)	Statistics	
				χ^2	P
Sex (M:F)	52:28	48:30	50:30	3.1326	0.209
Age (yr)				1.2375	0.975
40-	12	13	11		
50-	24	25	24		
60-	28	29	30		
70-	16	11	15		
Location				0.1920	0.996
Upper	11	10	12		
Middle	45	45	44		
Lower	24	23	24		
CT staging				0.1165	0.943
Ⅱ	35	33	36		
Ⅲ	45	45	44		

Pre-CRT: Preoperative chemoradiotherapy; Post-CRT: Postoperative CRT; S: Surgery alone; CT: Computed tomography.

Treatment

The surgical procedure used in this study was either a radical resection, which involved an esophagectomy through a left or right thoracotomy with 2-field lymphadenectomy, or palliative resection or esophageal bypass. All the patients who underwent palliative resection or esophageal bypass had taken traditional Chinese medicine themselves.

For patients in the preoperative arm, surgical resection was to be performed 4-6 wk after induction of CRT. The patients treated with postoperative CRT underwent surgery and received CRT 4-6 wk later. For patients treated with preoperative CRT, radiation was delivered in a total dose of 40 Gy (20 fractions at 2 Gy per fraction) in anteroposterior fields including esophageal tumors and enlarged lymph nodes, with a 4-5 cm proximal and distal margin and a 1-2 cm radial margin. For 30 out of 78 patients treated with postoperative CRT, radiation was delivered in daily fractions of 2 Gy to a total dose of 40 Gy over 4 wk by using the same double field technique as the preoperative CRT group, and the anteroposterior fields of the following 48 patients were extended from the sixth cervical vertebrae to the first lumbar vertebrae, including the origin of esophagus and lymph drainage that encompassed the supraclavicular regions and left gastric lymph nodes. Then a 10 Gy boost was delivered through parallel opposed lateral or oblique portals for limitation of spinal

cord radiation dose. Radiotherapy was carried out by linear accelerators with 6 MV photons; treatment ports were designed to include enlarged regional nodes based on CT evaluation and endoscopic ultrasound.

For chemotherapy, 2 cycles were administered on days 1-3 and days 22-24 of radiotherapy. A paclitaxel (PTX) + cisplatin (DDP) regimen was used, including PTX (135 mg/m^2 per day) administered as a short-term infusion on day 1 of each cycle, while DDP (20 mg/m^2 per day) was delivered as a continuous infusion over 24 h on days 1-3 of each cycle. The patients received the antiemetics granisetron and metoclopramide before and after the cisplatin infusion. The dose of chemotherapy in the second cycle was adjusted according to hematological toxicities.

Efficacy assessment

Any perioperative complications were observed and recorded. During treatment, the patients were monitored weekly with a physical examination and blood chemistry evaluation. Clinical evaluation was carried out by endoscopy, endoscopic ultrasonography, and CT scans. All results of the examination were collected and evaluated by the oncology experts. The 1-, 3-, 5- and 10-year survival were followed up.

Follow-up

Clinical follow-up after completion of treatment was based on periodic visits (every 3 mo during the first 2 years, every 6 mo after 2 years). The follow-up time for survivors ranged from 5 to 124 mo (median 45 mo).

Statistical analysis

STATA 10.0 for Windows (StataCorp, College Station, Texas 77845, USA) was used for statistical analysis. The differences in age group, sex, tumor location, and tumor staging, complications, and cause of death among groups were compared by the χ^2 test or Fisher's Exact test. The survival among groups were described by Kaplan-Meier curves and analyzed by the log-rank test. *P* values less than 0.05 were considered statistically significant. Progression free survival (PFS) was chosen as the primary endpoint by treatment arm measured from study entry until documented progression of disease or death from any cause. The secondary endpoint was overall survival (OS) determined as the time (in months) between the date of therapy and the date of death. Other factors determined were surgical and adjuvant therapy complications.

RESULTS

By June 30 2009, 228 out of all cases were followed up by means of telephone or outpatient service, and 10 cases were lost. There were 3.8% treatment-related deaths in preoperative CRT but no treatment-related deaths in the postoperative CRT and S group, and 51.3% of patients died from the local tumor recurrence and distant metastasis.

Median PFS was 46.5 mo (95% CI: 37.4-66.3) in the preoperative CRT group, 45 mo (95% CI: 35.8-67) in the postoperative CRT group, and 32.5 mo (95% CI: 25.4-42.3) in the S group. The 1-year PFS in preoperative CRT, postoperative CRT and S groups was 89.3%, 89.1% and 84.5%, respectively, with no significant differences (χ^2 = 0.64, *P* = 0.4123). However, the 3-, 5- and 10-year PFS of the preoperative CRT (61.3%, 37.5%, 18.1%, respectively) and postoperative CRT groups (61.1%, 37.2%, 17.8%, respectively) were significantly different (χ^2 = 4.16, *P* = 0.0319; χ^2 = 4.14, *P* = 0.0321; χ^2 = 5.38, *P* = 0.0203; respectively) from those of the S group (49.3%, 25.9%, 6.2%, respectively). There was no significant difference in PFS between the neoadjuvant and adjuvant therapy groups (χ^2 = 0.14, *P* = 0.7060) (Figure 1A). Median OS was 53 mo (95% CI: 43-64.3) in the preoperative CRT group, 48 mo (95% CI: 38.5-72.5) in the postoperative CRT group, and 36 mo (95% CI: 29.7-47.3) in the S group. The 1-year OS in the preoperative CRT, postoperative CRT and S groups was 91.3%, 91% and 87.5%, respectively, which were not significantly different (χ^2 = 0.72, *P* = 0.3970). However, the 3-, 5- and 10-year survival rates of the preoperative CRT (63.5%, 43.5%, 24.5%, respectively) and postoperative CRT groups (62.8%, 42.3%, 24.4%, respectively) were significantly different (χ^2 = 3.98, *P* = 0.0453; χ^2 = 4.76, *P* = 0.0402; χ^2 = 4.27, *P* = 0.0389; respectively) from those of the S group (51.3%, 33.8%, 12.5%, respectively). There was no significant difference in OS between the neoadjuvant and adjuvant therapy groups (χ^2 = 0.46, *P* = 0.4978) (Figure 1B).

For the patients who experienced radical resection, median PFS of the preoperative CRT group, postoperative CRT group and S group was 48 mo (95% CI: 40-67.0), 61 mo (95% CI: 44.0-75.4), and 39.5 mo (95% CI: 30-60), respectively. A significant difference in PFS was detected among the 3 arms (χ^2 = 6.82, *P* = 0.0331), however, there was no significant difference in PFS between neoadjuvant and adjuvant therapy groups (χ^2 = 0.22, *P* = 0.6416) (Figure 1C). There was a significant difference in OS among the 3 arms (χ^2 = 8.36, *P* = 0.0153). The median OS of the preoperative CRT group, postoperative CRT group and S group was 56.5 mo (95% CI: 44-72), 72 mo (95% CI: 49.6-88.4), and 41.5 mo (95% CI: 31.6-57.7), respectively. However, there was no significant difference in OS between neoadjuvant and adjuvant therapy groups (χ^2 = 0.16, *P* = 0.6873) (Figure 1D).

The local recurrence rates of the preoperative CRT group, postoperative CRT group and S group were 11.3%, 14.1% and 35% respectively, and showed a statistically significant difference (*P* = 0.011). There was no significant difference among the 3 groups when comparing perioperative complications but there was a tendency in favor of the postoperative CRT and S groups (*P* = 0.179).

For the 158 patients receiving CRT, incidence of grade 3 or greater leucopenia, thrombocytopenia, anemia and vomiting were 11.4% (18/158), 6.3% (10/158), 1.3% (2/158) and 6.3% (10/158), respectively. Postoperative pathologic staging and perioperative complications, and the causes of death are presented in Table 2.

DISCCUSION

Patients with resectable ESCC should receive multimod-

Table 2 Postoperative pathologic staging, perioperative complications, and cause of death *n* (%)

	Pre-CRT (*n* = 80)	Post-CRT (*n* = 78)	S (*n* = 80)	*n* = 238	Statistics	
					χ^2	*P*
Resection					-	0.011[1]
R	76 (97.4)	61 (78.2)	64 (80)	201 (84.5)		
P	4 (2.6)	13 (16.7)	13 (16.3)	30 (12.6)		
EB	0 (0)	4 (5.1)	3 (3.8)	7 (2.9)		
Stage					-	0.000[1]
Ⅰ	4 (2.6)	0 (0)	0 (0)	4 (1.7)		
Ⅱa	22 (27.5)	13 (16.7)	12 (15.4)	47 (19.7)		
Ⅱb	29 (36.3)	17 (21.8)	19 (23.8)	65 (27.3)		
Ⅲ	25 (31.3)	48 (61.5)	49 (61.3)	122 (51.3)		
Complications					-	0.179[1]
Hemorrhage during						
Surgery (> 300 mL)	8 (10.0)	2 (2.6)	2 (2.5)	12 (5.0)		
Stomal leakage	1 (1.3)	0 (0)	0 (0)	1 (0.4)		
Stomal stricture	2 (2.5)	3 (3.8)	1 (1.3)	6 (2.5)		
Reflux esophagitis	13 (16.3)	13 (16.7)	15 (18.8)	41 (17.2)		
Acute lung injury	3 (3.8)	0 (0)	0 (0)	3 (1.3)		
Death					-	0.011[1]
Local recurrence	9 (11.3)	11 (14.1)	28 (35)	48 (20.2)		
Distant metastasis	20 (25)	23 (29.5)	31 (38.8)	74 (31.1)		
Treatment related	3 (3.8)	0 (0)	0 (0)	3 (1.3)		
Not related	1 (1.3)	5 (6.4)	1 (1.3)	7 (2.9)		

[1]Fisher's Exact test. R: Radical resection; P: Palliative resection; EB: Esophageal bypass.

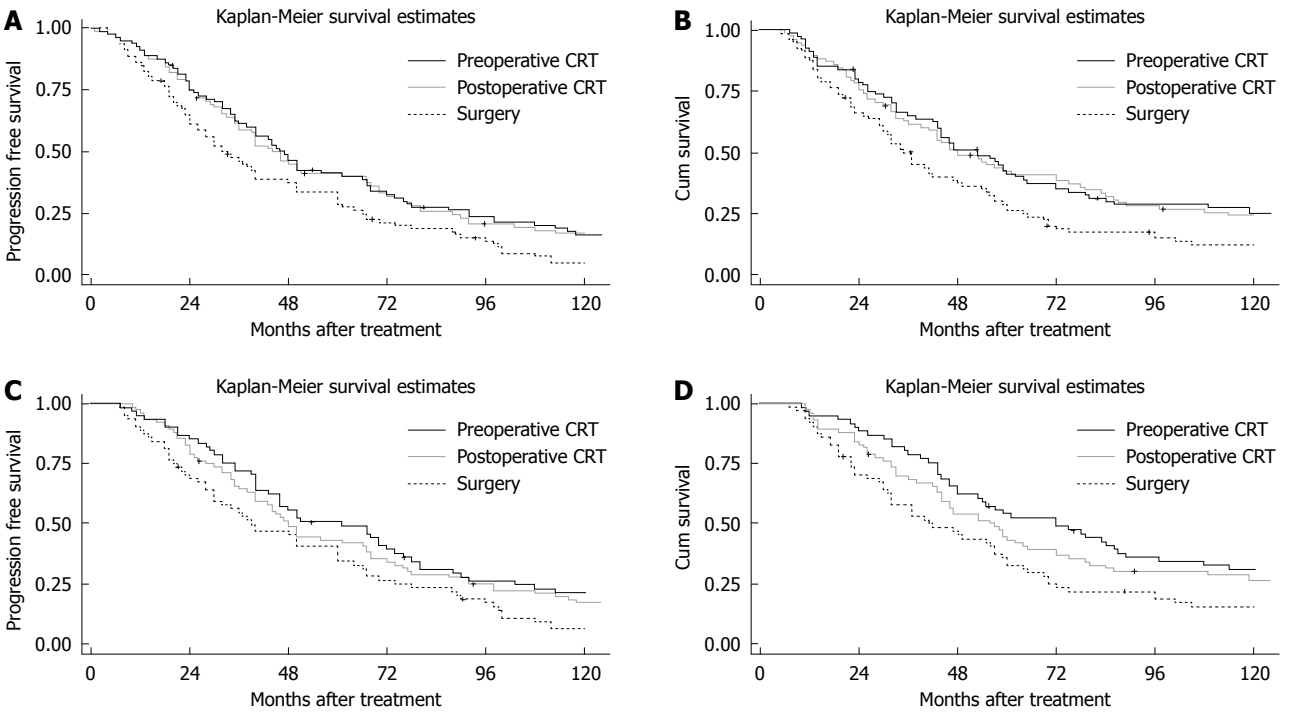

Figure 1 Kaplan-Meier curves. A: Postoperative progression-free survival. Logrank test: χ^2 = 8.39, *P* = 0.0151; "+": Loss to follow-up. Preoperative *vs* surgery: χ^2 = 6.81, *P* = 0.0091; Postoperative *vs* surgery: χ^2 = 5.38, *P* = 0.0203; Preoperative *vs* postoperative: χ^2 = 0.14, *P* = 0.7060; B: Postoperative overall survival. Logrank: χ^2 = 8.07, *P* = 0.0176; "+": Loss to follow-up. Preoperative *vs* surgery: χ^2 = 7.85, *P* = 0.0051; Postoperative *vs* surgery: χ^2 = 5.33, *P* = 0.0209; Preoperative *vs* postoperative: χ^2 = 0.46, *P* = 0.4978; C: Postoperative progression-free survival of radical resection. Logrank: χ^2 = 6.82, *P* = 0.0331; "+": Loss to follow-up. Preoperative *vs* surgery: χ^2 = 6.16, *P* = 0.0130; Postoperative *vs* surgery: χ^2 = 4.02, *P* = 0.0449; Preoperative *vs* postoperative: χ^2 = 0.22, *P* = 0.6416; D: Postoperative overall survival of radical resection. Logrank: χ^2 = 8.36, *P* = 0.0153; "+": Loss to follow-up. Preoperative *vs* surgery: χ^2 = 7.65, *P* = 0.0057; Postoperative *vs* surgery: χ^2 = 4.78, *P* = 0.0288; Preoperative *vs* postoperative: χ^2 = 0.16, *P* = 0.6873.

al treatment to prolong OS[11,12]. There is still controversy about how to improve prognosis and how to reduce local recurrence and distant metastasis. Both chemotherapy and radiotherapy may be active against different tumor cell populations, the chemotherapy may be effective against micrometastases while radiation counteracts spatial metastases. In the Western world, preoperative chemotherapy and CRT can increase OS by 4.4% and

6.4%, respectively, however, treatment-related mortality increases by 1.7% with neoadjuvant chemotherapy and by 3.4% with CRT, compared with surgery alone[13]. There were a few nonrandomized trials on postoperative CRT in treating esophageal carcinoma[14-19], however, the results had discrepancies. Regretfully, the most optimal sequence of CRT in relation to surgical resection is unclear. Thus our study is a unique randomized controlled study to evaluate the outcome of preoperative CRT in patients with local advanced thoracic ESCC, and it includes a long-term follow-up.

The present study showed a benefit in PFS and OS with neoadjuvant or adjuvant therapy. Meanwhile, our study indicated that preoperative CRT reduced the rate of local recurrence, and the survival benefit resulted from improved local cancer control brought about by the adjuvant arm. Although there was no significant difference found in 1-year PFS and OS, both preoperative CRT and postoperative CRT showed a significant advantage in longtime PFS and OS. A meta-analysis had suggested that preoperative CRT may improve survival and locoregional control but was associated with higher toxicity and increased mortality[3]. Our results also confirm this point. Rice and coworkers found that 31 patients treated with postoperative adjuvant CRT had improved survival, in a retrospective review[20]. Together with our present study, it further confirms that postoperative CRT may be an alternative option especially for locally advanced thoracic ESCC. Moreover, the results indicated that postoperative CRT may have almost the same long-term of efficacy as preoperative CRT, although the latter showed a nonsignificant trend of higher survival compared to the former.

To throw further light on the benefit in PFS and OS with neoadjuvant or adjuvant therapy for ESCC, we subsequently analyzed the data in patients who had undergone radical resection. The results also showed the same advantages as the above when including the palliative resection and esophageal bypass patients. The results also showed no significant difference in survival rates when comparing the preoperative CRT and postoperative CRT arms. It further clarifies that adjuvant CRT can provide almost the same long-term of efficacy as neoadjuvant CRT.

In addition, there was no suggestion that treatment-related mortality was increased by the use of postoperative CRT, which was accomplished with manageable toxicity. Most patients had less than grade 2 hematological toxicities. However, our results showed an increase in postoperative deaths and a trend for relatively higher perioperative complications in the neoadjuvant CRT arm. The involved reasons could be as follows: surgeons may undertake a challenging esophagectomy resulting in surgical difficulty and postoperative complications when performed after neoadjuvant CRT. For example, radiation might contribute to the failure of an anastomotic leak and postoperative acute lung injury. The results also showed that preoperative CRT can facilitate complete resection by downstaging tumors when compared to postoperative CRT and surgery alone. Thus, whether or not the survival benefit of neoadjuvant CRT can be negated by an increase in postoperative deaths should of concern. In addition, loss to follow-up was low (4.2%), with only 3 patients receiving preoperative CRT and 3 patients receiving postoperative CRT and 4 patients receiving surgery alone, thus our study is robust.

In conclusion, long-term survival is maximized by the use of CRT followed by surgery for locally advanced esophageal cancer. However, patients are more likely to develop toxicity. As therapies improve, it is likely that the toxicity may be reduced and neoadjuvant CRT may provide a more marked benefit in esophageal cancer. Meanwhile, postoperative CRT can also be safely administered and considered as the multimodal treatment of choice for locally advanced ESCC. In appropriately selected patients, either pre- or postoperative CRT is a viable strategy. Further comparison of pre- and postoperative CRT in treating esophageal cancer is required for verification through multicenter and large sample randomized clinical trials.

COMMENTS

Background

Esophagectomy is a standard treatment for resectable esophageal carcinoma but relatively few patients are cured. Combined neoadjuvant chemoradiotherapy (CRT) or adjuvant CRT with surgery may improve survival but there is concern about treatment morbidity and the best sequencing of CRT and surgery.

Research frontiers

This study investigated the overall survival and profession-free survival data (up to 10-year survival).

Innovations and breakthroughs

Some studies have demonstrated the effectiveness of neoadjuvant CRT and there are almost no randomized trials comparing adjuvant CRT with surgery alone. As yet no study is available to determine the best sequencing of CRT and surgery. The most optimal sequence of CRT in relation to surgical resection is unclear. This study was a unique randomized controlled study to evaluate the outcome of preoperative and postoperative CRT in patients with local advanced thoracic esophageal squamous cell carcinoma, and it includes a long-term follow-up.

Peer review

The authors present the results of a randomized prospective study which examined the efficacy and safety of 3 treatment regimens in esophageal squamous cell carcinoma stage Ⅱ and Ⅲ. The study is of interest to readers of the journal. The discussion is satisfactory and is limited to the topic. Tables depicted essential data and are well constructed.

REFERENCES

1 **Cao XF**, He XT, Ji L, Xiao J, Lv J. Effects of neoadjuvant radiochemotherapy on pathological staging and prognosis for locally advanced esophageal squamous cell carcinoma. *Dis Esophagus* 2009; **22**: 477-481

2 **Graham AJ**, Shrive FM, Ghali WA, Manns BJ, Grondin SC, Finley RJ, Clifton J. Defining the optimal treatment of locally advanced esophageal cancer: a systematic review and decision analysis. *Ann Thorac Surg* 2007; **83**: 1257-1264

3 **Lv J**, Cao XF, Zhu B, Ji L, Tao L, Wang DD. Effect of neoadjuvant chemoradiotherapy on prognosis and surgery for esophageal carcinoma. *World J Gastroenterol* 2009; **15**: 4962-4968

4 **Ruol A**, Portale G, Castoro C, Merigliano S, Cagol M, Cavallin F, Chiarion Sileni V, Corti L, Rampado S, Costantini M, Ancona E. Effects of neoadjuvant therapy on perioperative morbidity in elderly patients undergoing esophagectomy for esophageal cancer. *Ann Surg Oncol* 2007; **14**: 3243-3250

5 **Zemanova M**, Petruzelka L, Pazdro A, Kralova D, Smejkal M, Pazdrova G, Honova H. Prospective non-randomized study of preoperative concurrent platinum plus 5-fluorouracil-based chemoradiotherapy with or without paclitaxel in esophageal cancer patients: long-term follow-up. *Dis Esophagus* 2009; Epub ahead of print

6 **Natsugoe S**, Okumura H, Matsumoto M, Uchikado Y, Setoyama T, Yokomakura N, Ishigami S, Owaki T, Aikou T. Randomized controlled study on preoperative chemoradiotherapy followed by surgery versus surgery alone for esophageal squamous cell cancer in a single institution. *Dis Esophagus* 2006; **19**: 468-472

7 **Greer SE**, Goodney PP, Sutton JE, Birkmeyer JD. Neoadjuvant chemoradiotherapy for esophageal carcinoma: a meta-analysis. *Surgery* 2005; **137**: 172-177

8 **Dixit S**, Tilston M, Peter WM. Risk stratification for recurrence in patients with esophageal and junctional carcinoma treated with neoadjuvant chemotherapy and surgery. *Med Oncol* 2009; Epub ahead of print

9 **Bonnetain F**, Bouché O, Michel P, Mariette C, Conroy T, Pezet D, Roullet B, Seitz JF, Paillot B, Arveux P, Milan C, Bedenne L. A comparative longitudinal quality of life study using the Spitzer quality of life index in a randomized multicenter phase III trial (FFCD 9102): chemoradiation followed by surgery compared with chemoradiation alone in locally advanced squamous resectable thoracic esophageal cancer. *Ann Oncol* 2006; **17**: 827-834

10 **Macdonald JS**, Smalley SR, Benedetti J, Hundahl SA, Estes NC, Stemmermann GN, Haller DG, Ajani JA, Gunderson LL, Jessup JM, Martenson JA. Chemoradiotherapy after surgery compared with surgery alone for adenocarcinoma of the stomach or gastroesophageal junction. *N Engl J Med* 2001; **345**: 725-730

11 **Di Fiore F**, Lecleire S, Rigal O, Galais MP, Ben Soussan E, David I, Paillot B, Jacob JH, Michel P. Predictive factors of survival in patients treated with definitive chemoradiotherapy for squamous cell esophageal carcinoma. *World J Gastroenterol* 2006; **12**: 4185-4190

12 **Triboulet JP**, Mariette C. [Oesophageal squamous cell carcinoma stade III. State of surgery after radiochemotherapy (RCT)] *Cancer Radiother* 2006; **10**: 456-461

13 **Iyer R**, Wilkinson N, Demmy T, Javle M. Controversies in the multimodality management of locally advanced esophageal cancer: evidence-based review of surgery alone and combined-modality therapy. *Ann Surg Oncol* 2004; **11**: 665-673

14 **Bédard EL**, Inculet RI, Malthaner RA, Brecevic E, Vincent M, Dar R. The role of surgery and postoperative chemoradiation therapy in patients with lymph node positive esophageal carcinoma. *Cancer* 2001; **91**: 2423-2430

15 **Kurtzman SM**, Whittington R, Vaughn D, Rosato EF, Haller DG. Post-operative chemosensitized radiation with modulated 5-fluorouracil (5-FU) following resection of adenocarcinoma of the esophagus and esophagogastric (EG) junction. *Int J Radiat Oncol Biol Phys* 1995; **32**: 266

16 **Kang HJ**, Ebie N, Murthy AK, Galinsky DL, Tsekeris P, Griem K. Surgery followed by concomitant accel¬erated fractionation irradiation, cisplatin, and 5-FU for esophageal carcinoma. *Proc Am Soc Clin Oncol* 1992; **11**: 167

17 **Ebie N**, Kang HJ, Millikan K, Murthy AK, Griem K, Hartsell W, Recine DC, Doolas A, Taylor S 4th. Integration of surgery in multimodality therapy for esophageal cancer. *Am J Clin Oncol* 1997; **20**: 11-15

18 **Taylor SG**, Bonomi PD, Kiel KD, Slayton RE, Wolter J. Failure of simultaneous cisplatin/5FU infusion chemotherapy and radiation to improve control of esophageal cancer. *Proc Am Soc Clin Oncol* 1986; **5**: 88

19 **Saito T**, Shigemitsu Y, Kinoshita T, Shimoda K, Abe T, Nakamura A, Chikuba K, Kobayashi M. Cisplatin, vindesine, pepleomycin and concurrent radiation therapy following esophagectomy with lymph adenectomy for patients with an esophageal carcinoma. *Oncology* 1993; **50**: 293-297

20 **Rice TW**, Adelstein DJ, Chidel MA, Rybicki LA, DeCamp MM, Murthy SC, Blackstone EH. Benefit of postoperative adjuvant chemoradiotherapy in locoregionally advanced esophageal carcinoma. *J Thorac Cardiovasc Surg* 2003; **126**: 1590-1596

S- Editor Wang JL **L- Editor** Cant MR **E- Editor** Lin YP

World Journal of Gastroenterology

Online Submissions: http://www.wjgnet.com/1007-9327office
wjg@wjgnet.com
doi:10.3748/wjg.v16.i13.1655

World J Gastroenterol 2010 April 7; 16(13): 1655-1659
ISSN 1007-9327 (print)

BRIEF ARTICLE

Double-balloon enteroscopy for obscure gastrointestinal bleeding: A single center experience in China

Li-Hua Chen, Wen-Guo Chen, Hai-Jun Cao, Hong Zhang, Guo-Dong Shan, Lin Li, Bing-Ling Zhang, Cheng-Fu Xu, Kai-Li Ding, Ying Fang, Ying Cheng, Chen-Jiao Wu, Guo-Qiang Xu

Li-Hua Chen, Wen-Guo Chen, Hong Zhang, Guo-Dong Shan, Lin Li, Bing-Ling Zhang, Cheng-Fu Xu, Guo-Qiang Xu, Department of Gastroenterology, First Affiliated Hospital, College of Medicine, Zhejiang University, Hangzhou 310003, Zhejiang Province, China
Hai-Jun Cao, Department of Gastroenterology, First Affiliated Hospital, Zhejiang University of Chinese Medicine, Hangzhou 310003, Zhejiang Province, China
Kai-Li Ding, Department of Gastroenterology, Dongyang First People's Hospital, Jinhua 322100, Zhejiang Province, China
Ying Fang, Ying Cheng, Chen-Jiao Wu, Department of Endoscopy Center, First Affiliated Hospital, College of Medicine, Zhejiang University, Hangzhou 310003, Zhejiang Province, China
Author contributions: Chen LH, Zhang H, Shan GD, Li L, Fang Y, Cheng Y and Wu CJ performed the research; Xu GQ, Chen LH, Chen WG, Cao HJ, Zhang BL, Xu CF and Ding KL were involved in designing the study and editing the manuscript.
Correspondence to: Guo-Qiang Xu, MD, Department of Gastroenterology, First Affiliated Hospital, College of Medicine, Zhejiang University, Hangzhou 310003, Zhejiang Province, China. feng20081234@163.com
Telephone: +86-571-87236518 Fax: +86-571-87236611
Received: December 24, 2009 Revised: January 25, 2010
Accepted: February 1, 2010
Published online: April 7, 2010

Abstract

AIM: To evaluate the diagnostic value of double-balloon enteroscopy (DBE) for obscure gastrointestinal bleeding (OGIB).

METHODS: The data about 75 OGIB patients who underwent DBE in January 2007-June 2009 in our hospital were retrospectively analyzed.

RESULTS: DBE was successfully performed in all 75 patients without complication. Of the 75 patients, 44 (58.7%) had positive DBE findings, 22 had negative DBE findings but had potential bleeding at surgery and capsule endoscopy, *etc*. These 66 patients were finally diagnosed as OGIB which was most commonly caused by small bowel tumor (28.0%), angiodysplasia (18.7%) and Crohn's disease (10.7%). Lesions occurred more frequently in proximal small bowel than in distal small bowel (49.3% *vs* 33.3%, $P = 0.047$).

CONCLUSION: DBE is a safe, effective and accurate procedure for the diagnosis of OGIB.

Key words: Double-balloon enteroscopy; Capsule endoscopy; Obscure gastrointestinal bleeding; Diagnosis

Peer reviewers: Dr. Francesco Manguso, MD, PhD, UOC di Gastroenterologia, AORN A. Cardarelli, Via A. Cardarelli 9, Napoli 80122, Italy; Dr. Albert J Bredenoord, MD, Department of Gastroenterology, St Antonius Hospital, PO Box 2500, 3430 EM, Nieuwegein, The Netherlands; Shmuel Odes, Professor, MD, Department of Gastroenterology and Hepatology, Soroka Medical Center, PO Box 151, Beer Sheva 84101, Israel

Chen LH, Chen WG, Cao HJ, Zhang H, Shan GD, Li L, Zhang BL, Xu CF, Ding KL, Fang Y, Cheng Y, Wu CJ, Xu GQ. Double-balloon enteroscopy for obscure gastrointestinal bleeding: A single center experience in China. *World J Gastroenterol* 2010; 16(13): 1655-1659 Available from: URL: http://www.wjgnet.com/1007-9327/full/v16/i13/1655.htm DOI: http://dx.doi.org/10.3748/wjg.v16.i13.1655

INTRODUCTION

Obscure gastrointestinal bleeding (OGIB) is defined as recurrent or persistent gastrointestinal bleeding when gastric and colonic endoscopy is negative[1]. OGIB accounts for approximately 5% of all gastrointestinal bleeding events[2]. Most OGIB events are attributable to small bowel diseases.

The detection and management of small bowel bleeding are a challenge in the past due to the length and ana-

tomical position of small bowel. The diagnostic rate of conventional diagnostic strategies including small intestine radiography, abdominal computed tomography (CT), angiography, and red blood cell scan for small intestine disease is low[3]. Introduction of capsule endoscopy (CE) has significantly revolutionized the study of small bowel as it is a reliable method to evaluate the entire small bowel[4]. However, application of CE in diagnosis of OGIB is limited by the handing controllability, biopsy, endoscopic treatment, retention of capsule in stenosis intestine[5].

Etiological diagnosis of OGIB has been markedly improved with the development of double-balloon enteroscopy (DBE) since 2001[6]. DBE can be performed either through the mouth or through anus, and is thus able to explore a large part of the small bowel. DBE has the advantages including image clarity, handing controllability, biopsy, and endoscopic treatment over CE[7]. It has been demonstrated that DBE is a safe and useful procedure for the diagnosis of small intestinal disease, especially for OGIB[8]. In China, very few data are available on the diagnostic value of DBE for OGIB.

In this study, the data about 75 OGIB patients admitted to our hospital from January 2007 to June 2009 were retrospectively analyzed and the diagnostic value of DBE for OGIB was evaluated.

MATERIALS AND METHODS

Patients

DBE was performed in 75 OGIB patients (37 males, 38 females, at a mean age 51.5 ± 16.6 years, range 16-86 years) admitted to our hospital in January 2007-June 2009. Melena, hematemesis, hemafecia, and fecal occult bleeding were detected in the patients enrolled in this study. The duration of symptoms ranged 1 d-over 10 years. The main characteristics of patients are shown in Table 1. All the patients were suspected of small bowel diseases. However, standard gastric and colonic endoscopy for them was negative. Other routine methods such as CT and small intestine radiography showed no exact diagnosis of etiology.

DBE system

OGIB was detected in patients using a Fujinon enteroscope (EN450-P5/20, Fujinon Inc, Saitama, Japan) consisting of a mainframe, an enteroscope, an overtube and an air pump. Two soft latex balloons that can be inflated and deflated are attached to the tip of enteroscope and overtube. The balloons are connected to a pump through an air channel in the endoscope that can automatically modulate the air according to the different balloon pressures. By utilizing the overtube in combination with serial inflation and deflation of the balloons, endoscope can be inserted into the small bowel.

Preoperative preparation

The patients were fasted overnight and 2 boxes of polyethylene glycol electrolyte mixed with 3000 mL water were taken 4-5 h prior to DBE through anus or mouth. At the same time, 5-10 mg of midazolam and 10 mg of scopolamine butylbromide were also injected intramuscularly 10 min before DBE. The patients were anaesthetized with 10 mL of oral 2% lidocaine hydrochloride before DBE through mouth. Oxygen was inhaled with electrocardiography monitored when necessary.

Table 1 Characteristics of OGIB patients *n* (%)

Characteristics	*n* = 75
Age (yr)	51.5 ± 16.6 (16-86)
Sex (male/female)	37/38
Causes of OGIB	
Melena	45 (60.0)
Hematemesis and melena	7 (15.6)
Hemafecia	17 (22.7)
Occult bleeding	6 (8.0)
Duration of symptoms (mo)	
< 1	29 (38.7)
1-12	24 (32.0)
> 12	22 (29.3)

OGIB: Obscure gastrointestinal bleeding.

Procedure

DBE through mouth or anus was performed according to the suspected site of lesions. When the site was uncertain, DBE was performed through mouth.

DBE was not performed when the cause of bleeding could be explained, the operation time was too long to be tolerated, and more than half of the small intestine examined was negative.

Statistical analysis

Statistical analysis was performed using SPSS 11.5. Data were expressed as mean ± SD. Difference was detected by χ^2 test. $P < 0.05$ was considered statistically significant.

RESULTS

General information

DBE was performed 84 times in 75 patients, including 57 times through mouth and 27 through anus. Two patients completed DBE of the entire small bowel through mouth at one time.

All the procedures were successful without anesthesia. No hemorrhage, perforation, acute pancreatitis or other serious complications occurred. Nausea, vomiting, abdominal distension, and abdominal pain occurred in some patients during the procedure. However, these symptoms were transient and tolerable. In general, DBE through anus was more tolerable than through mouth.

DBE findings

Of the 75 patients, 44 (58.7%) had positive DBE, 22 had negative DBE with potential bleeding sites observed at surgery and CE, *etc*. The distribution of OGIB patients

Table 2 DBE findings in OGIB patients

Lesion	Diagnosed by DBE	Diagnosed by other methods	Location			Difference in proximal and distal small bowel
			Stomach and duodenum	Jejunum	Ileum	
Tumor	17	4	3	14	4	66.7% *vs* 19.0% (P = 0.002)
Gastrointestinal stromal tumor	7	1[2]	1	6[2]	1	
Non-hodgkin lymphoma	2	3	0	3	2	
Adenocarcinoma	3	0	1	1	1	
Lipoma	3	0	0	3	0	
Brunner adenoma	1	0	1	-	-	
Angioma	1	0	0	1	0	
Angiodysplasia	7	7	1	9	4	64.3% *vs* 28.6% (P = 0.128)
Crohn's disease	7	1	0	2	6	33.3% *vs* 66.7% (P = 0.132)
Diverticulum	3	2	0	4	1	
Henoch-Schönlein purpura	4[1]	0	0	2[1]	2	
Single ulcer	0	4	0	1	3	
Others	7	5	3	3	4	
Un-diagnosed	0	9	-	-	-	
Total	45	32	7	36	24	49.3% *vs* 33.3% (P = 0.047)

[1]One case was accompanied with ancylostomiasis; [2]One case was accompanied with heterotopic pancreas. DBE: Double-balloon enteroscopy.

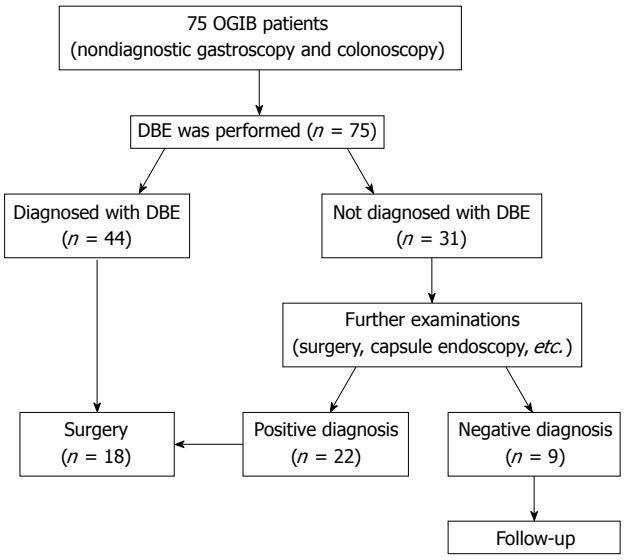

Figure 1 Distribution of obscure gastrointestinal bleeding (OGIB) patients enrolled in this study. DBE: Double-balloon enteroscopy.

enrolled in this study is shown in Figure 1. Among the 66 cases with positive DBE, OGIB was detected in upper digestive tract of 7 cases, in jejunum of 34 cases, in ileum of 24 cases, and at junction of jejunum and ileum of 1 case, respectively. The incidence of OGIB was higher in proximal small bowel (the third and fourth parts of duodenum, jejunum) than in distal small bowel (ileum) (49.3% *vs* 33.3%, P = 0.047). The DBE findings are presented in Table 2.

OGIB was most commonly caused by small bowel tumor (28.0%, 21/75), angiodysplasia (18.7%, 14/75) and Crohn's disease (10.7%, 8/75). Small bowel tumor was detected in duodenum of 3 cases, in jejunum of 14 cases, and in ileum of 4 cases, respectively. The incidence of small bowel tumor was higher in jejunum than in ileum (66.7% *vs* 19.0%, P = 0.002). Histological analysis showed that the tumor was benign in 7 cases (gastrointestinal stromal tumor in 2, lipoma in 3, duodenum adenoma in 1 and angioma in 1) and malignant in 14 cases (gastrointestinal stromal tumor in 6, non-hodgkin lymphoma in 5 and adenocarcinoma in 3) (Figure 1). The detection rate of benign tumor was lower than that of malignant tumor (33.3% *vs* 66.7%, P = 0.031).

Angiodysplasia was detected in jejunum of 9 cases, in ileum of 4 cases, and in dieulafoy of gastric fundus of 1 case, respectively, accounting for 18.7% of all the cases with no significant difference between them (P = 0.128). Crohn's disease was detected in jejunum and ileum of 2 and 6 cases, respectively, accounting for 10.7% of all the cases with no significant difference (P = 0.132). In addition, diverticulum, Henoch-Schönlein purpura, single ulcer, polyp, ancylostomiasis, tuberculosis, and nonspecific inflammation were also detected (Figure 2).

DBE detection rate of bleeding and duration of symptoms

Of the 75 cases, 45 presented with melena and 25 (55.6%) with positive DBE. Symptoms of hemafecia were detected in 17 cases with a DBE detection rate of 47.1% (8/17). There was no significant difference between the DBE detection rates of melena and hemafecia (55.6% *vs* 47.1%, P = 0.55). The DBE detection rates of occult bleeding, hematemesis and melena were not compared because of the limited number of cases.

The 75 patients were divided into 3 groups according to their bleeding time. There was no significance between the duration of OGIB symptoms and the DBE detection rates (Table 3).

Operation results

Of the 75 patients, 18 (24.0%) underwent operation. Gastrointestinal stromal tumor, non-hodgkin lymphoma, adenocarcinoma, lipoma and angioma were the most commonly detected tumors. Both gastrointestinal stromal tumor and bleeding from heterotopic pancreas were detected in 1 patient.

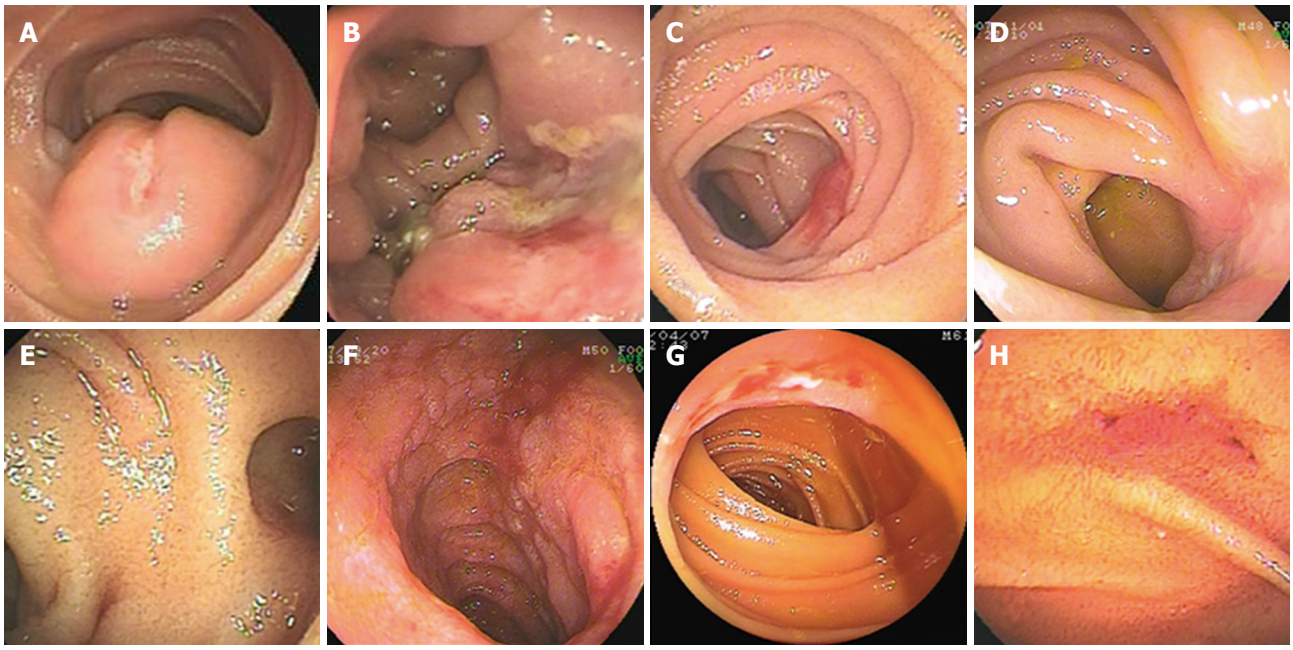

Figure 2 Typical endoscopic imaging. A: Gastrointestinal stromal tumor in jejunum; B: T cell lymphoma in jejunum; C: Angiodysplasia in jejunum; D: Crohn's disease in ileum; E: Diverticulum in jejunum; F: Henoch-Schönlein purpura in jejunum; G: Tuberculosis in ileum; H: Non-specific inflammation in jejunum.

Table 3 DBE detection rate of bleeding and duration of symptoms

	Patients	DBE findings	Detection rate (%)	*P*
Total	75	44	58.7	-
Causes of OGIB				
Melena	45	25	55.6	0.55[1]
Hematemesis and melena	7	5	71.4	-
Hemafecia	17	8	47.1	-
Occult bleeding	6	6	100.0	-
Duration of symptoms (mo)				
< 1	29	18	62.1	0.56[2]
1-12	24	13	53.8	0.74[3]
> 12	22	13	54.5	0.83[4]

[1]Difference between the DBE detection rates of melena and hemafecia; [2]Difference between the DBE detection rates of < 1 mo and 1-12 mo; [3]Difference between the DBE detection rates of 1-12 mo and > 12 mo; [4]Difference between the DBE detection rates of < 1 mo and > 12 mo.

DISCUSSION

OGIB is a common problem encountered by gastroenterologists. Its diagnostic rate has been greatly improved due to CE since 2000[9]. CE has a higher diagnostic rate of OGIB than conventional methods including small bowel barium radiography, push enteroscopy, and cross-sectional imaging[10]. However, CE may fail to identify lesions such as Meckel's diverticulum, angiodysplasia, and malignancies[11]. DBE can explore a large part of the small bowel, during which targeted tissue for biopsy can be taken. Moreover, endoscopic treatment procedures, including hemostasis, polypectomy, endoscopic mucosal resection, balloon dilation, and stent placement, can be performed at DBE[12].

In this study, the diagnostic value of DBE for OGIB was evaluated. The DBE detection rate of OGIB is consistent with the reported data[13,14]. No complication occurred in the 75 patients who underwent DBE without anesthesia, suggesting that DBE is a safe, tolerable, and effective procedure for the diagnosis of OGIB.

It was reported that 3%-6% of OGIB events are caused by small bowel tumor[15,16]. Sun *et al*[17] showed that the prevalence of gastrointestinal stromal tumor is the highest among different small bowel tumors. DBE can show lesions in about 50%-66% of the small intestine and even in the entire small intestine, thus providing a high diagnostic rate of small bowel tumor[18].

In this study, angiodysplasia was found to be another common etiology of OGIB, which is also in agreement with the reported data[19]. The detection rate of lesions was higher in jejunum than in ileum. Since Crohn's disease has been found to be the third commonest etiology of OGIB, and shows a higher incidence in distal intestine, DBE *via* anus is usually recommended[20].

The selection of DBE is still controversial. For those with no site of lesion indicated, DBE through mouth is preferred because our study and other studies showed that it has a higher diagnostic rate of lesions in proximal small bowel[21,22] and is relatively easier to perform without twisting the colon, which is also supported by Safatle-Ribeiro *et al*[23]. However, DBE through anus is also preferred by some endoscopists, since it has a better tolerance[18].

In summary, DBE is a safe, tolerable, accurate and effective procedure for the diagnosis of OGIB. OGIB is most commonly caused by small bowel tumor and angiodysplasia. Lesions occur more frequently in proximal small bowel and DBE through mouth is recommended as a prior consideration if no evidence indicates the location.

COMMENTS

Background

The diagnosis of obscure gastrointestinal bleeding (OGIB) was rather difficult in the past. Double-balloon enteroscopy (DBE) and capsule endoscopy (CE) have significantly revolutionized the diagnosis of small bowel lesions. Compared with CE, DBE has unique advantages such as handing controllability, biopsy, diagnosis and treatment, *etc*. Few data are available on the diagnostic value of DBE for OGIB.

Research frontiers

The data about 75 OGIB patients were retrospectively analyzed in this article. The DBE detection rate of OGIB and the feasibility of operation were evaluated. The incidence of common diseases in small bowel was compared. The DBE detection rate of lesions in proximal or distal small bowel was different.

Innovations and breakthroughs

Patients could tolerate the whole DBE process with no serious complication. The DBE detection rate of different bleeding events and symptoms of OGIB were compared. DBE through mouth was completed at one time.

Applications

In this study, DBE was proven to be a safe, accurate and effective procedure for the diagnosis of OGIB and can thus be performed in hospital for the diagnosis of OGIB.

Terminology

OGIB is defined as recurrent or persistent gastrointestinal bleeding when gastric and colonic endoscopy is negative. DBE and CE are both new methods enabling diagnostic endoscopy of the entire small intestine, which have their own *pros and cons* in the diagnosis of small bowel diseases.

Peer review

This is an interesting descriptive study concerning a single center experience with DBE for OGIB in China.

REFERENCES

1 American Gastroenterological Association medical position statement: evaluation and management of occult and obscure gastrointestinal bleeding. *Gastroenterology* 2000; **118**: 197-201

2 **Lewis BS**. Small intestinal bleeding. *Gastroenterol Clin North Am* 1994; **23**: 67-91

3 **Liu MK**, Yu FJ, Wu JY, Wu IC, Wang JY, Hsieh JS, Wang WM, Wu DC. Application of capsule endoscopy in small intestine diseases: analysis of 28 cases in Kaohsiung Medical University Hospital. *Kaohsiung J Med Sci* 2006; **22**: 425-431

4 **Girelli CM**, Porta P, Malacrida V, Barzaghi F, Rocca F. Clinical outcome of patients examined by capsule endoscopy for suspected small bowel Crohn's disease. *Dig Liver Dis* 2007; **39**: 148-154

5 **Rondonotti E**, Villa F, Mulder CJ, Jacobs MA, de Franchis R. Small bowel capsule endoscopy in 2007: indications, risks and limitations. *World J Gastroenterol* 2007; **13**: 6140-6149

6 **Yamamoto H**, Sekine Y, Sato Y, Higashizawa T, Miyata T, Iino S, Ido K, Sugano K. Total enteroscopy with a nonsurgical steerable double-balloon method. *Gastrointest Endosc* 2001; **53**: 216-220

7 **Matsumoto T**, Esaki M, Moriyama T, Nakamura S, Iida M. Comparison of capsule endoscopy and enteroscopy with the double-balloon method in patients with obscure bleeding and polyposis. *Endoscopy* 2005; **37**: 827-832

8 **Wu CR**, Huang LY, Song B, Yi LZ, Cui J. Application of double-balloon enteroscopy in the diagnosis and therapy of small intestinal diseases. *Chin Med J* (Engl) 2007; **120**: 2075-2080

9 **Chen X**, Ran ZH, Tong JL. A meta-analysis of the yield of capsule endoscopy compared to double-balloon enteroscopy in patients with small bowel diseases. *World J Gastroenterol* 2007; **13**: 4372-4378

10 **Triester SL**, Leighton JA, Leontiadis GI, Fleischer DE, Hara AK, Heigh RI, Shiff AD, Sharma VK. A meta-analysis of the yield of capsule endoscopy compared to other diagnostic modalities in patients with obscure gastrointestinal bleeding. *Am J Gastroenterol* 2005; **100**: 2407-2418

11 **Li XB**, Ge ZZ, Dai J, Gao YJ, Liu WZ, Hu YB, Xiao SD. The role of capsule endoscopy combined with double-balloon enteroscopy in diagnosis of small bowel diseases. *Chin Med J* (Engl) 2007; **120**: 30-35

12 **Kita H**, Yamamoto H, Yano T, Miyata T, Iwamoto M, Sunada K, Arashiro M, Hayashi Y, Ido K, Sugano K. Double balloon endoscopy in two hundred fifty cases for the diagnosis and treatment of small intestinal disorders. *Inflammopharmacology* 2007; **15**: 74-77

13 **Nakamura M**, Niwa Y, Ohmiya N, Miyahara R, Ohashi A, Itoh A, Hirooka Y, Goto H. Preliminary comparison of capsule endoscopy and double-balloon enteroscopy in patients with suspected small-bowel bleeding. *Endoscopy* 2006; **38**: 59-66

14 **Heine GD**, Hadithi M, Groenen MJ, Kuipers EJ, Jacobs MA, Mulder CJ. Double-balloon enteroscopy: indications, diagnostic yield, and complications in a series of 275 patients with suspected small-bowel disease. *Endoscopy* 2006; **38**: 42-48

15 **Pilleul F**, Penigaud M, Milot L, Saurin JC, Chayvialle JA, Valette PJ. Possible small-bowel neoplasms: contrast-enhanced and water-enhanced multidetector CT enteroclysis. *Radiology* 2006; **241**: 796-801

16 **Delvaux M**, Fassler I, Gay G. Clinical usefulness of the endoscopic video capsule as the initial intestinal investigation in patients with obscure digestive bleeding: validation of a diagnostic strategy based on the patient outcome after 12 months. *Endoscopy* 2004; **36**: 1067-1073

17 **Sun B**, Rajan E, Cheng S, Shen R, Zhang C, Zhang S, Wu Y, Zhong J. Diagnostic yield and therapeutic impact of double-balloon enteroscopy in a large cohort of patients with obscure gastrointestinal bleeding. *Am J Gastroenterol* 2006; **101**: 2011-2015

18 **Yamamoto H**, Kita H, Sunada K, Hayashi Y, Sato H, Yano T, Iwamoto M, Sekine Y, Miyata T, Kuno A, Ajibe H, Ido K, Sugano K. Clinical outcomes of double-balloon endoscopy for the diagnosis and treatment of small-intestinal diseases. *Clin Gastroenterol Hepatol* 2004; **2**: 1010-1016

19 **Schäfer C**, Rothfuss K, Kreichgauer HP, Stange EF. Efficacy of double-balloon enteroscopy in the evaluation and treatment of bleeding and non-bleeding small bowel disease. *Z Gastroenterol* 2007; **45**: 237-243

20 **Mehdizadeh S**, Han NJ, Cheng DW, Chen GC, Lo SK. Success rate of retrograde double-balloon enteroscopy. *Gastrointest Endosc* 2007; **65**: 633-639

21 **Descamps C**, Schmit A, Van Gossum A. "Missed" upper gastrointestinal tract lesions may explain "occult" bleeding. *Endoscopy* 1999; **31**: 452-455

22 **Hayat M**, Axon AT, O'Mahony S. Diagnostic yield and effect on clinical outcomes of push enteroscopy in suspected small-bowel bleeding. *Endoscopy* 2000; **32**: 369-372

23 **Safatle-Ribeiro AV**, Kuga R, Ishida R, Furuya C, Ribeiro U Jr, Cecconello I, Ishioka S, Sakai P. Is double-balloon enteroscopy an accurate method to diagnose small-bowel disorders? *Surg Endosc* 2007; **21**: 2231-2236

S- Editor Tian L **L- Editor** Wang XL **E- Editor** Zheng XM

World Journal of Gastroenterology

Online Submissions: http://www.wjgnet.com/1007-9327office
wjg@wjgnet.com
doi:10.3748/wjg.v16.i13.1660

World J Gastroenterol 2010 April 7; 16(13): 1660-1664
ISSN 1007-9327 (print)

BRIEF ARTICLE

Porcine hepatocyte isolation and reversible immortalization mediated by retroviral transfer and site-specific recombination

Fan-Ying Meng, Zhi-Shui Chen, Meng Han, Xin-Peng Hu, Xing-Xing He, Yong Liu, Wen-Tao He, Wei Huang, Hui Guo, Ping Zhou

Fan-Ying Meng, Zhi-Shui Chen, Meng Han, Xin-Peng Hu, Yong Liu, Wen-Tao He, Wei Huang, Hui Guo, Ping Zhou, Key Laboratory of Organ Transplantation, Ministry of Education, Ministry of Health, Institute of Organ Transplantation, Tongji Hospital, Tongji Medical College, Huazhong University of Science and Technology, Wuhan 430030, Hubei Province, China
Xing-Xing He, Institute of Liver Diseases, Tongji Hospital of Tongji Medical College, Huazhong University of Science and Technology, Wuhan 430030, Hubei Province, China
Author contributions: Meng FY, Chen ZS and Zhou P designed the study; Meng FY, Han M, Hu XP, He XX, Liu Y and He WT performed the majority of experiments; Guo H and Huang W provided vital reagents and analytical tools; Meng FY wrote the manuscript.
Supported by The Major Scientific and Technological Project of Hubei Province, No. 2007ABD005
Correspondence to: Ping Zhou, MD, PhD, Institute of Organ Transplantation, Tongji Hospital, Tongji Medical University, Huazhong University of Science and Technology, Wuhan 430030, Hubei Province, China. pzhou57@tjh.tjmu.edu.cn
Telephone: +86-27-83662655 Fax: +86-27-83662892
Received: March 9, 2009 Revised: December 20, 2009
Accepted: December 27, 2009
Published online: April 7, 2010

Abstract

AIM: To develop a hepatocyte cell line, we immortalized primary porcine hepatocytes with a retroviral vector SSR#69 containing the Simian Virus 40 T antigen (*SV40T*ag).

METHODS: We first established a method of porcine hepatocyte isolation with a modified four-step retrograde perfusion technique. Then the porcine hepatocytes were immortalized with retroviral vector SSR#69 expressing *SV40T* and hygromycin-resistance genes flanked by paired loxP recombination targets. *SV40T* cDNA in the expanded cells was subsequently excised by Cre/LoxP site-specific recombination.

RESULTS: The resultant hepatocytes with high viability (97%) were successfully immortalized with retroviral vector SSR#69. One of the immortalized clones showed the typical morphological appearance, TJPH-1, and was selected by clone rings and expanded in culture. After excision of the *SV40T* gene with Cre-recombinase, cells stopped growing. The population of reverted cells exhibited the characteristics of differentiated hepatocytes.

CONCLUSION: In conclusion, we herein describe a modified method of hepatocyte isolation and subsequently established a porcine hepatocyte cell line mediated by retroviral transfer and site-specific recombination.

Key words: Hepatocyte isolation; Porcine hepatocytes; Reversible immortalization; Simian virus 40 large T-antigen

Peer reviewers: Dean Y Kim, MD, Surgical Director, Department of Kidney and Pancreas Transplantation, Division of Hepatobiliary and Transplant Surgery, Henry Ford Hospital, 2799 W. Grand Blvd., Detroit, MI 48202, United States; Seong Gyu Hwang, MD, Professor, Department of Internal Medicine, CHA Bundang Medical Center, CHA University, #351, Yatap-Dong, Bundang-Gu, Seongnam, Gyeonggi-Do, 463-712, South Korea

Meng FY, Chen ZS, Han M, Hu XP, He XX, Liu Y, He WT, Huang W, Guo H, Zhou P. Porcine hepatocyte isolation and reversible immortalization mediated by retroviral transfer and site-specific recombination. *World J Gastroenterol* 2010; 16(13): 1660-1664 Available from: URL: http://www.wjgnet.com/1007-9327/full/v16/i13/1660.htm DOI: http://dx.doi.org/10.3748/wjg.v16.i13.1660

INTRODUCTION

A virtually unlimited supply of hepatocytes for metabolic studies, bio-artificial livers and cell transplantation would be highly desirable[1,2]. However, the utility of cultured hepatocytes is hampered by difficulties in timely obtained populations of primary cells, which have a limited life span *in vitro*. An attractive alternative source of hepatocytes would be immortalized cells which could make unlimited supplies of cells feasible and exhibit the characteristics of differentiated hepatocytes[3]. A series of studies have developed the strategy of cell immortalization[4,5]. However, the oncogene in the immortalized hepatocytes would expose patients to an unacceptable tumorigenic risk. An attractive solution for this problem could be the use of a novel strategy of reversible immortalization by using Cre/loxP site-specific recombination[6]. It has been reported that Cre/loxP recombination operates efficiently in primary cells[7]. The procedure of reversible immortalization was devised by retrovirus-mediated transfer of an oncogene that can be subsequently effectively excised by site-specific recombination[8].

A series of cells can be immortalized by retrovirus-mediated transfer of an immortalizing oncogene (*SV40T*)[9]. Although the hepatocytes can be transduced with retroviral vectors, the efficiency of transduction is significantly low[10]. In the process to successfully and effectively transduce retroviral vectors into hepatocytes, establishing an efficient technique of cell isolation seems to be meaningful.

To address these issues, we herein report an efficient procedure for porcine hepatocyte isolation, and subsequent successful immortalization by retrovirus-mediated transfer of *SV40T* which could be subsequently excised by Cre/LoxP-mediated site-specific recombination. The present study expands the strategy of hepatocyte reversible immortalization and represents an important step toward the development of immortalization of hepatocytes.

MATERIALS AND METHODS

Animals

A mini-pig weighing 13 kg was used in the present study. All procedures performed on the pig were approved by Tongji Medical College Animal Care and Use Committee and were within the guidelines for laboratory animals.

Porcine hepatocyte isolation

Porcine hepatocytes were isolated from a surgically resected liver segment with a modified four-step retrograde perfusion technique using dispase and collagenase (Figure 1). Briefly, the resected liver sample (47 g) was cannulated with a suitable pipette into the visible blood vessel on the cut surface (Figure 2A). Then the sample was flushed with a 500 mL calcium-free buffer solution (Step 1), 500 mL EDTA in buffer solution (Step 2) and another 500 mL of buffer solution at 37℃. Continuous recirculating perfusion was then carried out on the tissue using a pre-warmed

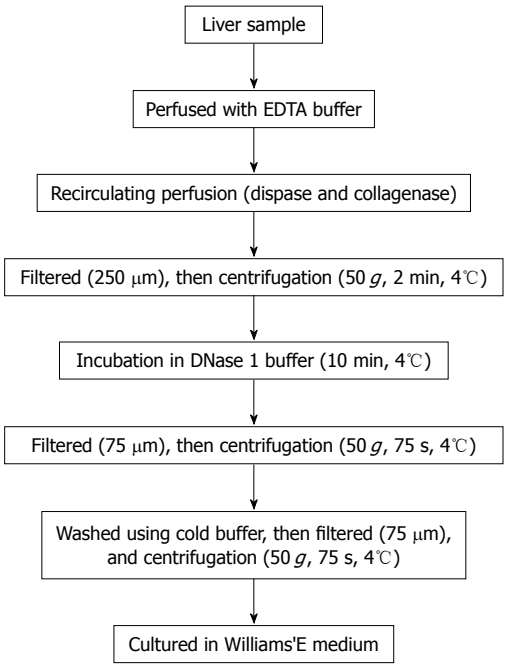

Figure 1 Flow diagram of the preparation of isolated hepatocytes with a modified four-step retrograde perfusion technique.

digestion buffer solution (8.4 g/L dispase Ⅱ and 0.5 g/L collagenase Ⅳ, Sigma, St. Louis, MO, USA) at 37℃ (Step 3). When digestion of the parenchyma was visualized, the liver tissue was finally flushed with 500 mL buffer solution (Step 4). Following sufficient digestion, the liver capsule was mechanically disrupted and the emerging cell suspension filtered through 250 μm nylon mesh and centrifuged (50 g, 2 min, 4℃). After that we employed a cell incubation step of 10 min using DNase1 (Sigma, St. Louis, MO, USA) containing buffer solution, during which cell clumps were broken up and damaged cells digested. Then, the resulting suspension was filtered through 75 μm nylon mesh, and the cells were harvested by low speed centrifugation at 50 g for 75 s. This was followed by washes using cold buffer solution and filtration through 75 μm nylon mesh and another centrifugation step (50 g, 75 s, 4℃). The resulting cell clumps were finally resuspended in culture medium (William's medium E, supplemented with 100 mU/mL penicillin, 100 μg/mL streptomycin and 10% fetal bovine serum). Hepatocyte yield and viability was determined using the standard trypan blue exclusion technique. Freshly isolated hepatocytes were seeded at a concentration of 4×10^5 per milliliter in culture flasks. The morphology of the cultured hepatocytes was assessed with a Nikon Diaphot inverted microscope at a magnification of 100 ×.

Porcine hepatocytes immortalization

The retroviral vector SSR#69 (kindly given by Naoya Kobayashi, Okayama University) containing SV40 large TAG and a gene resistant to hygromycin (Figure 3) was cultured in DMEM medium (Sigma, St. Louis, MO, USA) supplemented with 10% newborn calf serum. Freshly isolated primary porcine hepatocytes were transduced with 2 mL of SSR#69 cells supernatant per T25 flask at

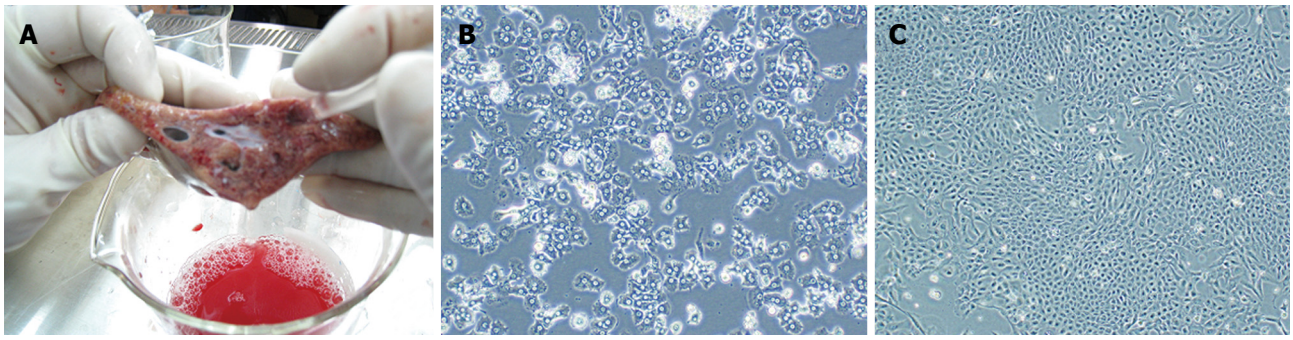

Figure 2 Isolation technique and microscopic appearance of primary and immortalized porcine hepatocytes. A: Perfusion was conducted by inserting a suitable pipette into vessels exposed on a cut surface of the sample; B: Non-immortalized primary porcine hepatocytes grow slowly with low plating efficiency and a short life span; C: Immortalized porcine hepatocytes grow rapidly as islands and had an extended life span. Magnifications: B and C 100 ×.

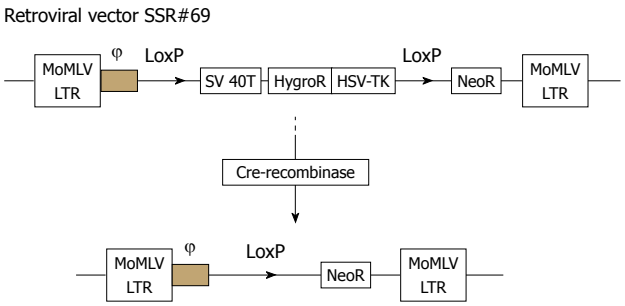

Figure 3 Schematic drawings of the integrating component of retroviral vector SSR#69 before and after Cre-recombination. SSR#69 contains the *hygromycin B resistance* gene (*Hyg R*) as a positive selectable marker and the *herpes simplex virus thymidine kinase* gene (*HSV-TK*) as a negative selectable marker. The *SV40T*, *Hyg R* and *HSV-TK* genes are flanked by loxP sites.

37℃ for 12 h each day for 5 d. Two days after the final transduction, selection was applied with 100 μg/mL hygromycin. After two weeks hygromycin selection, colonies of transduced hepatocytes emerged. One of the colonies displayed morphological characteristics of the primary hepatocytes, TJPH-1, and was isolated by cloning rings and expanded in culture. Finally, *SV40T* cDNA in the expanded cells was excised by Cre/loxP site-specific recombination.

Immunofluorescent analysis of SV40T antigen (SV40Tag) in immortalized cells

For detection of *SV40T*ag, indirect immunofluorescent staining was performed, using mouse monoclonal immunoglobulin G antibody to *SV40T*ag (Santa Cruz Biotechnology; Santa Cruz, CA, USA) and the second antibody, rhodamine (TRITC)-conjugated sheep anti-mouse IgG (Sigma, St. Louis, MO, USA). DAPI (4',6-diamidine-2'-phenylindole dihydrochloride, Roche, Cat. No. 10236276001) blue-fluorescent dye was used for staining nuclei (double-stranded DNA).

Gene expression of liver-specific functions in immortalized cells

Total RNA was extracted from immortalized cells and reverse transcription-polymerase chain reaction (RT-PCR) was performed according to the manufacturer's protocol. Primers used were as follows: *SV40T* (422 base pair, bp), CAGGCATAGAGTGTCTGC (5'primer), CAACAGCCTGTTGGCATATG (3'primer); porcine albumin (324 bp), CTTATTCCAGGGGTCTGTTTC (5'primer) and TCGTTTCTCTCAGGCTCTTCT (3'primer); porcine GAPDH (179 bp), CATCATCCCTGCTTCTACCG (5'primer), CCTGCTTCACCACTTTCTTG (3'primer).

RESULTS

Successful porcine hepatocytes isolation resulted in a cell yield of 1.05×10^7 cells/g liver. The viability of hepatocytes immediately after isolation, using the trypan blue exclusion technique, was 97%. The primary hepatocytes attached to the plates showed typical morphological appearance with a polygonal shape, granular cytoplasm and one or more nuclei (Figure 2B).

After transfection of porcine hepatocytes with *SV40T*, several clones (Figure 2C) grew steadily in the culture medium within 2 wk after 100 μg/mL hygromycin selection. One of the surviving cell colonies, TJPH-1, isolated by cloning rings displayed morphological characteristics of primary hepatocytes featuring a large round nucleus with a few nucleoli and multiple granules in the cytoplasm. After treatment with Cre recombinase, the expanded TJPH-1 cells reverted to their pre-immortalized state. The reverted cells lost expression of *SV40T* (Figure 4), resulting in loss of proliferation.

The *SV40T*ag was examined by immunofluorescent staining in the nuclei of all immortalized cells, as shown in Figure 5A. Immortalized and reverted cells expressed the albumin gene shown by RT-PCR, similar to normal porcine hepatocytes (Figure 4).

DISCUSSION

Cultured primary porcine hepatocytes provide a valuable tool for various research strategies and clinical applications, such as studying the regulation of cell growth and of certain differentiated hepatocyte functions and BAL (bioartificial liver) systems[11,12]. However, the utility of cultured hepatocytes is hampered by difficulties in obtaining populations of primary cells which cannot be expanded *in vitro*.

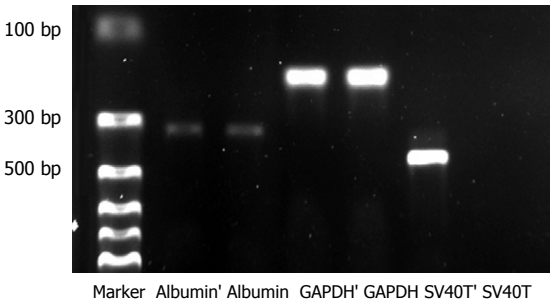

Figure 4 Gene expression of liver-specific functions in immortalized and reverted cells. Lines 1 to 7, from left to right, Marker, Albumin' (immortalized hepatocytes), Albumin (reverted hepatocytes), GAPDH' (immortalized hepatocytes), GAPDH (reverted hepatocytes), *SV40T'* (immortalized hepatocytes), *SV40T* (reverted hepatocytes), respectively.

Thus, other alternative sources of hepatocytes have to be explored[13]. Hepatocytes immortalized with a *SV40T*ag can make unlimited supplies of cells feasible. However, the continued presence of a *SV40T*ag in the immortalized hepatocytes would expose patients to an unacceptable tumorigenic risk. To surmount this hurdle, we herein established reversible immortalized porcine hepatocytes to intentionally control population expansion (Figure 5). Use of the Cre/LoxP-based reversible immortalization strategy represents an important step in the development of a potentially novel strategy for resolving the current limits of primary hepatocytes[2]. Different from a general gene transfer strategy, the novel strategy of reversible immortalization allows temporary expansion of cell populations by transfer of an oncogene which can be subsequently excised by site-specific recombination. Several studies have confirmed the utility, safety and efficiency of the reversible immortalization procedure[14]. This novel procedure has extended to several cell types, such as liver endothelial cells[15], hepatic stellate cells[16] and rat hepatocytes[17]. The present study expands the work to primary porcine hepatocytes.

Although porcine hepatocytes can be immortalized by retrovirus-mediated transfer of *SV40T*, the efficiency of transduction was significantly low[10]. A major challenge of successful transduction is represented by the availability of a sufficient amount of hepatocytes with high post-isolation viability. Thus, in the process to successfully and effectively transduce retroviral vectors into primary hepatocytes, establishing an efficient cell isolation technique would be meaningful.

Hepatocyte isolation started in the mid-1960s, when rat hepatocytes were isolated using a combined mechanical/enzymatic digestion technique[18]. It was not until 1976, when Seglen[19] introduced the two-step collagenase perfusion technique, that high-yield preparation of isolated intact hepatocytes was available. After that, different innovative techniques have been introduced to further improve isolation results[20,21]. In this study, we established a modified four-step collagenase retrograde perfusion technique. The modified four-step method of hepatocyte isolation, compared to the traditional two-step method, can

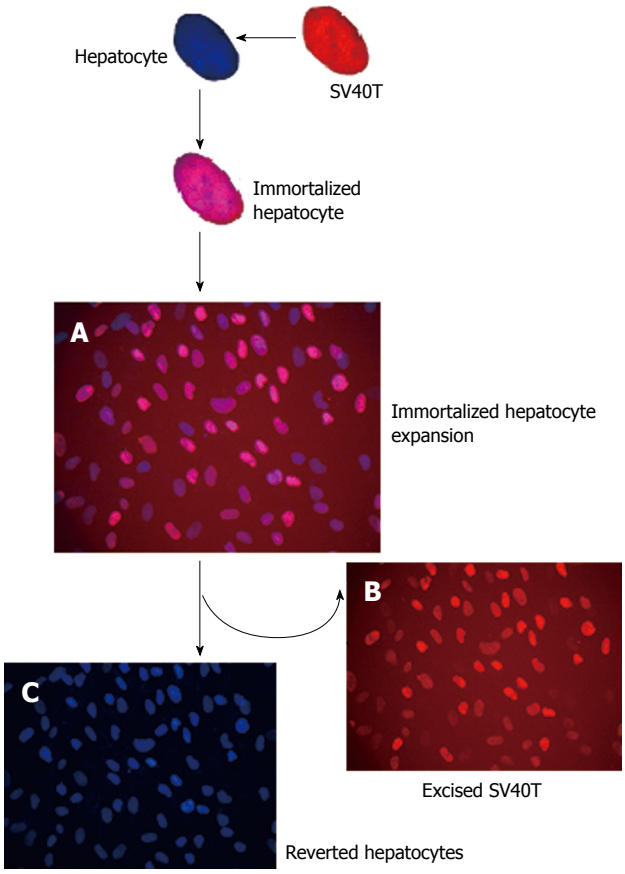

Figure 5 Scheme of reversible immortalization. The primary porcine hepatocytes were immortalized by transfer of an oncogene (*SV40T*). After expansion of the immortalized cells, Cre/loxP recombination was performed to remove the oncogene (*SV40T*) and the cells reverted to their pre-immortalized state. (A-C) Double immunofluorescence of immortalized hepatocytes stained with DAPI (blue), which binds, together with monoclonal antibody anti-*SV40T* revealed with texas red-antibody conjugate (red). Blue and red fluorescence merged as purple. *SV40T* expression is revealed by intense staining of the cell nucleus.

result in an improvement in cell viability and yield[22]. After cell isolation, we employed an incubation step of 10 min using DNase 1, during which cell clumps were broken up and damaged cells digested. This method resulted in a hepatocyte yield of 1.05×10^7 cells/g liver. The viability of the cells, using the trypan blue exclusion technique, was 97%.

In summary, we propose that the modified four-step technique would improve research results, allowing large-scale production of hepatocytes of high quality. Furthermore, the present study expanded the novel strategy of reversible immortalization to primary porcine hepatocytes. By permitting temporary and controlled expansion of hepatocyte populations, the reversible immortalized cells may therefore be used for various research strategies and clinical applications.

ACKNOWLEDGMENTS

We thank Dr. Naoya Kobayashi (Okayama University Graduate School of Medicine and Dentistry) for providing SSR#69 cells.

COMMENTS

Background

The limited lifespan of porcine hepatocytes is a major hurdle to their use. Furthermore, the functional activities of primary porcine hepatocytes decline rapidly after several days in culture. An attractive alternative source of liver cells would be reversible immortalized cells that could make unlimited supplies of cells feasible which would exhibit the characteristics of differentiated hepatocytes. Toward this goal, the authors have focused on reversible immortalization by using Cre/loxP site-specific recombination.

Research frontiers

Cre/loxP site-specific recombination was used to reversibly induce the proliferation of primary cells. A reversible immortalization system using the Cre-loxP site-specific recombination system has been widely used in establishing immortalized cell lines.

Innovations and breakthroughs

The authors described a modified four-step retrograde perfusion technique of hepatocyte isolation and subsequently established a porcine hepatocyte cell line mediated by retroviral transfer and site-specific recombination.

Applications

The modified four-step retrograde perfusion technique would improve research results, allowing large-scale production of hepatocytes of high quality. Furthermore, the present study expanded the novel strategy of reversible immortalization to primary porcine hepatocytes. This reversible immortalized cell line could provide an unlimited supply of cells for research and clinical use.

Terminology

Reversible immortalization: The procedure of reversible immortalization was devised by retrovirus-mediated transfer of an oncogene that can be subsequently effectively excised by site-specific recombination.

Peer review

This manuscript appears to be about two separate, but related topics of hepatocyte isolation and "reversible immortalization". In my opinion, by combining the two topics, it weakens the manuscript. It appears they were able to reproduce techniques described by others, which is good.

REFERENCES

1 **Pan T**, Cai M, Tang L, Zhou LQ, Li BJ, Zhu T, Li HZ, Li SY, Xiao X, Chen ZS. A novel approach of prophylaxis to HBV recurrence after liver transplantation. *Virology* 2008; **382**: 1-9

2 **Kobayashi N**, Okitsu T, Tanaka N. Cell choice for bioartificial livers. *Keio J Med* 2003; **52**: 151-157

3 **Totsugawa T**, Yong C, Rivas-Carrillo JD, Soto-Gutierrez A, Navarro-Alvarez N, Noguchi H, Okitsu T, Westerman KA, Kohara M, Reth M, Tanaka N, Leboulch P, Kobayashi N. Survival of liver failure pigs by transplantation of reversibly immortalized human hepatocytes with Tamoxifen-mediated self-recombination. *J Hepatol* 2007; **47**: 74-82

4 **Fujii S**, Maeda H, Wada N, Kano Y, Akamine A. Establishing and characterizing human periodontal ligament fibroblasts immortalized by SV40T-antigen and hTERT gene transfer. *Cell Tissue Res* 2006; **324**: 117-125

5 **Kobayashi N**. Artificial cells for the development of cell therapy. *Cell Transplant* 2008; **17**: 3-9

6 **Chapdelaine P**, Kang J, Boucher-Kovalik S, Caron N, Tremblay JP, Fortier MA. Decidualization and maintenance of a functional prostaglandin system in human endometrial cell lines following transformation with SV40 large T antigen. *Mol Hum Reprod* 2006; **12**: 309-319

7 **Westerman KA**, Leboulch P. Reversible immortalization of mammalian cells mediated by retroviral transfer and site-specific recombination. *Proc Natl Acad Sci USA* 1996; **93**: 8971-8976

8 **Kobayashi N**, Fujiwara T, Westerman KA, Inoue Y, Sakaguchi M, Noguchi H, Miyazaki M, Cai J, Tanaka N, Fox IJ, Leboulch P. Prevention of acute liver failure in rats with reversibly immortalized human hepatocytes. *Science* 2000; **287**: 1258-1262

9 **Narushima M**, Kobayashi N, Okitsu T, Tanaka Y, Li SA, Chen Y, Miki A, Tanaka K, Nakaji S, Takei K, Gutierrez AS, Rivas-Carrillo JD, Navarro-Alvarez N, Jun HS, Westerman KA, Noguchi H, Lakey JR, Leboulch P, Tanaka N, Yoon JW. A human beta-cell line for transplantation therapy to control type 1 diabetes. *Nat Biotechnol* 2005; **23**: 1274-1282

10 **Adams RM**, Soriano HE, Wang M, Darlington G, Steffen D, Ledley FD. Transduction of primary human hepatocytes with amphotropic and xenotropic retroviral vectors. *Proc Natl Acad Sci USA* 1992; **89**: 8981-8985

11 **He XX**, Chen T, Lin JS, Chang Y, Ye BX. Inhibition of the replication of hepatitis B virus in vitro by a novel 2,6-diaminopurine analog, beta-LPA. *Biochem Biophys Res Commun* 2008; **369**: 513-518

12 **Nyberg SL**, Hardin J, Amiot B, Argikar UA, Remmel RP, Rinaldo P. Rapid, large-scale formation of porcine hepatocyte spheroids in a novel spheroid reservoir bioartificial liver. *Liver Transpl* 2005; **11**: 901-910

13 **Meng FY**, Chen ZS, Han M, Hu XP, Zhou P. An improved purification approach with high cell viability and low cell loss for cryopreserved hepatocytes. *Cryobiology* 2010; **60**: 238-239

14 **Matsumura T**, Takesue M, Westerman KA, Okitsu T, Sakaguchi M, Fukazawa T, Totsugawa T, Noguchi H, Yamamoto S, Stolz DB, Tanaka N, Leboulch P, Kobayashi N. Establishment of an immortalized human-liver endothelial cell line with SV40T and hTERT. *Transplantation* 2004; **77**: 1357-1365

15 **Noguchi H**, Kobayashi N, Westerman KA, Sakaguchi M, Okitsu T, Totsugawa T, Watanabe T, Matsumura T, Fujiwara T, Ueda T, Miyazaki M, Tanaka N, Leboulch P. Controlled expansion of human endothelial cell populations by Cre-loxP-based reversible immortalization. *Hum Gene Ther* 2002; **13**: 321-334

16 **Watanabe T**, Shibata N, Westerman KA, Okitsu T, Allain JE, Sakaguchi M, Totsugawa T, Maruyama M, Matsumura T, Noguchi H, Yamamoto S, Hikida M, Ohmori A, Reth M, Weber A, Tanaka N, Leboulch P, Kobayashi N. Establishment of immortalized human hepatic stellate scavenger cells to develop bioartificial livers. *Transplantation* 2003; **75**: 1873-1880

17 **Cai J**, Ito M, Westerman KA, Kobayashi N, Leboulch P, Fox IJ. Construction of a non-tumorigenic rat hepatocyte cell line for transplantation: reversal of hepatocyte immortalization by site-specific excision of the SV40 T antigen. *J Hepatol* 2000; **33**: 701-708

18 **Howard RB**, Christensen AK, Gibbs FA, Pesch LA. The enzymatic preparation of isolated intact parenchymal cells from rat liver. *J Cell Biol* 1967; **35**: 675-684

19 **Seglen PO**. Preparation of isolated rat liver cells. *Methods Cell Biol* 1976; **13**: 29-83

20 **Müller P**, Aurich H, Wenkel R, Schäffner I, Wolff I, Walldorf J, Fleig WE, Christ B. Serum-free cryopreservation of porcine hepatocytes. *Cell Tissue Res* 2004; **317**: 45-56

21 **Vondran FW**, Katenz E, Schwartlander R, Morgul MH, Raschzok N, Gong X, Cheng X, Kehr D, Sauer IM. Isolation of primary human hepatocytes after partial hepatectomy: criteria for identification of the most promising liver specimen. *Artif Organs* 2008; **32**: 205-213

22 **Baccarani U**, Sanna A, Cariani A, Sainz-Barriga M, Adani GL, Zambito AM, Piccolo G, Risaliti A, Nanni-Costa A, Ridolfi L, Scalamogna M, Bresadola F, Donini A. Isolation of human hepatocytes from livers rejected for liver transplantation on a national basis: results of a 2-year experience. *Liver Transpl* 2003; **9**: 506-512

S- Editor Wang JL **L- Editor** Webster JR **E- Editor** Ma WH

World Journal of Gastroenterology

Online Submissions: http://www.wjgnet.com/1007-9327office
wjg@wjgnet.com
doi:10.3748/wjg.v16.i13.1665

World J Gastroenterol 2010 April 7; 16(13): 1665-1669
ISSN 1007-9327 (print)

CASE REPORT

Over-the-scope clip closure of two chronic fistulas after gastric band penetration

Federico Iacopini, Nicola Di Lorenzo, Fabrizio Altorio, Marc-Oliver Schurr, Agostino Scozzarro

Federico Iacopini, Agostino Scozzarro, Gastroenterology and Endoscopy Unit, Ospedale San Giuseppe, Albano Laziale, Roma 00041, Italy
Nicola Di Lorenzo, Fabrizio Altorio, Department of Surgical Science, Policlinico Università di Tor Vergata, Roma 00173, Italy
Marc-Oliver Schurr, Steinbeis University Berlin, IHCI-Institute, Tuebingen D-72076, Germany
Author contributions: Iacopini F, Di Lorenzo N, Altorio F and Scozzarro A contributed to this work; Iacopini F analyzed data and wrote the paper; Schurr MO revised the paper.
Correspondence to: Agostino Scozzarro, MD, Gastroenterology and Endoscopy Unit, Ospedale San Giuseppe, Via dell' Olivella, Albano Laziale, Rome 00041, Italy. a.scozzarro@virgilio.it
Telephone: +39-6-93273938 Fax: +39-6-93273216
Received: October 19, 2009 Revised: November 17, 2009
Accepted: November 24, 2009
Published online: April 7, 2010

Abstract

Gastrointestinal perforations are conservatively managed at endoscopy by through-the-scope endoclips and covered self expandable stents, according to the size and tissue features of the perforation. This is believed to be the first report of successful closure of two gastrocutaneous fistulas with over-the-scope clips (OTSCs). After laparoscopic gastric banding, a 45-year old woman presented with band erosion and penetration. Despite surgical band removal and gastric wall suturing, external drainage of enteric material persisted for 2 wk, and esophagogastroduodenoscopy demonstrated two adjacent 10-mm and 15-mm fistulous orifices at the esophagogastric junction. After cauterization of the margins, the 10-mm fistulous tract was grasped by the OTSC anchor, invaginated into the applicator cap, and closed by a traumatic OTSC. The other 15-mm fistula was too large to be firmly grasped, and a fully-covered metal stent was temporarily placed. No leak occurred during the following 6 wk. At stent removal: the OTSC was completely embedded in hyperplastic overgrowth; the 15-mm fistula significantly reduced in diameter, and it was closed by another traumatic OTSC. After the procedure, no external fistula recurred and both OTSCs were lost spontaneously after 4 wk. The use of the anchor and the OTSC seem highly effective for successful closure of small chronic perforations.

Key words: Gastrointestinal endoscopy; Fistula; Stent; Esophagogastric junction

Peer reviewer: Klaus R Herrlinger, MD, Department of Gastroenterology, Hepatology and Endocrinology, Robert-Bosch-Hospital, Auerbachstrasse, 110, D-70376 Stuttgart, Germany

Iacopini F, Di Lorenzo N, Altorio F, Schurr MO, Scozzarro A. Over-the-scope clip closure of two chronic fistulas after gastric band penetration. *World J Gastroenterol* 2010; 16(13): 1665-1669 Available from: URL: http://www.wjgnet.com/1007-9327/full/v16/i13/1665.htm DOI: http://dx.doi.org/10.3748/wjg.v16.i13.1665

INTRODUCTION

Gastrointestinal (GI) perforations require prompt closure and control of extraluminal fluid collections and sepsis. They have been managed traditionally by surgery[1-3], but a conservative endoscopic approach has recently been preferred with the advantages of negligible morbidity and mortality, a short hospital stay, and the possibility of prompt resumption of an oral diet[2,4-6].

Routine endoscopic methods to close GI perforations are endoclips and covered self-expandable stents; the choice being related to the width and tissue features of the margins[7,8]. Endoclips are metallic double-pronged clips loaded on a deployment catheter introduced through the operative channel of the scope [through-the-

scope (TTS) clips][7]. Although acute small (< 15 mm) perforations can be successfully closed with TTS clips[9], these devices achieve controversial results when used for larger perforations[10,11], and seem technically inadequate for chronic perforations, due to poor grasping ability and insufficient strength to close fibrotic margins[7]. Therefore, TTS clips have rarely closed chronic leaks[12-17] and are generally considered only as a supplementary technique[8].

Covered self-expandable metal stents (SEMSs) or self-expandable plastic stents (SEPSs) are an effective method for sealing and healing more than 80% of chronic GI leaks, but have drawbacks: the removal of partially-covered SEMSs may be difficult due to the ingrowth at uncovered ends and the risk of mucosal tears, hemorrhage and subcutaneous emphysema[4,18,19], whereas fully-covered stents show a migration rate of up to 50% and often require replacement[6,20,21].

The present case is the first successful closure of two gastro-cutaneous fistulas with the newly designed over-the-scope-clip (OTSC) (Ovesco Endoscopy, Tubingen, Germany).

CASE REPORT

Twenty-six months after laparoscopic gastric banding, a 45-year-old woman presented severe epigastric pain. The diagnosis of band erosion with penetration through two large tears at the posterior wall of the gastric fundus was established by esophagogastroduodenoscopy (EGD), and a subphrenic abscess was demonstrated by computed tomography (CT). Management included surgical band removal, suturing of the gastric wall with two omental patches, and abdominal drainage.

However, external drainage of enteric material persisted for 2 wk and the barium swallow revealed two fistulas at the esophagogastric junction (Figure 1). EGD showed two opposite perforations of 10 and 15 mm (Figure 2), with fistulous tracts partially and fully negotiable by the 9.8-mm endoscope, respectively.

After cauterization of the margins, the proximal segment of the 10-mm fistula was grasped by the OTSC anchor, invaginated into the applicator cap (Figure 3A), and closed by a 9-mm traumatic OTSC (Ovesco Endoscopy GmbH, Tuebingen, Germany) (Figure 3B). On the contrary, the 15-mm fistula was too wide to be firmly grasped by the anchor and therefore it was closed with a fully-covered esophageal self-expandable metal stent (SEMS; Niti-S, Taewoong, South Korea), which also covered the OTSC.

The barium swallow performed after 24 h confirmed the complete sealing of both fistulas (Figure 3C) and the patient was discharged on an oral diet.

After 6 wk, the fully-covered SEMS was easily removed, and the EGD showed that the OTSC was buried into an intense overgrowth reaction (Figure 4). The 15-mm fistula diameter was reduced to 8 mm, and therefore it was sealed by a second 9-mm traumatic OTSC (Figure 5).

During the following 8 wk, no external fistula or abdominal collection was observed by barium swallow (Figure 6) or the dye leak test with methylene blue. Both OTSCs were lost within the second and fourth weeks of follow-up after SEMS removal.

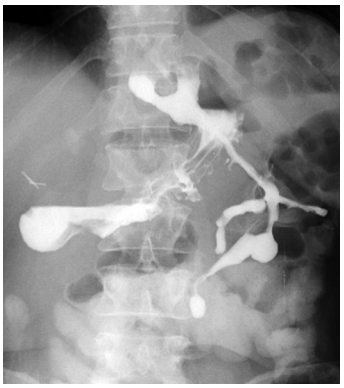

Figure 1 Barium swallow: two fistulas at the esophagogastric junction.

DISCUSSION

The OTSC has a different conception from TTS clips: (1) the OTSC is in nitinol with a "leghold trap" memory shape, is loaded on a cap placed on the scope tip, and has the capacity to grasp and compress the tissue more widely and with greater strength, without provoking ischemia or cutting the tissue; and (2) the target tissue needs to be caught and pulled into the cap by specifically developed devices that make addressing tangential lesions easier.

Preliminary small case series suggest that the OTSC is effective for hemostasis of non-variceal bleeding[22,23]. Moreover, results from a few human cases[22-24] and animal studies[25-27] have indicated that this device may be appropriate to close acute gastric and colonic perforations that occur during endoscopic mucosal resection, and natural orifice transluminal endoscopic surgery orifices up to 20 mm in size.

This is the first report of successful closure of two inveterate perforations by OTSCs. In our opinion, the success of the procedure should be attributed both to the anchor used to pull the tissue into the cap and to the OTSC itself. The three rigid hooks of the anchor firmly grasp the perforation margins at three equidistant points, permitting to pull the margins circumferentially into the cap. In the present case, the anchor was opened beyond the luminal margins of the fistulous orifice into the proximal segment of the fistolous tract that was partially invaginated into the cap before the release of the OTSC. This mechanical result would not have been achieved using the other OTSC device, the twin grasper, which has two independently movable branches that grasp the perforation margins at two opposite points. This two-point grasping method may be sufficient for acute perforations with normal elastic tissue margins, but not for fibrotic hard chronic ones that would be only partially invaginated into the cap (Figure 7).

Both traumatic OTSCs placed in the present case were lost after a period between the 2nd and 4th week after SEMS removal. Whether traumatic or atraumatic

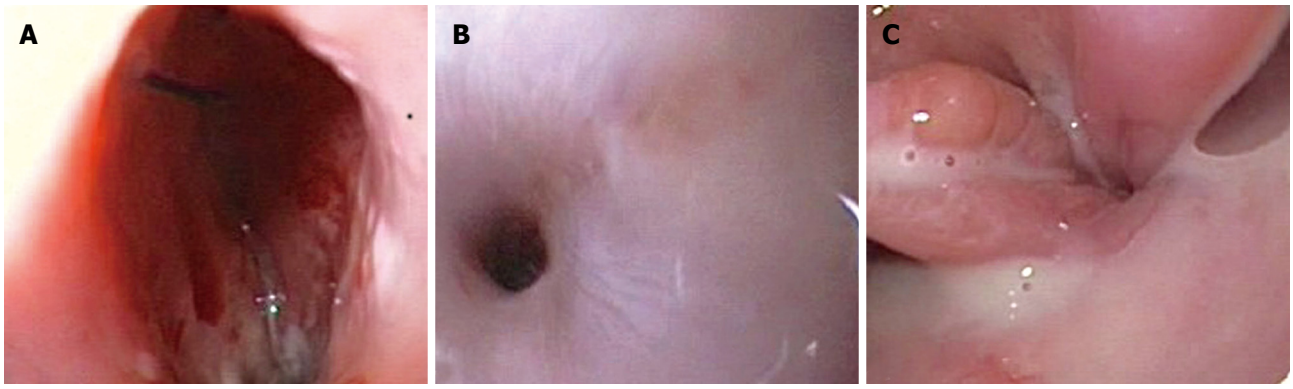

Figure 2 Endoscopic view of the 15-mm (A) and 10-mm (B) fistulous openings on the left and right sides, respectively, above the esophagogastric junction (C).

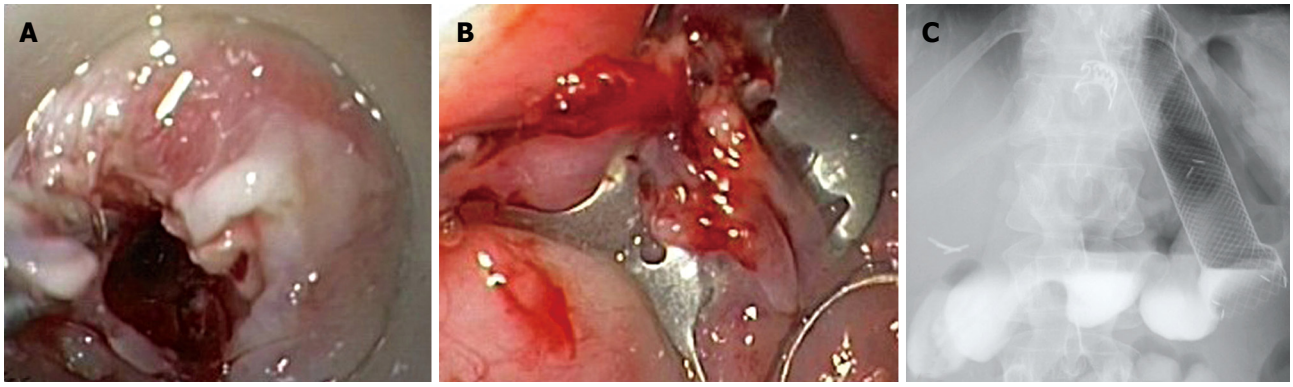

Figure 3 First OTSC placement. A: Invagination of the proximal segment of the 10-mm fistula into the OTSC applicator cap using the anchor; B: Closure of the 10-mm fistula; C: Barium swallow after the first OTSC and stent placement.

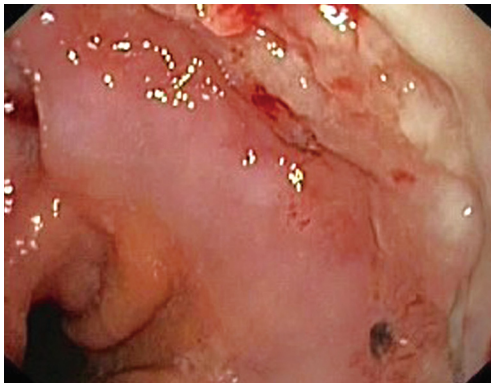

Figure 4 First OTSC completely embedded in hyperplastic overgrowth.

jaws have different "stay-in-place" periods is unknown. In previous studies, acute perforations have been successfully closed independently from the OTSC teeth shape after remaining in place for similar periods of time[22,26], and only occasionally for > 4 wk[24,26]. Although the traumatic teeth may reduce the possibility of hard tissue slipping out of the OTSC, prolonging its *in situ* stay, strong tissue compression could be more important to determine long-standing closure. Moreover, the use of oversized OTSCs may increase the capacity to grasp and close fibrotic margins of chronic perforations and its permanence.

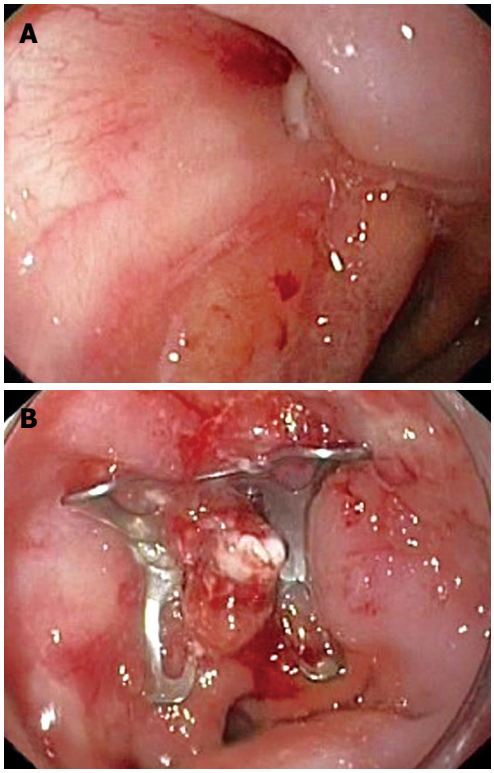

Figure 5 Second OTSC placement. A: Fistula opening reduced in size; B: Fistula closure.

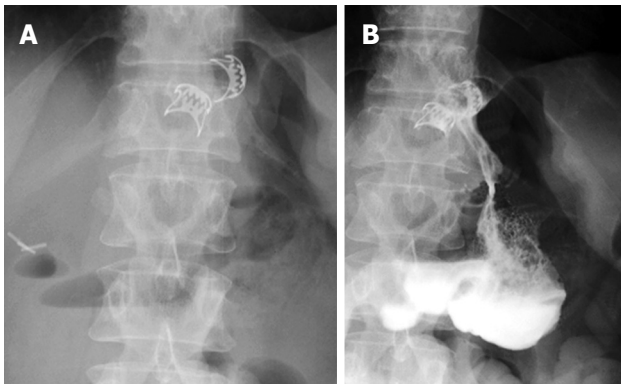

Figure 6 OTSC closure of the two fistulas. A: Two OTSCs in place; B: No leaks from both OTSCs at barium swallow.

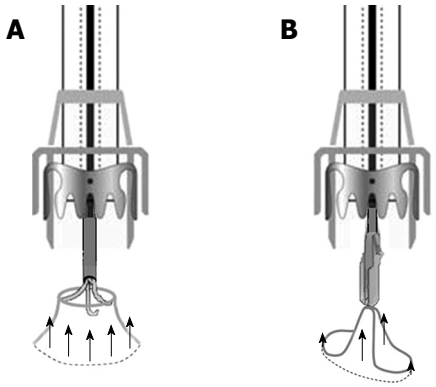

Figure 7 Mechanical results of OTSC devices pulling fibrotic margins of chronic perforations. A: Circumferential invagination using the anchor; B: Two-point invagination with the twin grasper.

Finally, no OTSC-related complications occurred. An intense overgrowth embedded the first OTSC after SEMS removal, but it did not prevent the spontaneous loss of the clip during follow-up. It remains to be established whether the overgrowth reaction would have occurred without the stent. Although endoscopic follow-up was not scheduled in previous studies, OTSC-related overgrowth has not been observed in humans[22-24], whereas Schurr *et al*[26] have observed minimal overgrowth in the colon of some pigs after 1 mo.

In conclusion, the OTSC may be the least invasive method to close chronic small fistulas or leaks, if prospective large comparative studies with fully-covered stents will confirm our observation.

REFERENCES

1 **Chung MA**, Wanebo HJ. Surgical management and treatment of gastric and duodenal fistulas. *Surg Clin North Am* 1996; **76**: 1137-1146

2 **Kiev J**, Amendola M, Bouhaidar D, Sandhu BS, Zhao X, Maher J. A management algorithm for esophageal perforation. *Am J Surg* 2007; **194**: 103-106

3 **Kingham TP**, Pachter HL. Colonic anastomotic leak: risk factors, diagnosis, and treatment. *J Am Coll Surg* 2009; **208**: 269-278

4 **Eisendrath P**, Cremer M, Himpens J, Cadière GB, Le Moine O, Devière J. Endotherapy including temporary stenting of fistulas of the upper gastrointestinal tract after laparoscopic bariatric surgery. *Endoscopy* 2007; **39**: 625-630

5 **Fischer A**, Thomusch O, Benz S, von Dobschuetz E, Baier P, Hopt UT. Nonoperative treatment of 15 benign esophageal perforations with self-expandable covered metal stents. *Ann Thorac Surg* 2006; **81**: 467-472

6 **Freeman RK**, Ascioti AJ, Wozniak TC. Postoperative esophageal leak management with the Polyflex esophageal stent. *J Thorac Cardiovasc Surg* 2007; **133**: 333-338

7 **Tierney W**, Chuttani R, Croffie J, DiSario J, Liu J, Mishkin DS, Shah R, Somogyi L, Petersen BT. Enteral stents. *Gastrointest Endosc* 2006; **63**: 920-926

8 **Chuttani R**, Barkun A, Carpenter S, Chotiprasidhi P, Ginsberg GG, Hussain N, Liu J, Silverman W, Taitelbaum G, Petersen B. Endoscopic clip application devices. *Gastrointest Endosc* 2006; **63**: 746-750

9 **Minami S**, Gotoda T, Ono H, Oda I, Hamanaka H. Complete endoscopic closure of gastric perforation induced by endoscopic resection of early gastric cancer using endoclips can prevent surgery (with video). *Gastrointest Endosc* 2006; **63**: 596-601

10 **Karahasanoglu T**, Altinli E, Hamzaoglu I, Aydogan F, Dobrucali A. Is intraluminal clip application an appropriate treatment for iatrogenic gastric perforation? *Eur Surg Res* 2003; **35**: 383-387

11 **Voermans RP**, Worm AM, van Berge Henegouwen MI, Breedveld P, Bemelman WA, Fockens P. In vitro comparison and evaluation of seven gastric closure modalities for natural orifice transluminal endoscopic surgery (NOTES). *Endoscopy* 2008; **40**: 595-601

12 **Raymer GS**, Sadana A, Campbell DB, Rowe WA. Endoscopic clip application as an adjunct to closure of mature esophageal perforation with fistulae. *Clin Gastroenterol Hepatol* 2003; **1**: 44-50

13 **Teitelbaum JE**, Gorcey SA, Fox VL. Combined endoscopic cautery and clip closure of chronic gastrocutaneous fistulas. *Gastrointest Endosc* 2005; **62**: 432-435

14 **Chryssostalis A**, Rosa I, Pileire G, Ozenne V, Chousterman M, Hagège H. Closure of refractory gastrocutaneous fistula using endoclipping. *Endoscopy* 2005; **37**: 924

15 **Siddiqui AA**, Kowalski T, Cohen S. Closure of a nonhealing gastrocutaneous fistula using an endoscopic clip. *South Med J* 2007; **100**: 75-76

16 **Qadeer MA**, Dumot JA, Vargo JJ, Lopez AR, Rice TW. Endoscopic clips for closing esophageal perforations: case report and pooled analysis. *Gastrointest Endosc* 2007; **66**: 605-611

17 **John BK**, Cortes RA, Feinerman A, Somnay K. Successful closure of a rectovaginal fistula by using an endoscopically placed Resolution clip. *Gastrointest Endosc* 2008; **67**: 1192-1195

18 **Doniec JM**, Schniewind B, Kahlke V, Kremer B, Grimm H. Therapy of anastomotic leaks by means of covered self-expanding metallic stents after esophagogastrectomy. *Endoscopy* 2003; **35**: 652-658

19 **Amrani L**, Ménard C, Berdah S, Emungania O, Soune PA, Subtil C, Brunet C, Grimaud JC, Barthet M. From iatrogenic digestive perforation to complete anastomotic disunion: endoscopic stenting as a new concept of "stent-guided regeneration and re-epithelialization". *Gastrointest Endosc* 2009; **69**: 1282-1287

20 **Langer FB**, Wenzl E, Prager G, Salat A, Miholic J, Mang T, Zacherl J. Management of postoperative esophageal leaks with the Polyflex self-expanding covered plastic stent. *Ann Thorac Surg* 2005; **79**: 398-403; discussion 404

21 **Holm AN**, de la Mora Levy JG, Gostout CJ, Topazian MD, Baron TH. Self-expanding plastic stents in treatment of benign esophageal conditions. *Gastrointest Endosc* 2008; **67**: 20-25

22 **Kirschniak A**, Kratt T, Stüker D, Braun A, Schurr MO, Königsrainer A. A new endoscopic over-the-scope clip system for treatment of lesions and bleeding in the GI tract:

first clinical experiences. *Gastrointest Endosc* 2007; **66**: 162-167
23 **Repici A**, Arezzo A, De Caro G, Morino M, Pagano N, Rando G, Romeo F, Del Conte G, Danese S, Malesci A. Clinical experience with a new endoscopic over-the-scope clip system for use in the GI tract. *Dig Liver Dis* 2009; **41**: 406-410
24 **Kirschniak A**, Traub F, Kueper MA, Stüker D, Königsrainer A, Kratt T. Endoscopic treatment of gastric perforation caused by acute necrotizing pancreatitis using over-the-scope clips: a case report. *Endoscopy* 2007; **39**: 1100-1102
25 **Kratt T**, Küper M, Traub F, Ho CN, Schurr MO, Königsrainer A, Granderath FA, Kirschniak A. Feasibility study for secure closure of natural orifice transluminal endoscopic surgery gastrotomies by using over-the-scope clips. *Gastrointest Endosc* 2008; **68**: 993-996
26 **Schurr MO**, Hartmann C, Ho CN, Fleisch C, Kirschniak A. An over-the-scope clip (OTSC) system for closure of iatrogenic colon perforations: results of an experimental survival study in pigs. *Endoscopy* 2008; **40**: 584-588
27 **von Renteln D**, Schmidt A, Vassiliou MC, Rudolph HU, Gieselmann M, Caca K. Endoscopic closure of large colonic perforations using an over-the-scope clip: a randomized controlled porcine study. *Endoscopy* 2009; **41**: 481-486

S- Editor Wang YR **L- Editor** Kerr C **E- Editor** Ma WH

World Journal of Gastroenterology

Online Submissions: http://www.wjgnet.com/1007-9327office
wjg@wjgnet.com
doi:10.3748/wjg.v16.i13.1670

World J Gastroenterol 2010 April 7; 16(13): 1670-1672
ISSN 1007-9327 (print)

CASE REPORT

Therapeutic angiography for giant bleeding gastro-duodenal artery pseudoaneurysm

Ram Elazary, Mahmoud Abu-Gazala, Avraham Schlager, Noam Shussman, Avraham I Rivkind, Allan I Bloom

Ram Elazary, Mahmoud Abu-Gazala, Avraham Schlager, Noam Shussman, Avraham I Rivkind, Department of Surgery, Hadassah-Hebrew University Medical Center, Jerusalem 91120, Israel
Allan I Bloom, Department of Radiology, Section of Interventional Radiology, Hadassah-Hebrew University Medical Center, Jerusalem 91120, Israel
Author contributions: Elazary R, Abu-Gazala M, Schlager A and Shussman N treated the patient in the emergency room and surgical department and participated in writing the article; Rivkind AI is the chief of surgery who was responsible for the transfer of the patient to our center and for the treatment; Bloom AI performed the angiography and participated in writing the article.
Correspondence to: Ram Elazary, MD, Department of Surgery, Hadassah-Hebrew University Medical Center, Jerusalem 91120, Israel. ramelazary@hadassah.org.il
Telephone: +972-2-6778800 Fax: +972-2-6449412
Received: October 28, 2009 Revised: January 14, 2010
Accepted: January 21, 2010
Published online: April 7, 2010

Abstract

We present the case of an 18-year-old female transferred to our center from an outside hospital due to persistent gastrointestinal bleeding. Two weeks prior to her transfer she underwent duodenal omentopexy for a perforated duodenal peptic ulcer. The patient underwent a computed tomography angiogram which identified the source of bleeding as a giant gastro-duodenal artery (GDA) pseudoaneurysm. The patient was taken to interventional radiology where successful microcoil embolization was performed. We present this rare case of a giant GDA pseudoaneurysm together with imaging and a review of the medical literature regarding prevalence, etiology and treatment options for visceral arterial aneurysms.

Key words: Gastro-duodenal artery; Gastrointestinal; Bleeding; Angiography; Pseudoaneurysm

Peer reviewer: Klaus Thaler, MD, One Hospital Drive, McHany Hall, MC 413, Columbia, MO 65212, United States

Elazary R, Abu-Gazala M, Schlager A, Shussman N, Rivkind AI, Bloom AI. Therapeutic angiography for giant bleeding gastro-duodenal artery pseudoaneurysm. *World J Gastroenterol* 2010; 16(13): 1670-1672 Available from: URL: http://www.wjgnet.com/1007-9327/full/v16/i13/1670.htm DOI: http://dx.doi.org/10.3748/wjg.v16.i13.1670

INTRODUCTION

Upper gastrointestinal bleeding (UGIB) is one of the leading causes of admission to the emergency department. While the vast majority of these bleeding episodes resolve spontaneously and most of the remaining cases are successfully managed endoscopically, a small percentage of patients require treatment using more invasive procedures such as therapeutic angiography and surgery. UGIB can be caused by a number of various pathologies. Gastro-duodenal artery (GDA) pseudoaneurysm is a rare but potentially fatal complication of surgery and, hence, early recognition and management of this complication is critical[1]. Although open surgery has traditionally been the treatment of choice, therapeutic angiography is emerging as an effective treatment modality for selected cases[2]. In this article we present such a case as well as remarkable images of the giant GDA aneurysm. Additionally, we discuss the pathophysiology of the condition, the treatment options and our rationale for opting for angiographic intervention over surgery.

CASE REPORT

An 18-year-old female was transferred to our surgery department due to unsuccessful treatment of acute upper gastrointestinal bleeding. Seven months prior to this admission she was diagnosed with Crohn's disease of the ileo-cecal region. She was treated with oral steroids and

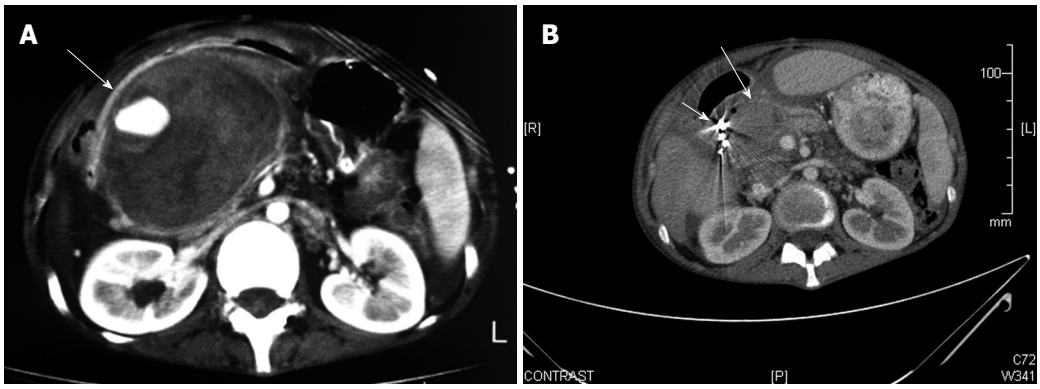

Figure 1 Computed tomography angiography (CTA). A: CTA arterial late phase showing the giant GDA pseudoaneurysm (arrow); B: CTA eight days post the procedure which shows the reduction in size of the pseudoaneurysm (long arrow), angiographic coils (short arrow) and no perfusion.

mesalamine (Pentasa) with gradual improvement of the disease symptoms. Five months later she was admitted to a local community hospital due to acute abdominal pain. She was taken immediately to the operating theatre. At that time, a perforated duodenal ulcer was identified and treated with duodenal omentopexy (Graham's patch). On post-operative day 14, the patient began bleeding from the surgical wound and experiencing episodes of UGIB. She was transfused with multiple units of packed blood cells and was transferred to a second hospital where she underwent an upper endoscopy (Figure 1A). The endoscopy showed erosive gastritis and blood clots without active bleeding. Due to unsatisfactory explanation for the source of the hemorrhage she underwent computed tomography angiography (CTA) which demonstrated a giant pseudoaneurysm of the GDA, surrounded by fresh clots of blood. The patient was transfused with an additional five units of packed blood cells and transferred to our institution as the initial hospital did not have an interventional radiology unit. Upon arrival at the emergency department, the patient's pulse was 80 bpm and blood pressure was 110/70 mmHg. A pulsatile abdominal mass was palpated at the right upper quadrant. Blood tests showed hemoglobin level of 11.6 mg/dL and normal coagulation studies. A naso-gastric tube was inserted which drained multiple clots of blood, at which time she was treated with intravenous omeprazole and taken to the angiography suite. After cannulation of the celiac trunk and the superior mesenteric artery *via* a right trans-femoral approach, the giant pseudoaneurysm emerging from the GDA was demonstrated. Arterial embolization was performed by placement of several detachable micro-coils until flow-arrest was obtained. The procedure was performed without complication. Eight days following the procedure she underwent CTA which showed the angiographic coils surrounded by a small collection of fluid and no signs of perfusion in the GDA (Figure 1B). She was discharged on the 10th d of hospitalization. After two years of follow up, the patient is asymptomatic and has not been hospitalized due to recurrent UGIB.

DISCUSSION

Visceral artery pseudoaneurysms are considered rare pathologies. Nevertheless, pseudoaneurysm rupture and bleeding can lead to significant morbidity and mortality. The visceral arteries which most commonly develop pseudoaneurysm are the splenic artery, hepatic arteries, gastric and gastroepiploic arteries, gastro-duodenal artery and branches of the mesenteric arteries[3]. The most common artery involved is the splenic. GDA aneurysms are considered to be extremely rare. Although pseudoaneurysms and aneurysms of splanchnic arteries have traditionally been considered uncommon clinical entities, the prevalence discovered during autopsy study was surprisingly high (10.4%)[1]. More recent, higher rates of detection are likely related to increased frequency of imaging studies such as ultrasonography and computed tomography. There are multiple etiologies for development of pseudoaneurysms including: atherosclerosis, trauma, surgery, pancreatitis, infection, collagen vascular disease and congenital abnormalities. Infection and trauma are probably the most common causes. Infection can occur as a direct process around the vessel or as lymphatic spread from a primary focus such as *Mycobacterium tuberculosis* located away from the vessel[4]. Patients with pseudoaneurysm may be asymptomatic or present with symptoms of gastrointestinal bleeding, intraperitoneal hemorrhage, obstructive jaundice due to external pressure by the pseudoaneurysm, hematobilia and rupture into the portal vein.

A review of visceral aneurysms conducted by Moore *et al*[5] concluded that 35% of GDA aneurysms are ruptured at presentation, carrying a mortality rate of 21%. In the past, these pseudoaneurysms were treated surgically. However, in the last two decades, radiographic intervention has emerged as an attractive method for treating these patients. Surgical treatments include resection of the aneurysm and placing an interposition graft or performing aneurysmectomy with or without patching using a great saphenous vein. Endovascular treatments used are embolization or stent graft repair of the aneurysm. A laparoscopic procedure has also been reported for treating splenic artery aneurysm[6]. The potential complications of angiography, aside from those of standard femoral cannulation, include infarction of viscera and abscess

formation. Fortunately, the complication rate regarding the former is relatively low due to rich collateral blood supply. Saltzberg *et al*[7] retrospectively reviewed the outcome of 65 patients diagnosed with visceral aneurysm, 18 of whom were treated by angiography and 9 by surgery. He reported that the initial technical success rate of the endovascular procedures was 94.4% (17/18). Major complications occurred in 22.2% (4/18). However, all four of these were in patients who were treated for splenic artery aneurysms. They concluded from their experience that endovascular management of visceral artery aneurysms is a reasonable alternative to open surgical repair, except for patients with splenic artery aneurysm. Carrafiello *et al*[8] published a case report of a patient with an evolving asymptomatic GDA pseudoaneurysm who underwent a combination of percutaneous, ultrasound-guided thrombin injection directly into the pseudoaneurysm sac and microcoil embolization of the gastro-duodenal artery. They concluded that thrombin injection may reduce the pseudoaneurysm's wall tension and probably diminishes the risk for rupture.

Our patient presumably developed the pseudoaneurysm due to a leak occurring after the omentopexy repair for her perforated duodenal ulcer which initiated an infectious/inflammatory process in the region of the GDA area, causing damage to the vessel wall. Bleeding into the peritoneal space or the gastrointestinal tract beginning several days following an operation should be a cause for suspicion for the possibility of a ruptured pseudoaneurysm. Any operation which involves handling of an infected space or organ is a risk factor for infecting the peritoneal cavity and developing the pseudoaneurysm. Angioembolic occlusion of this giant aneurysm provided an effective treatment with minimal morbidity risk. Surgical repair in this case would have been particularly challenging and possibly morbid as it would have required re-exploring a previously operated space. We conclude that angiographic management is not only a feasible but possibly preferred treatment modality in selected cases of visceral artery aneurysms.

REFERENCES

1 **Lee CH**, Lan CC, Wang CC, Chan CY, Wu YK. Spontaneous rupture of gastroduodenal artery pseudoaneurysm following vigorous cough. *Am J Gastroenterol* 2009; **104**: 529-530

2 **Salam TA**, Lumsden AB, Martin LG, Smith RB 3rd. Nonoperative management of visceral aneurysms and pseudoaneurysms. *Am J Surg* 1992; **164**: 215-219

3 **Chong WW**, Tan SG, Htoo MM. Endovascular treatment of gastroduodenal artery aneurysm. *Asian Cardiovasc Thorac Ann* 2008; **16**: 68-72

4 **Seith A**, Gulati MS, Nandi B, Bhatia V, Garg PK, Bandhu S, Paul SB. Tuberculous pseudoaneurysm of gastroduodenal artery. *Clin Imaging* 2003; **27**: 408-410

5 **Moore E**, Matthews MR, Minion DJ, Quick R, Schwarcz TH, Loh FK, Endean ED. Surgical management of peripancreatic arterial aneurysms. *J Vasc Surg* 2004; **40**: 247-253

6 **Pulli R**, Dorigo W, Troisi N, Pratesi G, Innocenti AA, Pratesi C. Surgical treatment of visceral artery aneurysms: A 25-year experience. *J Vasc Surg* 2008; **48**: 334-342

7 **Saltzberg SS**, Maldonado TS, Lamparello PJ, Cayne NS, Nalbandian MM, Rosen RJ, Jacobowitz GR, Adelman MA, Gagne PJ, Riles TS, Rockman CB. Is endovascular therapy the preferred treatment for all visceral artery aneurysms? *Ann Vasc Surg* 2005; **19**: 507-515

8 **Carrafiello G**, Laganà D, Recaldini C, Mangini M, Lumia D, Giorgianni A, Leonardi A, Fugazzola C. Combined percutaneous thrombin injection and endovascular treatment of gastroduodenal artery pseudoaneurysm (PAGD): case report. *Emerg Radiol* 2007; **14**: 51-54

S- Editor Tian L **L- Editor** Logan S **E- Editor** Ma WH

World Journal of Gastroenterology

Online Submissions: http://www.wjgnet.com/1007-9327office
wjg@wjgnet.com
doi:10.3748/wjg.v16.i13.1673

World J Gastroenterol 2010 April 7; 16(13): 1673-1675
ISSN 1007-9327 (print)

CASE REPORT

A geriatric patient with diffuse idiopathic skeletal hyperostosis

Berrin Karadag, Huseyin Cat, Selma Aksoy, Banu Ozulu, Ali Osman Ozturk, Sukru Oguz, Yuksel Altuntas

Berrin Karadag, Huseyin Cat, Banu Ozulu, Ali Osman Ozturk, Yuksel Altuntas, Sisli Etfal Research and Training Hospital, 2. Internal Medicine Clinic, Sisli, 34377, İstanbul, Turkey
Selma Aksoy, Sisli Etfal Research and Training Hospital, Neurology Clinic, Sisli, 34377, İstanbul, Turkey
Sukru Oguz, Sisli Etfal Research and Training Hospital, Radiology Clinic, Sisli, 34377, İstanbul, Turkey
Author contributions: Karadag B, Cat H, Ozturk AO and Altuntas Y designed the work; Karadag B and Ozulu B wrote the paper; Karadag B, Cat H, Aksoy S and Oguz S followed up the patient; Karadag B, Altuntas Y and Ozulu B reviewed the article.
Correspondence to: Berrin Karadag, MD, Sisli Etfal Research and Training Hospital, 2. Internal Medicine Clinic, Sisli, 34377, İstanbul, Turkey. bekaradag@yahoo.com
Telephone: +90-212-2312209 Fax: +90-212-2341121
Received: December 9, 2009 Revised: January 5, 2010
Accepted: January 12, 2010
Published online: April 7, 2010

Abstract

The most frequent health problems seen in senility are chronic and degenerative diseases. A 75-year-old male patient with the complaints of weight loss and difficulty in swallowing was admitted to our hospital from a nursing home. Upper system fiber-optic gastrointestinal endoscopy was performed and a mass at the junction of the hypopharynx and esophagus just below recessus piriformis obstructing almost the whole of the lumen and blocking the distal passage was detected. Computed tomography revealed marked narrowing secondary to osseous hypertrophy in the air column of the hypopharynx and proximal esophagus. Diffuse idiopathic skeletal hyperostosis or Forestier's disease is an idiopathic disease characterized by the ossification of the anterior longitudinal ligament of vertebra and some of the extraspinal ligaments. In the present case we aim to discuss an elderly patient who suffered from dysphagia and weight loss and the diagnostic stages.

Key words: Dysphagia; Diffuse idiopathic skeletal hyperostosis; Elderly; Weight loss

Peer reviewers: Dr. Shahab Abid, Associate Professor, Department of Medicine, Aga Khan University, Stadium Road, PO Box 3500, Karachi 74800, Pakistan; Jai Dev Wig, MS, FRCS, Former Professor and Head, Department of General Surgery, Postgraduate Institute of Medical Education and Research, Chandigarh 160012, India

Karadag B, Cat H, Aksoy S, Ozulu B, Ozturk AO, Oguz S, Altuntas Y. A geriatric patient with diffuse idiopathic skeletal hyperostosis. *World J Gastroenterol* 2010; 16(13): 1673-1675 Available from: URL: http://www.wjgnet.com/1007-9327/full/v16/i13/1673.htm DOI: http://dx.doi.org/10.3748/wjg.v16.i13.1673

INTRODUCTION

Diffuse idiopathic skeletal hyperostosis (DISH) is a common but often unrecognized systemic disorder observed mainly in elderly people[1]. All papers related to DISH demonstrate a consistent and marked increase of the disease with advancing age[2]. Various local structural lesions such as oropharyngeal tumors, vascular pathologies, retropharyngeal abscesses, and anterior cervical osteophytes may lead to mechanical esophageal dysphagia[3-5]. The prevalence of DISH in adults over the age of 50 years is around 25% for men and 15% for women, with an increased incidence in patients with obesity, gout and diabetes[6].

Although most patients with cervical spine involvement are either asymptomatic or have limited cervical spine movement and unspecified pain, possible complications described in the literature are dysphagia[7], stridor[8] dyspnea[9], ossification of the posterior longitudinal ligament and/or myelopathy[10] and hoarseness[11].

CASE REPORT

A 75-year-old male patient was found drunk and unconsci-

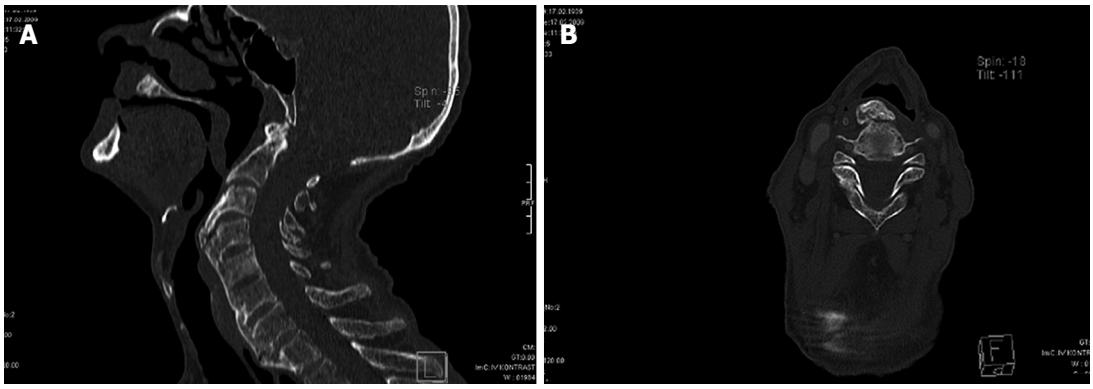

Figure 1 Cervical CT. A: Sagittal section revealed hypertrophic bridging alterations of anterior corpus parts at the level of C3-T1 vertebra and restriction of the esophagus due to osteophytic sprue formations; B: Axial section revealed osteophytic formations on the anterior parts of vertebral corpus.

ous on the street in November 9, 2008 and was transferred to the nearest state hospital. After an operation for intertrochanteric femur fracture he was sent to a nursing home. Because of progressive weight loss and swallowing difficulty, some blood tests were done and Hb and erythrocyte sedimentation rate (ESR) were found to be 9 g/dL and 75 mm/h, respectively. The patient was then transferred to our hospital on 28 January, 2009 with the preliminary diagnosis of malignancy. His height was 160 cm, weight 41 kg and body mass index was 16 kg/m^2. Physical examination revealed only cachectic appearance and limited neck movements; the other findings were normal, and the thyroid gland was nonpalpable. Due to detected anemia two packs of erythrocyte suspensions were transfused. In the biochemical analyses hepatic and renal functions were normal; he didn't have any electrolyte imbalance or systemic disease (fasting plasma glucose: 79 mg/dL, blood urea nitrogen: 22 mg/dL, creatinine: 1.0 mg/dL, uric acid: 4.8 mg/dL, aspartate aminotransferase: 8 U/L, alanine aminotransferase: 3 U/L, potassium: 4.3 mmol/L, iron: 41 μg/dL total iron binding capacity: 173 μg/L). His vitamin B12 and folic acid levels were 57 pg/mL and 1.46 ng/mL respectively. Total protein value was 5.7 g/dL and albumin was 2.3 g/dL. Evaluation of cognitive functions revealed his Mini Mental State Examination score was 12. There was not any evidence for malignancy in his thoracic and abdominal CT scans. Upper system fiber-optic gastrointestinal endoscopy was performed and a mass at the junction of the hypopharynx and esophagus just below recessus piriformis obstructing almost whole of the lumen and blocking the distal passage was detected. Biopsy couldn't be performed because of the risk of bleeding and aspiration. As a result of ear-nose-throat clinic consultation, and after laryngoscopic examination, anesthesia confirmation and cervical CT was performed for taking a biopsy from the mass thought to have originated from the pharyngeal area. Cervical CT revealed hypertrophic bridging alterations of anterior corpus parts at the level of C3-T1 vertebra (Figure 1A and B). At the hypopharynx and proximal parts of esophagus restriction secondary to osseous hypertrophy was demonstrated and this aspect was evaluated as consistent with DISH or Forrestier disease. As a result of multidisciplinary evaluation, an operation wasn't planned because of the patient's poor general condition. Patient's nutrition was regulated with fluid foods. No problem was established during nutrition with fluids. The patient was sent back to nursing home after recovery of general status.

DISCUSSION

Although mortality decreases and life expectancy gets longer with developing technology and medicine, chronic diseases remain common problems of elderly patients. In the differential diagnosis for dysphagia, larynx, lung and mediastinal tumors, esophagus motility disorders, esophagitis, restriction of esophagus, spinal tumors, vascular abnormalities, Zencker diverticule, Plummer-Vinson syndrome, gastroesophageal reflux and globus histericus should be kept in mind. For differentiating these disorders barium esophagography has a great importance[12].

A medical history should be taken in detail and questions about anatomical structure and functions of the oral cavity, pharynx, larynx, and esophagus should be examined when a patient complaining of dysphagia applies to ear-nose and throat clinics. Physical examination of the oral cavity, pharynx, larynx and neck should be done for determining the possible pathologies. Esophageal cancer, web, achalasia, diffuse esophageal spasm and esophagitis are common causes of esophageal dysphagia. Rarely, mediastinal tumors pressing the esophagus, vertebral bone processes and impressions due to the aorta can be the causes[13]. In our case, the patient's complaints were anemia, weight loss and difficulty in swallowing and initially esophageal malignancy was thought to be the cause of these complaints and upper gastrointestinal system endoscopy was planned. As a result of these evaluations, hypertrophic bridging alterations of anterior corpus parts at the level of C3-T1 vertebra were revealed. It was reported that perforation during esophagoscopy improves because of compression due to cervical osteophytes[14].

Treatment for DISH is primarily conservative, nonsteroidal anti-inflammatory drugs and myorelaxants are used. But in refractory cases there are two surgical approaches to remove osteophytes by lateral cervical or

peroral transpharyngeal ways[15]. In our case, we initially preferred a medical approach and started treatment with anti-inflammatory drugs and nutrition with liquid foods, after recovery of oral intake we maintained with high calorie formulas.

In our case, the patient hadn't applied to any hospital in the period that he lived alone but after he began to stay in the nursing home for elderly these complaints and problems were established and he was transferred to our hospital. At the present time, it is emphasized that without increasing the quality of the life, longer life will have no meaning and health expectancy is more important than life expectancy. Consequently, while treatment is the target in a young population, in a geriatric population the main target is the preservation of quality of life. We avoided the complications of surgical management and anesthesia, we tried nutrition with liquids and facilitated oral intake. Eventually, recovery in our patient's status and weight gain started. Gastrostomy may be planned if necessary and the patient is followed at particular intervals. During the evaluation of elderly patients, social status, cognitive functions and exhaustive physical examination should be performed definitely.

In conclusion, DISH should be considered an important, although rare, cause of dysphagia among older adults. However, it should not be accepted as the cause of dysphagia until all other causes have been ruled out.

REFERENCES

1 **Belanger TA**, Rowe DE. Diffuse idiopathic skeletal hyperostosis: musculoskeletal manifestations. *J Am Acad Orthop Surg* 2001; **9**: 258-267

2 **Weinfeld RM**, Olson PN, Maki DD, Griffiths HJ. The prevalence of diffuse idiopathic skeletal hyperostosis (DISH) in two large American Midwest metropolitan hospital populations. *Skeletal Radiol* 1997; **26**: 222-225

3 **Lambert JR**, Tepperman PS, Jimenez J, Newman A. Cervical spine disease and dysphagia. Four new cases and a review of the literature. *Am J Gastroenterol* 1981; **76**: 35-40

4 **Srinivas P**, George J. Cervical osteoarthropathy: an unusual cause of dysphagia. *Age Ageing* 1999; **28**: 321-322

5 **Uzunca K**, Birtane M, Tezel A. Dysphagia induced by a cervical osteophyte: Acase report of cervical spondylosis. *Chin Med J* (Engl) 2004; **117**: 478-480.

6 **Masiero S**, Padoan E, Bazzi M, Ponzoni A. Dysphagia due to diffuse idiopathic skeletal hyperostosis: an analysis of five cases. *Rheumatol Int* 2010; **30**: 681-685

7 **Masiero S**, Marchese Ragona R, Bottin R, Volante D, Ortolani M. An unusual cause of aspiration pneumonia. *Aging Clin Exp Res* 2006; **18**: 78-82

8 **Curtis JR**, Lander PH, Moreland LW. Swallowing difficulties from "DISH-phagia". *J Rheumatol* 2004; **31**: 2526-2527

9 **Nelson RS**, Urquhart AC, Faciszewski T. Diffuse idiopathic skeletal hyperostosis: a rare cause of Dysphagia, airway obstruction, and dysphonia. *J Am Coll Surg* 2006; **202**: 938-942

10 **Epstein NE**. Simultaneous cervical diffuse idiopathic skeletal hyperostosis and ossification of the posterior longitudinal ligament resulting in dysphagia or myelopathy in two geriatric North Americans. *Surg Neurol* 2000; **53**: 427-431; discussion 431

11 **Kritzer RO**, Rose JE. Diffuse idiopathic skeletal hyperostosis presenting with thoracic outlet syndrome and dysphagia. *Neurosurgery* 1988; **22**: 1071-1074

12 **Rotés-Querol J**. Clinical manifestations of diffuse idiopathic skeletal hyperostosis (DISH). *Br J Rheumatol* 1996; **35**: 1193-1194

13 **Alper F**, Akgun M, Kantarci M, Eroglu A, Ceyhan E, Onbas O, Duran C, Okur A. Demonstration of vascular abnormalities compressing esophagus by MDCT: special focus on dysphagia lusoria. *Eur J Radiol* 2006; **59**: 82-87

14 **Vrouenraets BC**, Been HD, Brouwer-Mladin R, Bruno M, van Lanschot JJ. Esophageal perforation associated with cervical spine surgery: report of two cases and review of the literature. *Dig Surg* 2004; **21**: 246-249

15 **Uppal S**, Wheatley AH. Transpharyngeal approach for the treatment of dysphagia due to Forestier's disease. *J Laryngol Otol* 1999; **113**: 366-368

S- Editor Wang YR **L- Editor** O'Neill M **E- Editor** Ma WH

World Journal of Gastroenterology

Online Submissions: http://www.wjgnet.com/1007-9327office
wjg@wjgnet.com
doi:10.3748/wjg.v16.i13.1676

World J Gastroenterol 2010 April 7; 16(13): 1676-1679
ISSN 1007-9327 (print)

CASE REPORT

Peeling a giant ileal lipoma with endoscopic unroofing and submucosal dissection

Takashi Morimoto, Kuang-I Fu, Hironori Konuma, Yuko Izumi, Syujirou Matsuyama, Kanako Ogura, Akihisa Miyazaki, Sumio Watanabe

Takashi Morimoto, Kuang-I Fu, Hironori Konuma, Yuko Izumi, Syujirou Matsuyama, Akihisa Miyazaki, Department of Gastroenterology, Juntendo University Nerima Hospital, Tokyo 177-8521, Japan
Kanako Ogura, Department of Pathology, Juntendo University Nerima Hospital, Tokyo 177-8521, Japan
Sumio Watanabe, Department of Gastroenterology, Juntendo University School of Medicine, Tokyo 113-8421, Japan
Author contributions: Morimoto T and Fu KI supplemented the data about the patient; Konuma H, Izumi Y, Matsuyama S, Ogura K, Miyazaki A and Watanabe S analyzed the data about the patient; Morimoto T and Fu KI wrote the paper.
Correspondence to: Kuang-I Fu, MD, PhD, Department of Gastroenterology, Juntendo University Nerima Hospital, 3-1-10 Nerimatakanodai, Nerima, Tokyo 177-8521, Japan. fukuangi@hotmail.com
Telephone: +81-3-59233111 Fax: +81-3-59233111
Received: December 5, 2009 Revised: January 1, 2010
Accepted: January 8, 2010
Published online: April 7, 2010

Abstract

Lipoma is relatively common in the colon but is less often in the small intestine. Most lipomas are incidentally detected at endoscopy and are usually small and asymptomatic. However, some of them can present with obstruction and/or intussusceptions. Surgical resection is commonly recommended to remove such significant lipomas with a limited pedicle and larger than 2 cm in size, as endoscopic resection may result in unfavorable complications such as intestinal perforations. We report a case of 62-year-old man presenting with hematochezia. Colonoscopy showed a submucosal tumor, about 50 mm in size, in the terminal ileum. A clinical diagnosis of lipoma was established based on the findings of colonoscopy and abdominal computed tomography (CT). As the patient complained of hematochezia and mild iron deficiency anemia associated with repeated tumor prolapse, we decided to remove his lipoma. Consequently, the lesion was completely removed *en bloc*. Although abdominal CT immediately after removal of the lesion showed a small amount of free air, conservative treatment was successfully carried out for the perforation. Histologically, the removed lesion was a lipoma.

Key words: Lipoma; Endoscopic submucosal dissection; Endoscopic unroofing; Perforation

Peer reviewers: Venkatesh Shanmugam, MBBS, MS (Gen. Surg.), Dip.NB (Gen. Surg.), FRCS (Glasg.), MD, Specialist Registrar (Trent Deanery), Royal Derby Hospital, Uttoxeter Road, Derby, DE22 3NE, United Kingdom; Dr. Zoran Krivokapic, Professor, MD, FRCS, Institute for Digestive Disease, First Surgical Clinic, Clinical Center of Serbia, 6, Dr Koste Todorovica, Belgrade 11000, Serbia

Morimoto T, Fu KI, Konuma H, Izumi Y, Matsuyama S, Ogura K, Miyazaki A, Watanabe S. Peeling a giant ileal lipoma with endoscopic unroofing and endoscopic submucosal dissection. *World J Gastroenterol* 2010; 16(13): 1676-1679 Available from: URL: http://www.wjgnet.com/1007-9327/full/v16/i13/1676.htm DOI: http://dx.doi.org/10.3748/wjg.v16.i13.1676

INTRODUCTION

Lipoma is relatively common in the colon (65%-75%) but is less often in the small intestine (20%-25%). Most lipomas are incidentally detected at endoscopy and are usually small (less than 2 cm) and asymptomatic. However, some of them can present with obstruction and/or intussusceptions[1]. Surgical resection is commonly recommended to remove such lipomas with a limited pedicle and larger than 2 cm in size, as endoscopic resection may result in unfavorable complications such as intestinal perforations[2]. We herein report a case of a large lipoma, 50 mm in diameter, arising from the end of ileum, which was completely removed with the so-called endoscopic

unroofing technique in combination with endoscopic submucosal dissection (ESD)[3,4].

CASE REPORT

A 62-year-old man presented with hematochezia. Colonoscopy showed a pedunculated lesion, about 50 mm in size, originating from the ileum end. With peristalsis, the lesion prolapsed through the ileocecal valve into the cecum and ascending colon (Figure 1). The surface was regularly covered with normal mucosa, except for a part of nodular change suggesting hyperplastic mucosa due to repeated prolapse, and "Cushion-sign" was positive[5]. Moreover, computed tomography (CT) showed a uniform mass with a very low-density in the ileum end corresponding to the above detected lesion (Figure 2A and B). A clinical diagnosis of ileal lipoma was established based on the above findings. Although there was not any symptom of intestinal intussusception, multiple erosions were seen in the ascending colon perhaps caused by the tumor prolapsing with peristalsis. As oozing of blood was also seen, the ileal lipoma was considered as the bleeding source of his hematochezia. Therefore, local resection was decided for treatment. At first, conventional endoscopic mucosal resection (EMR, lift and cut technique) was attempted under CO_2 insufflation. However, the tumor was too large for the largest commercially available snare with a maximum diameter of 33 mm in our department to capture the whole lesion after injection of glycerol at the base of the lesion (Figure 3A). Alternatively, endoscopic submucosal resection (ESD) was conducted with an IT-knife for removal. Unfortunately, the muscle layer was lacerated and serosal membrane was observed during dissection (Figure 3B). Thus, we used the snare to break the mucosal layer on the top of the lipoma, and then dissection from the defect on the top rather than from the base of the lesion was continued. Capsulated fat tissue extruding through the overlying mucosa during dissection (naked fat sign) was seen (Figure 3C)[5,6]. Finally, the lesion was completely removed *en bloc* (Figure 3D). The vital signs were stable and no abdominal distension or discomfort was found during the whole procedure. The lacerated muscle layer could not be completely but only partially sutured with metallic clips due to the narrow lumen in the terminal ileum. Abdominal CT immediately after removal, however, showed only a small amount of free air around the ileum end without ascites. Conservative treatment including withholding of oral intake, intravenous administration of antibiotics and hyperalimentation was started after consultation with the surgeons. The vital signs were stable except for fever (at the highest degree of 38℃) for 2 d. No sign of peritoneal irritation suggesting diffuse peritonitis was seen on close physical examination. Oral intake was restarted on the fifth day after ESD, and the patient was discharged uneventfully 2 d thereafter. Histologically, the removed lesion was a lipoma.

DISCUSSION

This lipoma could be correctly diagnosed before resection, as endoscopically it was a submucosal tumor with a positive "Cushion sign", and moreover computed tomography disclosed a round and smooth, well-demarcated tumor with a fat attenuation[7,8]. Although, lipohyperplasia, frequently discovered at the right-sided colon (especially in the ileocecal valve), should be included in the differential diagnosis, the encapsulated yellowish adipose tissue detected during endoscopic dissection finally supported the endoscopic diagnosis of a lipoma rather than lipohyperplasia before histological evaluation. We decided to treat this ileal lipoma, as the patient complained of hematochezia and mild iron deficiency anemia associated with erosions caused by repeated tumor prolapse. Various techniques including endoscopic

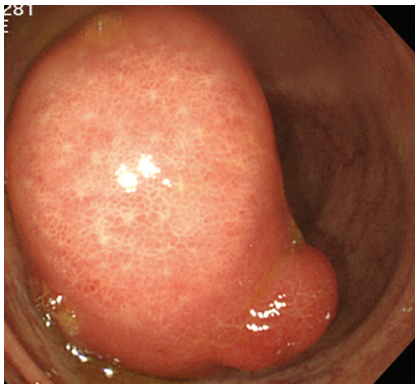

Figure 1 Colonoscopy showing a large pedunculated tumor, 50 mm in size, originating from the ileum end.

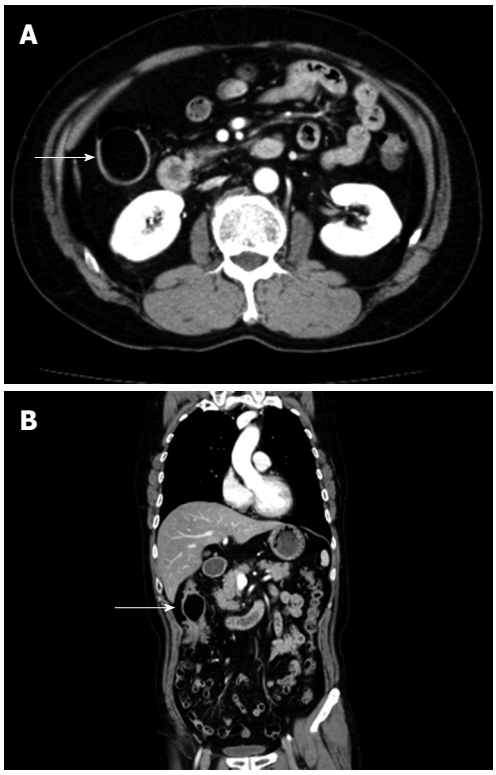

Figure 2 Abdominal CT showing a round, smooth and well-demarcated tumor at the end of the ileum (A) with a fat attenuation coefficient of -116 Hounsfield units (arrows) (B).

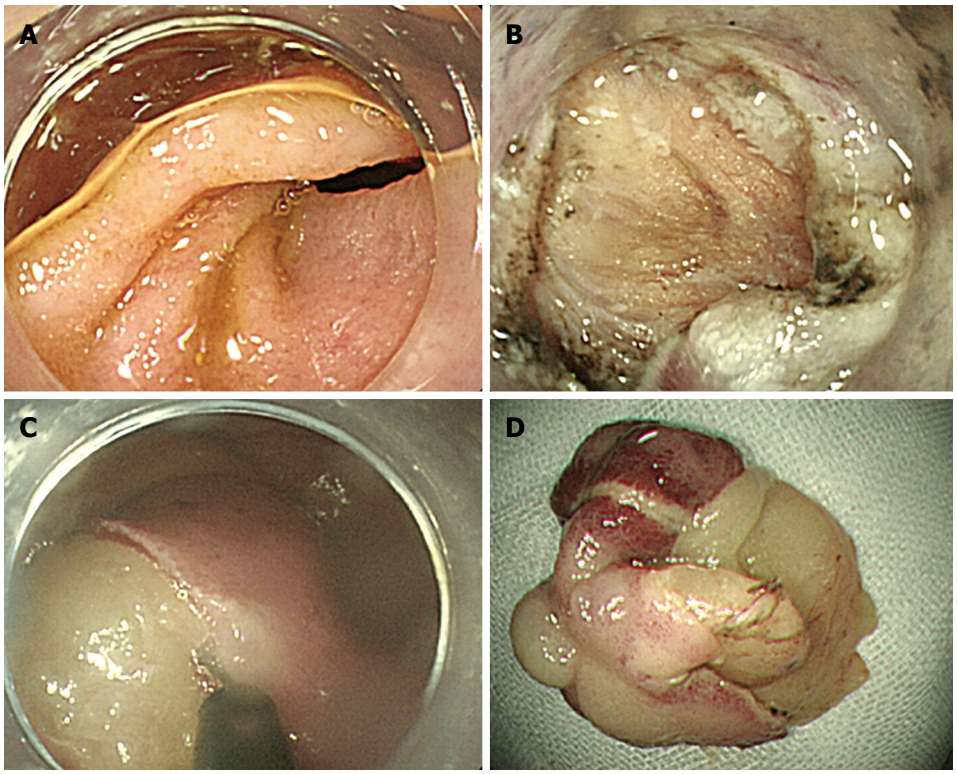

Figure 3 Whole captured lesion after injection of glycerol at the base of the lesion. The base of the lipoma (A), lacerated muscle layer (B), dissected overlying mucosa and capsule (C), and completely removed lipoma (D).

removal and surgical resection have been reported[9,10]. We firstly attempted conventional EMR. However, unfortunately the tumor could not be completely captured with the largest snare. Piecemeal resection was also tried but failed to electrosurgically resect the tumor with the snaring technique. We therefore used the ESD technique to remove this large lesion, as this newly developed technique can remove this kind of large lesions *en bloc*[11].

During dissection, since laceration of the muscle layer and thereafter the serosa were unfortunately endoscopically identified, we modified the ESD technique for removal. We enrolled the reported unroofing technique in combination with ESD for endoscopic resection[3,4,12]. At first, the overlying mucosa and capsule of the lipoma were peeled off with the tip of the snare and IT knife from the top to the bottom of the tumor. The underlying adipose tissue was thereafter seen like a peeling banana. This modified technique finally enabled us to completely remove the lipoma *en bloc*. Different from the submucosal direct dissection at the base, we dissected this lipoma from the top to the bottom rather than from the base. We believe that this modified technique can remove large lipomas more safely and quickly than ESD[11].

Perhaps, perforation is one of the most serious complications associated with endoscopic resection. We did not close the lacerated muscle layer immediately, as the clips in the narrow lumen of ileum would disturb continuing the endoscopic procedure. Fortunately, we could complete the endoscopic removal, as the patient did not develop pneumoperitoneum and the lumen was not collapsed. Furthermore, we could not close the perforation completely with metallic clips. However, conservative treatment was carried out successfully. Our case was treated successfully without laparotomy. However, the choice of conservative or surgical treatment for iatrogenic colonic perforation remains controversial. In this case, non-surgical treatment was selected because the vital signs of the patient were stable, the abdominal pain was mild and localized, no unexplained peritoneal fluid was found in the abdominal CT, and the colonic preparation was extremely good. We also believe that CO_2 insufflation plays an important role in this successful conservative treatment, as room air insufflation would lead to pneumoperitoneum collapsing the lumen and vital signs (abdominal compartment syndrome)[13-16].

In conclusion, large ileal lipoma can be completely removed with the modified ESD procedure in combination with endoscopic unroofing technique (from the top to the bottom like peeling a banana).

REFERENCES

1 **Rogers SO Jr**, Lee MC, Ashley SW. Giant colonic lipoma as lead point for intermittent colo-colonic intussusception. *Surgery* 2002; **131**: 687-688
2 **Yu JP**, Luo HS, Wang XZ. Endoscopic treatment of submucosal lesions of the gastrointestinal tract. *Endoscopy* 1992; **24**: 190-193
3 **Hizawa K**, Kawasaki M, Kouzuki T, Aoyagi K, Fujishima M. Unroofing technique for the endoscopic resection of a large duodenal lipoma. *Gastrointest Endosc* 1999; **49**: 391-392
4 **Mimura T**, Kuramoto S, Hashimoto M, Yamasaki K, Kobayashi K, Kobayashi M, Oohara T. Unroofing for lymphangioma of the large intestine: a new approach to endoscopic treatment. *Gastrointest Endosc* 1997; **46**: 259-263
5 **Pfeil SA**, Weaver MG, Abdul-Karim FW, Yang P. Colonic lipomas: outcome of endoscopic removal. *Gastrointest Endosc* 1990; **36**: 435-438
6 **Messer J**, Waye JD. The diagnosis of colonic lipomas--the

naked fat sign. *Gastrointest Endosc* 1982; **28**: 186-188
7 **Urbano J**, Serantes A, Hernandez L, Turegano F. Lipoma-induced jejunojejunal intussusception: US and CT diagnosis. *Abdom Imaging* 1996; **21**: 522-524
8 **Heiken JP**, Forde KA, Gold RP. Computed tomography as a definitive method for diagnosing gastrointestinal lipomas. *Radiology* 1982; **142**: 409-414
9 **Yu HG**, Ding YM, Tan S, Luo HS, Yu JP. A safe and efficient strategy for endoscopic resection of large, gastrointestinal lipoma. *Surg Endosc* 2007; **21**: 265-269
10 **Tsushimi T**, Matsui N, Kurazumi H, Takemoto Y, Oka K, Seyama A, Morita T. Laparoscopic resection of an ileal lipoma: Report of a case. *Surg Today* 2006; **36**: 1007-1011
11 **Okada K**, Shatari T, Suzuki K, Tamada T, Sasaki T, Suwa T, Hori M, Sakuma M. Is endoscopic submucosal dissection really contraindicated for a large submucosal lipoma of the colon? *Endoscopy* 2008; **40** Suppl 2: E227
12 **Huang WH**, Peng CY, Yu CJ, Chou JW, Feng CL. Endoloop-assisted unroofing for the treatment of symptomatic duodenal lipomas. *Gastrointest Endosc* 2008; **68**: 1234-1236
13 **Bretthauer M**, Lynge AB, Thiis-Evensen E, Hoff G, Fausa O, Aabakken L. Carbon dioxide insufflation in colonoscopy: safe and effective in sedated patients. *Endoscopy* 2005; **37**: 706-709
14 **Sumanac K**, Zealley I, Fox BM, Rawlinson J, Salena B, Marshall JK, Stevenson GW, Hunt RH. Minimizing postcolonoscopy abdominal pain by using CO(2) insufflation: a prospective, randomized, double blind, controlled trial evaluating a new commercially available CO(2) delivery system. *Gastrointest Endosc* 2002; **56**: 190-194
15 **Saito Y**, Uraoka T, Matsuda T, Emura F, Ikehara H, Mashimo Y, Kikuchi T, Kozu T, Saito D. A pilot study to assess the safety and efficacy of carbon dioxide insufflation during colorectal endoscopic submucosal dissection with the patient under conscious sedation. *Gastrointest Endosc* 2007; **65**: 537-542
16 **Fu K**, Ishikawa T, Yamamoto T, Kaji Y. Paracentesis for successful treatment of tension pneumoperitoneum related to endoscopic submucosal dissection. *Endoscopy* 2009; **41** Suppl 2: E245

S- Editor Wang JL **L- Editor** Wang XL **E- Editor** Ma WH

World Journal of Gastroenterology

Online Submissions: http://www.wjgnet.com/1007-9327office
wjg@wjgnet.com
doi:10.3748/wjg.v16.i13.1680

World J Gastroenterol 2010 April 7; 16(13): 1680-1682
ISSN 1007-9327 (print)

CASE REPORT

Upper gastrointestinal hemorrhage caused by superwarfarin poisoning

Shu-Lei Zhao, Peng Li, Ming Ji, Ye Zong, Shu-Tian Zhang

Shu-Lei Zhao, Peng Li, Ming Ji, Ye Zong, Shu-Tian Zhang, Department of Gastroenterology, Beijing Friendship Hospital Affiliated to Capital Medical University, Beijing 100050, China
Author contributions: Zhang ST designed the research; Li P, Ji M, Zong Y and Zhao SL performed the research; Zhao SL collected the data and wrote the manuscript.
Correspondence to: Shu-Tian Zhang, MD, Department of Gastroenterology, Beijing Friendship Hospital Affiliated to Capital Medical University, Yongan Road 95, Beijing 100050, China. zhangst@ccmu.edu.cn
Telephone: +86-10-63138702 Fax: +86-10-63138067
Received: December 2, 2009 Revised: December 19, 2009
Accepted: December 26, 2009
Published online: April 7, 2010

Abstract

Superwarfarins are a class of rodenticides. Gastrointestinal hemorrhage is a fatal complication of superwarfarin poisoning, requiring immediate treatment. Here, we report a 55-year-old woman with tardive upper gastrointestinal hemorrhage caused by superwarfarin poisoning after endoscopic cold mucosal biopsy.

Key words: Esophagogastroduodenoscopy; Upper gastrointestinal hemorrhage; Superwarfarin poisoning

Peer reviewers: Subbaramiah Sridhar, MB, BS, MPH, FRCP, FRCP, FRCP, FRSS, FRCPC, FACP, FACG, FASGE, AGAF, Section of Gastroenterology, BBR 2544, Medical College of Georgia, 15th Street, Augusta, GA 30912, United States; Michael Leitman, MD, FACS, Chief of General Surgery, Beth Israel Medical Center, 10 Union Square East, Suite 2M, New York, NY 10003, United States

Zhao SL, Li P, Ji M, Zong Y, Zhang ST. Upper gastrointestinal hemorrhage caused by superwarfarin poisoning. *World J Gastroenterol* 2010; 16(13): 1680-1682 Available from: URL: http://www.wjgnet.com/1007-9327/full/v16/i13/1680.htm DOI: http://dx.doi.org/10.3748/wjg.v16.i13.1680

INTRODUCTION

Superwarfarins are anticoagulants similar to warfarin. As substitutes for acute rodenticides, superwarfarins are usually the first choice of rodenticide, especially in rural areas. Esophagogastroduodenoscopy (EGD) is a common tool for diagnostic and therapeutic goals. Significant bleeding after cold mucosal biopsy is seldom seen. Here, we report a woman with severe upper gastrointestinal hemorrhage after gastroscopic mucosal biopsy, which is a rare and previously unreported complication of superwarfarin poisoning.

CASE REPORT

A 55-year-old woman was referred to our hospital for epigastric pain and abdominal distention. Her medical history and physical examination were unremarkable. She had no history of anticoagulation therapy or use of non-steroid anti-inflammatory drugs. She came to the outpatient department for further evaluation.

Routine EGD revealed an uneven granular mucosa and several erosion lesions scattering in the stomach, covered with fresh blood crusts (Figure 1). Five mucosal biopsies of the stomach, two from the gastric angle and three from the lesser curvature side of gastric antrum, were performed for pathological analysis and *Helicobacter pylori* (*H. pylori*) detection. Gastric biopsy specimens revealed atrophic gastritis accompanying intestinal metaplasia. Rapid urease test was negative for *H. pylori* infection. No active bleeding was seen immediately after endoscopic biopsy and throughout the whole endoscopic procedure. However, she was admitted to the emergency department of our hospital because of hematemesis and melena the next day after EGD examination.

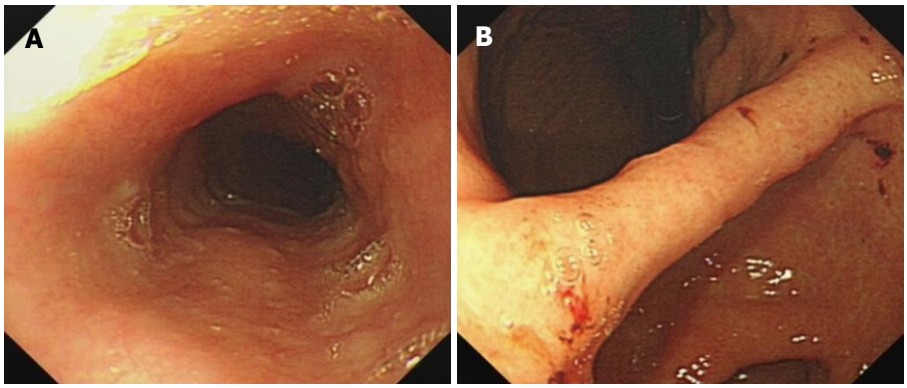

Figure 1 Initial esophagogastroduodenoscopy (EGD) demonstrating normal esophageal mucosa (A) and erosion lesions scattering in the stomach (B).

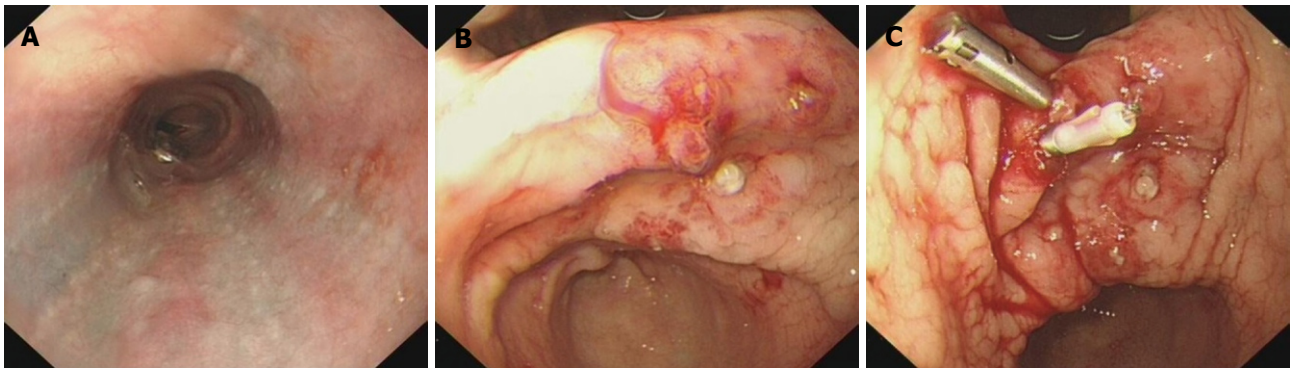

Figure 2 Second EGD showing submucosal congestion in the esophagus (A), active bleeding in the original biopsy sites (B), and titanium clips used for hemostasis (C).

Table 1 Findings in hematologic and coagulation laboratory tests

Variables	Normal range	Day 2	Day 4	Day 8
RBC (10^{12}/L)	3.5-5.5	1.7	2.25	2.72
Hemoglobin (g/L)	110-160	55	74	89
Prothrombin time (s)	11.0-14.0	> 180	16.8	13.8
Activated partial thromboplastin time (s)	35.0-55.0	94.3	30.5	26.9

Routine blood test showed 1.7 × 10^{12} erythrocytes per liter (normal 3.5-4.5 erythrocytes/liter) and 56 g hemoglobin per liter (Table 1). Coagulation function test revealed a prolonged prothrombin time (PT > 180 s) and an activated partial thromboplastin time (APTT = 94.3 s) (Table 1), both of which could be corrected when mixed with normal plasma at a 1:1 ratio. Other blood tests, such as platelet count, fibrinogen, renal function, and liver function, were normal (data not shown).

Superwarfarin poisoning was taken into consideration. The patient's serum and urine specimens were sent to Affiliated 307 Hospital of Academy of Military Sciences of China for toxicology analysis. Laboratory evaluation for some common superwarfarins was performed with the help of reverse-phase high performance enzyme-linked chromatography, showing that the level of brodifacoum and bromadiolone in serum was 1665 ng/mL and 132 ng/mL, respectively, and 216 ng/mL and 15 ng/mL in urine, respectively. The diagnosis of superwarfarin poisoning was confirmed. The patient was also allowed to have intentionally ingested rodenticides to commit suicide 10 d before the routine EGD examination because of severe depression.

Emergency EGD showed submucosal congestion of the esophagus (Figure 2A), and five hemorrhagic sites in the stomach, which were still bleeding during the endoscopic procedure (Figure 2B). All the bleeding sites were closed with 5 titanium clips to achieve hemostasis (Figure 2C).

The patient was treated with concentrated red blood cells, fresh frozen plasma and intravenous vitamin K (30 mg/d) for 8 d until her coagulation parameters returned to normal, RBC count and hemoglobin concentration were greatly improved (Table 1). She began to have oral vitamin K1 (30 mg/d) from day 9 after admission. Toxicology analysis on day 7 showed a brodifacoum concentration of 986 ng/mL and a bromadiolone concentration of 36 ng/mL in serum. Brodifacoum (7 ng/mL) could only be detected in the urine specimen. On day 10, EGD showed that the submucosal congestion of esophagus was absorbed with no sign of bleeding in the stomach, and titanium clips in good condition (Figure 3). Plain radiography and CT scanning revealed 5 titanium clips in the stomach (Figure 4).

Two days after the last EGD examination, the patient was discharged from our hospital and oral vitamin K1 was prescribed (10 mg/d) for 1 mo. Weekly PT, prothrombin activity and international normalized ratio measurements

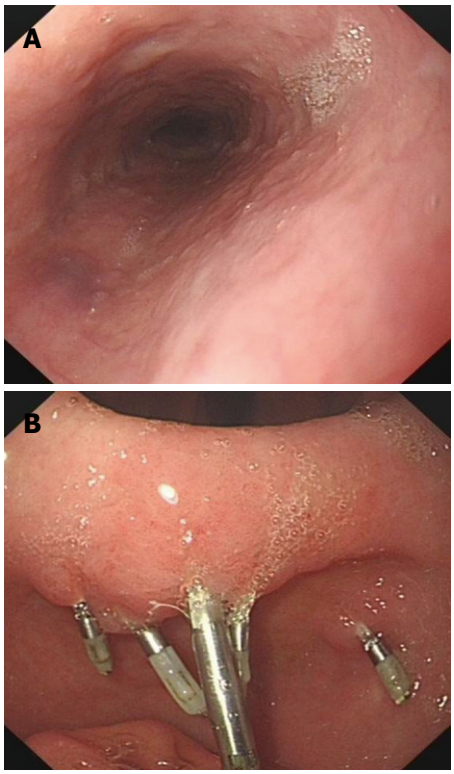

Figure 3 Final EGD showing the absorbed esophageal submucosal congestion (A) and bleeding in the stomach with titanium clips in good condition (B).

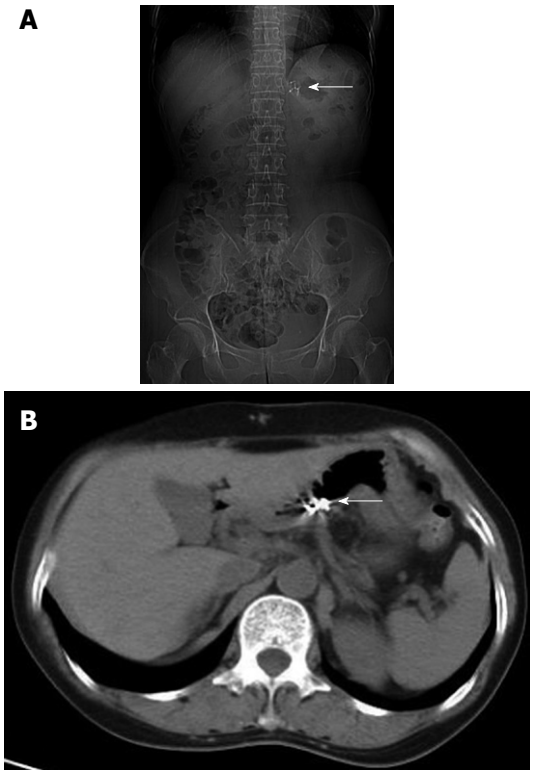

Figure 4 Plain radiography (A) and CT scanning (B) revealing 5 titanium clips in the stomach (arrows).

were also advised. During the 1-mo following-up after discharge, her coagulation parameters remained normal with no recurrent bleeding.

DISCUSSION

Superwarfarins, a class of rodenticides with brodifacoum and bromadiolone as their representative, are long acting anticoagulants[1,2] and are 100 times as potent as warfarin. The half life of brodifacoum and bromadiolone can be as long as 24 d[3] or 30 d[1] and 31 d[2], respectively.

Superwarfarins are supposed as the first-line rodenticides all over the world. However, superwarfarin poisoning cases are often reported, especially in rural areas. The number of superwarfarin poisoning cases has also increased in the USA[4,5]. The causes of superwarfarin poisoninginclude accidental exposure, suicide intention and occupational exposure. In addition to oral intake, inhalation and skin absorption can also result in superwarfarin poisoning.

Gastrointestinal hemorrhage is a fatal complication of superwarfarin poisoning, requiring immediate treatment. Treatment modalities include use of antidotes, such as vitamin K1, often requiring a high dose (20-125 mg/d) and a prolonged time because of the long half-life of superwarfarins[2].

Endoscopic treatment for hemostasis is somewhat effective. Due to the extensive bleeding and hemodynamic instability of our patient, blood transfusion and fluid infusion should also be applied to correct the blood volume before emergency endoscopy. In this case, hemostasis was achieved by placing five titanium tips to clip the bleeding sites with the help of an EGD.

In conclusion, with the help of antidotes against superwarfarins and EGD, upper gastrointestinal hemorrhage caused by superwarfarin poisoning after endoscopic cold mucosal biopsy can be successfully and safely controlled.

REFERENCES

1 **Laposata M**, Van Cott EM, Lev MH. Case records of the Massachusetts General Hospital. Case 1-2007. A 40-year-old woman with epistaxis, hematemesis, and altered mental status. *N Engl J Med* 2007; **356**: 174-182
2 **Pavlu J**, Harrington DJ, Voong K, Savidge GF, Jan-Mohamed R, Kaczmarski R. Superwarfarin poisoning. *Lancet* 2005; **365**: 628
3 **Bruno GR**, Howland MA, McMeeking A, Hoffman RS. Long-acting anticoagulant overdose: brodifacoum kinetics and optimal vitamin K dosing. *Ann Emerg Med* 2000; **36**: 262-267
4 **Chua JD**, Friedenberg WR. Superwarfarin poisoning. *Arch Intern Med* 1998; **158**: 1929-1932
5 **Watson WA**, Litovitz TL, Rodgers GC Jr, Klein-Schwartz W, Reid N, Youniss J, Flanagan A, Wruk KM. 2004 Annual report of the American Association of Poison Control Centers Toxic Exposure Surveillance System. *Am J Emerg Med* 2005; **23**: 589-666

S- Editor Wang JL **L- Editor** Wang XL **E- Editor** Zheng XM

World Journal of Gastroenterology

Online Submissions: http://www.wjgnet.com/1007-9327office
wjg@wjgnet.com
www.wjgnet.com

World J Gastroenterol 2010 April 7; 16(13): I
ISSN 1007-9327 (print)

Acknowledgments to reviewers of *World Journal of Gastroenterology*

Many reviewers have contributed their expertise and time to the peer review, a critical process to ensure the quality of *World Journal of Gastroenterology*. The editors and authors of the articles submitted to the journal are grateful to the following reviewers for evaluating the articles (including those published in this issue and those rejected for this issue) during the last editing time period.

Rakesh Aggarwal, Additional Professor, Department of Gastroenterology, Sanjay Gandhi Postgraduate Institute of Medical Sciences, Lucknow 226014, India

Akira Andoh, MD, Department of Internal Medicine, Shiga University of Medical Science, Seta Tukinowa, Otsu 520-2192, Japan

Albert J Bredenoord, MD, Dr., Department of Gastroenterology, St Antonius Hospital, PO Box 2500, 3430 EM, Nieuwegein, The Netherlands

Wan-Long Chuang, MD, PhD, MS, Professor, Director, Hepatobiliary Division, Department of Internal Medicine, Kaohsiung Medical University, No. 100 Shih-Chuan 1st Road, Kaohsiung 807, Taiwan, China

Jeremy FL Cobbold, PhD, Dr., Clinical Lecturer in Hepatology, Department of Hepatology and Gastroenterology, Liver Unit, Imperial College London, St Mary's Hospital, 10th Floor, QEQM building, Praed Street, London, W2 1NY, United Kingdom

Joseph J Cullen, Dr., MD, Professor, Department of Surgery, University of Iowa Carver College of Medicine, 4605 JCP, University of Iowa Hospitals and Clinics, 200 Hawkins Drive, Iowa City, IA 52242, United States

Giovanni D De Palma, Professor, Department of Surgery and Advanced Technologies, University of Naples Federico II, School of Medicine, Naples 80131, Italy

Willemijntje A Hoogerwerf, MD, Assistant Professor, Internal Medicine, Division of Gstroenterology, University of Michigan, 2215 Fuller Road, Ann Arbor, MI 48105, United State

Masahiro Iizuka, MD, PhD., Director, Akita Health Care Center, Akita Red Cross Hospital, 3-4-23, Nakadori, Akita, 010-0001, Japan

Yoshiaki Iwasaki, Dr., Department of Gastroenterology and Hepatology, Okayama University Graduate School of Medicine, Dentistry, and Pharmaceutical Sciences, 2-5-1, Shikata-cho, Okayama 700-8558, Japan

Marcela Kopacova, Associate Professor, MD, PhD, 2nd Department of Internal Medicine, Charles University Teaching Hospital, Sokolska 581, 500 05 Hradec Kralove, Czech Republic

Michael Koutsilieris, Professor, Experimental Physiology, Medical School, National & Kapodistrian University of Athens, Goudi, Athens, 11527, Greece

Michael Leitman, MD, FACS, Chief of General Surgery, Beth Israel Medical Center, 10 Union Square East, Suite 2M, New York, NY 10003, United States

Susumu Ohwada, Associate Professor, Department of Surgery, Gunma University Graduate School of Medicine, 3-39-15 Shoma-Machi, Maebashi 371-8511, Japan

George Papatheodoridis, MD, Assistant Professor in Medicine & Gastroenterology, 2nd Department of Internal Medicine, Athens University Medical School, Hippokration General Hospital of Athens, 114 Vas. Sophias Ave., 115 27 Athens, Greece

Vasiliy I Reshetnyak, MD, PhD, Professor, Scientist Secretary of the Scientific Research Institute of General Reanimatology, 25-2, Petrovka str., 107031, Moscow, Russia

Gerardo Rosati, MD, Medical Oncology Unit, "S. Carlo" Hospita, Via Potito Petrone, 1, Potenza 85100, Italy

Francis Seow-Choen, MBBS, FRCSEd, FAMS, Professor, Seow-Choen Colorectal Centre, Mt Elizabeth Medical Centre, Singapore, 3 Mt Elizabeth Medical Centre #09-10, 228510, Singapore

Scott Steele, MD, FACS, FASCRS,Chief, Colon & Rectal Surgery, Department of Surgery,Madigan Army Medical Center, Fort Lewis, WA 98431, United States

Alberto Tommasini, Dr., MD, Professor, Laboratory of Immunopathology, Institute for Maternal and Child Health, IRCCS Burlo Garofolo, Via dell'Istria 65/1, Trieste 34137, Italy

Eric WC Tse, Dr., MB, PhD, Department of Medicine, The University of Hong Kong, Queen Mary Hospital, Pokfulam, Hong Kong, China

Akihito Tsubota, Assistant Professor, Institute of Clinical Medicine and Research, Jikei University School of Medicine, 163-1 Kashiwashita, Kashiwa, Chiba 277-8567, Japan

Lea Veijola, MD, PhD, Consultant Gastroenterologist, Herttoniemi Hospital, Health Care of City of Helsinki, Kettutie 8, Helsinki, 00800, Finland

World Journal of Gastroenterology

Online Submissions: http://www.wjgnet.com/1007-9327office
wjg@wjgnet.com
www.wjgnet.com

World J Gastroenterol 2010 April 7; 16(13): I
ISSN 1007-9327 (print)

Meetings

Events Calendar 2010

January 25-26
Tamilnadu, India
International Conference on Medical Negligence and Litigation in Medical Practice

January 25-29
Waikoloa, HI, United States
Selected Topics in Internal Medicine

January 26-27
Dubai, United Arab Emirates
2nd Middle East Gastroenterology Conference

January 28-30
Hong Kong, China
The 1st International Congress on Abdominal Obesity

February 11-13
Fort Lauderdale, FL, United States
21th Annual International Colorectal Disease Symposium

February 26-28
Carolina, United States
First Symposium of GI Oncology at The Caribbean

March 04-06
Bethesda, MD, United States
8th International Symposium on Targeted Anticancer Therapies

March 05-07
Peshawar, Pakistan
26th Pakistan Society of Gastroenterology & Endoscopy Meeting

March 09-12
Brussels, Belgium
30th International Symposium on Intensive Care and Emergency Medicine

March 12-14
Bhubaneswar, India
18th Annual Meeting of Indian National Association for Study of the Liver

March 23-26
Cairo, Egypt
14th Pan Arab Conference on Diabetes PACD14

March 25-28
Beijing, China
The 20th Conference of the Asian Pacific Association for the Study of the Liver

March 27-28
San Diego, California, United States
25th Annual New Treatments in Chronic Liver Disease

April 07-09
Dubai, United Arab Emirates
The 6th Emirates Gastroenterology and Hepatology Conference, EGHC 2010

April 14-17
Landover, Maryland, United States
12th World Congress of Endoscopic Surgery

April 14-18
Vienna, Austria
The International Liver Congress™ 2010

April 28-May 01
Dubrovnik, Croatia
3rd Central European Congress of surgery and the 5th Croatian Congress of Surgery

May 01-05
New Orleans, LA, United States
Digestive Disease Week Annual Meeting

May 06-08
Munich, Germany
The Power of Programming: International Conference on Developmental Origins of Health and Disease

May 15-19
Minneapolis, MN, United States
American Society of Colon and Rectal Surgeons Annual Meeting

June 04-06
Chicago, IL, United States
American Society of Clinical Oncologists Annual Meeting

June 09-12
Singapore, Singapore
13th International Conference on Emergency Medicine

June 14
Kosice, Slovakia
Gastro-intestinal Models in the Research of Probiotics and Prebiotics-Scientific Symposium

June 16-19
Hong Kong, China
ILTS: International Liver Transplantation Society ILTS Annual International Congress

June 20-23
Mannheim, Germany
16th World Congress for Bronchoesophagology-WCBE

June 25-29
Orlando, FL, United States
70th ADA Diabetes Scientific Sessions

August 28-31
Boston, Massachusetts, United States
10th OESO World Congress on Diseases of the Oesophagus 2010

September 10-12
Montreal, Canada
International Liver Association's Fourth Annual Conference

September 11-12
La Jolla, CA, United States
New Advances in Inflammatory Bowel Disease

September 12-15
Boston, MA, United States
ICAAC: Interscience Conference on Antimicrobial Agents and Chemotherapy Annual Meeting

September 16-18
Prague, Czech Republic
Prague Hepatology Meeting 2010

September 23-26
Prague, Czech Republic
The 1st World Congress on Controversies in Gastroenterology & Liver Diseases

October 07-09
Belgrade, Serbia
The 7th Biannual International Symposium of Society of Coloproctology

October 15-20
San Antonio, TX, United States
ACG 2010: American College of Gastroenterology Annual Scienitfic Meeting

October 23-27
Barcelona, Spain
18th United European Gastroenterology Week

October 29-November 02
Boston, Massachusetts, United States
The Liver Meeting® 2010--AASLD's 61st Annual Meeting

November 13-14
San Francisco, CA, United States
Case-Based Approach to the Management of Inflammatory Bowel Disease

December 02-04
San Francisco, CA, United States
The Medical Management of HIV/AIDS

World Journal of Gastroenterology

Online Submissions: http://www.wjgnet.com/1007-9327office
wjg@wjgnet.com
www.wjgnet.com

World J Gastroenterol 2010 April 7; 16(13): I-IV
ISSN 1007-9327 (print)

Instructions to authors

GENERAL INFORMATION

World Journal of Gastroenterology (*World J Gastroenterol*, *WJG*, print ISSN 1007-9327, DOI: 10.3748) is a weekly, open-access (OA), peer-reviewed journal supported by an editorial board of 1096 experts in gastroenterology and hepatology from 60 countries.

The biggest advantage of the OA model is that it provides free, full-text articles in PDF and other formats for experts and the public without registration, which eliminates the obstacle that traditional journals possess and usually delays the speed of the propagation and communication of scientific research results. The open access model has been proven to be a true approach that may achieve the ultimate goal of the journals, i.e. the maximization of the value to the readers, authors and society.

The role of academic journals is to exhibit the scientific levels of a country, a university, a center, a department, and even a scientist, and build an important bridge for communication between scientists and the public. As we all know, the significance of the publication of scientific articles lies not only in disseminating and communicating innovative scientific achievements and academic views, as well as promoting the application of scientific achievements, but also in formally recognizing the "priority" and "copyright" of innovative achievements published, as well as evaluating research performance and academic levels. So, to realize these desired attributes of *WJG* and create a well-recognized journal, the following four types of personal benefits should be maximized. The maximization of personal benefits refers to the pursuit of the maximum personal benefits in a well-considered optimal manner without violation of the laws, ethical rules and the benefits of others. (1) Maximization of the benefits of editorial board members: The primary task of editorial board members is to give a peer review of an unpublished scientific article via online office system to evaluate its innovativeness, scientific and practical values and determine whether it should be published or not. During peer review, editorial board members can also obtain cutting-edge information in that field at first hand. As leaders in their field, they have priority to be invited to write articles and publish commentary articles. We will put peer reviewers' names and affiliations along with the article they reviewed in the journal to acknowledge their contribution; (2) Maximization of the benefits of authors: Since *WJG* is an open-access journal, readers around the world can immediately download and read, free of charge, high-quality, peer-reviewed articles from *WJG* official website, thereby realizing the goals and significance of the communication between authors and peers as well as public reading; (3) Maximization of the benefits of readers: Readers can read or use, free of charge, high-quality peer-reviewed articles without any limits, and cite the arguments, viewpoints, concepts, theories, methods, results, conclusion or facts and data of pertinent literature so as to validate the innovativeness, scientific and practical values of their own research achievements, thus ensuring that their articles have novel arguments or viewpoints, solid evidence and correct conclusion; and (4) Maximization of the benefits of employees: It is an iron law that a first-class journal is unable to exist without first-class editors, and only first-class editors can create a first-class academic journal. We insist on strengthening our team cultivation and construction so that every employee, in an open, fair and transparent environment, could contribute their wisdom to edit and publish high-quality articles, thereby realizing the maximization of the personal benefits of editorial board members, authors and readers, and yielding the greatest social and economic benefits.

The major task of *WJG* is to report rapidly the most recent results in basic and clinical research on esophageal, gastrointestinal, liver, pancreas and biliary tract diseases, *Helicobacter pylori*, endoscopy and gastrointestinal surgery, including: gastroesophageal reflux disease, gastrointestinal bleeding, infection and tumors; gastric and duodenal disorders; intestinal inflammation, microflora and immunity; celiac disease, dyspepsia and nutrition; viral hepatitis, portal hypertension, liver fibrosis, liver cirrhosis, liver transplantation, and metabolic liver disease; molecular and cell biology; geriatric and pediatric gastroenterology; diagnosis and screening, imaging and advanced technology.

The columns in the issues of *WJG* will include: (1) Editorial: To introduce and comment on the substantial advance and its importance in the fast-developing areas; (2) Frontier: To review the most representative achievements and comment on the current research status in the important fields, and propose directions for the future research; (3) Topic Highlight: This column consists of three formats, including (A) 10 invited review articles on a hot topic, (B) a commentary on common issues of this hot topic, and (C) a commentary on the 10 individual articles; (4) Observation: To update the development of old and new questions, highlight unsolved problems, and provide strategies on how to solve the questions; (5) Guidelines for Basic Research: To provide Guidelines for basic research; (6) Guidelines for Clinical Practice: To provide guidelines for clinical diagnosis and treatment; (7) Review: To systemically review the most representative progress and unsolved problems in the major scientific disciplines, comment on the current research status, and make suggestions on the future work; (8) Original Article: To originally report the innovative and valuable findings in gastroenterology and hepatology; (9) Brief Article: To briefly report the novel and innovative findings in gastroenterology and hepatology; (10) Case Report: To report a rare or typical case; (11) Letters to the Editor: To discuss and make reply to the contributions published in *WJG*, or to introduce and comment on a controversial issue of general interest; (12) Book Reviews: To introduce and comment on quality monographs of gastroenterology and hepatology; and (13) Guidelines: To introduce Consensuses and Guidelines reached by international and national academic authorities worldwide on basic research and clinical practice gastroenterology and hepatology.

CSSN
ISSN 1007-9327 (print)
CN 14-1219/R

Indexed and Abstracted in
Current Contents®/Clinical Medicine, Science Citation Index Expanded (also known as SciSearch®), Journal Citation Reports®, Index Medicus, MEDLINE, PubMed, PubMed Central, Digital Object Identifer, and EMBASE/Excerpta Medica. ISI, Thomson Reuters, 2008 Impact Factor: 2.081 (32/55 Gastroenterology and Hepatology).

Published by
Beijing Baishideng BioMed Scientific Co., Ltd.

SUBMISSION OF MANUSCRIPTS

Manuscripts should be typed in 1.5 line spacing and 12 pt. Book Antiqua with ample margins. Number all pages consecutively, and start each of the following sections on a new page: Title Page,

Abstract, Introduction, Materials and Methods, Results, Discussion, Acknowledgements, References, Tables, Figures, and Figure Legends. Neither the editors nor the publisher are responsible for the opinions expressed by contributors. Manuscripts formally accepted for publication become the permanent property of Beijing Baishideng BioMed Scientific Co., Ltd, and may not be reproduced by any means, in whole or in part, without the written permission of both the authors and the publisher. We reserve the right to copy-edit and put onto our website accepted manuscripts. Authors should follow the relevant guidelines for the care and use of laboratory animals of their institution or national animal welfare committee. For the sake of transparency in regard to the performance and reporting of clinical trials, we endorse the policy of the International Committee of Medical Journal Editors to refuse to publish papers on clinical trial results if the trial was not recorded in a publicly-accessible registry at its outset. The only register now available, to our knowledge, is http://www. clinicaltrials.gov sponsored by the United States National Library of Medicine and we encourage all potential contributors to register with it. However, in the case that other registers become available you will be duly notified. A letter of recommendation from each author's organization should be provided with the contributed article to ensure the privacy and secrecy of research is protected.

Authors should retain one copy of the text, tables, photographs and illustrations because rejected manuscripts will not be returned to the author(s) and the editors will not be responsible for loss or damage to photographs and illustrations sustained during mailing.

Online submissions

Manuscripts should be submitted through the Online Submission System at: http://www.wjgnet.com/1007-9327office. Authors are highly recommended to consult the ONLINE INSTRUCTIONS TO AUTHORS (http://www.wjgnet.com/1007-9327/g_info_20100315215714.htm) before attempting to submit online. For assistance, authors encountering problems with the Online Submission System may send an email describing the problem to wjg@wjgnet.com, or by telephone: +86-10-5908-0039. If you submit your manuscript online, do not make a postal contribution. Repeated online submission for the same manuscript is strictly prohibited.

MANUSCRIPT PREPARATION

All contributions should be written in English. All articles must be submitted using word-processing software. All submissions must be typed in 1.5 line spacing and 12 pt. Book Antiqua with ample margins. Style should conform to our house format. Required information for each of the manuscript sections is as follows:

Title page

Title: Title should be less than 12 words.

Running title: A short running title of less than 6 words should be provided.

Authorship: Authorship credit should be in accordance with the standard proposed by International Committee of Medical Journal Editors, based on (1) substantial contributions to conception and design, acquisition of data, or analysis and interpretation of data; (2) drafting the article or revising it critically for important intellectual content; and (3) final approval of the version to be published. Authors should meet conditions 1, 2, and 3.

Institution: Author names should be given first, then the complete name of institution, city, province and postcode. For example, Xu-Chen Zhang, Li-Xin Mei, Department of Pathology, Chengde Medical College, Chengde 067000, Hebei Province, China. One author may be represented from two institutions, for example, George Sgourakis, Department of General, Visceral, and Transplantation Surgery, Essen 45122, Germany; George Sgourakis, 2nd Surgical Department, Korgialenio-Benakio Red Cross Hospital, Athens 15451, Greece

Author contributions: The format of this section should be: Author contributions: Wang CL and Liang L contributed equally to this work; Wang CL, Liang L, Fu JF, Zou CC, Hong F and Wu XM designed the research; Wang CL, Zou CC, Hong F and Wu XM performed the research; Xue JZ and Lu JR contributed new reagents/analytic tools; Wang CL, Liang L and Fu JF analyzed the data; and Wang CL, Liang L and Fu JF wrote the paper.

Supportive foundations: The complete name and number of supportive foundations should be provided, e.g., Supported by National Natural Science Foundation of China, No. 30224801

Correspondence to: Only one corresponding address should be provided. Author names should be given first, then author title, affiliation, the complete name of institution, city, postcode, province, country, and email. All the letters in the email should be in lower case. A space interval should be inserted between country name and email address. For example, Montgomery Bissell, MD, Professor of Medicine, Chief, Liver Center, Gastroenterology Division, University of California, Box 0538, San Francisco, CA 94143, United States. montgomery.bissell@ucsf.edu

Telephone and fax: Telephone and fax should consist of +, country number, district number and telephone or fax number, e.g., Telephone: +86-10-59080039 Fax: +86-10-85381893

Peer reviewers: All articles received are subject to peer review. Normally, three experts are invited for each article. Decision for acceptance is made only when at least two experts recommend an article for publication. Reviewers for accepted manuscripts are acknowledged in each manuscript, and reviewers of articles which were not accepted will be acknowledged at the end of each issue. To ensure the quality of the articles published in *WJG*, reviewers of accepted manuscripts will be announced by publishing the name, title/position and institution of the reviewer in the footnote accompanying the printed article. For example, reviewers: Professor Jing-Yuan Fang, Shanghai Institute of Digestive Disease, Shanghai, Affiliated Renji Hospital, Medical Faculty, Shanghai Jiaotong University, Shanghai, China; Professor Xin-Wei Han, Department of Radiology, The First Affiliated Hospital, Zhengzhou University, Zhengzhou, Henan Province, China; and Professor Anren Kuang, Department of Nuclear Medicine, Huaxi Hospital, Sichuan University, Chengdu, Sichuan Province, China.

Abstract

There are unstructured abstracts (no more than 256 words) and structured abstracts (no more than 480). The specific requirements for structured abstracts are as follows:

An informative, structured abstracts of no more than 480 words should accompany each manuscript. Abstracts for original contributions should be structured into the following sections. AIM (no more than 20 words): Only the purpose should be included. Please write the aim as the form of "To investigate/study/…; MATERIALS AND METHODS (no more than 140 words); RESULTS (no more than 294 words): You should present *P* values where appropriate and must provide relevant data to illustrate how they were obtained, e.g. 6.92 ± 3.86 *vs* 3.61 ± 1.67, $P < 0.001$; CONCLUSION (no more than 26 words).

Key words

Please list 5-10 key words, selected mainly from *Index Medicus*, which reflect the content of the study.

Text

For articles of these sections, original articles, rapid communication and case reports, the main text should be structured into the following sections: INTRODUCTION, MATERIALS AND METHODS, RESULTS and DISCUSSION, and should include appropriate Figures and Tables. Data should be presented in the main text or in Figures and Tables, but not in both. The main text format of these sections, editorial, topic highlight, case

report, letters to the editors, can be found at: http://www.wjgnet.com/1007-9327/g_info_20100315215714.htm.

Illustrations

Figures should be numbered as 1, 2, 3, *etc.*, and mentioned clearly in the main text. Provide a brief title for each figure on a separate page. Detailed legends should not be provided under the figures. This part should be added into the text where the figures are applicable. Figures should be either Photoshop or Illustrator files (in tiff, eps, jpeg formats) at high-resolution. Examples can be found at: http://www.wjgnet.com/1007-9327/13/4520.pdf; http://www.wjgnet.com/1007-9327/13/4554.pdf; http://www.wjgnet.com/1007-9327/13/4891.pdf; http://www.wjgnet.com/1007-9327/13/4986.pdf; http://www.wjgnet.com/1007-9327/13/4498.pdf. Keeping all elements compiled is necessary in line-art image. Scale bars should be used rather than magnification factors, with the length of the bar defined in the legend rather than on the bar itself. File names should identify the figure and panel. Avoid layering type directly over shaded or textured areas. Please use uniform legends for the same subjects. For example: Figure 1 Pathological changes in atrophic gastritis after treatment. A:...; B:...; C:...; D:...; E:...; F:...; G: …*etc.* It is our principle to publish high resolution-figures for the printed and E-versions.

Tables

Three-line tables should be numbered 1, 2, 3, *etc.*, and mentioned clearly in the main text. Provide a brief title for each table. Detailed legends should not be included under tables, but rather added into the text where applicable. The information should complement, but not duplicate the text. Use one horizontal line under the title, a second under column heads, and a third below the Table, above any footnotes. Vertical and italic lines should be omitted.

Notes in tables and illustrations

Data that are not statistically significant should not be noted. $^{a}P < 0.05$, $^{b}P < 0.01$ should be noted ($P > 0.05$ should not be noted). If there are other series of P values, $^{c}P < 0.05$ and $^{d}P < 0.01$ are used. A third series of P values can be expressed as $^{e}P < 0.05$ and $^{f}P < 0.01$. Other notes in tables or under illustrations should be expressed as ^{1}F, ^{2}F, ^{3}F; or sometimes as other symbols with a superscript (Arabic numerals) in the upper left corner. In a multi-curve illustration, each curve should be labeled with ●, ○, ■, □, ▲, △, *etc.*, in a certain sequence.

Acknowledgments

Brief acknowledgments of persons who have made genuine contributions to the manuscript and who endorse the data and conclusions should be included. Authors are responsible for obtaining written permission to use any copyrighted text and/or illustrations.

REFERENCES

Coding system

The author should number the references in Arabic numerals according to the citation order in the text. Put reference numbers in square brackets in superscript at the end of citation content or after the cited author's name. For citation content which is part of the narration, the coding number and square brackets should be typeset normally. For example, "Crohn's disease (CD) is associated with increased intestinal permeability[1,2]". If references are cited directly in the text, they should be put together within the text, for example, "From references[19,22-24], we know that..."

When the authors write the references, please ensure that the order in text is the same as in the references section, and also ensure the spelling accuracy of the first author's name. Do not list the same citation twice.

PMID and DOI

Pleased provide PubMed citation numbers to the reference list, e.g. PMID and DOI, which can be found at http://www.ncbi.nlm.nih.gov/sites/entrez?db=pubmed and http://www.crossref.org/SimpleTextQuery/, respectively. The numbers will be used in E-version of this journal.

Style for journal references

Authors: the name of the first author should be typed in bold-faced letters. The family name of all authors should be typed with the initial letter capitalized, followed by their abbreviated first and middle initials. (For example, Lian-Sheng Ma is abbreviated as Ma LS, Bo-Rong Pan as Pan BR). The title of the cited article and italicized journal title (journal title should be in its abbreviated form as shown in PubMed), publication date, volume number (in black), start page, and end page [PMID: 11819634 DOI: 10.3748/wjg.13.5396].

Style for book references

Authors: the name of the first author should be typed in bold-faced letters. The surname of all authors should be typed with the initial letter capitalized, followed by their abbreviated middle and first initials. (For example, Lian-Sheng Ma is abbreviated as Ma LS, Bo-Rong Pan as Pan BR) Book title. Publication number. Publication place: Publication press, Year: start page and end page.

Format

Journals

English journal article (list all authors and include the PMID where applicable)

1 **Jung EM**, Clevert DA, Schreyer AG, Schmitt S, Rennert J, Kubale R, Feuerbach S, Jung F. Evaluation of quantitative contrast harmonic imaging to assess malignancy of liver tumors: A prospective controlled two-center study. *World J Gastroenterol* 2007; **13**: 6356-6364 [PMID: 18081224 DOI: 10.3748/wjg.13.6356]

Chinese journal article (list all authors and include the PMID where applicable)

2 **Lin GZ**, Wang XZ, Wang P, Lin J, Yang FD. Immunologic effect of Jianpi Yishen decoction in treatment of Pixu-diarrhoea. *Shijie Huaren Xiaohua Zazhi* 1999; **7**: 285-287

In press

3 **Tian D**, Araki H, Stahl E, Bergelson J, Kreitman M. Signature of balancing selection in Arabidopsis. *Proc Natl Acad Sci USA* 2006; In press

Organization as author

4 **Diabetes Prevention Program Research Group**. Hypertension, insulin, and proinsulin in participants with impaired glucose tolerance. *Hypertension* 2002; **40**: 679-686 [PMID: 12411462 PMCID:2516377 DOI:10.1161/01.HYP.0000035706.28494.09]

Both personal authors and an organization as author

5 **Vallancien G**, Emberton M, Harving N, van Moorselaar RJ; Alf-One Study Group. Sexual dysfunction in 1, 274 European men suffering from lower urinary tract symptoms. *J Urol* 2003; **169**: 2257-2261 [PMID: 12771764 DOI:10.1097/01.ju.0000067940.76090.73]

No author given

6 21st century heart solution may have a sting in the tail. *BMJ* 2002; **325**: 184 [PMID: 12142303 DOI:10.1136/bmj.325.7357.184]

Volume with supplement

7 **Geraud G**, Spierings EL, Keywood C. Tolerability and safety of frovatriptan with short- and long-term use for treatment of migraine and in comparison with sumatriptan. *Headache* 2002; **42** Suppl 2: S93-99 [PMID: 12028325 DOI:10.1046/j.1526-4610.42.s2.7.x]

Issue with no volume

8 **Banit DM**, Kaufer H, Hartford JM. Intraoperative frozen section analysis in revision total joint arthroplasty. *Clin Orthop Relat Res* 2002; (**401**): 230-238 [PMID: 12151900 DOI:10.1097/00003086-200208000-00026]

No volume or issue

9 Outreach: Bringing HIV-positive individuals into care. *HRSA Careaction* 2002; 1-6 [PMID: 12154804]

Books

Personal author(s)

10 **Sherlock S**, Dooley J. Diseases of the liver and billiary system. 9th ed. Oxford: Blackwell Sci Pub, 1993: 258-296

Chapter in a book (list all authors)

11 **Lam SK**. Academic investigator's perspectives of medical treatment for peptic ulcer. In: Swabb EA, Azabo S. Ulcer disease: investigation and basis for therapy. New York: Marcel Dekker, 1991: 431-450

Author(s) and editor(s)

12 **Breedlove GK**, Schorfheide AM. Adolescent pregnancy. 2nd ed. Wieczorek RR, editor. White Plains (NY): March of Dimes Education Services, 2001: 20-34

Conference proceedings

13 **Harnden P**, Joffe JK, Jones WG, editors. Germ cell tumours V. Proceedings of the 5th Germ cell tumours Conference; 2001 Sep 13-15; Leeds, UK. New York: Springer, 2002: 30-56

Conference paper

14 **Christensen S**, Oppacher F. An analysis of Koza's computational effort statistic for genetic programming. In: Foster JA, Lutton E, Miller J, Ryan C, Tettamanzi AG, editors. Genetic programming. EuroGP 2002: Proceedings of the 5th European Conference on Genetic Programming; 2002 Apr 3-5; Kinsdale, Ireland. Berlin: Springer, 2002: 182-191

Electronic journal (list all authors)

15 Morse SS. Factors in the emergence of infectious diseases. Emerg Infect Dis serial online, 1995-01-03, cited 1996-06-05; 1(1): 24 screens. Available from: URL: http//www.cdc.gov/ncidod/EID/eid.htm

Patent (list all authors)

16 **Pagedas AC**, inventor; Ancel Surgical R&D Inc., assignee. Flexible endoscopic grasping and cutting device and positioning tool assembly. United States patent US 20020103498. 2002 Aug 1

Statistical data

Write as mean ± SD or mean ± SE.

Statistical expression

Express *t* test as *t* (in italics), *F* test as *F* (in italics), chi square test as χ^2 (in Greek), related coefficient as *r* (in italics), degree of freedom as υ (in Greek), sample number as *n* (in italics), and probability as *P* (in italics).

Units

Use SI units. For example: body mass, m (B) = 78 kg; blood pressure, p (B) = 16.2/12.3 kPa; incubation time, t (incubation) = 96 h, blood glucose concentration, c (glucose) 6.4 ± 2.1 mmol/L; blood CEA mass concentration, p (CEA) = 8.6 24.5 μg/L; CO_2 volume fraction, 50 mL/L CO_2, not 5% CO_2; likewise for 40 g/L formaldehyde, not 10% formalin; and mass fraction, 8 ng/g, *etc.* Arabic numerals such as 23, 243, 641 should be read 23 243 641.

The format for how to accurately write common units and quantums can be found at: http://www.wjgnet.com/1007-9327/g_info_20100315223018.htm.

Abbreviations

Standard abbreviations should be defined in the abstract and on first mention in the text. In general, terms should not be abbreviated unless they are used repeatedly and the abbreviation is helpful to the reader. Permissible abbreviations are listed in Units, Symbols and Abbreviations: A Guide for Biological and Medical Editors and Authors (Ed. Baron DN, 1988) published by The Royal Society of Medicine, London. Certain commonly used abbreviations, such as DNA, RNA, HIV, LD50, PCR, HBV, ECG, WBC, RBC, CT, ESR, CSF, IgG, ELISA, PBS, ATP, EDTA, mAb, can be used directly without further explanation.

Italics

Quantities: *t* time or temperature, *c* concentration, *A* area, *l* length, *m* mass, *V* volume.
Genotypes: *gyrA*, *arg* 1, *c myc*, *c fos*, *etc.*
Restriction enzymes: *Eco*RI, *Hin*dI, *Bam*HI, *Kbo* I, *Kpn* I, *etc.*
Biology: *H. pylori*, *E coli*, *etc.*

RESUBMISSION OF THE REVISED MANUSCRIPTS

Please revise your article according to the revision policies of *WJG*. The revised version includes manuscript and high-resolution image figures. The author should re-submit the revised manuscript online, along with printed high-resolution color or black and white photos; Copyright transfer letter, and responses to the reviewers, and science news are sent to us *via* email.

Editorial Office

World Journal of Gastroenterology
Editorial Department: Room 903, Building D,
Ocean International Center,
No. 62 Dongsihuan Zhonglu,
Chaoyang District, Beijing 100025, China
E-mail: wjg@wjgnet.com
http://www.wjgnet.com
Telephone: +86-10-5908-0039
Fax: +86-10-85381893

Language evaluation

The language of a manuscript will be graded before it is sent for revision. (1) Grade A: priority publishing; (2) Grade B: minor language polishing; (3) Grade C: a great deal of language polishing needed; and (4) Grade D: rejected. Revised articles should reach Grade A or B.

Copyright assignment form

Please download a Copyright assignment form from http://www.wjgnet.com/1007-9327/g_info_20100315222818.htm.

Responses to reviewers

Please revise your article according to the comments/suggestions provided by the reviewers. The format for responses to the reviewers' comments can be found at: http://www.wjgnet.com/1007-9327/g_info_20100315222607.htm.

Proof of financial support

For paper supported by a foundation, authors should provide a copy of the document and serial number of the foundation.

Science news releases

Authors of accepted manuscripts are suggested to write a science news item to promote their articles. The news will be released rapidly at EurekAlert/AAAS (http://www.eurekalert.org). The title for news items should be less than 90 characters; the summary should be less than 75 words; and main body less than 500 words. Science news items should be lawful, ethical, and strictly based on your original content with an attractive title and interesting pictures.

Publication fee

Authors of accepted articles must pay a publication fee.
EDITORIAL, TOPIC HIGHLIGHTS, BOOK REVIEWS and LETTERS TO THE EDITOR are published free of charge.